# Modelling of $CO_2$ Behaviour at the Interface between the Storage Formation and the Caprock

Seyed Mohammad Shariatipour

Submitted for the degree of Doctor of Philosophy

Institute of Petroleum Engineering
Heriot-Watt University
Edinburgh
UK

May 2013

# ABSTRACT

Carbon Capture and Storage (CCS) is a possible option to mitigate the rise in anthropogenic $CO_2$. When $CO_2$ is injected into a storage formation, it migrates upwards under buoyancy until it reaches the caprock. Of the $CO_2$ that does not dissolve, some may be trapped under the caprock as a free phase and the rest will migrate laterally, which could subsequently cause a risk of $CO_2$ leakage out of a storage complex.

Many studies assume a smooth, abrupt interface between the storage and the sealing formations, whereas typically the surface is irregular, due to sedimentological and stratigraphic effects or structural deformation. In this study, the area where the $CO_2$ migrates beneath the caprock is investigated. A set of numerical simulations was conducted to investigate the impacts of various factors on $CO_2$ storage, such as top morphology, tilt and $k_V/k_H$, and the presence of a transition zone, where there is a gradational change from storage formation to caprock. These effects were also examined on a realistic field (Lincolnshire Model). It is concluded that a transition zone can increase the security of storage by lessening the amount of $CO_2$ accumulating underneath the caprock. Regarding the top morphology, it is determined that ridges with higher amplitude (larger than the plume thickness) provide more structural trapping if they are perpendicular to the tilt. However, ridges parallel to the tilt provide a pathway for rapid $CO_2$ up dip migration. On the other hand, more $CO_2$ is dissolved due to more migration. Therefore it is important to characterise the interface in terms of the size of irregularities and also in terms of the existence of any transition zone. The latter has not been addressed in previous works. The role of an unconformity at the interface between the caprock and storage formation was also investigated. It is concluded that this can have both positive and negative effects on $CO_2$ storage capacity and security. For example a very thin weathered zone can contribute significantly to pressure diffusion across the model.

A novel approach for $CO_2$ injection is presented to minimize vertical migration of $CO_2$ in the storage formation thereby reducing the risk of $CO_2$ leakage. This is achieved by downhole-mixing of $CO_2$ and brine. It is demonstrated that vertical migration of $CO_2$ in the reservoir can be limited due to viscous effects during the injection period, and that during the subsequent shut-in period gravity segregation displaces the $CO_2$ saturated brine *downwards*, thereby increasing the storage security.

*Dedicated to my Dear Family*

# Acknowledgements

This thesis is submitted in partial fulfilment of the requirements for the Ph.D. degree at Heriot-Watt University. This work has been conducted at the Institute of Petroleum from November 2010 to May 2013 under the supervision of Dr. Gillian Pickup and Professor Eric Mackay.

The project has been financed by grants by Scottish Carbon Capture and Storage (SCCS) Consortium and Foundation CMG, which are gratefully acknowledged.

I was quite fortunate to have the right supervisors, whose conscientious supervision and unflagging support challenged me to settle for nothing less than quality. They provided me freedom to explore different ideas. Gillian was always accessible, and constantly provided insightful reviews and timely responses throughout the various stages of this work. They gave me insightful suggestions and guidance. For this, I express my deepest gratitude to my supervisors, Dr. Gillian Pickup and Professor Eric Mackay.

Also in this regard, I would like to thank my colleague Dr. Min Jin for his close collaboration and fruitful discussions. Additionally, I greatly appreciate the help from Professor Dorrik Stow, Dr. Helen Lever, and Dr. Andy Gardner for their constructive geology related discussions and all the colleagues as well as friends in the Carbon Storage group and in the Institute of Petroleum Engineering (IPE) making my stay in Edinburgh very pleasant and provided me with any help needed. I wish to express my thanks to the Institute of Petroleum Engineering, Heriot-Watt University.

I would like to thanks my Iranian friends Amir, Hadi, Hamidreza, Hamid, Alireza, Mobeen, Yousef, Jalal, Hajar, Shayda and Zahra who have made my stay in Edinburgh amazing.

A special thanks goes to my office colleagues Peter, Sally, Mohammad, Usman, and Mustapha.

I greatly appreciate the invaluable comments from my examiner, Professor Philip Ringrose and Professor Bahman Tohidi which significantly improved the quality of my work.

Last, but by no means least, I am extremely grateful to my parents, my brothers, my sisters and my sisters in law. Words cannot express how much I thank them for their continuous support through my graduate research. I would not have come this far without their inspiration and unyielding support.

# TABLE OF CONTENTS

# Table of Contents

## List of Figures

# List of Tables

## Nomenclature

| | |
|---|---|
| $a$ | intermolecular attraction |
| $aq$ | liquid phase |
| $b$ | intermolecular repulsion |
| $B_b$ | brine formation volume factor |
| $c_b$ | formation brine compressibility |
| $D$ | molecular diffusion coefficient |
| g | gas phase |
| $k$ | constant = $1.38058 \times 10^{-12}$ |
| $K^0$ | thermodynamic equilibrium constant |
| $m$ | molality |
| mD | mile Darcy |
| $M_w$ | molecular weight |
| $n$ | mole |
| $p$ | pressure |
| Par | parameter, it can be either $\lambda$ or $\zeta$ |
| $R$ | gas constant |
| $R_s$ | dissolved $CO_2$–brine ratio |
| $T$ | absolute temperature (K) |
| $V$ | volume |
| $\bar{V}$ | molar volume |
| $V_\phi$ | apparent molar volume |
| $x$ | mole fraction in aqueous phase |
| $y$ | mole fraction in $CO_2$-rich phase |

Greek symbols

| | |
|---|---|
| $\gamma$ | activity coefficient |
| $\varphi$ | fugacity coefficient |
| $\kappa$ | equilibrium constant |
| $\lambda$ | second-order interaction parameters |
| $\mu$ | viscosity |
| $\nu$ | stoichiometric number of ions in the dissolved salt |
| $\pi$ | pressure |
| $\theta$ | temperature (°C) |
| $\rho$ | mass density |
| $\bar{\rho}$ | molar density |
| $\omega$ | $CO_2$ mass fraction in aqueous phase |

Subscripts

| | |
|---|---|
| b | brine |
| c | critical |
| i | component index |
| j | component index |
| k | component index |
| L | liquid |
| h | horizontal |
| mix | mixture |
| res | Reservoir condition |
| sat | saturated |
| sc | standard condition |
| p | pore volume |
| w | water |

## Abbreviations

| | |
|---|---|
| CASSEM | $CO_2$ Aquifer Storage Site Evaluation & Monitoring |
| CCS | Carbon Capture and storage |
| EKP | Ennis-King and Paterson |
| FPR | Field Average Pressure |
| FWCD | $CO_2$ Dissolved in Water Phase |
| GEP | Gillian Pickup |
| HHZ | Hassan Hassanzadeh |
| Imb | Imbibition |
| IPCC | International Panel on Climate Change |
| LGR | Local Grid Refinement |
| RESV | Reservoir Volume Injection Control |
| WBHP | Well Bottom Hole Pressure |
| PARA | Parallel |
| PERM | Permeability |
| PERP | Perpendicular |
| PORO | Porosity |
| TRANS | Transition |

## List of Publications and Invited Presentations by the Candidate

- Shariatipour, S.M., Pickup, G.E., Stow, D., Mackay, E.J., 2011, *The Effects of Aquifer/Caprock Interface on $CO_2$ Storage,* UKCCSC Biannual Meeting, UK Carbon Capture and Storage Conference, 1-2 September, Edinburgh, UK.

- Shariatipour, S.M., Pickup, G.E., Mackay, E.J., 2011, *A Novel Method to Minimize Leakage Risk in $CO_2$ Sequestration.* Iranian Ministry of Science, Research and Technology, Tehran International Exhibition, 13 - 19 December, Tehran, Iran.

- Shariatipour, S.M., Pickup, G.E., Mackay, E.J., 2012, Heinemann, N., *Flow Simulation of $CO_2$ Storage in Saline Aquifer Using Black Oil Simulator" SPE 151042,* Carbon Management Technology Conference, 7-9 February 2012, Orlando, Florida, USA.

- Shariatipour, S.M., Pickup, G.E., Stow, D.A.V., Mackay, E.J., 2012, *The Effects of Aquifer/Caprock Interface on $CO_2$ Storage Capacity and Security,* 3rd EAGE CO2 Geological Storage Workshop, 26-27 March, Edinburgh, UK.

- Shariatipour, S.M., Pickup, G.E., Mackay, E.J., 2012, *A Novel Method for $CO_2$ Injection that Enhances Storage Capacity and Security,* 74th EAGE Conference & Exhibition incorporating SPE EUROPEC, 4 - 7 June, Copenhagen, Denmark.

- Shariatipour, S.M., Pickup, G.E., Mackay, E.J., 2012, *The Impact of Aquifer/Caprock Morphology on $CO_2$ Storage in Saline Aquifer*s, The 3rd EAGE International Conference on Fault and Top Seals, 1 - 3 October, Montpellier, France.

- Shariatipour, S.M., Pickup, G.E., Mackay, E.J., 2012, Jin, M., *A Novel Method for Increasing the Security of $CO_2$ Storage by Eliminating Buoyant Migration using Down-Hole Mixing (DHM),* 4th Annual Knowledge Exchange (KE) Scotland Conference, 4 - 5 October, Edinburgh, UK.

- Shariatipour, S.M., Pickup, G.E., Mackay, E.J., Lever, H., 2013, *The Impact of Angular Unconformity at the Caprock Interface on $CO_2$ Storage,* 74th EAGE Conference & Exhibition incorporating SPE EUROPEC, 10 - 13 June, London, UK.
- Shariatipour S.M., Mackay E.J. and Pickup G.E., 2013, *Could this be the Future of Secure $CO_2$ Storage?,* 2nd Sustainable Earth Sciences: Technologies for Sustainable Use of the Deep Sub-surface, 30 Sep – 4 Oct 2013, Pau, France.

**Invited talks**

- *$CO_2$ Storage in depleted Oil Hydrocarbon Reservoir and Saline Aquifers*, School of Chemical and Petroleum Engineering, Shiraz University, December 2011,Shiraz, Iran.

- *The Effect of Convective Mixing During the Post Injection Period of Carbon Dioxide in Saline Aquifers***,** Winter School, Imperial College London, 8-11 February 2011, London, UK.

**Contest**

- *A Novel Engineering Solution for Minimizing the $CO_2$ Vertical Migration to Increase Storage Capacity and Security*: It was reviewed, selected and shortlisted by SPE to be presented in the SPE Europe Student Paper Contest 2013 in PhD Division, Offshore Mediterranean Conference, 20-22 March 2013, Ravenna, Italy.

# Chapter 1

# Introduction

## 1.1 Greenhouse Gases (GHGs)

Carbon Capture and Storage (CCS) is one of several possible options for the reduction of $CO_2$ emissions to the atmosphere and it has the possibility to allow a huge decrease in $CO_2$ emissions arising from large point sources of $CO_2$ emissions (IPCC 2005).

Power plants are the main sources to apply $CO_2$ capture (Abanades et al. 2004). Pre-combustion capture, post combustion capture, oxy-fuel combustion capture and capture from industrial processes are four main types of $CO_2$ capture (IPCC 2005). In this study $CO_2$ capture is not addressed further because the focus of this thesis is on $CO_2$ storage.

In order to achieve a decrease in $CO_2$ emissions a variety of storage methods are being considered, such as geological formations (deep saline aquifers, oil and gas fields, unmineable coal beds (Figure 1.1)) ocean storage and industrial fixation of $CO_2$ into inorganic carbonates. Regarding oil and gas reservoirs, it has been suggested to inject $CO_2$ either into reservoirs during production leading to enhanced oil recovery, or into abandoned reservoirs.

Amongst all types of storage methods, it is considered that deep saline aquifers have the largest potential volume to store $CO_2$ worldwide (Bachu and Adams 2003) so this thesis focuses on storage in deep saline aquifers.

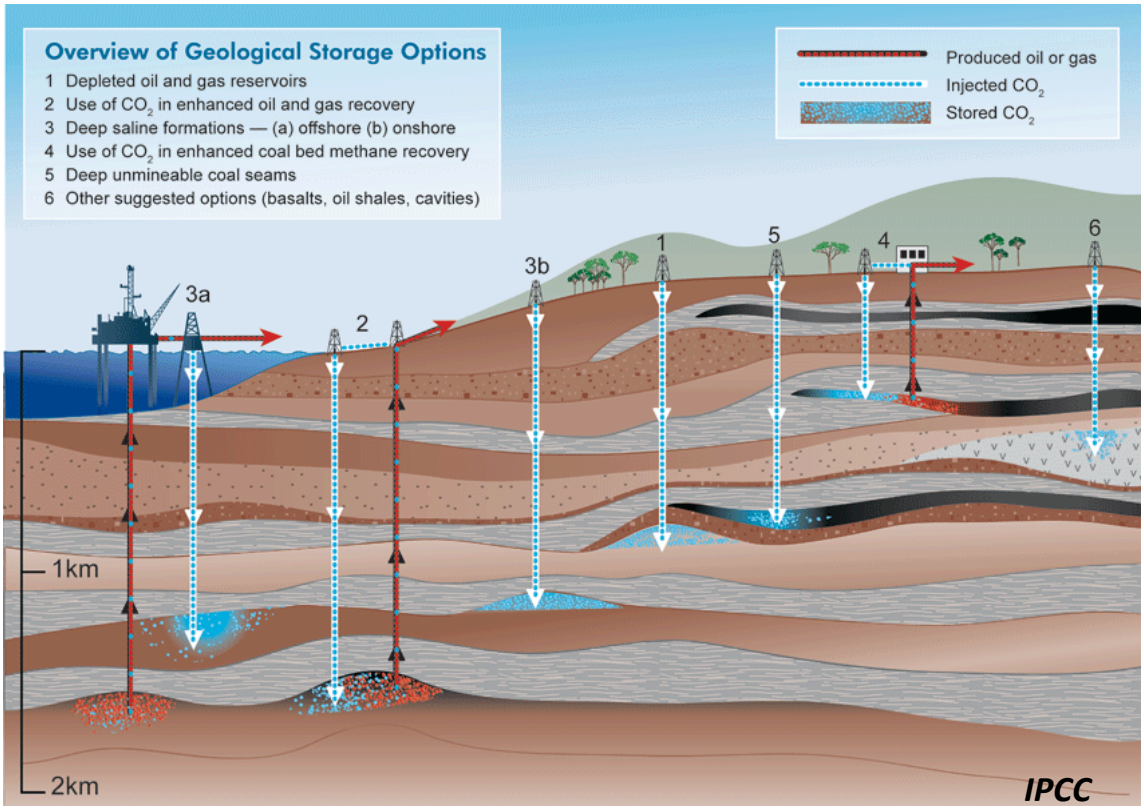


*Figure 1.1 Geological storage options.*

## 1.2 Oil and Gas Experience

Injecting $CO_2$ into oil and gas reservoirs ($CO_2$EOR) was patented in 1958 (Sweatman et al. 2011). Since then, many oil and gas companies have been using $CO_2$ commercially to recover oil from geological formations by enhanced oil recovery (EOR). Thus, millions of tonnes of $CO_2$ have been used for this purpose. For example, around 33 million tonnes of $CO_2$ is used per year at more than 74 EOR project in the United State (IEAGHG 2005). About 5% of the total U.S. crude oil production is provided by this method. Although $CO_2$ EOR is currently the most economic method for reducing anthropogenic carbon dioxide, it is not sufficient, considering both capacity and site availability, to meet all the criteria for $CO_2$ storage (IEAGHG 2005). Therefore, considering other storage options is vital.

## 1.3 Storage Process in Saline Aquifers

It should be noted that in most geological storage cases being considered, $CO_2$ is injected in a supercritical state, which is above $31.1\,^{\circ}C$ and 73.9 bars. Supercritical $CO_2$ is a fluid with a liquid-like density and a gas-like viscosity (Winterfeld et al. 2011), which generally occurs at a depth of storage of more than 800 meters depending on temperature gradient. It is important to be aware of the processes and parameters of the $CO_2$ migration in a saline aquifer. $CO_2$ is retained in situ through four basic trapping mechanisms: structural, dissolution, residual trapping and mineral trapping (Figure 1.2).

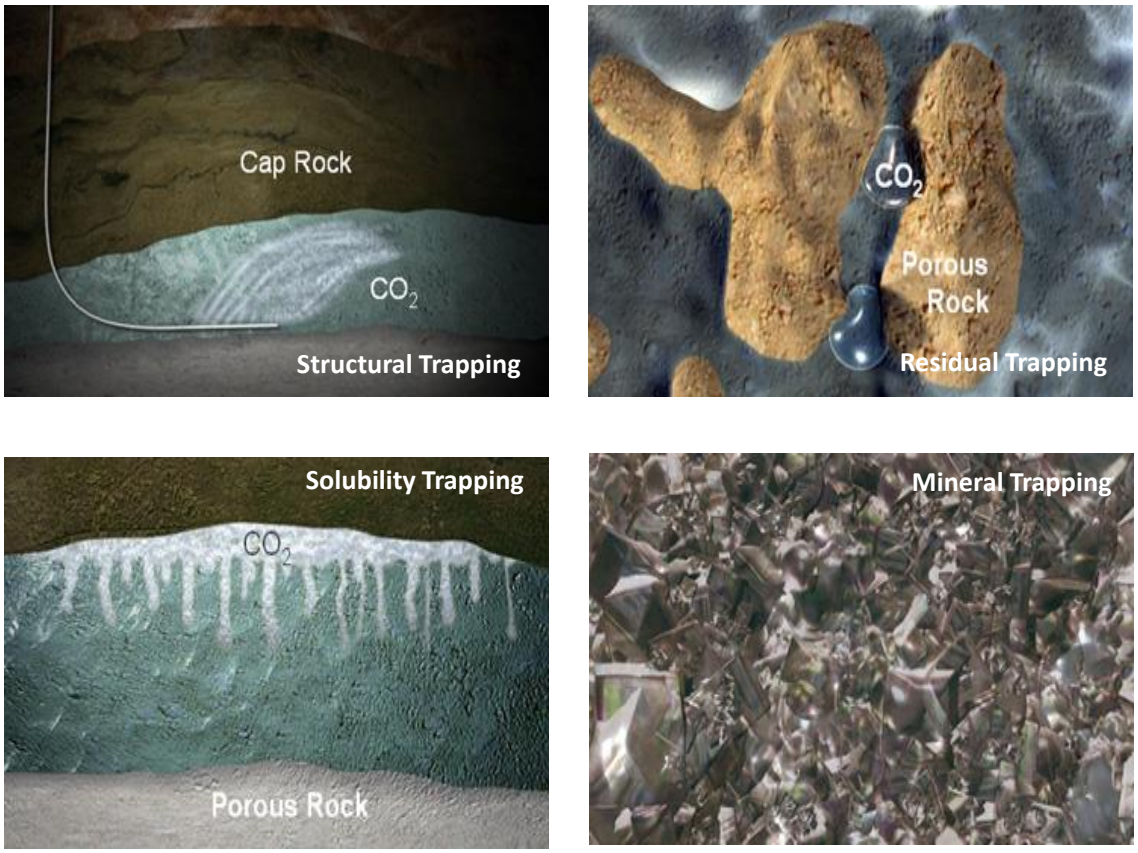


*Figure 1.2 $CO_2$ trapping mechanisms: structural trapping top left picture, residual trapping top right picture, solubility trapping bottom left, and mineral trapping bottom right picture. (http://www.co$_2$captureproject.org/co$_2$_trapping.html).*

Figure 1.3 shows that in the short term, throughout injection, structural trapping is the most significant trapping mechanism (IPCC 2005), because it prevents $CO_2$, which migrates upward due to buoyancy, from reaching the surface. This migration will continue until $CO_2$ reaches a very low permeability seal. Therefore, the existence of a laterally extensive confining layer, immediately overlying the storage formation, is vital (Corcoran, 2006).

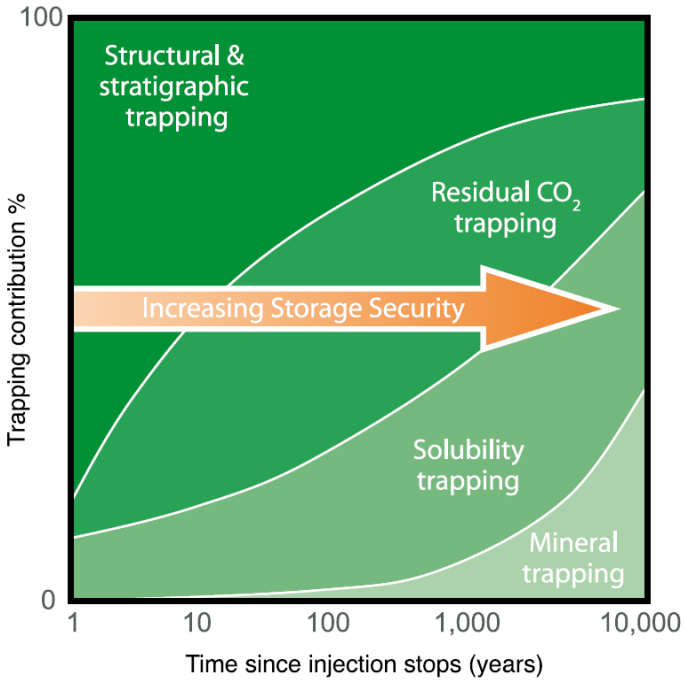


*Figure 1.3 Storage Security depends on a combination of physical and geochemical trapping (IPCC 2005).*

Additional physical trapping can be provided by capillary forces that retain $CO_2$ in the pore spaces of the storage formation (IPCC 2005). During the $CO_2$ injection into the storage formation $CO_2$ bubbles could be immobilized due to capillary snap-off (Taku Ide et al. 2007). Capillary trapping is more efficient in heterogeneous reservoirs where there are permeability contrasts (Salimi and Wolf 2012).

Dissolution of $CO_2$ in formation water is anticipated to occur on the decade's time-scale depending on the heterogeneity of the storage formations (Lindeberg and Bergmo 2003). Dissolution of $CO_2$ into brine decreases as salinity and temperature increase (IPCC 2005) and increases as pressure increase (Spycher et al., 2003). The formation brine becomes acidic due to the dissolution of $CO_2$ in the brine (see Equation 1.1), altering the brine pH.

$$CO_2(g) + H_2O \leftrightarrow H_2CO_3 \leftrightarrow HCO_3^- + H^+ \leftrightarrow CO_3^{2-} + 2H^+ \qquad (1.1)$$

Once $CO_2$ is dissolved, the density of the brine increases by 0.1% - 1% (Lindeberg and Bermo, 2003; Kneafsey et al., 2011), therefore eliminating the buoyant force that drive it upward (IPCC 2005). The $CO_2$ saturated brine is denser than pure brine so when the $CO_2$ saturated brine layer is thick enough, instability occurs. During the long-term storage of $CO_2$, convection is one of the important functions that plays a role in the

dissolution of the $CO_2$ in the saline aquifers (Hassanzadeh et al., 2005; Ennis-King et al., 2005; Riaz et al., 2006).

The minerals of the matrix could be dissolved in the weak acidic fluid depending on the type of rock (Xu et al., 2004) or could precipitated (Ennis-King and Paterson 2003). In siliciclastic aquifer, reactions of calcium and magnesium minerals with acidic brine increase storage capacity in comparison to other aquifer mineralogies (Gunter et al., 1993; Ennis-King and Paterson 2003). It is considered that mineral dissolution is a very slow process (i.e. probably tens of hundreds of years Gunter et al., 1993).

## 1.4 Examples of $CO_2$ Storage Projects

There are examples of planned and active large- scale $CO_2$ storage projects around the world. Amongs these the Sleipner and Snohvit projects are offshore CCS pojects and In Salah is an on shore project, where $CO_2$ is injected into deep saline aquifers. The Weyburn project in Canada is a dual purpose EOR and $CO_2$ storage project (Preston et al. 2009). Capture type in all the aforementioned projects is pre-combustion and $CO_2$ is transported through pipelines. Eiken et al. (2011) presented a paper on the experience and knowledge learnt from Sleipner, In Salah and Snohvit. They concluded that for the $CO_2$ storage capacity evaluation, detailed $CO_2$ site characterisation is required. In this section we will give an overview on Sleipner in Norway and In Salah in Algeria.

### *1.4.1 Sleipner*

The Sleipner field is located in the North Sea and it has been used to pioneer the carbon capture and storage concept (Singh et al. 2010). When the Sleipner West gas field was planned, tests showed that natural gas in the reservoir contained around 9% $CO_2$ (Sleipner Project Website). After the $CO_2$ tax was introduced by the Norwegian government in 1991 to reduce emissions offshore, Statoil decided to capture and store the $CO_2$ in an adjacent aquifer (Sleipner Project Website). In Sleipner the water depth is 80 m and the storage formation depth is around 700 m below the seafloor (Eiken et al. 2011). In this project $CO_2$ is transported at near critical point conditions a short distance between two connected offshore platforms, as the $CO_2$ capture is on one unit and the wellhead is connected to the other unit (Li et al. 2011). $CO_2$ injection started in 1996 at an annual rate of approximately 0.85Mt (Zweigel et al. 2004). $CO_2$ is being injected into the highly porous (35%-40%) and extremely permeable (approximately 2 D) (Zweigel et al. 2004) 200-300 m thick storage formation with a net to gross ratio of 95% (Eiken

et al. 2011). The storage formation also contains low permeability interbeded shale layers (around 1 m thick) (Zweigel et al. 2004). Migration of $CO_2$ over the years has been monitored using 4D seismic. Figure 1.4 (upper panels) shows the effect of low permeability interbeded shale layers and the growth of $CO_2$ plume from successive time-lapse seismic surveys at Sleipner. Figure 1.4 (lower panels) shows the effect of the morphology of the caprock.

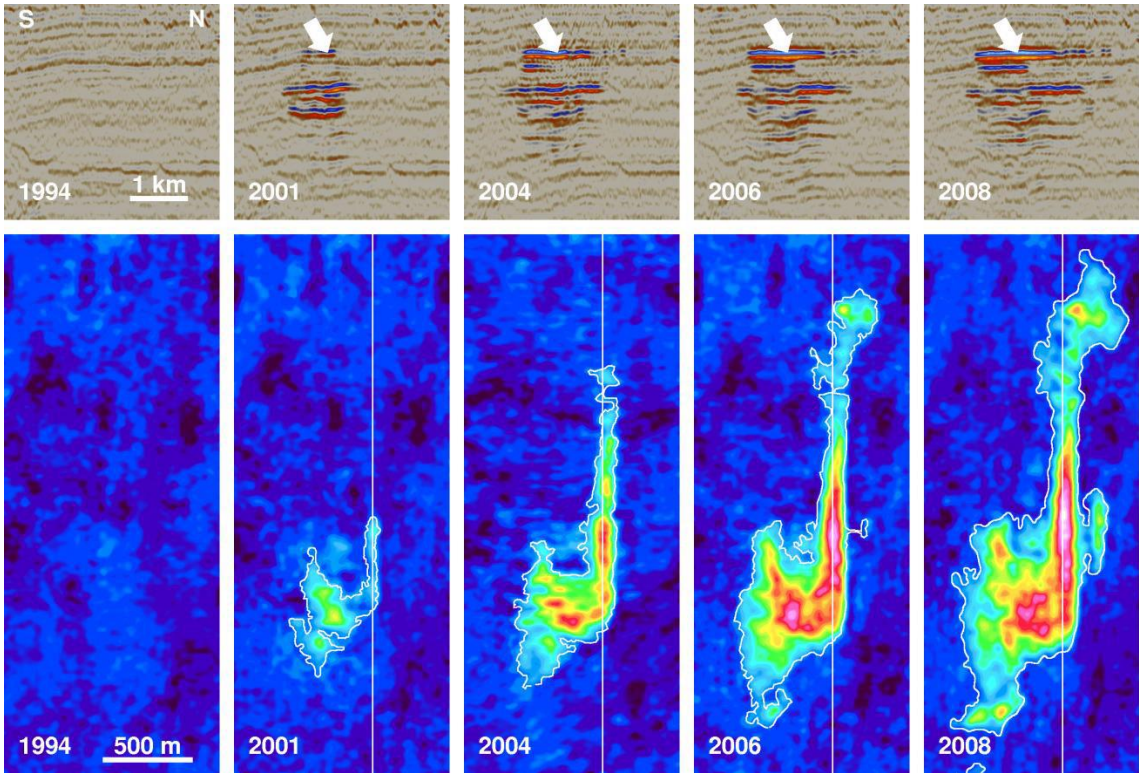


*Figure 1.4 Upper panels display vertical cross sections from successive seismic surveys at Sleipner. The strong reflections, absent in the 1994 data, denote the growing CO2 plume. The topmost plume reflection is highlighted with an arrow. The lower panels show the total reflection amplitude of the expanding topmost layer in plan view (White et al. 2013).*

Based on ten years' experience of monitoring $CO_2$ injection in the storage formation at Sleipner there was no indication of $CO_2$ leakage through the caprock. Thus $CO_2$ storage in this field is considered to be a very successful project (Arts et al. 2008).

### *1.4.2 In Salah*

$CO_2$ storage in In Salah is an industrial-scale project in Algeria which started in 2004 (Ringrose et al. 2009). The initial plan was to store up to 17 million tonnes of $CO_2$ over the lifetime of the project. The storage formation is 20m thick, fractured at the depth of around 1900m underground (Mathieson et al. 2009; 2011). This Carboniferous sandstone comprises a gentle anticline (Ringrose et al. 2011). Around 0.5-1 million tonnes of $CO_2$ per year has been injected in the water-leg of the Krechba gas reservoir (Rutqvist et al. 2010). $CO_2$ was injected through three horizontal injectors which were drilled perpendicular to the main fracture orientation (Mathieson et al. 2011). This was designed in order to help maximize $CO_2$ injectivity. The porosity of the reservoir ranges from 0.1 – 0.18 and the average permeability of the reservoir is around 10mD (Mathieson et al. 2011).

In 2005 a Joint Industry Project between BP, Sonatrach and Statoil was set up to monitor the $CO_2$ storage process such as $CO_2$ migration, rock deformation, etc. A variety of monitoring techniques such as geophysical, geochemical and production data were selected to be used over an initial 5 year period (Mathieson et al. 2011).

Interferometric Synthetic Aperture Radar (InSAR) was used, and this showed that few millemetres per year ground displacement occured as a result of $CO_2$ injection into the storage formation in this field (Rutqvist and Rinaldi 2013). $CO_2$ injection at In Salah has now ceased (Mathieson, A., personal communication).

## 1.5 Thesis Overview

### *1.5.1 Motivation*

By definition, a hydrocarbon accumulation implies the presence of a caprock that prevents vertical fluid migration out of the reservoir. However, for $CO_2$ storage in saline aquifers it may not be known a priori whether the caprock is sealing. Since $CO_2$ migrates along the underside of the caprock, it contacts a large area of the underside of the caprock. Therefore, the integrity of the caprock is very important.

Often simulations assume a distinct and smoothly undulating boundary between the aquifer and the caprock (Gasda et al., 2010). However studies of outcrops show that a variety of types of interface may arise in nature, depending on the depositional setting. For example, Shariatipour et al. (2012) have shown that there may be a gradual transition from sand-rich facies in the aquifer to mud-rich facies in the caprock. Nilsen

et al. (2012) have investigated the impact of top-seal morphology on $CO_2$ storage capacity and migration patterns, and concluded that it is important to model geological details in order to predict $CO_2$ migration. In this study the interface between caprock and storage formation will be examined.

There are concerns about long term storage integrity in aquifers, due to the high uncertainty in their structure and the sealing capacity of a caprock. Good characterisation of the top of an aquifer and the bottom of the caprock is vital in a $CO_2$ storage study. In addition, ideas for methods which could reduce the migration of $CO_2$ towards the interface between the aquifer and the caprock are developed.

### *1.5.2 Objectives*

This project will study the migration of $CO_2$ which has been injected into a saline aquifer. Calculations will be performed to identify the impact of structure, rugosity, dip angle, and dissolution on the migration of $CO_2$. Different types of interface between caprock and storage formation will be studied. Modelling of $CO_2$ behaviour in some types of formation such as: tilted, interbedded, and unconformable stratigraphic boundaries will be performed.

Density of free phase $CO_2$ is much lower than formation brine. Therefore, when free phase $CO_2$ is injected into saline aquifers, it rises up under buoyancy, until it become trapped under a caprock. Then it migrates laterally beneath the seal; this migration is also influenced by gravity, and thus $CO_2$ preferentially moves up dip. Finally, while the $CO_2$ diffuses it dissolves gradually into the brine and after sometime, dissolved $CO_2$ sinks, as dissolved $CO_2$ is denser than unsaturated brine. The density of brine saturated with $CO_2$ is approximately 0.1% - 1% greater than unsaturated brine (Lindeberg and Bermo, 2003; Kneafsey et al., 2011).

$CO_2$ is less dense than the native brine that fills the pore space in aquifers, and therefore when it is injected as a free phase, as noted, it migrates to the top of the structure, from where there is a risk that it may leak to surface. This study will also evaluate the condition under which $CO_2$ may not migrate upward and develop ideas for more effective and secure storage of $CO_2$ in subsurface geological formations. Reservoir flow simulation tools applied in the oil industry will be used to develop and test the technical viability of a novel method for $CO_2$ injection that enhances storage capacity and security by injecting the $CO_2$ pre-dissolved in brine. In this novel proposed

injection system, brine is extracted from the target aquifer by means of a lateral horizontal completion located near the top of the formation. A pump is used to extract the brine and boost its pressure, before it mixes with $CO_2$ that is being injected down the vertical section of the well. The mixing takes place in the vertical section of the well below the upper lateral. The $CO_2$–brine mix is then injected into the same formation in a lower lateral.

### *1.5.3 Methodology*

A range of 2D and 3D numerical simulations has been conducted on a variety of heterogeneous and homogeneous models to study the different types of aquifer/caprock interfaces on $CO_2$ storage. In addition, a hypothetical onshore site in Lincolnshire was used to demonstrate the $CO_2$/brine down-hole mixing method. All models were constructed in Petrel (Schlumberger, 2011a). The reservoir models were input to the ECLIPSE compositional reservoir simulator with the CO2STORE option (Schlumberger, 2011b). Temperature and pressure data used in this study were based on assumptions of a geothermal gradient of 35 C°/Km (Spycher et al. 2003), and a hydrostatic pressure gradient of 100 bar/Km (Sun and Duan 2007).

### *1.5.4 Thesis Outline*

This thesis is divided into five sections followed by the discussion of the main findings and recommended future work.

In the next chapter the background of simulation of $CO_2$ storage in subsurface geological formations will be discussed. Methods for calculating $CO_2$ dissolution in brine will be presented. Different types of traps will be presented here. From there, some types of interface will be chosen which are the basis of Chapters 3 and 4.

Chapter 3 is divided into three main sections. In the first section, the impact of aquifer/caprock morphology on $CO_2$ storage in saline aquifers is investigated. In the second section, a transition zone, where there is a gradational change from storage formation to caprock, will be presented as a new uncertainty in the study of $CO_2$ storage in underground formations. The effect of aquifer/caprock interface on $CO_2$ storage capacity and security will be investigated. In addition, calculation of the effective aquifer volume will be presented in this part. Also, the effect of irregularity of the interface on the effective aquifer volume will be studied. In the third section, a set of very detailed models will be studied to investigate the effect of top morphology,

transition zone, tilt, and $k_V/k_H$ ratio on the amount of $CO_2$ dissolution and plume migration.

Chapter 4 covers the effect of unconformities, which could be considered as one type of interface between storage formation and caprock, on the storage capacity and security. In this study the focus will be on angular unconformities. A range of 2D and 3D numerical simulations will be conducted to investigate the influence of unconformities on $CO_2$ storage. Prior to this study, an examination on the effect of the method of gridding the unconformities is described.

In Chapter 5, the potential to increase storage capacity and security by use of a novel method for $CO_2$ injection in which $CO_2$ is dissolved in brine down-hole is investigated. The method involves extracting water using a lateral producer at the top of the aquifer, mixing with injected $CO_2$ using a down-hole tool, and then injecting the $CO_2$-brine solution into the formation via another lateral branch of the well.

In Chapter 6, the effect of a transition zone will be studied using a realistic field model. The reason for choosing this model is that, in this model the aquifer and the caprock are the same types of rock (Sherwood Sandstone and Mercia Mudstone) as in the preliminary models in Chapter 3. In the initial model (Smith et al. 2012) it was assumed that there is a sharp boundary between the aquifer and the caprock. In this chapter the top aquifer layer is modified to represent a transition zone and the results of $CO_2$ storage in this model are compared with the base case.

The application of the down-hole mixing method will also be investigated in this model. Placement of the laterals (the water extraction and injection of dissolved $CO_2$ in brine) in the well will also be studied.

Chapter 7 presents the main concluding remakes of this study and recommendations for future work.

# Chapter 2

# Background

## 2.1 Introduction

The depositional environment and depositional processes need to be considered in a study of saline aquifers in order to understand the texture and structure of the sediment and to have a better understanding of distribution of petrophysical properties. The properties of caprocks must also be studied because they are important for storage security. The interface between an aquifer and caprock is particularly important, because $CO_2$ migrates to the top of an aquifer and then along the underside of the caprock.

The types of rocks which are of major importance as reservoirs are clastic sedimentary rocks (sandstone) and carbonated sedimentary rocks (limestone and dolomite).

In clastic sedimentary rocks permeability and porosity are heavily dependent on the texture of the rock, which is determined mostly by the depositional processes and partially by the diagenetic processes which the rock has undergone. On the other hand, the properties of carbonate rocks are governed mostly by the diagenetic history of the rock and partially by the original texture.

### *2.1.1 Saline Aquifers*

Aquifers are most commonly found in sandstone formations. Due to complex inter-bedded successions of various types of sedimentary rocks, sandstone aquifers usually are surrounded by low permeable rock such as shale (Miller 1999). Shales are the most abundant lithologies in most sedimentary basins. Mudrocks are defined as fine-grained rocks with high content of clay minerals. The origins of clay minerals in mudrocks may be due to weathering of igneous and metamorphic rocks, by erosion of older shales and mudrocks, from volcanic ash, and by diagenesis on the seafloor and during burial (Bjorlykke 2010).

Structural deformation, such as folding and faulting of sandstones may affect water movement through aquifers and may even compartmentalize an aquifer (Miller 1999). Aquifers are generally aerially widespread and may be overlain or underlain by a low-permeable bed.

The content of dissolved solids in underground water varies widely in different parts of the world, both in terms of specific composition (e.g. halite, anhydrite, carbonates, gypsum, fluoride-salts, and sulphate-salt) and regarding the level of concentration. The latter, often called salinity level is a convenient macro-parameter for a first general characterization of water quality. It is usually expressed as Total Dissolved Solids (TDS). Table ***2.1*** illustrates the simple classification of water salinity (Van Weert et al. 2009).

*Table 2.1 Classification of water salinity*

| **Class Name** | Class Limits (TDS range, in mg/l) |
|---|---|
| **Fresh Water** | 0 – 1,000 |
| **Brackish Water** | 1,000 – 10,000 |
| **Saline Water** | 10,000 – 100,000 |
| **Brine** | >100,000 |

(After Freeze and Cherry, 1979)

### *2.1.2 Seal*

A seal is a very fine grained or crystalline, low permeable rock that prevents $CO_2$ migration upward. Clay-rich rocks are the most common seals worldwide. Salt and anhydrite are other forms of seal. The effectiveness of seals is determined by the capillary entry pressure into the pores of the fine-grained rock overlying a $CO_2$ plume which must be greater than the buoyancy force of the underlying $CO_2$ column. Corcoran (2006) investigated the stratigraphic traps for hydrocarbons and presented 14 applicable sealing surfaces in the Central North Sea. Some of these are of interest in this study. For example, there is an unconformity at the top seal of the Alba Field (Corcoran 2006), and unconformities are discussed in Chapter 4. Studying the classification of different types of seals (Milton and Bertram 1992, Corcoran 2006) provides an appropriate framework for the screening the proposed $CO_2$ storage sites.

### *2.1.3 Traps*

In petroleum engineering a trap is a place where oil and gas accumulate, because very low permeable rocks are preventing further rise due to buoyancy. Traps (physically bound traps or structures) which occur in the sedimentary basins are usually occupied by saline aquifers, oil or gas (CO2CARE 2011).

Regarding the trapping classification, various schemes have been proposed by, Levorsen 1967, Milton and Bertram (1992), and Corcoran 2006. Table ***2.2*** illustrates, Levorsen (1967) classifications based on the relation of sealing surfaces with top seals. Traps can be stratigraphic traps, structural traps or a combination of them.

Stratigraphic traps are formed by the changes in rock type caused by variation in the depositional sequences. A low-permeability rock may overlie sandstone formations, such as those deposited in the river valleys, beaches, sand bars and delta fronts, to create traps of many varied shapes and sizes. Examples of Stratigraphic traps formed by depositional pinchout include aeolian dunes encased in lacustrine mudstone, sand filled fluvial channels cut into mud rich over bank deposits, shallow marine bar sandstones surrounded by marine shales, and submarine fan sands trapped within the domain of pelagic mud (Gluyas and Swarbrick 2004).

Structural traps are formed by the occurrence of folds, faults and other deformation structures, which can be from hundreds of kilometres long to microscopic in size. Some faults act as permeability barriers and others as pathways for fluid flow. These deformations can occur in any environmental setting and will change the stress and

strain of the rocks. The range of structural traps in a basin can be deduced based on the knowledge of the basin evolution (Gluyas and Swarbrick 2004).

*Table 2.2 Classification schemes of petroleum traps (after Levorsen 1967).*

| **Levorsen (1967)** |
|---|
| Structural traps<br>Folding<br>Faulting |
| Stratigraphic traps<br>Primary (lenses of clastic and igneous rocks)<br>Secondary(lenses of biochemical) |
| Combination traps (including salt domes) |

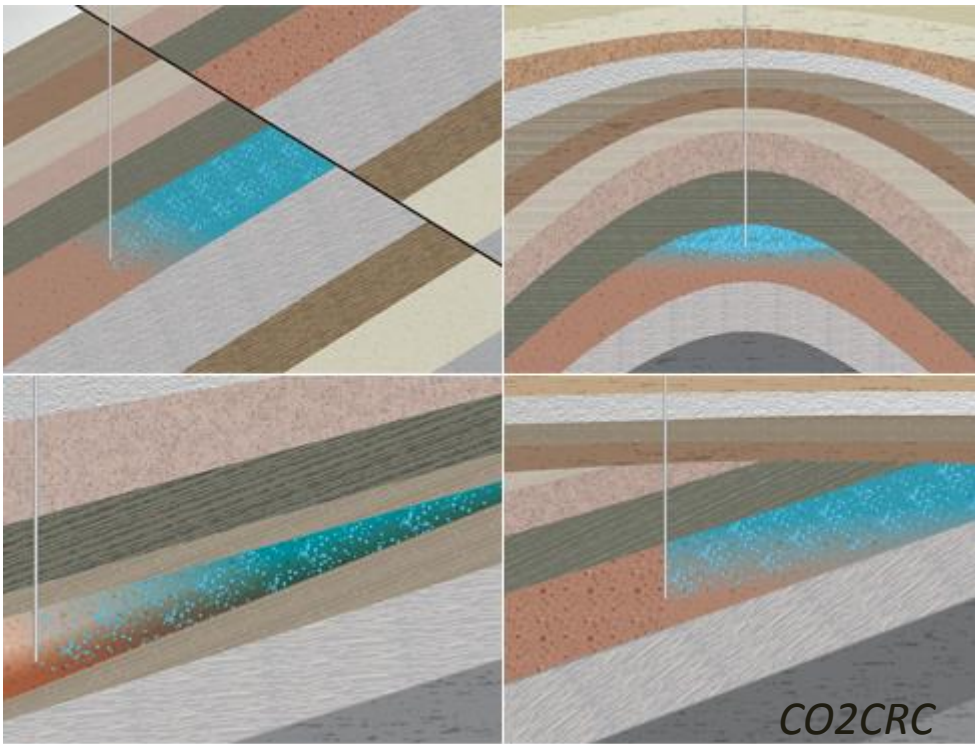


*Figure 2.1 Top cartoons illustrate structural trapping (top left, fault and top right, folding) and bottom cartoons shows stratigraphic trapping (left, pinch out and right, unconformity) CO2CRC.*

Traps have been studied and widely explored in the petroleum industry. A classification for the different traps on the UK Continental Shelf is presented by Stoker et al. (2006) based on the oil and gas fields which had been discovered by the end of 2003. This study shows that most of the oil and gas reservoirs are formed by structural traps (75% by volume) and only 20% and 5% are formed by stratigraphic traps and combination stratigraphic/structural traps, respectively. For $CO_2$ storage in geological formations, either in depleted oil and gas reservoirs or in saline aquifers, references such as Stoker et al. (2006) which discuss traps are very relevant, because if a very low permeable caprock prevents oil and gas from upward migration, it could do so for $CO_2$ also.

The function of faults for $CO_2$ storage in subsurface geological formation can be studied from two perspectives. Firstly, fault closure traps which are potential traps. Secondly, fault-rock seals result from mechanical and chemical changes that take place and in fault zones as a result of faulting processes. These changes may or may not make the fault plane or zone a barrier to fluid flow (Sorkhabi and Tsuji, 2005).

The height of a trap and the trap geometry are essential factors in determining the $CO_2$ storage capacity (Sales 1997). $CO_2$ capacity is controlled by the caprock capillary properties. If the buoyancy force of a column of $CO_2$ is greater than the capillary entry pressure, then $CO_2$ will invade the caprock. The top seal capillary properties and seal capacity can be estimated from the equivalent grain size (EGS) method (Sawamura and Nakayama, 2005).

Capillary entry pressure is a function of the size of the pore throats, the interfacial tension (IFT) between two immiscible fluids, and the contact angle. The threshold capillary entry pressure ( $P_{c,th}$ ) is expressed as:

$$P_{c,th} = \sigma\left(\frac{\cos\theta_{seal}}{r_t} - \frac{\cos\theta_{res}}{r_p}\right) \approx \frac{\sigma\cos\theta}{R} \qquad \textbf{(2.1)}$$

Where

$\sigma$ interfacial tension between two fluids (gas and brine)

$\theta_{seal}$ contact angle in the wetting phase (i.e. brine) with the caprock

$\theta_{res}$ contact angle in the wetting phase (i.e. brine) with the reservoir

$r_t$ pore radius in the seal

$r_p$ pore radius in the reservoir

$R$ the size of the largest pore throats or microfractures in the porous caprck

$\theta$ contact angle (measured in the brine phase) of the caprock mineral/brine/gas system

Chiquet et al., (2007) highlighted that the threshold capillary entry pressure for $CO_2$ is lower than the one of natural gas due to their differences in the interfacial tension (IFT) and the wettability. However, buoyancy force on the seal for a fixed column height is lower for $CO_2$ than natural gas due to its high density under reservoir conditions (Naylor et al., 2011).

## 2.2 Fluid Properties

$CO_2$ storage in saline aquifers with a sufficient storage capacity and security is one promising approach to reduce the levels of $CO_2$ in the atmosphere (IPCC 2005, Bachu 2008, Birkholzer et al. 2008). In order to investigate the numerical modelling of the $CO_2$ storage in saline aquifers it is important to understand the theory behind the dissolution of $CO_2$ in brine. Within the temperature and pressure range of a normal targeted aquifer for $CO_2$ storage (more than 800 meters depth) typically, two phases co-exist: a $CO_2$-rich gas or supercritical phase and an $H_2O$-rich liquid phase (Spycher et al. 2003) (Figure ***2.2***). In the following sections the properties of brine and $CO_2$ such as density and viscosity, the density of $CO_2$ saturated brine, and the solubility of $CO_2$ in brine will be discussed.

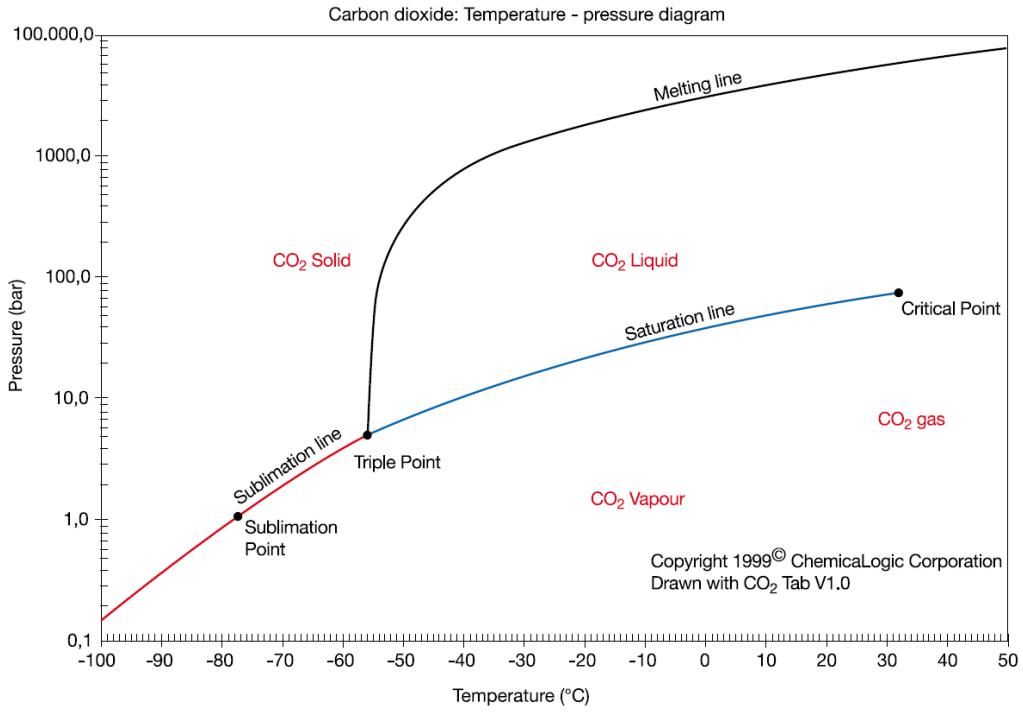


*Figure 2.2 Phase Diagram of Pure $CO_2$ (obtained from IPCC, 2005).*

### *2.2.1 $CO_2$ Properties*

$CO_2$ is in the gas phase at standard conditions (IPCC 2005). Physical properties of $CO_2$ vary with temperature and pressure (Figure ***2.2***). At very low temperature and high pressure $CO_2$ is in the solid state. At the temperatures range from -56.5 C (triple point) to 31.1 $^{\circ}C$ (critical point), $CO_2$ could be either in the vapour phase at lower pressure or in the liquid phase at higher pressure. Table ***2.3*** shows some physical properties for $CO_2$ and a few related components. Density and viscosity of $CO_2$ and the solubility of $CO_2$ in brine are described in the following sections.

*Table 2.3 $CO_2$ thermodynamic data*

| Property | Value |
|---|---|
| Molecular weight | 44.01 |
| Critical temperature | 31.1°C |
| Critical pressure | 73.9 bar |
| Critical density | 467 kg $m^{-3}$ |
| Triple point temperature | -56.5 °C |
| Triple point pressure | 5.18 bar |
| Boiling (sublimation) point (1.013 bar) | -78.5 °C |
| ***Gas Phase*** | |
| Gas density (1.013 bar at boiling point) | 2.814 kg $m^{-3}$ |
| Gas density (@ STP) | 1.976 kg $m^{-3}$ |
| Specific volume (@ STP) | 0.506 $m^3$ $kg^{-1}$ |
| Cp (@ STP) | 0.0364 kJ ($mol^{-1}$ $K^{-1}$) |
| Cv (@ STP) | 0.0278 kJ ($mol^{-1}$ $K^{-1}$) |
| Cp/Cv (@ STP) | 1.308 |
| Viscosity (@ STP) | 13.72 µN.s $m^{-2}$ (or µPa.s) |
| Thermal conductivity (@ STP) | 14.65 mW (m $K^{-1}$) |
| Solubility in water (@ STP) | 1.716 vol $vol^{-1}$ |
| Enthalpy (@ STP) | 21.34 kJ $mol^{-1}$ |
| Entropy (@ STP) | 117.2 J mol $K^{-1}$ |
| Entropy of formation | 213.8 J mol $K^{-1}$ |
| ***Liquid Phase*** | |
| Vapour pressure (at 20 °C) | 58.5 bar |
| Liquid density (at -20 °C and 19.7 bar) | 1032 kg $m^{-3}$ |
| Viscosity (@ STP) | 99 µN.s $m^{-2}$ (or µPa.s) |
| ***Solid Phase*** | |
| Density of carbon dioxide snow at freezing point | 1562 kg $m^{-3}$ |
| Latent heat of vaporisation (1.013 bar at sublimation point) | 571.1 kJ $kg^{-1}$ |

Where STP stands for Standard Temperature and Pressure, which is 0°C and 1.013 bar.
Sources: Air Liquide gas data table; Kirk-Othmer (1985); NIST (2003).

***Density***

Gas density can be computed from a cubic equation of state tuned to calculate the density of compressed gas phase accurately by Spycher and Pruess (2005). Figure ***2.3*** illustrates the density of $CO_2$ versus depth, in the upper diagram, and $CO_2$ density versus temperature, in the lower diagram (Bachu, 2010).

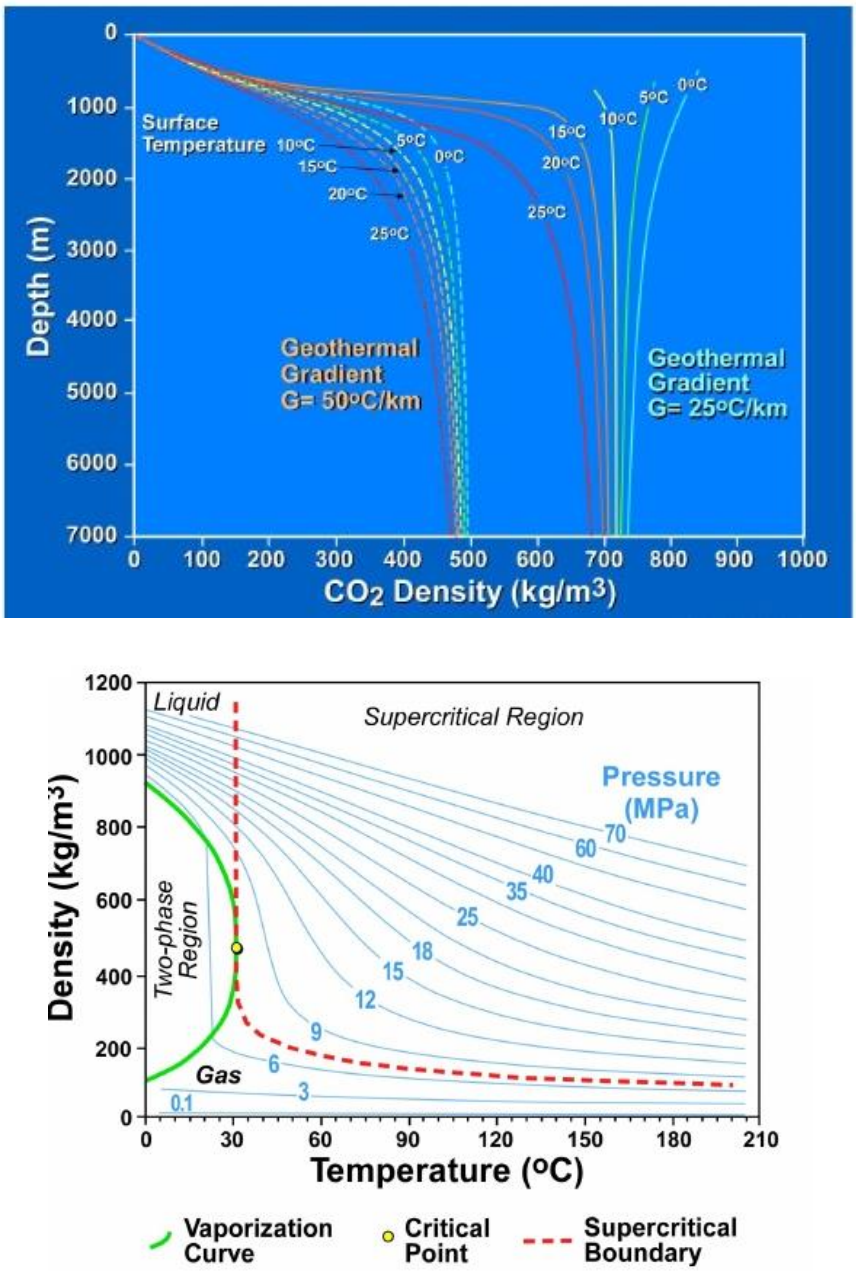


*Figure 2.3 $CO_2$ density versus depth (top diagram), and $CO_2$ density as a function of pressure versus temperature (bottom diagram) (Bachu, 2010).*

***Viscosity***

$CO_2$ viscosity had been studied extensively by Vesovic et al. (1990). This is the source which the ECLIPSE reservoir simulation suite uses in calculation of viscosity of $CO_2$. ECLIPSE has used a method whereby viscosity is decomposed into three separate contributions:

1. Viscosity in the zero-density limit

$$\eta_0(T) = \frac{1.00697 T^{1/2}}{\varsigma_\eta^*(T^*)}, \tag{2.2}$$

where $\eta_0(T)$ is the zero-density viscosity $(\mu Pa)$, and $\varsigma_\eta^*(T^*)$ is the reduced effective cross section:

$$\ln \varsigma_\eta^*(T^*) = \sum_{i=0}^{4} a_i (\ln T^*)^i, \tag{2.3}$$

Where $a_i$ are coefficients of the correlation of the zero density transport properties of carbon dioxide and $T^*$ is the reduced temperature given by

$$T^* = kT/\varepsilon \tag{2.4}$$

where the scaling parameter is $\varepsilon/k = 251.196\,\mathrm{K}$

2. Viscosity in the critical region

The viscosity in the critical region ($\eta$) reveals a multiplicative anomaly and this is due to the fact that critical viscosity enhancement is proportional to the background viscosity ($\overline{\eta}$).

$$\eta = \overline{\eta}(\Omega\xi)^z$$

where $\Omega$ is a system dependent amplitude, $\xi$ is the correlation length of the density fluctuations which diverges at the critical point ($T_c = 304.107K$, $p_c = 7.3721MPa$, and $\rho_c = 467.69kg/m^{-3}$) and the exponent ($z$) is a universal quantity and it has the same value for all fluids (0.06).

3. Excess viscosity

The equation below shows the viscosity of the fluid outside of the critical region.

$$\Delta\eta(\rho,T)=\sum_{i=1}^{n} b_i(T)\rho^i \text{ ,} \tag{2.5}$$

where $b_i(T)$ is the temperature dependence of the density coefficient.

### *2.2.2 Water Properties*

Water properties such as density and viscosity can be computed from Ezrokhi's method (Schlumberger, 2011).

***Density***

Water density can be computed from the equation below.

$$\log 10(\rho)=\log 10(\rho_0(P,T))+\sum_i A_i(T)w_i \tag{2.6}$$

where, $w_i$ is the weight fraction of the non-water component $i$ (salt) and $\rho_0(P.T)$ is the density of pure water. The coefficients are a polynomial in temperature:

$$A_i(T)=a_{0,i}+a_{1,i}T+a_{2,i}T^2 \tag{2.7}$$

where temperature is specified in $^\circ C$ and $a_{0,i}, a_{1,i},$ and $a_{2,i}$, are the three regression coefficients for each component.

***Viscosity***

Water viscosity can be calculated from the equation below.

$$\log 10(\mu)=\log 10(\mu_0(P,T))+\sum_i B_i(T)w_i \tag{2.8}$$

where, $w_i$ is the weight fraction of the non-water component $i$ and $\mu_0(P,.T)$ is the density of pure water. The coefficients are a polynomial in temperature:

$$B_i(T)=b_{0,i}+b_{1,i}T+b_{2,i}T^2 \tag{2.9}$$

where temperature is specified in $^\circ C$.

### *2.2.3 Solubility of $CO_2$ in Brine*

The solubility of carbon dioxide in brine depends on the balance between the chemical potential in the liquid phase and in the gas phase, and it can be written in terms of fugacity in the vapour phase and activity in the liquid phase (Duan and Sun (2003)).

At equilibrium, when $CO_2$ is dissolved in water, the chemical equilibrium reaction will be followed as Equation (2.10). Therefore, $CO_2$ is either in the gas phase (g) or in the liquid phase (aq).

$$CO_2(g) = CO_2(aq) \tag{2.10}$$

The chemical potentials are equals in the gas and aqueous phases, thus:

$$\mu_{CO_2}(g) = \mu_{CO_2}(aq) \tag{2.11}$$

The fugacities of $CO_2$ in the coexisting phases ( $f_{CO_2(g)}$, $f_{CO_2(aq)}$) are defined as a factor of fugacity coefficient $(\Phi)$, partial pressure of $CO_2$ $(P_{CO_2})$ in the gas phase and molality $(m_{CO_2})$ and activity coefficient $(\gamma_{CO_2})$ of $CO_2$ in the aqueous phase:

$$f_{CO_2(g)} = \Phi P_{CO_2} \tag{2.12}$$

$$f_{CO_2(aq)} = m_{CO_2}\gamma_{CO_2} \tag{2.13}$$

The solubility of $CO_2$ in the aqueous phase is then given by:

$$y_{CO_2} = \frac{f_{CO_2(aq)}}{H} = \frac{\Phi P_{CO_2}}{H} \tag{2.14}$$

Where H is the Henry's constant. By calculating the fugacity coefficient, the solubility of $CO_2$ in the aqueous phase can be achieved. The fugacity coefficient of $CO_2$ can be computed from the cubic equation of state (e.g. Redlich and Kwong, 1949, Peng and Robinson (1976), and Span and Wagner, 1996). A semi empirical equation of state which was presented by Duan et al. (1992) also enables us to calculate the fugacity coefficients of $CO_2$.

The more accurate the EOS is, the more complex the calculations. Some of these EOS have limitations in terms of the pressure, temperature, and salinity ranges used. Some of them are too computationally intensive for their integration into effective multiphase flow simulators. Therefore different $CO_2$-$H_2O$ models have been proposed to estimate the $CO_2$ solubility in the aqueous phase. These solubility models include: Li and Nghiem (1986), Enick and Klara (1990), Pruess and Garcia (2002), Duan and Sun

(2003), Spycher et al. (2003), and Spycher and Pruess (2005; 2009). Some of these models (e.g. Spycher et al. 2003, Spycher and Pruess (2005, 2009)) are computationally efficient and cover mutual solubility of $CO_2$ and $H_2O$ over a wide range of pressures and temperatures. Table ***2.4*** presents the parameters (T, P, and S) ranges and the EOS used in different $CO_2$ solubility models in the aqueous phase.

*Table 2.4 Temperature, pressure, and salinity ranges and the EOS used in different solubility models (after Gundogan 2011)*

| Solubility Model | Temperature $\left({}^{0}C\right)$ | Pressure (bar) | Salinity (up to) (M) | EOS |
|---|---|---|---|---|
| Akinfiev and Diamond | 22 - 100 | Up to1000 | any | Span and Wagner |
| Spycher and Pruess (2009) | 12 - 300 | Up to 600 | 6 | Modified Redlich - Kwong |
| Spycher and Pruess (2005) | 12 - 100 | Up to 600 | 6 | Modified Redlich - Kwong |
| Portier and Rochelle | up to 300 | Up to 300 | 3 | Peng - Robinson |
| Spycher et al. (2003) | 12 - 100 | Up to 600 | 0 | Modified Redlich - Kwong |
| Duan and Sun | 0 - 260 | Up to 2000 | 4.5 | Duan et al. |
| Pruess and Garcia | 25 - 350 | Up to 1000 | 5 | Spycher and Reed |
| Enick and Klara | 25 - 250 | 30 - 850 | 5 | Peng - Robinson |
| Li and Nghiem | up to 200 | up to 1000 | 4 | Peng - Robinson |
| GEM | up to 150 | up to 600 | 5 | Soave - Redlich-Kwong |
| TOUGHREACT | 50 – 350 | Up to 500 | 6 | Spycher and Reed |
| ECLIPSE | 12 - 250 | Up to 600 | 6 | Spycher and Preuss |

The ECLIPSE300 simulator with the CO2STORE option will be used to study $CO_2$ storage in aquifers in the work presented in this thesis. The Spycher and Pruess Model is implemented in this simulator, and therefore this model will be described in this section.

Spycher et al. (2003) tried to gain a better understanding of the phase equilibrium and the mutual solubilities of $CO_2$ from 12 to 110 °C and $H_2O$ from 15 to 100 °C and up to 600 bar. A number of researchers, King et al. (1992), Teng et al. (1997), Wibe and Gaddy (1940) and Anderson (2002) have published papers in this area, but those focused on high temperatures and pressures applicable to metamorphic processes. However all these pieces of research are in good agreement.

Spycher et al. (2003) used the modified Redlich-Kwong equation of state to express departure from ideal behaviour (Equation 2.15). They concluded that the solubility of $CO_2$ rises dramatically with increasing pressure up to saturation pressure, but decreases with rising temperature. In this paper, there is quite a good match between experimental and calculated solubilities from 12 up to 50 °C and up to a pressure of 600 bars, which is important for geological sequestration purposes.

$$P = \left(\frac{RT}{V-b}\right) - \left(\frac{a}{T^{0.5}V(V+b)}\right) \tag{2.15}$$

where the volume of the compressed gas at T and P is shown by V in this equation. R is the gas constant. The intermolecular attraction and the repulsion are shown by a and b respectively, and are derived at critical conditions. The fugacity coefficient can be expressed as:

$$\ln(\Phi_k) = \ln\left(\frac{V}{V-b_{mix}}\right) + \left(\frac{b_k}{V-b_{mix}}\right) - \left(\frac{2\sum_{i=1}^{n} y_i a_{ik}}{RT^{1.5} b_{mix}}\right) \ln\left(\frac{V+b_{mix}}{V}\right) + \left(\frac{a_{mix} b_k}{RT^{1.5} b_{mix}^2}\right)\left[\ln\left(\frac{V+b}{V}\right) - \left(\frac{b_{mix}}{V+b_{mix}}\right)\right] - \ln\left(\frac{PV}{RT}\right) \tag{2.16}$$

Spycher and Pruess (2005) describe a continuation of the work of the previous study on mutual solubilities of $CO_2$ and $H_2O$, including the partitioning in chloride brines at the same pressures and temperatures as in the previous study. They examined the effect of chloride salts in the aqueous phase based on correlations presented by Spycher et al. (2003). They carried out some research on the computation of mutual solubilities in a non-iterative manner for solutions up to 6 molal NaCl and 4 molal $CaCl_2$. They presented an extended formulation of the basic model (Spycher et al. 2003), which accounted for the effect of dissolved salts. The water mole fraction in the $CO_2$ rich phase ($y_{H_2O}$) and the $CO_2$ mole fractions in the aqueous phase ($x_{CO_2}$) are respectively expressed as:

$$x_{CO_2} = \frac{\Phi_{CO_2}\left(1-y_{H_2O}\right)P_{tot}}{55.508 a_{CO_2} K^0_{CO_2}} \exp\left(-\frac{\left(P-P^0\right)\overline{V}_{CO_2}}{RT}\right) \tag{2.17}$$

$$y_{H_2O} = \frac{K^0_{H_2O} a_{H_2O}}{\Phi_{H_2O} P_{tot}} \exp\left( \frac{\left(P - P^0\right)\overline{V}_{H_2O}}{RT} \right) \tag{2.18}$$

where, $K^0$ is the thermodynamic equilibrium constant for each component at temperature T.

Spycher and Pruess (2010) extended their previous work to a much higher temperature for the purposes of geothermal studies, using the same equation of state (modified Redlich-Kwong). The range of temperature in this phase-partitioning Model is 12 – $300\,^0C$. This method relies on the experimental data between $CO_2$ and NaCl brines.

### *2.2.4 Density of Brine and $CO_2$*

An accurate calculation of the amount of $CO_2$ that can be dissolved in brine is crucial both for the storage capacity estimation and for investigations of the interactions between rock and fluid due to the low pH of the $CO_2$ saturated brine (Gundogan 2011). After $CO_2$ has dissolved in brine, the density of the solution is expected to follow Eq. 2.19 which shows the influence of dissolved carbon dioxide on brine density (Garcia 2001). In practice, $CO_2$ dissolved in brine is denser than unsaturated in-situ formation brine.

$$\rho = \rho_b + M_{CO_2} C - C\rho_b V_\varphi \tag{2.19}$$

where,

$\rho$ Brine density including dissolved $CO_2$ ($kg/m^3$)

$\rho_b$ Brine density without dissolved $CO_2$ ($kg/m^3$)

$M_{CO_2}$ Molecular weight of $CO_2$ (kg/mol)

C Concentration of dissolved $CO_2$ (mole $CO_2/m^3$ solution)

$V_\varphi$ Molar volume of dissolved $CO_2$ ($m^3$/mol)

## 2.3 Fate of Injected $CO_2$

The important issue in $CO_2$ sequestration in a geological formation is to understand the processes that govern $CO_2$ displacement such as: buoyancy, diffusivity and convection. $CO_2$ and brine are miscible fluids, and consequently $CO_2$ dissolves in brine and this dissolution is limited by pressure, temperature and salinity (Duan and Sun, 2003, Spycher and Pruess, 2005). Buoyancy is the dominant force during the $CO_2$ injection

phase where $CO_2$ is injected into the site. Thereafter, it is thought that residual trapping and dissolution are of primary importance in the post injection period (Riaz and Tchelepi, 2008). Chemical reactions and dissolution driven gravitationally unstable flow are important mechanisms in the latter stages of a $CO_2$ sequestration project (Riaz and Tchelepi, 2008).

### *2.3.1 Convection*

The density of $CO_2$ is less than that of brine, and therefore it goes upward due to buoyancy until reaches a sealing formation (Ghanbari et al. 2006). $CO_2$ dissolves in brine and this dissolution is dependent on the brine pressure, temperature and salinity (Duan and Sun, 2003; Spycher and Pruess, 2005). Once $CO_2$ has dissolved into fresh brine, the density of the brine increases by 0.1% - 1% (Kneafsey et al. 2011). A convective process may arise, in which $CO_2$ saturated brine is denser than fresh brine, and therefore it migrates downward (Ennis-King and Paterson, 2003; Ennis-King et al. 2005; Riaz et al. 2006) (Figure ***2.4***). This gravitational instability may be a significant driver for the $CO_2$ dissolution in aquifers (Gasda et al. 2012; Kneafsey and Pruess, 2010; Orr, 2009).

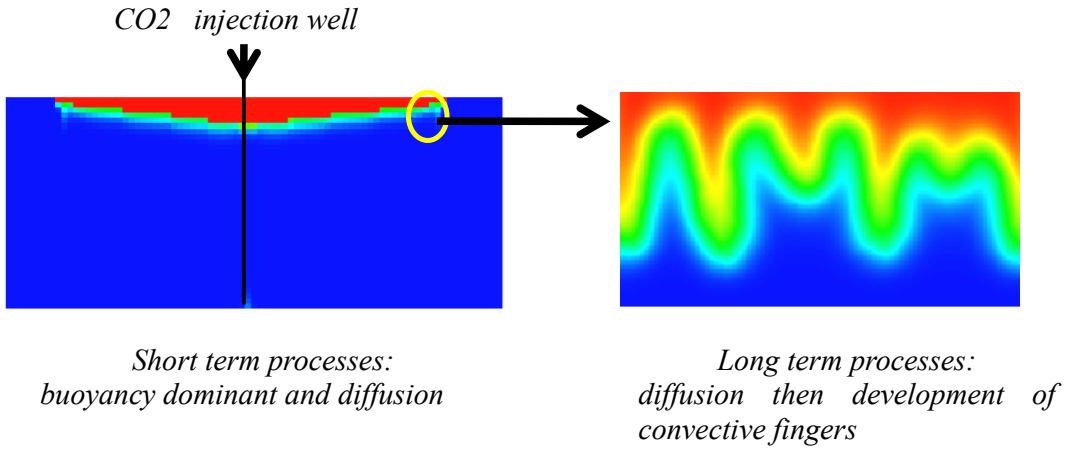


*Figure 2.4 Convective mixing processes during CO2 storage*

Some parameters associated with convective flow, such as the onset of instability ($t_c$) and the critical wavelength ($\lambda_c$) have been investigated (Ennis-King et al. (2005); Riaz et al. (2006); Hassanzadeh et al. (2007)). These researchers derived equations for the critical time and the critical wavelength using stability analysis. These equations show

that in isotropic homogeneous models the critical wavelength is inversely proportional to permeability, and the time to onset of convection is inversely proportional to the square of permeability. As shown below, there are slight differences between their presented equations due to different assumptions used in the derivation.

Ennis King et al. (2005):

$$t_c = 80\frac{(\phi\mu_w)^2 D}{(k\Delta\rho g)^2}$$

$$\lambda_c = 90\frac{\phi\mu D}{k_h \Delta\rho g}$$

Riaz et al. (2006):

$$t_c = 146\frac{\phi\mu^2 D}{(k\Delta\rho g)^2}$$

$$\lambda_c = \frac{2\pi\mu D}{0.07k\Delta\rho g}$$

Hassanzadeh et al. (2007):

$$t_c = 500\frac{(\phi\mu_w)^2 D}{(k\Delta\rho g)^2}$$

$$\lambda_c = 40\pi\frac{\phi\mu d}{k_h \Delta\rho g}$$

Pau et al. (2010) studied the convection process alongside the dissolution and the diffusion of $CO_2$ in aquifers. These authors studied the effect of formation properties on the convection process and concluded that the variation in porosity led to faster onset time than the variation in permeability. One of the parameters which has a significant role in the study of stability is the Rayleigh number (Eq. 2.20). It is used to compare the rate of convection and the rate of diffusive transport, and thus indicates whether convection is likely to occur or not (Kneafsey and Pruess 2010). Both the initial wavelength and the onset of instability are independent of the porous layer thickness at the high Rayleigh number (Hassanzadeh et al. 2005).

$$R_a = \frac{Kg\Delta\rho H}{\mu\varphi D} \tag{2.20}$$

where:

$\Delta\rho = \beta\rho_0 C^*$ is the density differences

$C^*$ is the $CO_2$ equilibrium concentration at the initial pressure

$\beta$ is partial derivative of density $\rho_0$ with respect to concentration

D is the molecular diffusion coefficient of $CO_2$ in water

### *2.3.2 Numerical Simulations of $CO_2$*

Modelling and simulations of $CO_2$ behaviour in saline aquifers have been extensively carried out. Different reservoir simulators (e.g. TOUGH family, ECLIPSE, Permedia, and CMG) have been used for these purposes. The TOUGH family of codes

(TOUGHT2, TOUGH2-MP, TOUGH2/ECO2N, TOUGH-FLAC, and TOUGHREACT) have largely been used by the researchers in the Lawrence Berkeley National Laboratory (Pruess et al. 1999, 2003; Pruess and Spycher, 2007 and Birkholzer et al. 2008).

Kumar et al. (2004) studied reservoir simulation of $CO_2$ storage in deep saline aquifers by using GEM to quantify estimates of the $CO_2$ storage mechanisms. In this study they investigated three modes of $CO_2$ storage: firstly the pore-level trapping of $CO_2$, then, dissolution of $CO_2$ into brine and finally the possible contribution of mineralization to $CO_2$ storage. A set of 2D and 3D numerical simulations was used to study the aforementioned processes. They stated that using an accurate model for the solubility of $CO_2$ in brine is an important factor in evaluating $CO_2$ storage in saline aquifers. In their study they investigated the effect of aquifer properties on $CO_2$ storage. They concluded that an increase in permeability results in greater injectivity, which in turn leads to greater migration of $CO_2$ in the reservoir. The most important finding of Kumar et al. (2004) was the significant effect of residual gas saturation on $CO_2$ storage in deep saline aquifers.

Juanes et al. (2006) performed a series of numerical simulations using ECLIPSE to investigate the impact of relative permeability hysteresis on $CO_2$ storage in saline aquifers as an important factor in the assessment of $CO_2$ sequestration projects. In their simulations they proved that one of the main storage processes is trapping, but only during the post injection period. They injected the same amount of $CO_2$ into a model with hysteresis (Case 1) and without hysteresis (Case 2) in order to investigate the effect of hysteresis and trapping. In both cases $CO_2$ was injected during 10 years, and after that the model was run for 490 years to study the $CO_2$ plume migration. In Case 1 where there was no hysteresis associated with the gas relative permeability, the $CO_2$ plume migrates up dip under buoyancy without leaving any residual $CO_2$ behind. Consequently, after 490 years post injection a gas cap of mobile $CO_2$ formed at the top of the aquifer (Figure ***2.5***, left diagram). In case 2, they considered hysteresis with gas relative permeability. In this case trapping prevents the entire injected $CO_2$ from migrating upwards (Figure ***2.5***, right diagram). The effect of injection rate also was investigated. They concluded that for lower injection rates snap-off will reduce during the imbibition period, whereas higher injection rates lead to an increase in the macroscopic trapping.

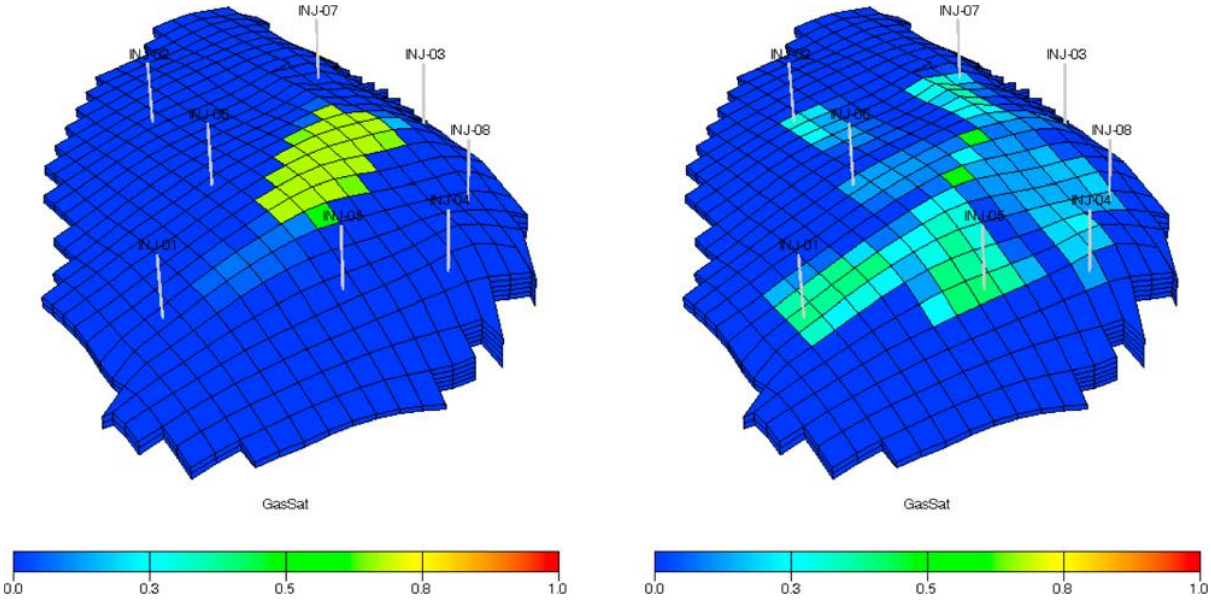


*Figure 2.5 Distributions of CO2 saturation after 500 years (10 years injection period and 490 years post injection period) in the model without hysteresis (left diagram) and the model with hysteresis (right diagram) (Juanes et al. 2006).*

Compositional simulation was originally developed for modelling enhanced oil recovery processes, such as miscible gas injection. More recently, compositional simulation packages have been extended to model $CO_2$ injection into saline aquifers, including the mutual solubility of $CO_2$ and brine and the increase of the density of brine with dissolved $CO_2$ (e.g. CO2STORE module, Schlumberger, 2011). However, assuming the $CO_2$ is pure and is always in a supercritical state, the simulation of $CO_2$ storage is a simpler procedure than miscible gas injection. In this case, fully compositional simulation is unnecessary, and the PVT properties can be input using pre-calculated tables. One method of doing this is to adapt black-oil simulators for $CO_2$ storage. In this case, oil is used to represent brine and hydrocarbon gas represents supercritical $CO_2$. Shariatipour et al. (2012) tested the accuracy of flow simulation of $CO_2$ storage in saline aquifers using ECLIPSE 100 (a black oil simulator) compared with ECLIPSE 300 with the CO2STORE option (a compositional simulator). They concluded that the results compared well, while the ECLIPSE 100 simulations were a factor of four faster than the ECLIPSE 300 simulations.

However, ECLIPSE 300 with the CO2STORE option has been used by different researchers around the world for simulation of $CO_2$ in saline aquifers (e.g. Nordbotten et al. 2012; Williams et al. 2013; Jin et al. 2012).

Permedia $CO_2$ software (an invasion percolation modelling approach) is used to simulate $CO_2$ migration in saline aquifers (Cavanagh and Ringrose, 2011). Singh et al. (2010) used monitoring data from Sleipner and compared results of reservoir simulation of $CO_2$ plumes in the Permedia $CO_2$ software against conventional reservoir simulations. They concluded that there was a better initial match to observed data in the Permedia $CO_2$ software than in other reservoir simulations.

Hassanzadeh et al. (2008) developed an efficient algorithm to convert compositional data from EOS to black oil PVT data. Their algorithm is capable of generating $CO_2$ - brine density, solubility and formation volume factors, which are necessary for using black - oil flow simulations of $CO_2$ storage in geological formations. Spycher et al. (2003), and Spycher et al. (2005), presented a thermodynamic model and mutual solubility of $CO_2$ - $H_2O$. Hassanzadeh et al. (2008) used the equations which were presented by Spycher et al. (2003) to generate their algorithm and finally to generate PVT data for a Black oil model from a compositional model. In their calculation, they used a constant mole fraction for salt as they believed that $CO_2$ solubility in the aqueous phase is fairly low for the pressure and temperature range of $CO_2$ storage in the saline aquifers.

### *2.3.3 CO2STORE Option*

Regarding simulation of $CO_2$ storage in ELIPSE 300 there are several options under various conditions (ECLIPSE Technical Manual 2011).

COAL option can be employed when $CO_2$ is injected into a coal bed methane reservoir.

GASWAT option is a general equation of state for Gas-Water systems.

CO2SOL option can be applied to investigate $CO_2$ storage in oil reservoirs.

CO2STORE can be used to study $CO_2$ storage in saline aquifers ($CO_2$ – $H_2O$ systems with salt).

Since the current study investigates $CO_2$ storage in saline aquifers, the CO2STORE option was used. Three phases are considered in this option, $H_2O$ as the liquid phase, $CO_2$ rich phase, and a solid phase (ECLIPSE Technical Manual 2011). The $CO_2$ rich phase is labelled the gas phase therefore saturation of $CO_2$ in brine will be presented as

gas saturation. Spycher and Pruess (2010) calculations were used to identify mutual solubilities of $CO_2$ – $H_2O$ under typical $CO_2$ storage conditions: 12 – 100 C and up to 600 bar.

In terms of limitation, the CO2STORE option has the fluid properties built in, so you cannot change them. Some researchers prefer to use ECLIPSE 300 with alternative EOS. However, this does not affect our results because the focus of this study was not on the EOS.

## 2.4 Caprock Integrity for $CO_2$ Storage

Capillary entry pressure is a function of the size of the pore throats and the interfacial tension (IFT) between two immiscible fluids. Generally, it is assumed that if the sealing capacity of the caprock was sufficient to seal the original hydrocarbon in the reservoir for a long period of time, then it is adequate to stop the injected $CO_2$ from migrating through the caprock. However, the sealing capacity of caprock is reduced when the hydrocarbons in a reservoir are replaced with the injected $CO_2$. Li et al., (2005) showed that the contact angle of $CO_2$ – water systems is close to that of other gases such as $CH_4$ and $N_2$ and water. Therefore this reduction in sealing capacity is mainly due to lower interfacial tension (IFT) of $CO_2$/water system relative to that of the hydrocarbon/water system; see Table ***2.5*** (Li et al., 2006; Chiquet et al., 2007). Therefore, it is important to re-examine the sealing capacity of the caprock of the depleted oil and gas reservoir for $CO_2$ storage purposes.

*Table 2.5 IFT for different fluids system (after Li et al., 2006).*

| System | Pressure (MPa) | Temperature (C) | IFT (mN/m) |
|---|---|---|---|
| $CH_4$/water | 10 - 30 | 40 - 80 | 48.60 - 61.70 |
| Medium oil/water | > 6.9 | 54.4 - 81.1 | 30 - 35 |
| N-alkane($C_6$-$C_{16}$)/water | 10 - 30 | 25 - 50 | 49 - 54 |
| $CO_2$/water | 10 - 30 | 40 - 80 | 16 - 30 |

Rutqvist (2012) presented an extensive review paper of the modelling of the geo-mechanics associated with $CO_2$ storage in deep saline aquifers. The different geo-mechanical aspects included the sealing performance of the caprock. The strain and stress in the caprock and storage formation were discussed and the geo-mechanical observations at In Salah were also integrated in their work. Geo-mechanical property changes in a $CO_2$ storage formation are in direct relation with the specific formation geo-mechanical conditions (Rutqvist 2010). For example at the In Salah project significant changes arose, whereas at the Sleipner $CO_2$ project site this is not the case (Rutqvist 2012).

Ringrose et al. (2011) stated that the structural geology aspects such as rock mechanical issues related to the reservoir, are vital during the early stages of the $CO_2$ injection (up to 10 years) and the characterisation of the pore space is more important afterwards.

When $CO_2$ is injected into a storage formation the pressure will rise, depending on the injection rate and the properties of the formation. Initially, the pressure will rise in the near-well region, but with time will diffuse further into the formation. Birkholzer et al. (2008) studied pressure response of $CO_2$ storage in layered systems. They indicated that the pressure disturbance may reach the near surface formation if the permeability of the caprock is more than 10E-7 mD. However, pressure builds up in the storage formation even 100km away from the injection region. They concluded that the permeability of the sealing formation has an important impact on the pressure build-up.

Casabianca and Cosgrove (2012) presented a new approach to estimate hydraulic seals based on geo-mechanical properties. They address the fact that there is a waste zone at the lower section of the caprock based on the six case studies in the UK Central Graben. They investigated the hydrocarbons accumulated in the formation between base Cretaceous Unconformity and the base of the Chalk Group, and concluded that the Jurassic Kimmeridge Clay formation may not be the seal for these traps. This waste zone consists of fractures from the top of the reservoir to the base of the caprock.

### *2.4.1 Top Surface Morphology*

Nilsen et al. (2012) created a series of stochastic models to study the effect of different top-surface morphologies on the $CO_2$ storage capacity (Figure ***2.6***). The fault populations and orientations were anisotropic and two hundred faults were generated for each model (Table ***2.6***). They have applied five types of structural models in the three

types of stratigraphical models, resulting in fifteen models. The size of the models was 60 km by 30 km with different heights. $CO_2$ was injected from a single well at the bottom (lowest point) of the models.

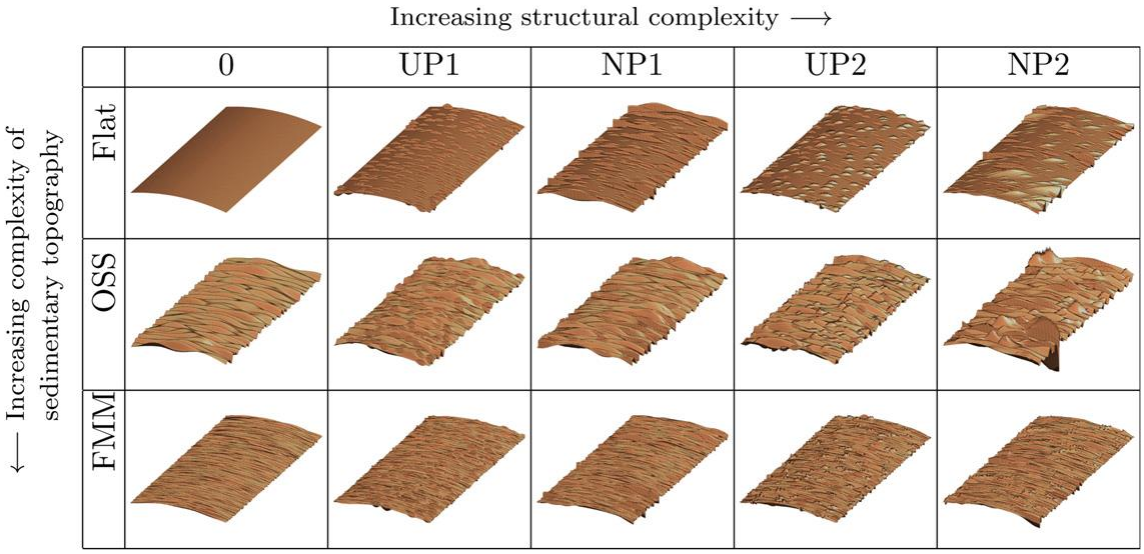


*Figure 2.6 Overview in terms of a heterogeneity matrix for the selected geological features, OSS stands for offshore sand ridges and FMM stands for flooded marginal marine. The columns show different structural scenarios and the rows different depositional settings (Nilsen et al.2012).*

*Table 2.6 Geometric definitions of fault populations (Nilsen et al. 2012)*

| | UP1 | NP1 | UP2 | NP2 |
|---|---|---|---|---|
| Displacement | Uniform; 100m | Random; 20-150m | Uniform; 100m | Random; 20-150m |
| Length | Uniform; 4000m | Random; 300-6000m | Uniform; 4000m | Random; 300-6000m |
| Strike | Uniform; 90° | Uniform; 90° | Uniform; 30° and 90° | Uniform; 30° and 90° |

They concluded that the top-surface morphology plays a significant role in the $CO_2$ migration and the capacity of $CO_2$ storage. Figure ***2.7*** shows that $CO_2$ migrates laterally before migrating up-slope. In addition, they investigated two approaches to estimate $CO_2$ trapping in saline aquifers. They believed that the spill-point approach can be used to obtain a rough estimate of structural trapping, whereas for estimating the residual trapping, a very detailed flow simulation is required.

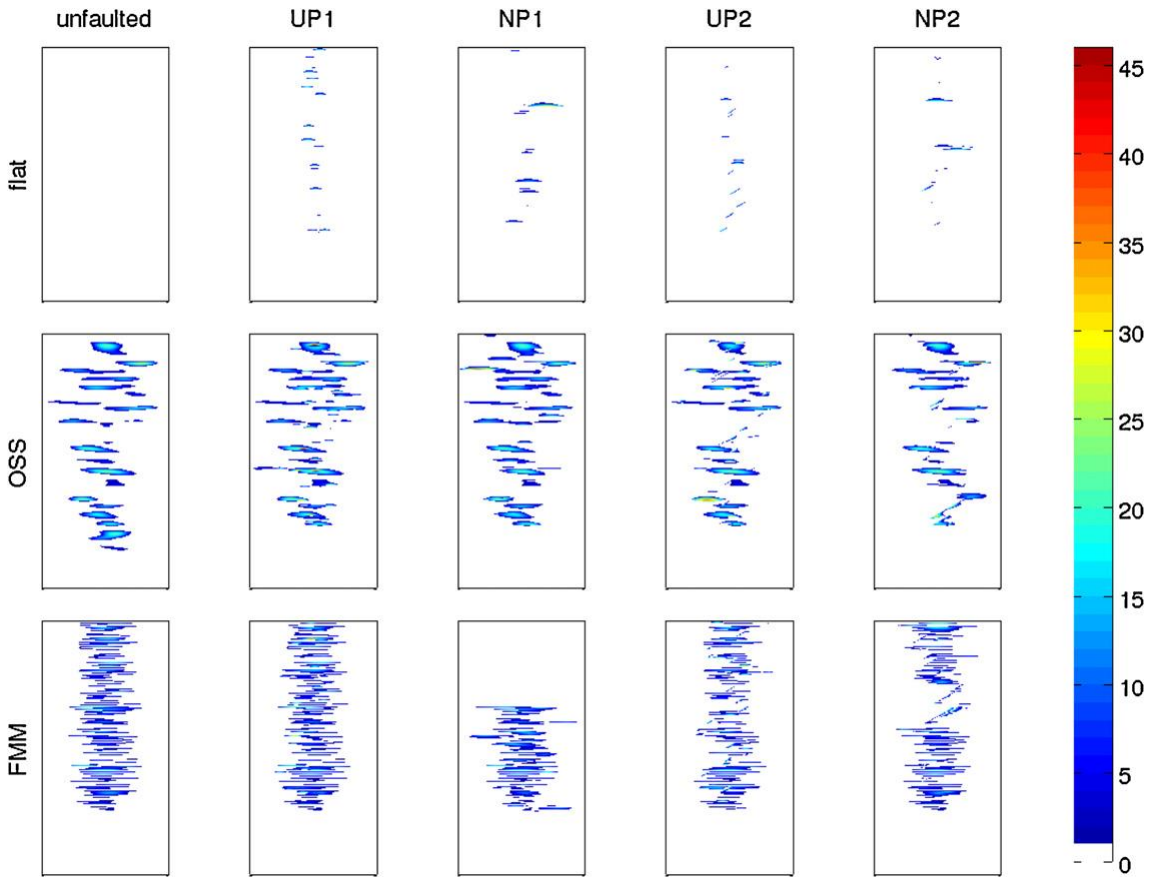


*Figure 2.7 Height in meters inside structural traps computed by a spill-point analysis.*

They observed that an increase in pressure beneath the caprock during the injection period is not affected by the morphology of the top of the aquifer. They understood that the effect of faulting on free and residual volumes is less than the effect of top-surface morphology. They demonstrated that the presence of faults could increase the structural trapping; however, this is dependent on the transmissibility of the faults and their orientations. Faults normal to the flow direction (UP1 and NP1) create the most structural trapping amongst all types of faults. Furthermore, they concluded that offshore sand ridges have the largest capacity for structural trapping.

Gammer et al. (2011) presented the methodology used in creating the estimate of capacity for the geological storage of $CO_2$ on the UK continental shelf (UKCS) in the UK Storage Appraisal Project (UKSAP). They used production and injection data for estimating the storage capacity of depleted hydrocarbon reservoirs. Saline aquifers were classified into two groups, either fully confined or open units. They explained that due to the geographical extent of the project and consequently the large number of the storage units, it was impossible for them to consider more detailed reservoir modelling. This meant that the localised closures at the interface between caprock and the storage formation which could buoyantly trap $CO_2$ were not considered in all cases. Therefore

there is an uncertainty in their calculation in estimating the actual pore volume and consequently in the real capacity of the geological storage of $CO_2$ in the UK continental shelf.

Goater et al. (2013) studied the effect of top-surface morphology and heterogeneity on the storage capacity in open aquifers. They used a model based on the Forties aquifer for their studies. In their studies they considered three models, homogeneous smooth, homogeneous with top-surface topography, and heterogeneous with top-surface topography (Figure ***2.8***). The range of arithmetic average permeability and average aquifer dip were 11mD -1000mD and 0.27° - 3° respectively.

They observed that most studies on the storage capacity were either on the effect of heterogeneity (e.g. Lengler et al. 2010) or on the effect of heterogeneity where top-surface morphology was included (e.g. Chadwick and Noy 2010). Goater et al. (2013) investigated the effect of permeability and the aquifer dip on the $CO_2$ migration and pressure build-up. Their studies include the detailed account of the simulations described in Gammer et al. (2011) on the dynamic modelling of $CO_2$ storage in a dipping open aquifer. They concluded that the structural closure due to top-surface morphology increases storage efficiency whereas regions of high dip decrease storage efficiency.

Goater et al. (2013) concluded that the effect of top-surface topography on the storage efficiency could be neglected in models with a very low permeability and a very low aquifer dip angle. However, in other cases this effect could be greater by at least a factor of two. Top-surface channels reduce storage efficiency whereas the lower dip routes to escape increase storage efficiency when low migration velocity storage is considered.

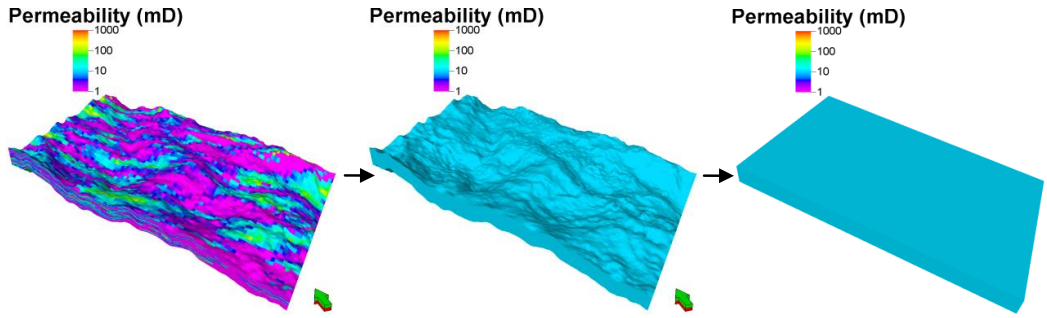


*Figure 2.8 Forties base case model. From right to left, homogeneous smooth Model, homogeneous with top-surface topography, and heterogeneous with top-surface topography (vertical exaggeration x15)(Goater et al. 2011).*

Okwen et al., (2010) presented a simple analytical solution for estimating storage efficiency of geological sequestration of $CO_2$. They used some of the analytical expressions developed by Nordbotten et al., 2005 and Nordbotten and Celia (2006), in their calculations. They did not consider dry-out process in their calculations, in which residual brine saturation is evaporated by injected $CO_2$ (Nordbotten and Celia, 2006). In order to estimate the storage efficiency of saline aquifers the following equations were presented by Okwen et al., (2010):

$$\varepsilon \approx (1-S_r)\frac{1}{\lambda} \qquad 0 \le \Gamma \prec 0.5$$

$$\varepsilon \approx \frac{2(1-S_r)}{(0.0324\lambda - 0.0952)\Gamma + (0.1778\lambda + 5.9682)\Gamma^{1/2} + 1.6962\lambda - 3.0472} \qquad 0.5 \le \Gamma \prec 50 \qquad (2.21)$$

where, ($S_r$) is residual brine saturation, ($\lambda$) is the ratio of $CO_2$ mobility to brine mobility, and ($\Gamma$) is a dimensionless term that quantifies the $CO_2$ buoyancy to the $CO_2$ injection rate (gravity factor).

They found that the storage efficiency depends on the mobilities of $CO_2$ and brine, residual brine saturation, and gravity factor. Therefore, for cases where $CO_2$ injection rate is high enough that gravity factor can be neglected (i.e. $\Gamma \prec 0.5$), the storage efficiency depends only on the ratio of $CO_2$ mobility to brine mobility and the residual brine saturation.

The work presented in this thesis extends the work of (Nilsen et al. 2012 and Goater et al. 2013) on the impact of top-surface morphology on $CO_2$ storage capacity. A transition zone, where there is a gradational change from storage formation to caprock,

will be presented as a new uncertainty in the study of $CO_2$ storage in underground formations. The morphology of the aquifer/caprock interface depends on the sedimentalogical setting and structural deformation. Below some of these factors, which can affect the interface between caprock and aquifer, are described.

### *2.4.2 Tilted Beds*

Most sedimentary rocks are deposited within a few degrees of horizontal (Gasda et al. 2008). However, these layers may become tilted due to lateral tectonic stress (Figure ***2.9***). When $CO_2$ is injected into dipping aquifers the plume migrates asymmetrically beneath the caprock and the plume moves further up dip (Gasda et al. 2012), and the residual trapping due to this migration of $CO_2$ will be increased (Klaus 2007).

*Figure 2.9 Tilted rock layers (near Denver, http://raider.mountunion.edu).*

Nordbotten et al., (2005) and Nordbotten and Celia (2006) presented analytical solution for fluid injection into confined aquifers. The interface between two fluids during the injection phase can be obtained based on their calculations, analytically. However, they did not consider the effect of tilt in their calculations.

Gasda et al., (2008) showed that slope of the interface between storage formation and caprock plays an important role in the $CO_2$ plume migration. They have conducted a series of 1D and 2D numerical simulations, to investigate the effects of tilt as well as some others system properties such as rock permeability, fluid viscosity and density on the plume migration. Two different tilt angles, $0.1^{\circ}$ to $1^{\circ}$, and two different permeabilites, 50 mD and 3 D, were tested. Figure ***2.10*** and Table ***2.7*** show a sketch of their model and their model properties used in their simulations respectively. In their

simulation, one million tonnes of $CO_2$ was injected per year through one horizontal well for 15 years.

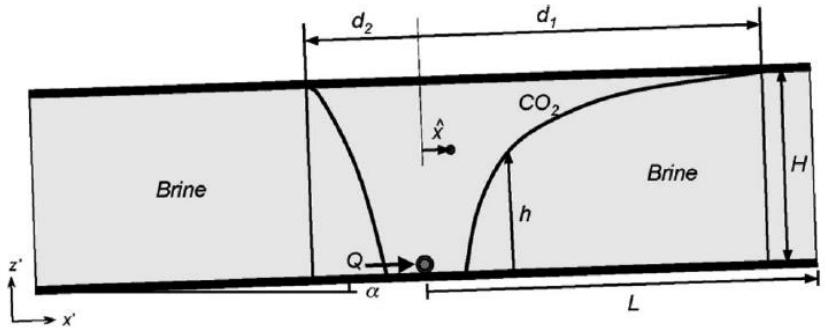


*Figure 2.10 Representation of domain of interest, showing the CO2-brine interface, the horizontal centroid, $\hat{x}$, and other system parameters (Gasda et al., 2008).*

*Table 2.7 Models properties (Gasda et al., 2008).*

| Aquifer property | Value |
|---|---|
| $H$ | 50 m |
| $\phi$ | 0.15 |
| $k$ | $5 \times 10^{-14}$ m$^2$ |

| Subsurface conditions | Viscosity (mPa · s) | | Density (kg/m$^3$) | |
|---|---|---|---|---|
| | $CO_2$ | Brine | $CO_2$ | Brine |
| Warm, deep | 0.0395 | 0.2535 | 479 | 1045 |
| Cold, shallow | 0.0577 | 1.1875 | 741 | 1121 |

They have shown that $CO_2$-brine interface in the more unstable viscous ratios cases (cold, shallow aquifers) extends three times farther than the more stable cases. They concluded that increasing dip angle from $0.1^{\circ}$ to $1^{\circ}$ degree, leads to an increase in the horizontal position of centroid ($\hat{x}$) by one order of magnitude in low permeability and high permeability results in 1D models. The centroid for the high permeability cases increased around two log-units, which shows the effect of high permeability formation on the $CO_2$ up dip migration.

### *2.4.3 Unconformities*

Unconformity traps are broadly classified as a class of stratigraphic traps but they may be influenced by diagenetic processes (Rittenhouse 1972). Usually there is a major gap in the geological sequence between a rock which has overlain another rock (Figure ***2.11***). The Southern Gas Basin Carboniferous under the base Permian is one example of an unconformity in the UK continental shelf (Stoker et al. 2006). When an unconformity is the main seal (caprock) of a hydrocarbon reservoir, it may allow hydrocarbons to migrate through the bedding planes under the unconformity, and perhaps escape from the trap (Corcoran 2006). In addition, the risk of gas escape might increase if the unconformable seal was formed of different lithologies with different sealing efficiencies. Therefore, a depleted hydrocarbon reservoir or a saline aquifer underlying an unconformity may not be a very promising $CO_2$ storage site.

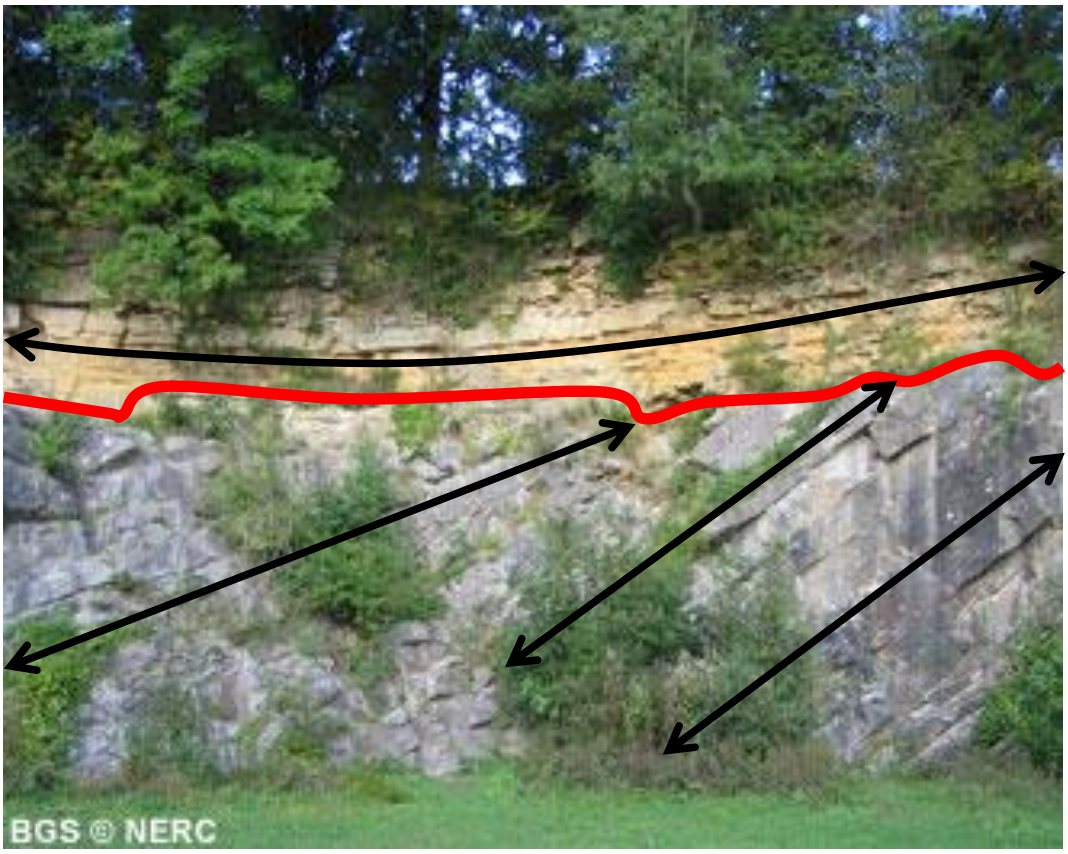


*Figure 2.11 Unconformity exposed in a quarry in Somerset. The grey coloured Carboniferous-age limestone below the unconformity was deeply-buried, folded (tilted), re-exposed and eroded by the sea before the overlying yellow-coloured flat-lying. The Red line represents the unconformity surface and the black arrows show layers orientation above and below the unconformity.*

### *2.4.4 Interbedded*

Interbedded sandstones and shales may arise due to variations in sea level. $CO_2$ storage in the Utsira formation is an example where there are interbedded mud layers in the sandstone which act like an obstacle for vertical migration of $CO_2$ and enhance the lateral migration of the plume (Figure ***2.12*** and Figure ***2.13***). In Sleipner there are nine layers of $CO_2$ trapped beneath the interbeded mud layers (White et al. 2013). Boait et al. (2011) concluded that the $CO_2$ plume is thining and shrinking. $CO_2$ seems to migrate right through the interbeded mud layers. This is probably because of a progressive increase in effective permeablities within the interbeded mud layers (Boait et al. 2011).

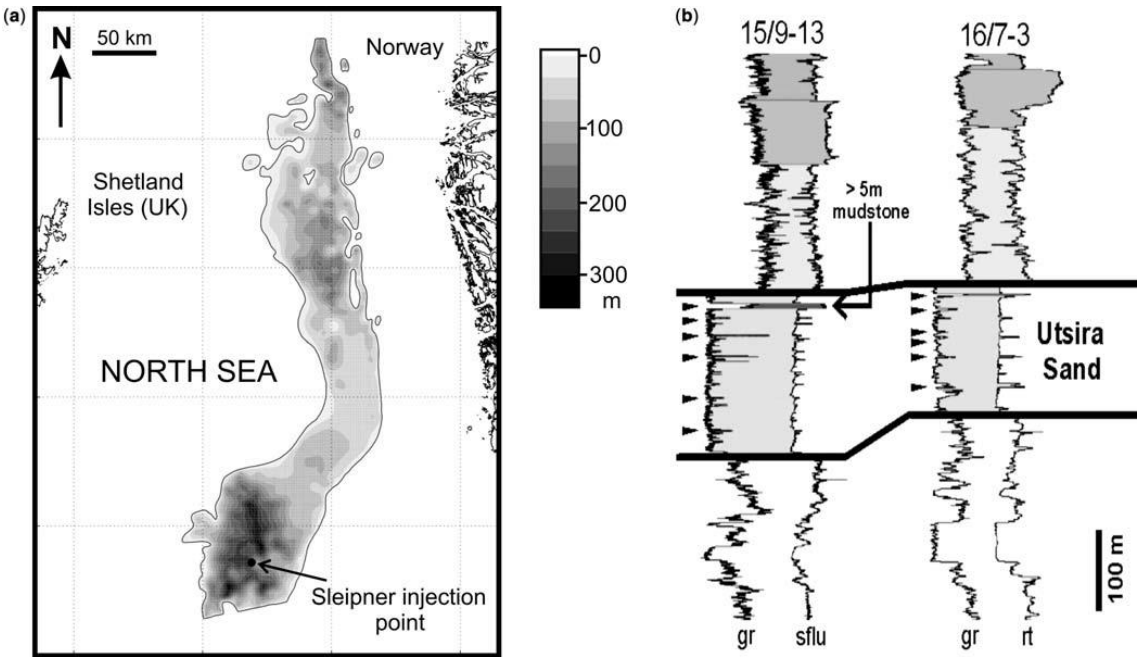


*Figure 2.12 (a) Location of the Sleipner (b) Geophysical logs through the Utsira Sand showing GR and resistivity peaks corresponding to thin intra-reservoir mudstones (Chadwick et al. 2009).*

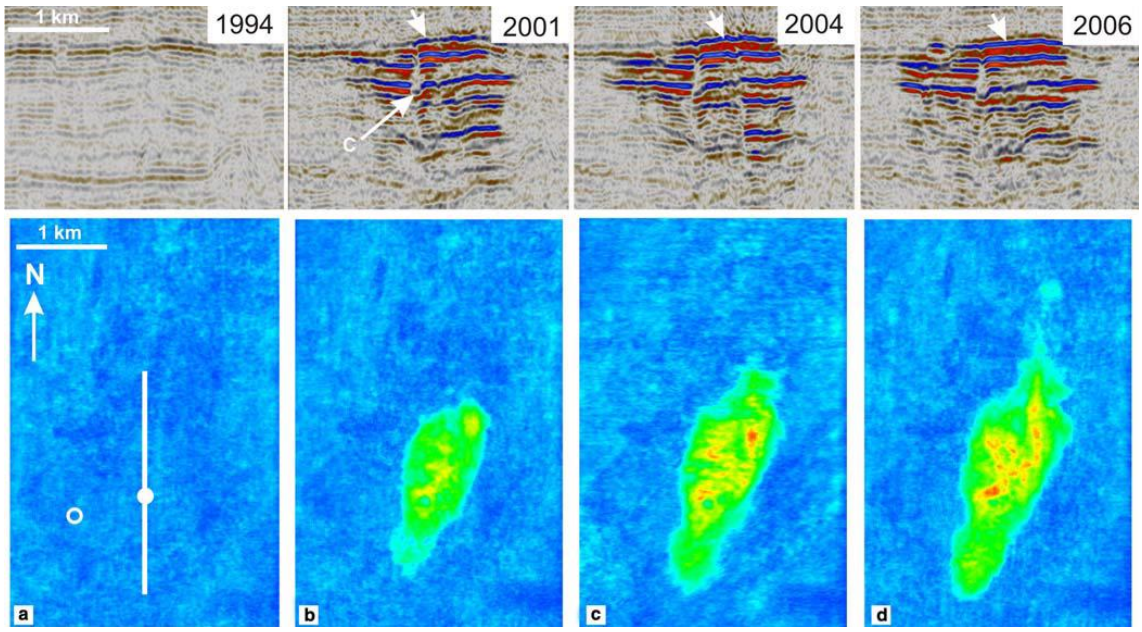


*Figure 2.13 The top row shows a north–south seismic section through the plume, white arrows show the $CO_2$ layer beneath the top seal and C denotes where $CO_2$ goes easily through the interbedded shale; the bottom row demonstrates plan views of the plume displayed as total reflection amplitude (Chadwick et al. 2009).*

## 2.5 Outlines of Cases to be Studied

Storage security is one of the most important issues in $CO_2$ storage in geological formations. Before storing $CO_2$ in a particular aquifer, a thorough characterization of the geological properties must be carried out. In the next chapter the importance of characterization of the interface between caprock and storage formation will be demonstrated.

# Chapter 3

# Interface between Caprock and Aquifer

## 3.1 The Impact of Aquifer/Caprock Morphology on $CO_2$ Storage in Saline Aquifers

### *3.1.1 Introduction*

The $CO_2$ storage project at Sleipner has shown that the topography of the aquifer/caprock interface can have a significant effect on the migration paths of $CO_2$ in an aquifer (e.g. Singh et al., 2010). Therefore, when appraising any reservoir or aquifer for $CO_2$ storage, it is important to characterise the interface and to ensure that it is modelled adequately.

Often simulations assume a sharp smooth boundary between the aquifer and the caprock. However, studies of outcrops show that a variety of types of interface may arise in nature, depending on the depositional setting. Nilsen et al. (2012) have investigated the impact of top-seal morphology on $CO_2$ storage capacity and migration patterns, and concluded that it is important to model geological details in order to predict $CO_2$ migration.

The aim of this work is to investigate different types of caprock/aquifer interface to determine how these affect the pressure build-up under the caprock and the amount of $CO_2$ which dissolves in brine. This will enable us to identify which type of aquifer/caprock has the greatest potential for storing $CO_2$ securely.

There are three main factors that affect the interface:

1. The depositional setting and the nature of the transition from sandstone to mudstone.

2. Post-depositional processes, such as bending due to tectonic processes.

3. Diagenetic processes

Other related factors could include faulting due to tectonic processes, compaction and cementation which may affect the permeabilities in the aquifer and caprock. In this study, these effects and also diagenetic processes are not considered.

### *3.1.2 Methodology*

A range of numerical simulations on a variety of heterogeneous aquifer/caprock models has been conducted to investigate the impact of the different types of aquifer/caprock interfaces.

The models all have dimensions of 3000 m × 10 m × 40 m in the X, Y, and Z directions were discretized into 600×1×34 cells. The statistics for the porosity and permeability of the models were taken from the CASSEM study (Pickup et al. 2011). The aquifer data is based on the Sherwood Sandstone Group and the caprock on the Mercia Mudstone Group (Figure 3.1). Table ***3.1*** shows the porosity and the permeability values. It is assumed that the permeability is isotropic. The models represented part of a larger aquifer, and the pore volume of the five outer cells on each side was multiplied by a factor of 1000, to take account of this.

*Table 3.1 Models Properties*

| Formation | Geometric Ave. Permeability (mD) | Std Dev ln(Permeability) | Ave. Porosity | Std. Dev. Porosity | Min | Max |
|---|---|---|---|---|---|---|
| Sherwood sandstone | 1000 | 0.5 | 0.25 | 0.02 | 0.16 | 0.28 |
| Mercia Mudstone | 0.00006 | 0.1 | 0.1 | 0.03 | 0.06 | 0.20 |

In all cases, a single injection well was placed in the centre of the model. Initial pressure and initial temperature were set to 100 bar and 35 $^{\circ}C$ at 1000 m depth. The control mode for injection was the surface rate which was set to 600 $m^3$/day. The injector was shut after 20 years and the simulation was continued for a further 100 years. Initially, it was assumed that the reservoir contained 100% brine, with mole fractions of 0.967 and 0.033 for $H_2O$ and NaCl respectively. The simulations were performed using the ECLIPSE 300 compositional simulator with the CO2STORE option (Schlumberger, 2011).

Figure ***3.1*** illustrates three models which were generated in order to investigate the effect of rugosity on storage capacity and security. The lithostratigraphic units are the Sherwood Sandstone Group (yellow) and the Mercia Mudstone Group (Green). Model 1 is a tilted aquifer. Model 2 shows an aquifer with a few domes at the interface between the caprock and the sandstone. Model 3 is based on Model 1, with some irregularities at the interface between caprock and aquifer formation.

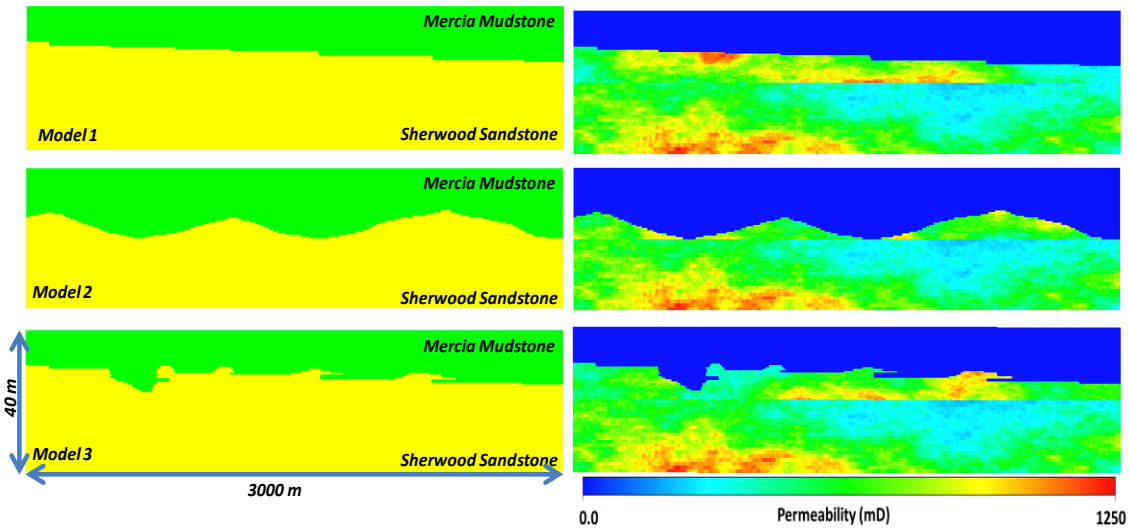


*Figure 3.1 Model dimensions and morphology (left) and permeabilities in X direction (right).*

### *3.1.3 Results*

Figure ***3.2*** and Figure ***3.3*** illustrate gas saturation for all three models at the end of the injection period (20 years) and 30 years post injection, respectively. They illustrate how the rugosity of the interface affects the migration of the $CO_2$. After $CO_2$ is injected into the aquifer in the middle of each model, it migrates upward under buoyancy until it reaches the caprock (structural trapping). Then, depending on the nature of the interface between the caprock and the storage formation (which depends on sedimentological and stratigraphic effects or structural deformation), the plume spreads laterally. $CO_2$ tends to move upslope unless prevented by a baffle (Model 3) or it reaches a dome where it will fill to the spill point (Model 2).

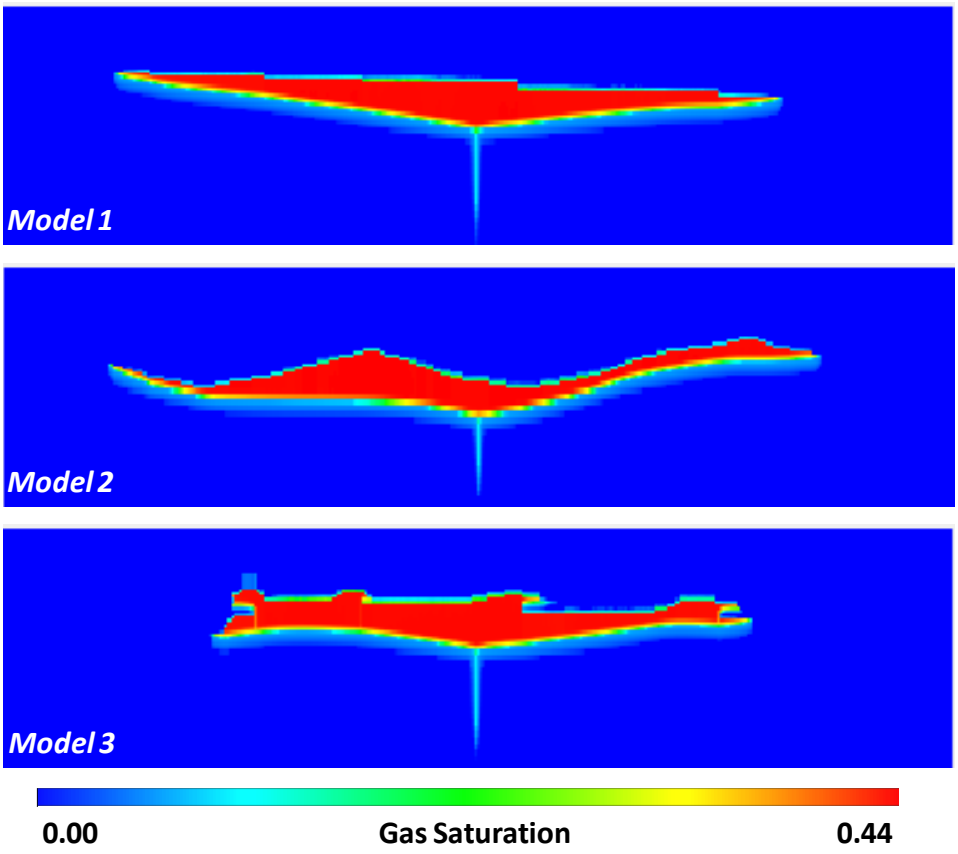


*Figure 3.2 Gas saturation at the end of injection period (20 years) for all models.*

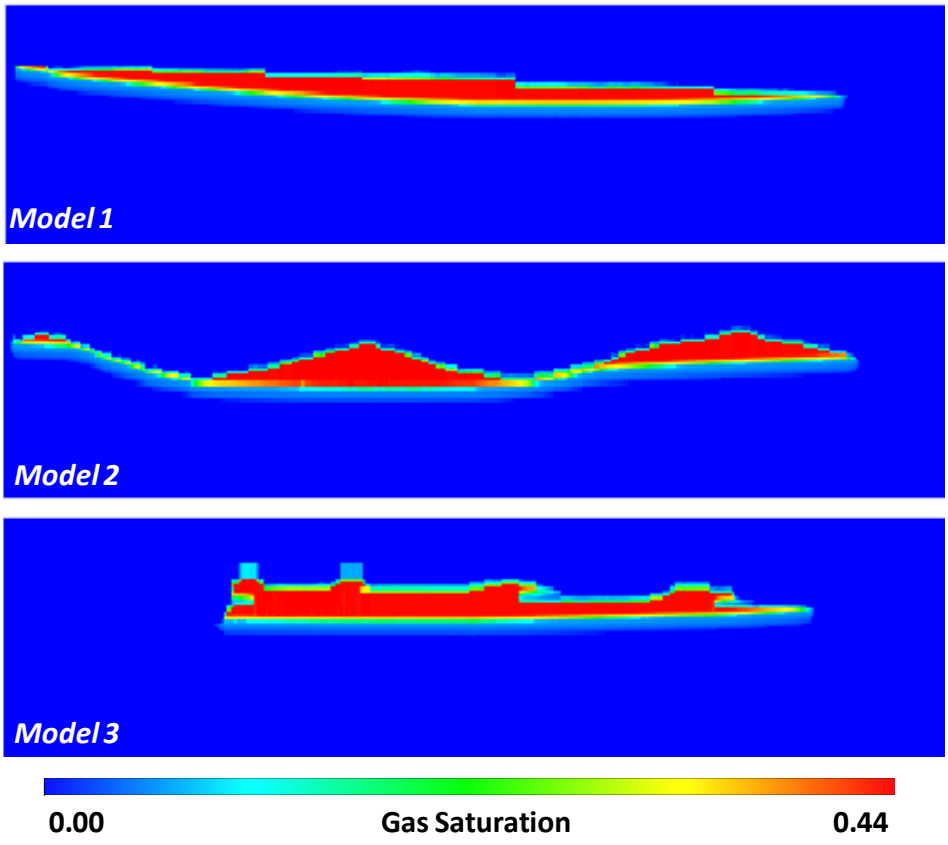


*Figure 3.3 Gas saturation after 30 years post injection.*

Figure ***3.4*** shows the amount of $CO_2$ dissolved in brine in these models. During the injection period, when the migration of $CO_2$ is governed by both the viscous force and buoyancy, the differences in the amount of dissolution are negligible. However, in the post-depositional period the effects of the different aquifer/caprock interfaces become apparent. The greatest amount of dissolution occurs in Model 1, because the interface is tilted, but smooth, so $CO_2$ is free to migrate up dip, thereby coming into contact with the most brine. In Model 3 (which is also tilted), the dissolution initially rises at the same rate as in Model 1. However, after 30 years post injection, the rate of dissolution declines because $CO_2$ is trapped in the irregularities at the interface. The least amount of dissolution takes place in the domed model (Model 2): $CO_2$ fills the domes so there is a lower area of interface between $CO_2$ and brine.

Figure ***3.5*** illustrates pressure increase in Model 2 which had the highest pressure increase of the models. Although the pressure increase at the aquifer/caprock interface is not large in this case (only 3 bars), it gives an indication of the highest pressure at the crest.

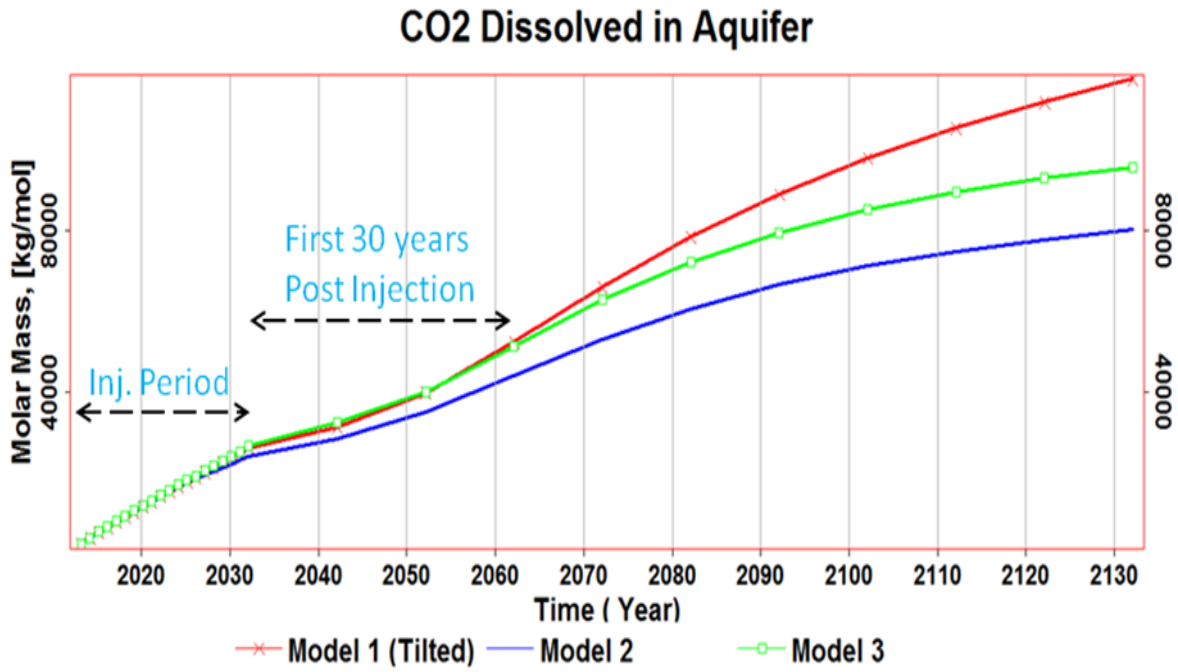


*Figure 3.4 The amount of $CO_2$ that can be dissolved in all three models.*

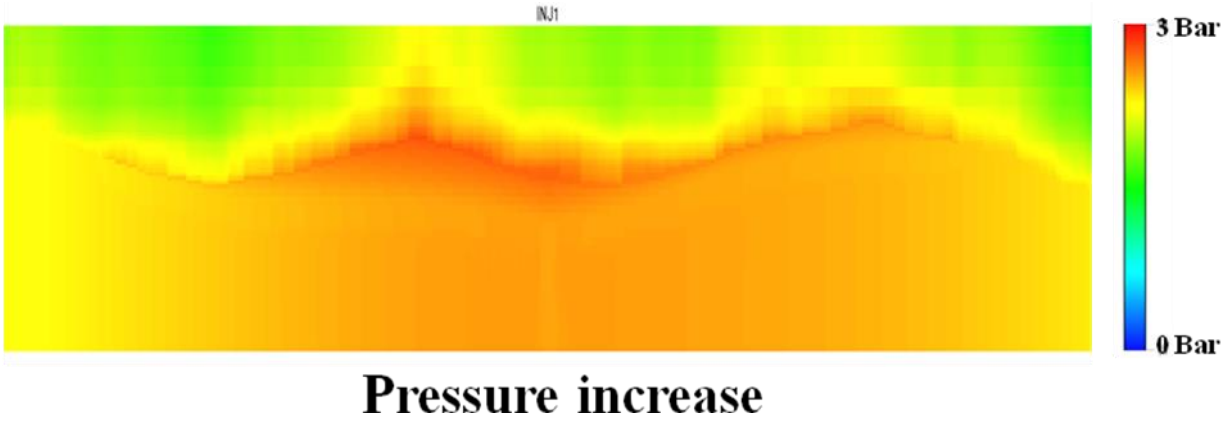


*Figure 3.5 Pressure increase in Model 2*

### *3.1.4 Discussion*

There are advantages and disadvantages in the models studied in this work. On the one hand a domed model, like Model 2, will limit the amount of migration which increases storage efficiency as also observed by Nilsen et al. (2012) and Goater et al. (2013), but on the other hand, there will be less dissolution of $CO_2$.

Model 3, represents an irregular interface between the aquifer and the caprock. In this case, the amplitude of the irregularities was small. The small high points in the sandstone limited the migration of $CO_2$ to a certain extent, and the $CO_2$ distribution was intermediate between that of Model 1 and that of Model 2. Also, the amount of dissolution was intermediate.

## 3.2 The Effects of Aquifer/Caprock Interface on $CO_2$ Storage Capacity and Security

### *3.2.1 Introduction*

In simulations of $CO_2$ storage in saline aquifers, it is often assumed that there is a sharp boundary between the aquifer and the caprock. However, this is not always the case. This was investigated during a field trip to the Wessex Basin in South of England.

The following terminologies will be used in this section.

Interface between caprock/storage formation is the contact surface between the caprock and the geological storage formation.

Transition zone is a zone where there is a gradual change from reservoir rock to caprock over a distance of a few metres.

### *3.2.2 Wessex Basin*

This is a large basin covering some parts of southern UK, the English Channel and Northern France (See Appendix A). The geological evolution of this basin includes a few stages, starting in the Permo-Triassic period when the basin was formed. Figure ***3.6*** shows the stratigraphic position of the different rocks of the Wessex Basin.

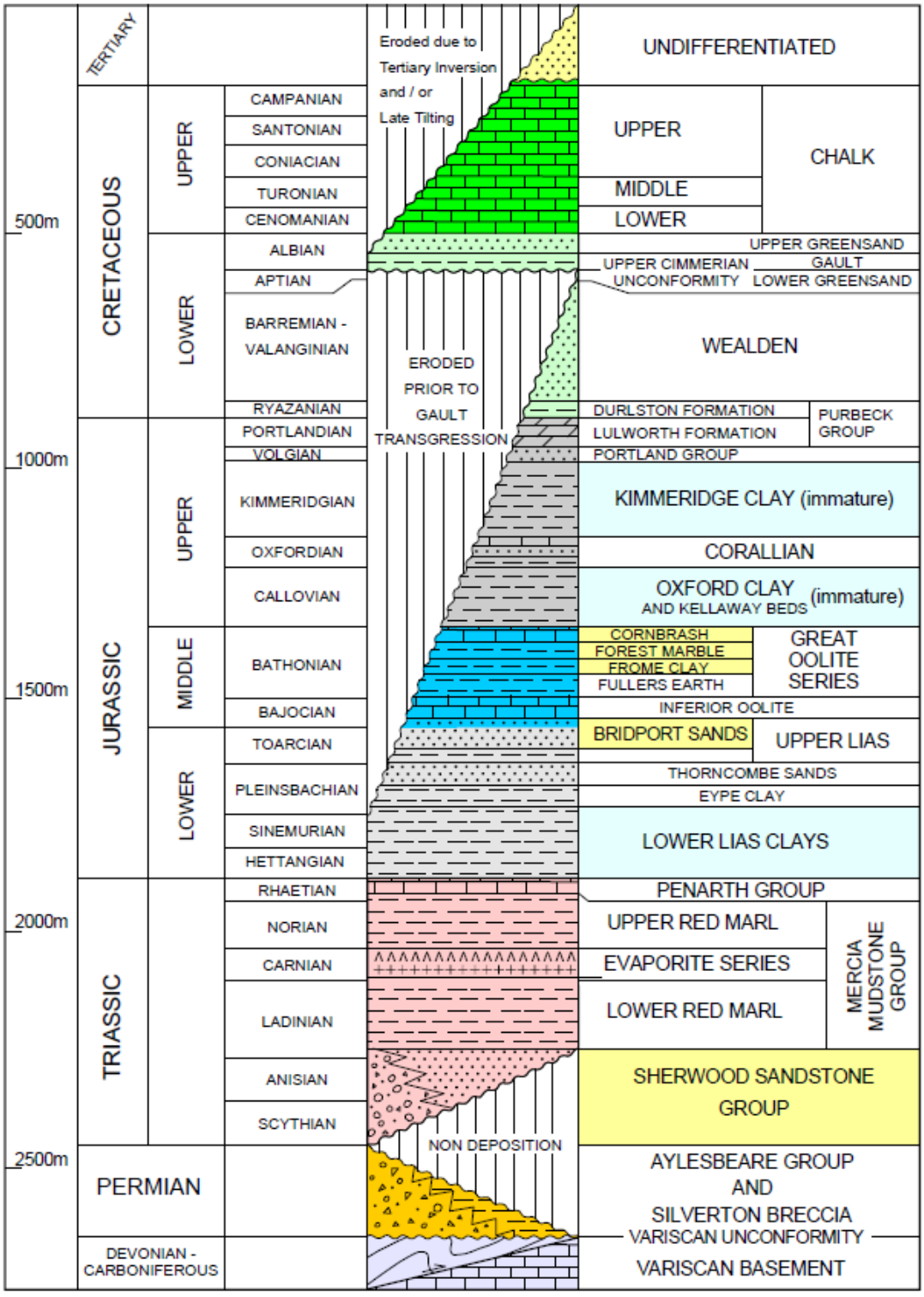


*Figure 3.6 Stratigraphy of the Wessex Basin ( DECC 2012).*

A few outcrops were visited in the South Devon Coast to the west of Sidmouth to study the interface between caprock and storage formation. One site visited was Ladram Bay which has a series of well-developed cliffs, stacks and shore platforms cut in the red sandstones of the Triassic rocks belonging to the Otter Sandstone Formation, a component part of the Sherwood Sandstone Group. Regarding the lithofacies, this

sequence consists of mainly fluvial sandstones comprising some thin layers of mudstone and breccias (Figure *3.7*).

*Figure 3.7 Ladram Bay outcrop*

Sidmouth was the second outcrop chosen for further investigation of characterisation of the caprock/formation interface. The Sidmouth exposure is a vertical cliff cut in the red sandstone of the Triassic rocks belonging to the Otter Sandstone Formation, a component part of the Sherwood Sandstone Group (SSG). It has the same lithofacies as Ladram Bay (Figure ***3.8***). The Sherwood Sandstone Group is composed of alluvial sandstones with distributary channels (Underhill and Stoneley 1998). At the Wytch Farm it was reported that SSG was deposited in a mixed fluvial and alluvial plain setting (Holloway et al. 1989; Bowman et al. 1993; Underhill and Stoneley 1998).

*Figure 3.8 Sidmouth outcrop, Professor Dorrik Stow (in the picture) is describing the Sidmouth outcrop.*

It was observed at the Sidmouth outcrop that this outcrop consists of largely fluvial Sherwood Sandstone and Mercia Mudstone (Figure *3.8*). The outcrop was classified into three sections. The first section, which was the top section, consists of Mercia Mudstone. The second section involved a sequence of sandstone layers including mudstone layers. The third section, which was underlying the second section, consists mainly of sandstone (Figure *3.8* and Figure *3.9*).

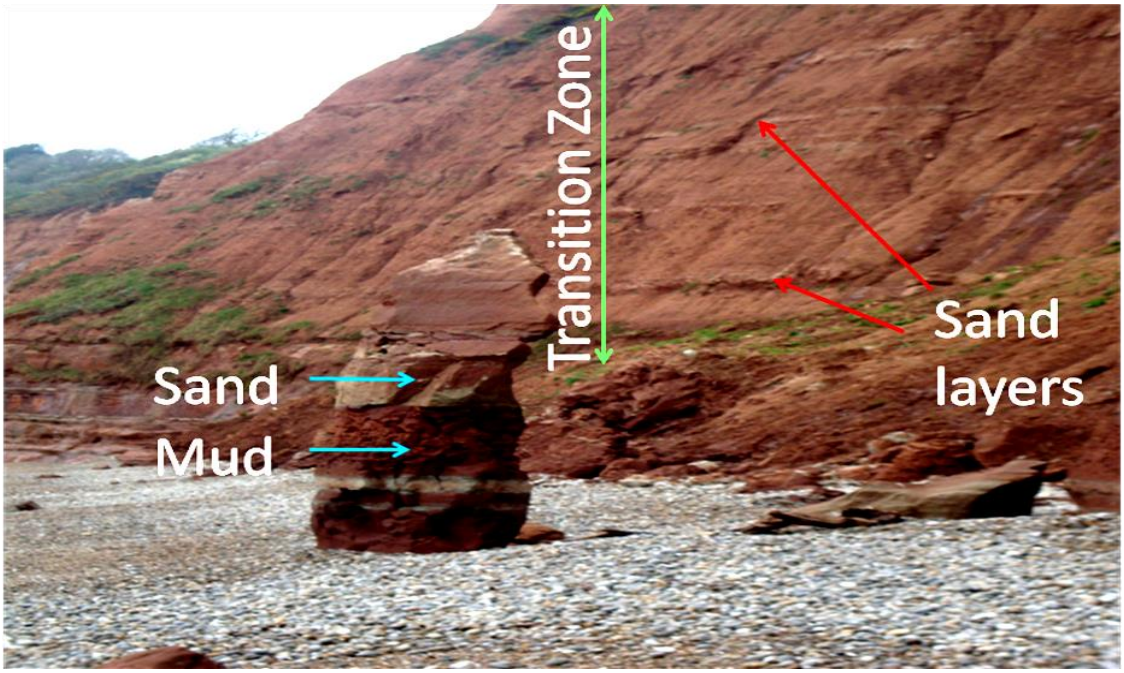


*Figure 3.9 outcrop of the interface between the Sherwood Sandstone Group and the Mercia Mudstone Group near Sidmouth, Devon, England, UK.*

The observations at this outcrop show that there is a gradual transition between sand rich facies and mud rich facies (Figure ***3.9***). This suggests that transition zones may arise in other potential $CO_2$ storage sites, and this is a factor which has not been considered previously in simulations of $CO_2$ storage. Moreover, some simulations assume a smooth interface based on the source of interpretations (e.g. from well logs Figure ***3.10***), whereas typically the surface is irregular, due to sedimentological and stratigraphic effects or structural deformation.

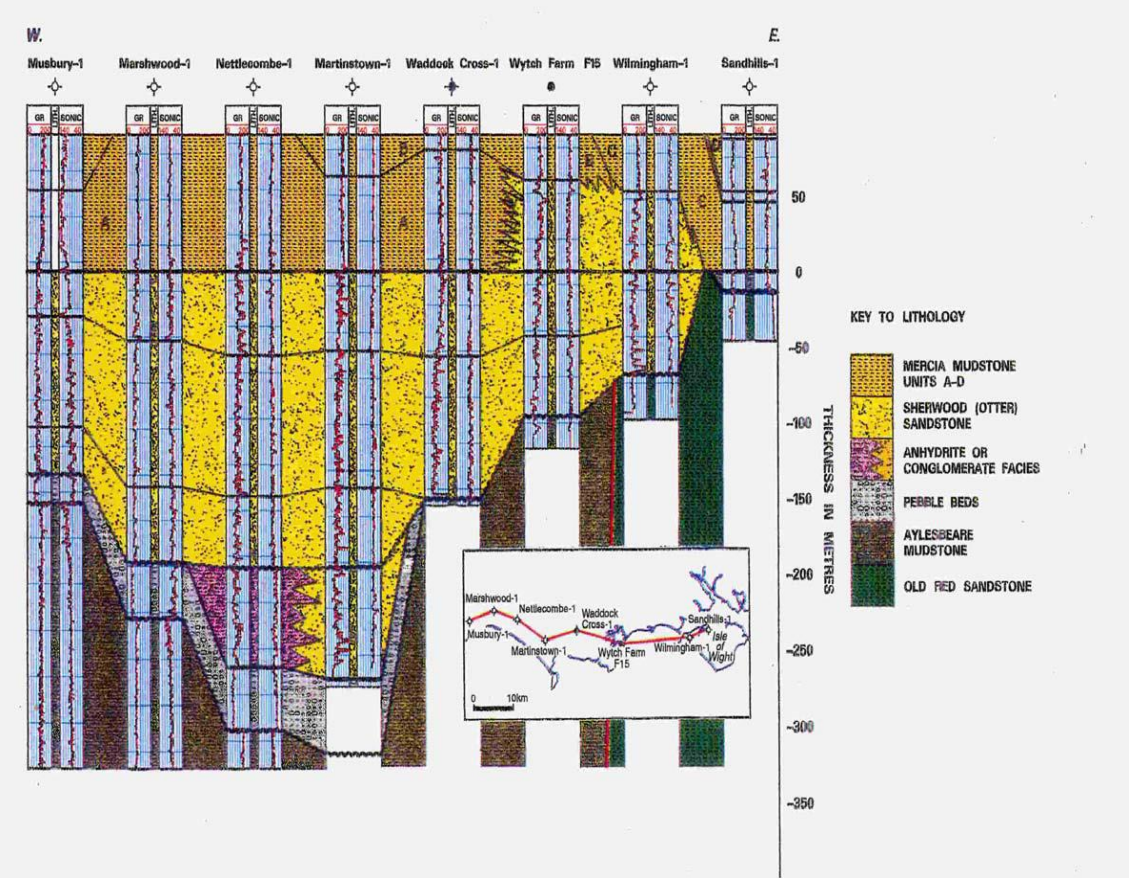


*Figure 3.10 Regional Sherwood Sandstone correlation (after Butler, 1998). It can be seen from this figure that the interpreter assumed that there is a sharp boundary between Sherwood Sandstone and Mercia Mudstone.*

### *3.2.3 Methodology*

In this study, a range of models was generated in Petrel in order to investigate the effect of uncertainty in the aquifer/caprock interface on storage capacity. The 2D models all have dimensions of 3000 m × 10 m × 40 m in X, Y and Z directions respectively. Model 1, which is assumed here to be "reality", is based on observations of the interface between the Sherwood Sandstone Group and the Mercia Mudstone Group near Sidmouth, Devon. Here there is a gradual transition from the sand-rich facies in the aquifer to the mud-rich facies in the caprock. See Figure ***3.11***, Model 1.

It was estimated at the Sidmouth outcrop that the transition zone may be up to 10 m in places, therefore transition zone in Model 1 is assumed to be 10 m. Models 2 and 3 are interpretations which might be made using seismic reflection data. Model 2 will overestimate the storage capacity whereas Model 3 will under estimate the storage capacity.

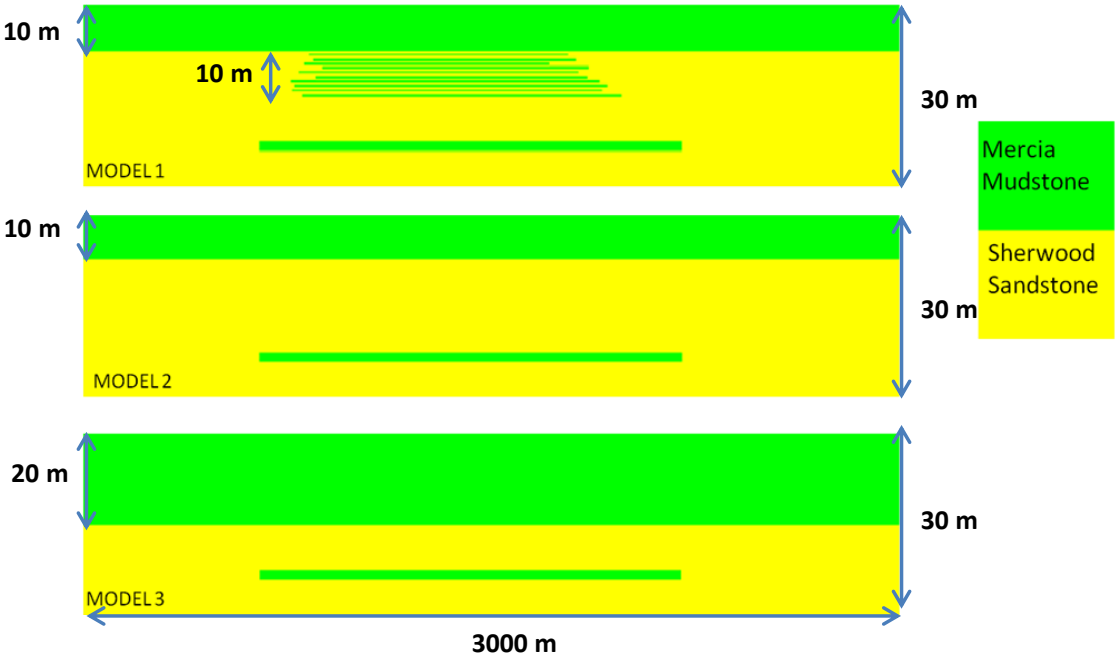


*Figure 3.11: Model 1, which is assumed here as "reality"; models 2 and 3 are two interpretations which might be made*

***Effect of Irregularity of the Interface in the Effective Aquifer Volume***

The irregularity of the transition zone may also lead to uncertainty in the effective aquifer volume. Top-surface structure can either decrease or increase storage efficiency (Goater et al. (2013)). Figure ***3.12***, shows the base case model (Model 1) with a model which has irregularity at the interface (Model 4).

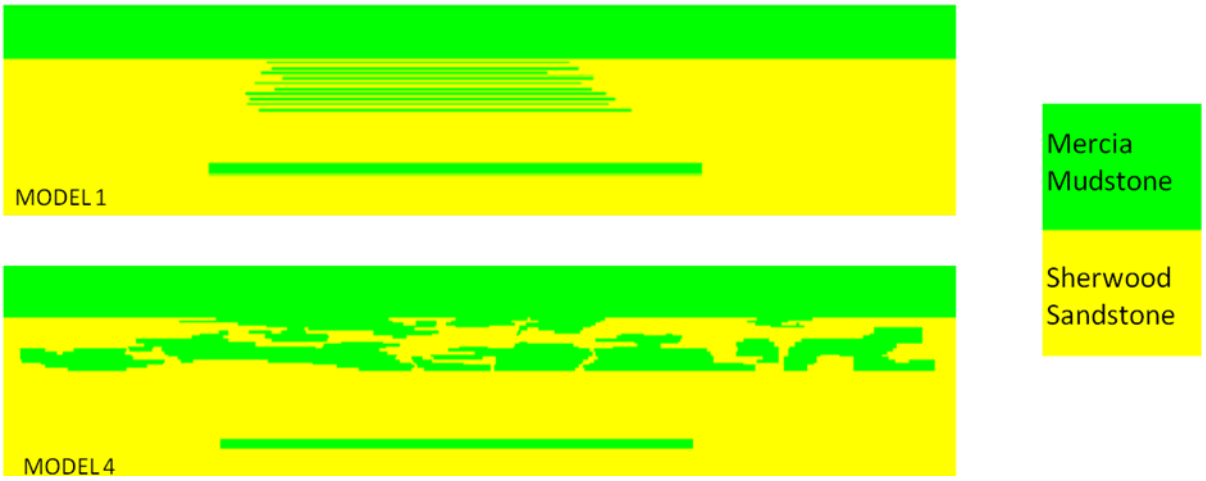


*Figure 3.12: Model 1 and model 4*

### *3.2.4 Results*

Table ***3.2*** shows that assuming that the transition zone is part of the reservoir will overestimate the storage by up to 6% (see Figure ***3.11*** for models dimensions). However, including the transition zone as a part of the caprock will under estimate the storage capacity by up to 29% for this model. Storage efficiency (E) can be 1% to 2% for an open system depending on boundary conditions (Goater et al. (2013)). In this study, E is assumed to be 1.5%.

*Table 3.2: Calculation of the storage capacity. E is storage efficiency.*

| ***Storage models*** | ***A ($m^2$)*** | ***H(m)*** | ***N/G*** | ***Porosity*** | ***PV ($m^3$)*** | ***$CO_2$ density ($kg/m^3$)*** | ***E (%)*** | ***$CO_2$ stored (Mkg)*** | ***Over- or under-estimate of storage (%)*** |
|---|---|---|---|---|---|---|---|---|---|
| ***Model 1*** | 30000 | 30 | 0.92 | 0.20 | 165600 | 760 | 1.5 | 2 | 0 |
| ***Model 2*** | 30000 | 30 | 0.98 | 0.20 | 176400 | 760 | 1.5 | 2.01 | + 6.3 |
| ***Model 3*** | 30000 | 20 | 0.97 | 0.20 | 116400 | 760 | 1.5 | 1.33 | - 29.6 |

This graph (Figure ***3.13***) shows the overestimation or underestimation ratio of the storage capacity as a function of the total thickness of reservoir, assuming that the transition zone has a constant thickness. The results reveal how a transition zone can have a significant effect on the storage capacity in this particular model.

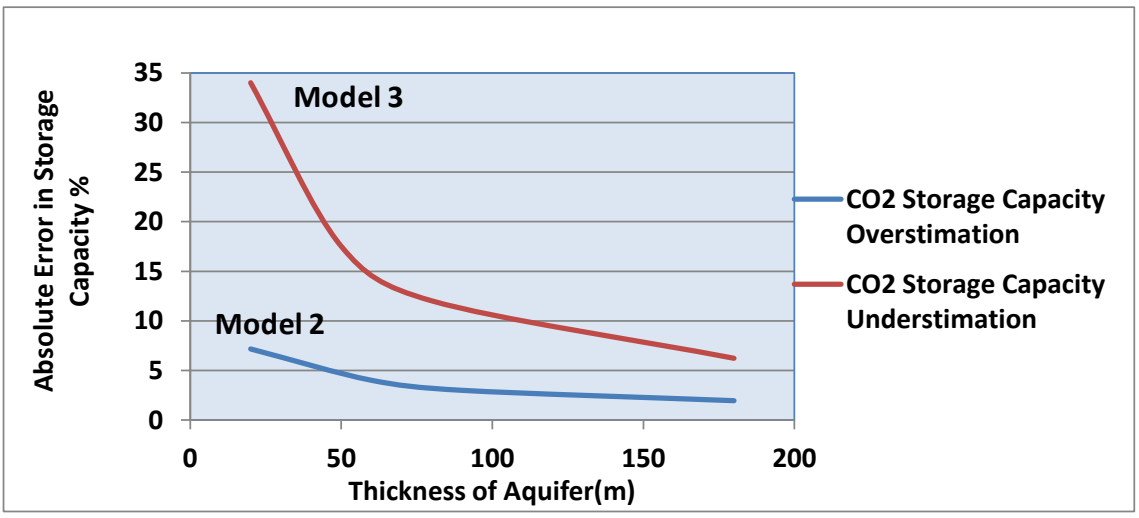


*Figure 3.13: Dependency of ratio of storage capacity to thickness of aquifer*

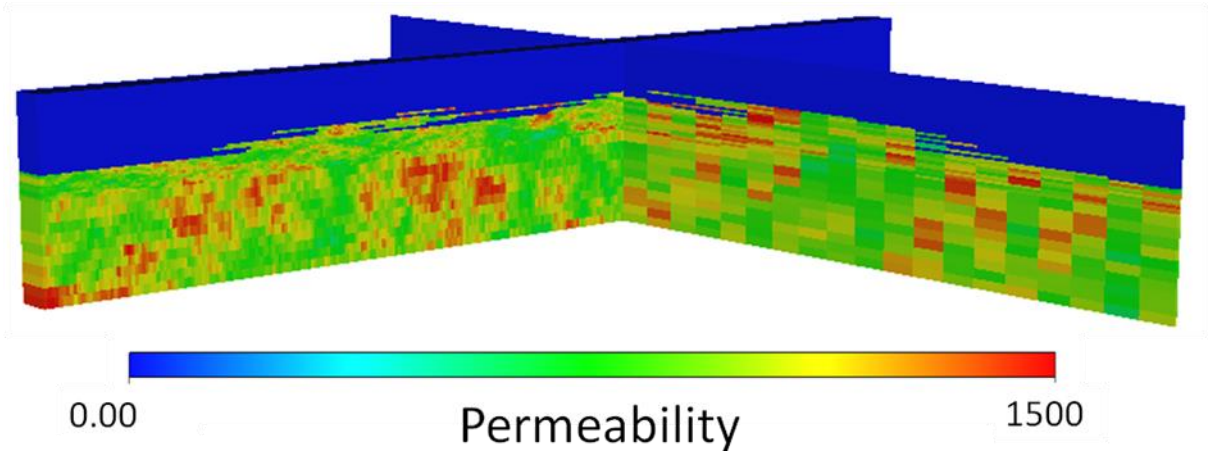


*Figure 3.14: Permeability distribution in a 3D model*

Figure ***3.14*** shows the permeability distribution in a 3D model with dimensions of 3000 m × 3000 m × 40 m which was discretized into 600×60×34 cells (Table ***3.3***). $CO_2$ was injected for 30 years through two vertical injectors and wells were completed in the bottom 3 layers of the aquifer. Simulation was continued for 100 years after the wells were shut in to predict the extent of $CO_2$ migration at the top of the aquifer. 2D models with dimensions of 3000 m × 100 m × 40 m which were discretized into 600×1×34 cells (Table ***3.3***) were also created. One vertical well was placed at the centre of the 2D models and the bottom three layers were completed. In all 2D models, the injectors were shut in after 30 years and the simulations were continued for 100 years. The same porosity and permeability values were used for sandstone and mudstone in the 2D and 3D models as they were used in the previous section (Table ***3.1***).

Figure ***3.15*** and Figure ***3.16*** show gas saturation in the 3D model and 2D models, respectively. After $CO_2$ is injected into the aquifer it rises up under buoyancy until it reaches any low permeable layer and then migrates laterally. This can be seen in both 2D and 3D models. These results reveal how the irregularity of the interface can have an effect on the security of $CO_2$ storage in the saline aquifer. This can have a negative effect if there are some paths in the interface to allow $CO_2$ to migrate through it and reach the caprock faster; otherwise it might have a positive effect by delaying the migration of $CO_2$ towards the caprock.

*Table 3.3 Layers and the sizes of layers in all (2D and 3D) models*

| | Layers | Thickness (m) | Thickness of each layer (m) |
|---|---|---|---|
| **Caprock** | 1- 4 | 10 | 2.5 |
| **Transition Zone** | 5 - 24 | 10 | 0.5 |
| **Aquifer** | 25 - 34 | 20 | 2 |

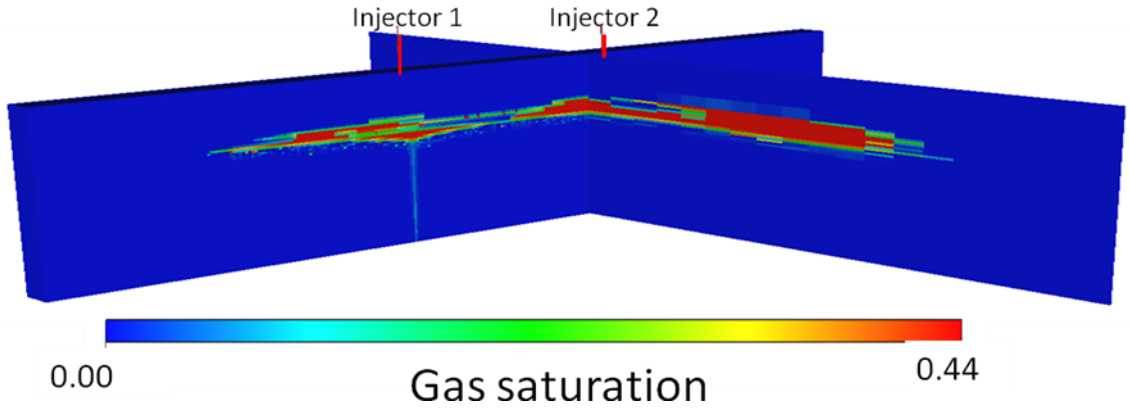


*Figure 3.15: Gas Saturation after 100 years post injection in a 3D model.*

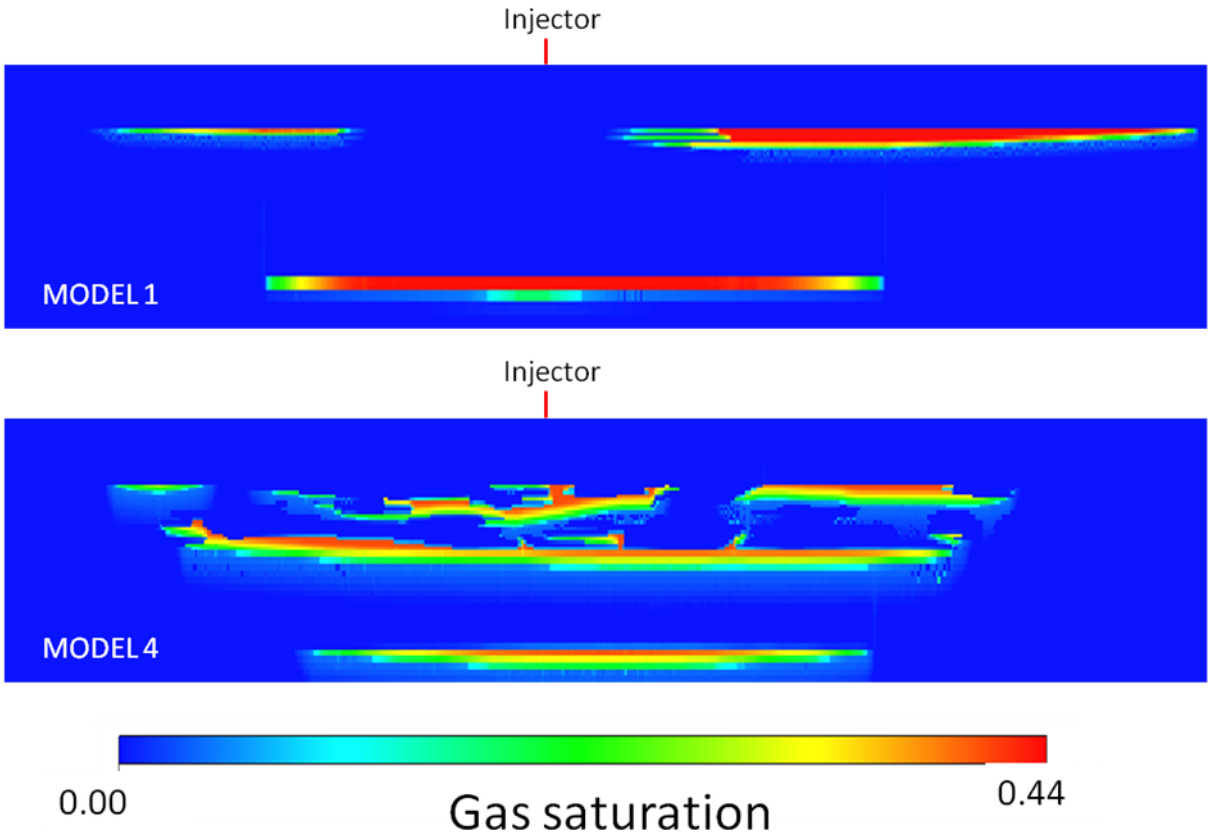


*Figure 3.16: Gas Saturation after 100 years post injection, in the 2D models.*

## 3.3 Study of the effect of top surface morphology assumes a homogeneous model

### *3.3.1 Introduction:*

Although, Nilsen et al. (2012) used a semi-analytical spill-point analysis and vertical equilibrium in order to calculate the storage capacity, they did not consider a combination of all relevant effects such as top morphology, tilt, and $k_V/k_H$ on the $CO_2$ storage. They did not study the effect of a transition zone either. The existence of any transition zone has not been addressed in previous works. The length and width of plume migration with transition zone and amplitude of ridges, which are very important for security of $CO_2$ storage, also have not been addressed. Therefore, this section has described a systematic study of the effect of parallel and perpendicular ridges to determine their effect on up-dip and lateral migration. A set of numerical simulations was conducted to investigate the impacts of the transition zone, top morphology, tilt and $k_V/k_H$ on the $CO_2$ storage. For this reason two types of models were created. The first type was created to study the impact of aquifer/caprock morphology. The second type was created to study the impact of transition zone (refered to as "*trans"*). In the former two main scenarios were considered. In the first one, ridges are perpendicular to the tilt ("*perp"* models). In the second one ridges are parallel to the tilt (it is called "*para"*).

### *3.3.2 Model Specifications*

Equation 3.1 was used to make top surfaces for the ridges. A simple model was chosen for the top surface, so that the properties could be studied methodically.

$$Z = Z_0 + A(Sin(\frac{2\pi x}{\lambda})) + x(\tan\theta) \quad (3.1)$$

where,

$A$ refers to amplitude of the ridges (m)

$x$ denotes the length of each point in the X (horizontal) direction (m)

$\lambda$ refers to wavelength which is 1000m here

$\theta$ refers to tilt angle

As depicted in Figure ***3.17***, the sizes of all the models are 8 km × 8 km × 100 m. One injector was placed on the left hand side of model and $CO_2$ injected through perforations at the bottom of the aquifer (bottom 50 layers). The models represented part of a larger aquifer, and the pore volume of the outer column of cells on the opposite

side of where injector was placed, was multiplied by a factor of 10E+9, to take account of this.

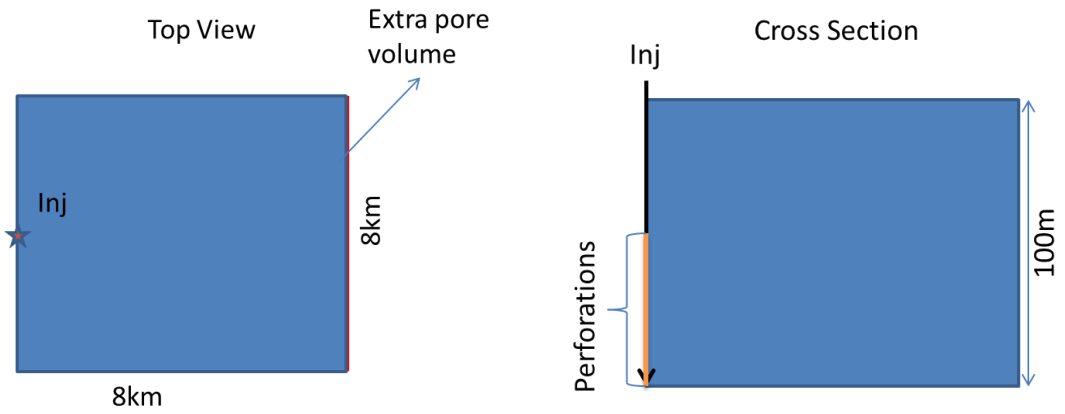


*Figure 3.17 Schematic top view (left picture) and cross section (right picture) of model. The injector is placed at the edge of models on the left side.*

Table ***3.4*** shows all the scenarios (144 models) that were used in this study (for more detail see Appendix B1). All models have the same dimensions and the same grid cell sizes (100 m × 100 m × 1 m). In all the models, the sandstone was homogeneous with constant porosity (0.2) and constant permeability (500 mD) and impermeable for mud layers in *trans* models. The datum depth was set to be 1500 m to keep the models always below 800 m, even in the tilted models, in order to keep injected $CO_2$ in the supercritical phase.

*Table 3.4***:** *Model Specifications*

| **Perp/Para/*Trans*** | **Amplitude (m)** | **Angle (θ)** | **$k_V/k_H$** |
|---|---|---|---|
| | **0** | **0** | **0.01** |
| | **3** | **1** | **0.1** |
| | **6** | **2** | **1** |
| | **9** | **5** | |

It should be noted that amplitude in the *trans* models refers to the half of thickness of the transition zone. Sequential Gaussian simulation was used to generate the facies distribution and the permeability and porosity were correlated with that.

The $CO_2$ injection rate was chosen to be half of the $CO_2$ emissions of a 500 MW coal-fired power plant which is around 2 million tons of $CO_2$ per year. The well was controlled by surface rate with a maximum pressure limit of 220 bars. However, in all models studied here the same amount of $CO_2$ was injected into the models, as the pressure did not reach the maximum bottom-hole pressure. The injector was shut in after 6 years and the simulation was continued for 100 years.

The models are described by four parameters:
The first part is the type of the model, which could be *para*, *perp* or *trans*.
The second one is the amplitude (A).
The third one is the tilt (D).
The forth one is $k_V/k_H$ ratio (K).

For instance, Model Perp-A9-D5-K001 refers to a simulation with perpendicular ridges, amplitude of 9 m, tilt equals 5 degrees and $k_V/k_H$ ratio equals 0.01. Figure 3.18 shows top morphology of models with amplitudes equal 9 metres and different tilts (0-5, degrees).

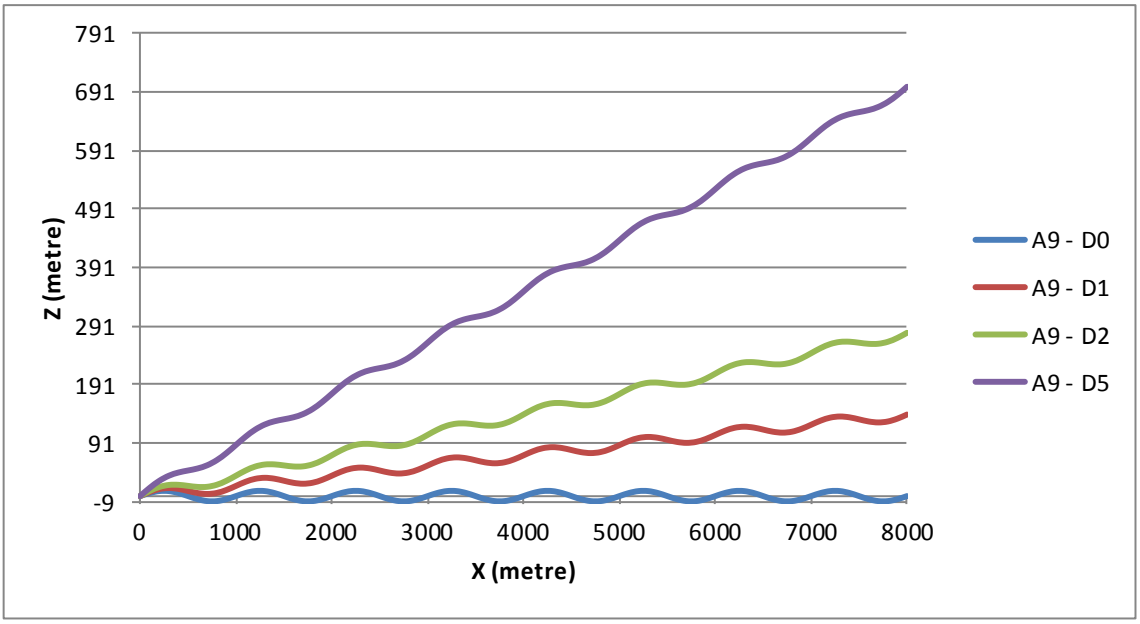


*Figure 3.18 Top morphology of perp models with amplitudes equal 9 metres and different tilts (D0-D5).*

### *3.3.3 Results and Discussion*

***Para Models, Injection Period***

Figure *3.19*, Figure *3.20* and Figure *3.21* demonstrate the relation between the amounts of dissolved $CO_2$ (in percentage) at the end of injection period with $k_V/k_H$ ratio, amplitude and tilt respectively. It is very clear that the results are more sensitive to the $k_V/k_H$ ratio than other parameters.

The lower the $k_V/k_H$ ratio the higher the amount of dissolved $CO_2$. This is because the low permeability is preventing the rise of $CO_2$ therefore more $CO_2$ spreads laterally during the injection. Thus, more free $CO_2$ phase is in contact with fresh brine resulting in more $CO_2$ dissolution in the model with lower $k_V/k_H$ ratio (Figure *3.22*).

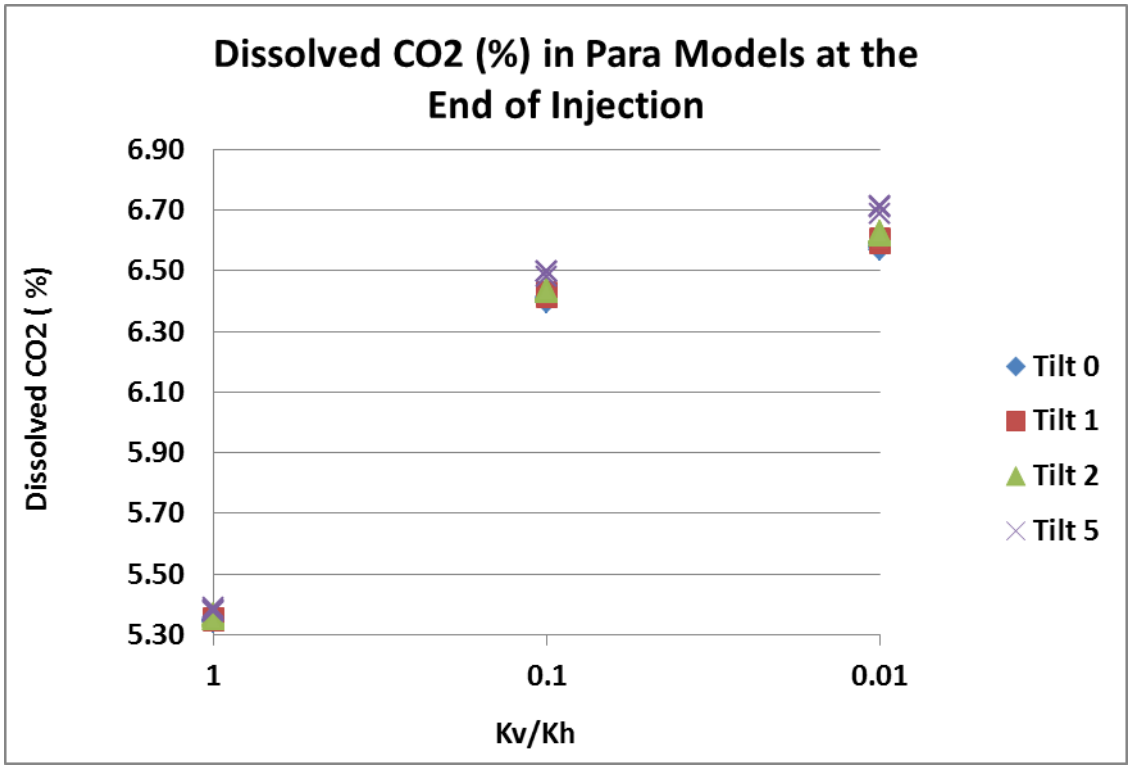


*Figure 3.19 The amount of dissolved $CO_2$ in the para models at the end of injection comparing $k_V/k_H$ ratio and tilt.*

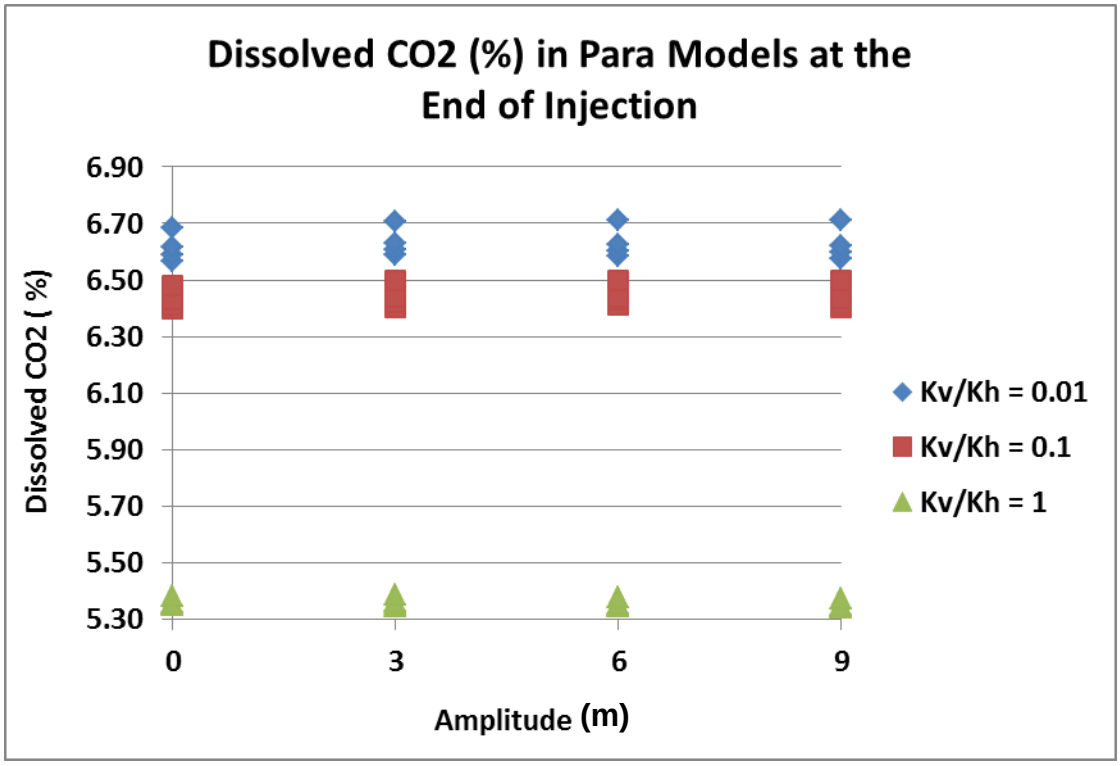


*Figure 3.20 The amount of dissolved $CO_2$ in the para models at the end of injection comparing amplitude and $k_V/k_H$ ratio.*

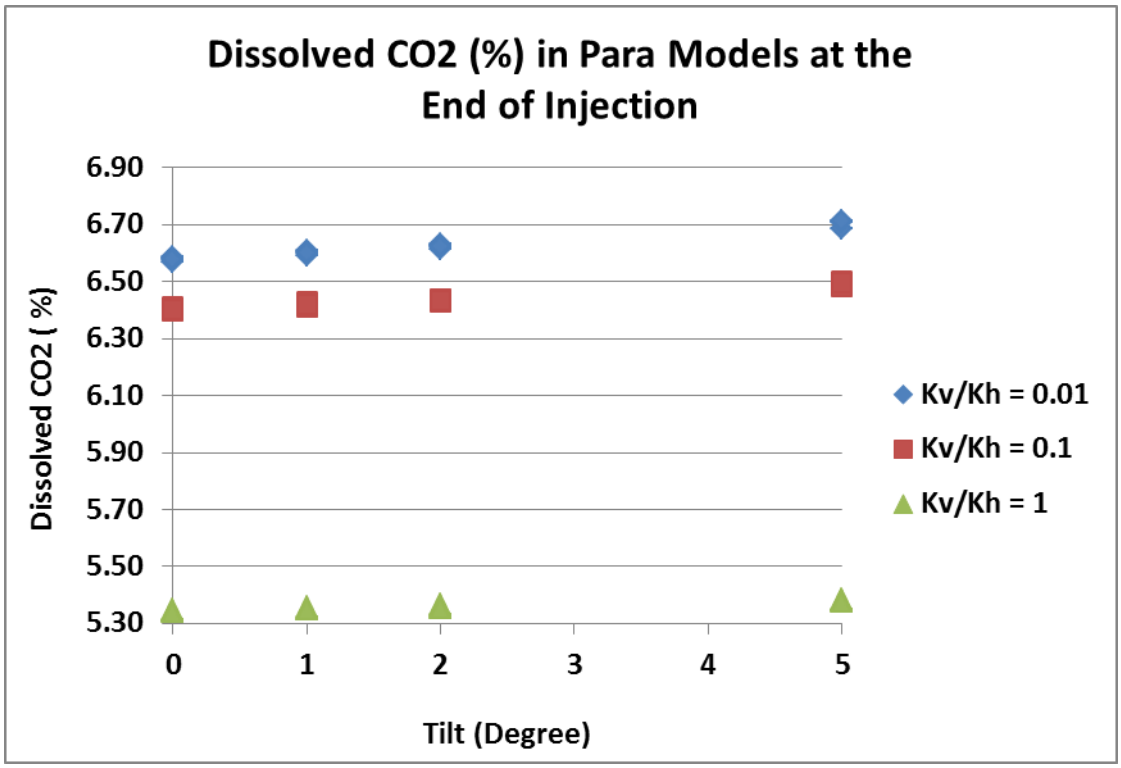


*Figure 3.21 The amount of dissolved $CO_2$ in the para models at the end of injection comparing tilt and $k_V/k_H$ ratio.*

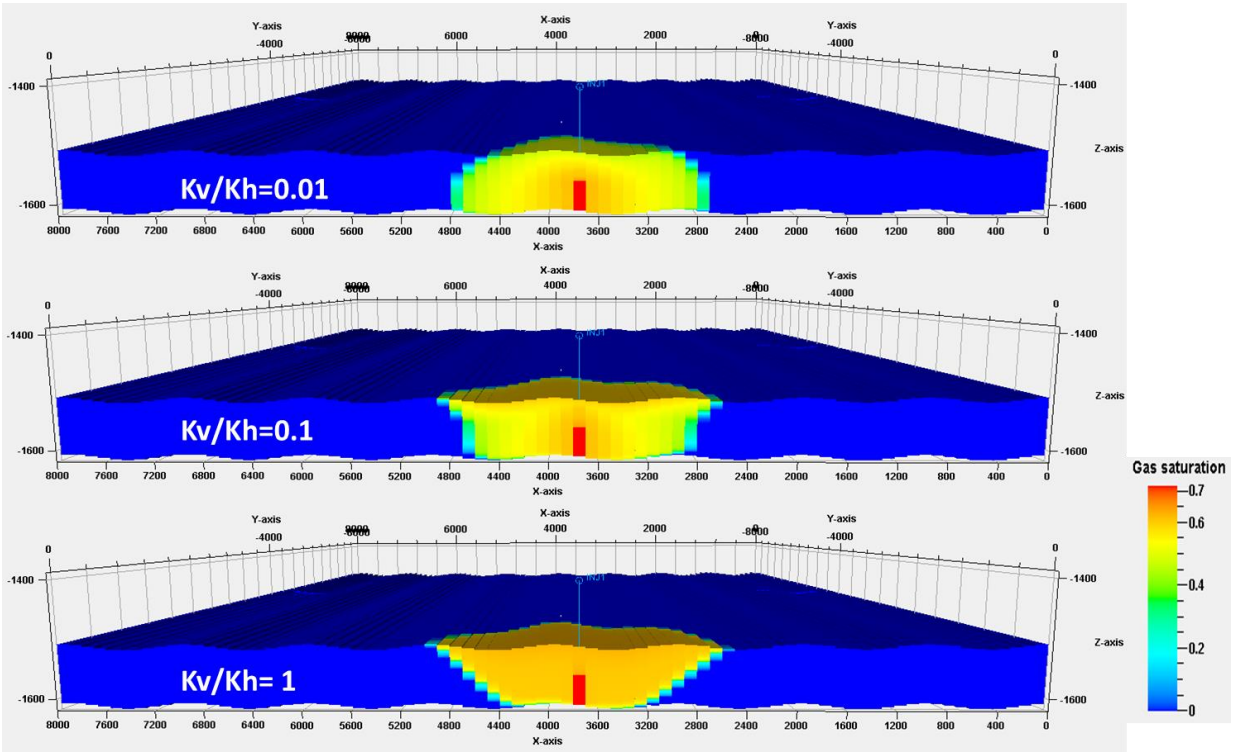


*Figure 3.22 Gas saturation at the end of injection in para models which have zero tilt with the same amplitudes (9) and different $k_V/k_H$ ratios. More $CO_2$ spreads out around the injector at the model with lower $k_V/k_H$ ratio (top picture).*

***Para Models, Post Injection Period***

Figure *3.23*, *Figure 3.24* and *Figure 3.25* show percentage of injected gas which exists as dissolved gas in all *para* models with respect to tilt, $k_V/k_H$ ratio and amplitude 100 years post injection. During this period the amount of dissolved $CO_2$ is sensitive to the tilt and $k_V/k_H$ ratio (Figure *3.23* and *Figure 3.24*) whereas the effect of amplitude is negligible. Below these results are discussed in more detail.

**Effect of Tilt:**

The effect of tilt is more important as the higher the tilt the more $CO_2$ migrates up-dip (Figure *3.26*) and therefore more $CO_2$ is in contact with fresh brine resulting in more $CO_2$ dissolved in models with higher tilt. From 0 to 2 degrees tilt approximately 1% more $CO_2$ is dissolved per 1 degree tilt. However, this change is more than 1% when tilt is increased to 5 degree.

The higher the tilt angle the more segregation between results of models with high and intermediate $k_V/k_H$ ratio.

**Effect of $k_V/k_H$ ratio:**

If the models are flat, most $CO_2$ is dissolved in the models with the intermediate $k_V/k_H$ ratio, next the models with lowest $k_V/k_H$ ratio and the least $CO_2$ is dissolved in the isotropic models ($k_V/k_H$ =1). By increasing the tilt angle to 5 degrees, more $CO_2$ is dissolved in the isotropic models. This is because greater $CO_2$ migrates upwards resulting in more $CO_2$ in contact with fresh brine.

**Effect of Amplitude:**

Results show that despite increasing the amplitude from 0 to 9 m, approximately the same amount of $CO_2$ is dissolved 100 years post injection period in all models. This is due to the fact that when the $CO_2$ reaches the top sand layer, it starts to fill and migrate along the closest ridge. If the thickness of the plume is more than the amplitude, $CO_2$ moves laterally to the next ridges and fills them while migrating parallel to them. Therefore there is no obstacle to prevent $CO_2$ migration. Therefore amplitude does not have a significant effect on the amount of $CO_2$ dissolution in the *para* models.

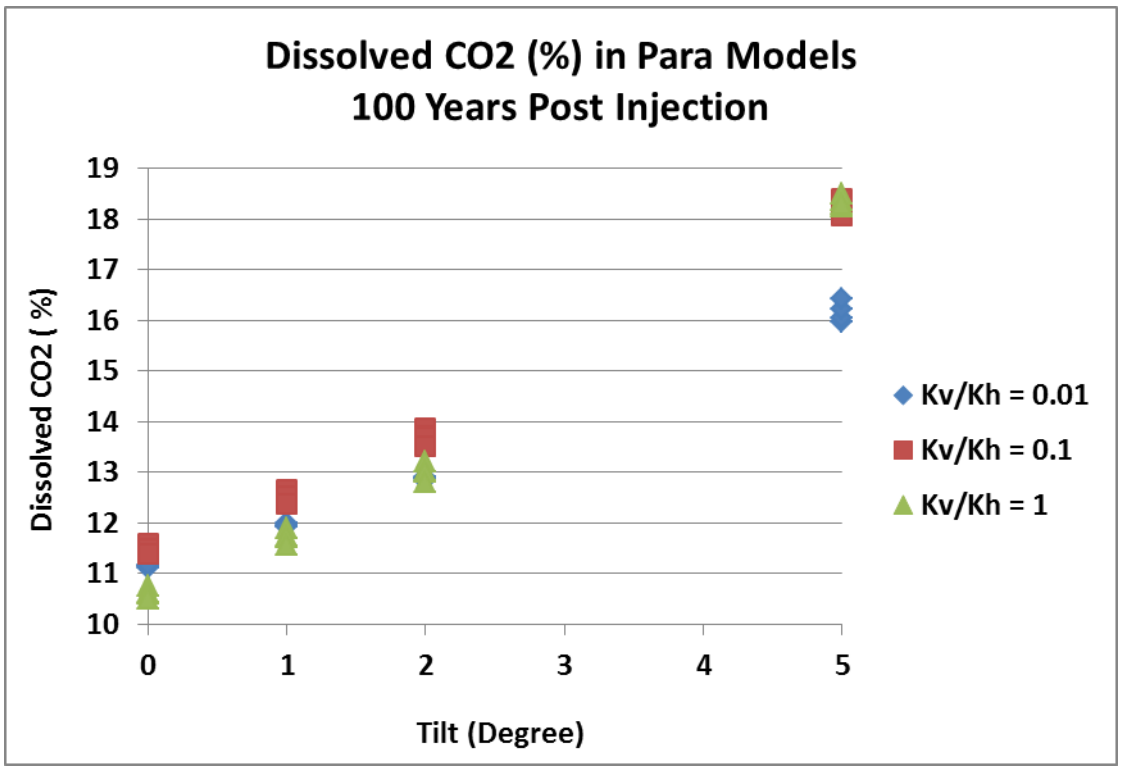


*Figure 3.23 The amount of dissolved $CO_2$ in the para models 100 years post injection period comparing tilt and $k_V/k_H$ ratio.*

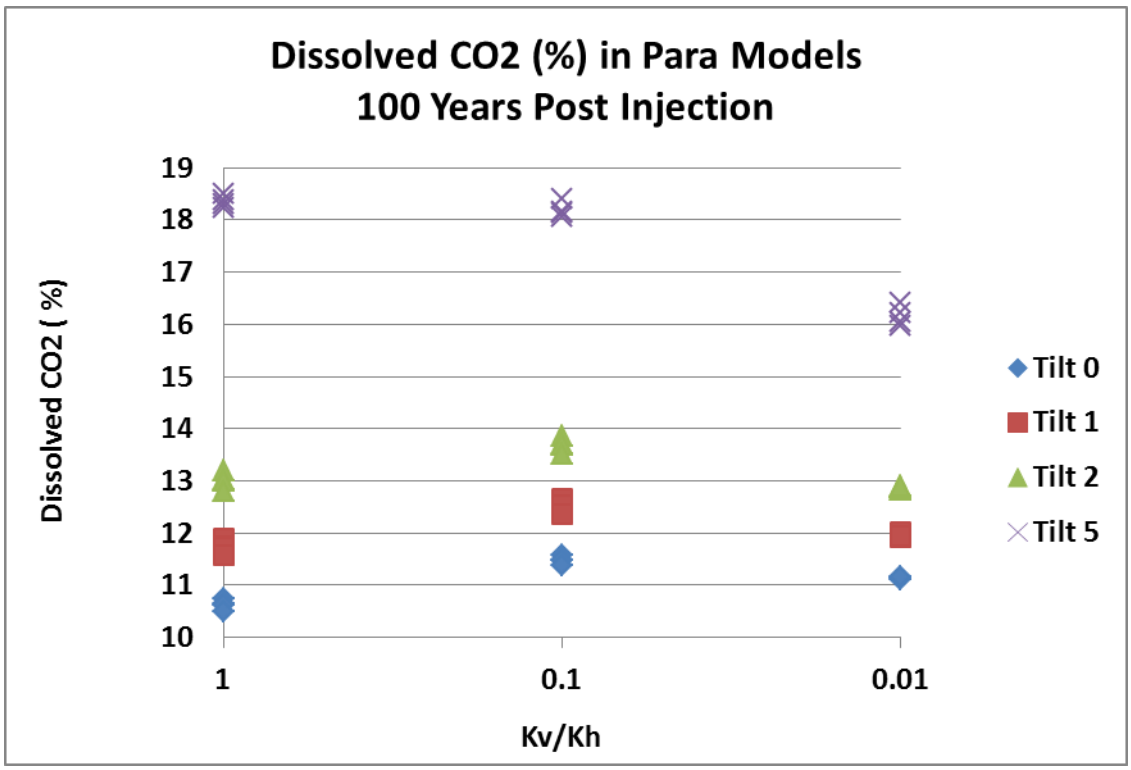


*Figure 3.24 The amount of dissolved $CO_2$ in percentage in para models 100 years post injection period with $k_V/k_H$ ratio and tilt.*

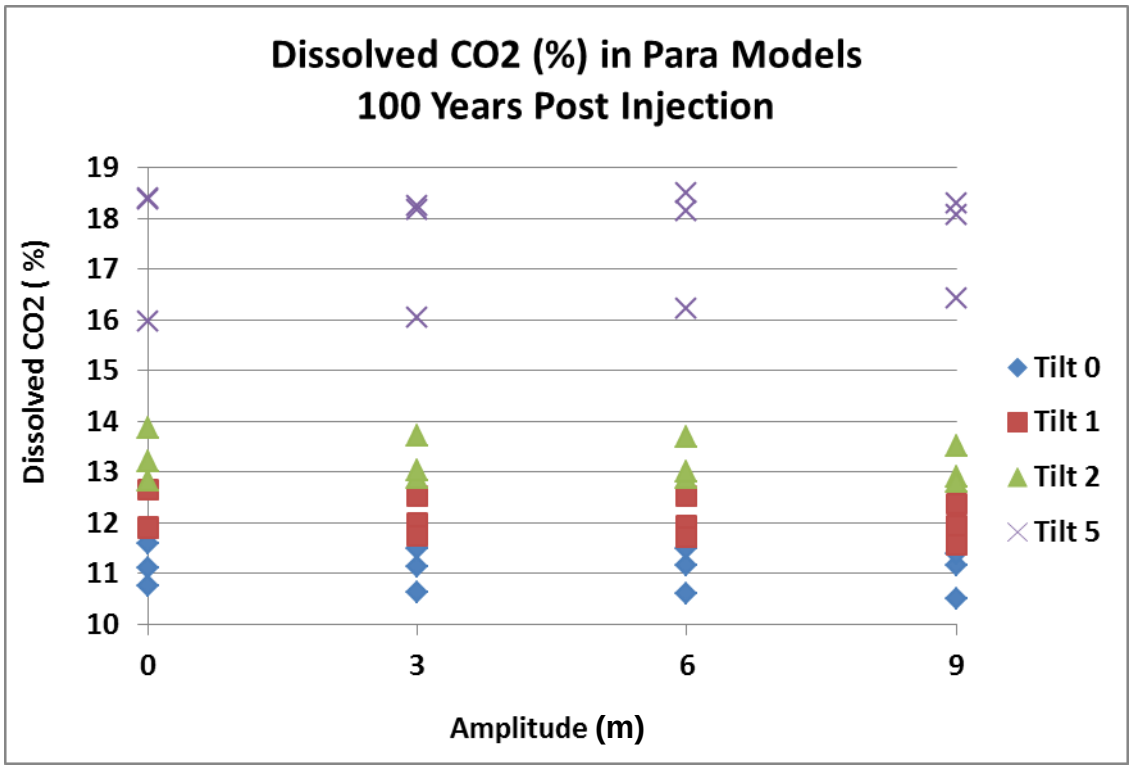


*Figure 3.25 The amount of dissolved $CO_2$ in percentage in para models 100 years post injection period with amplitude and tilt.*

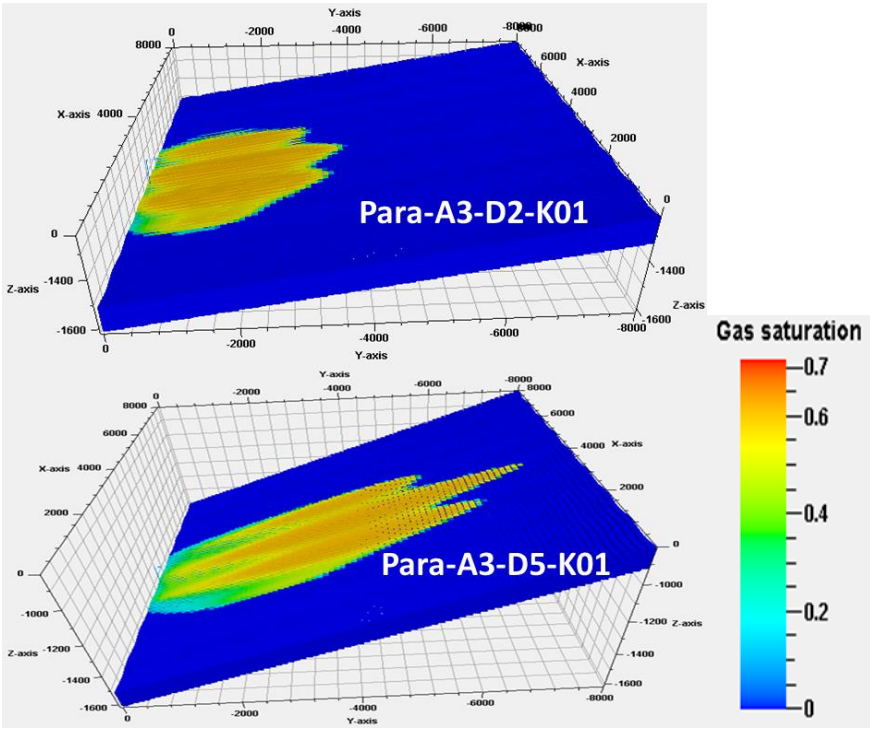


*Figure 3.26 Gas saturation 100 years post injection period in two para models. Top picture refers to a para model with amplitude 3, 2 degree tilted and $k_V/k_H$ equals 0.01. Bottom picture refers to a para model with the same amplitude and $k_V/k_H$ ratio with the top one but 5 degree tilted.*

***Perp Models***

Results show that the effect of the $k_V/k_H$ ratio and tilt on the amount of $CO_2$ dissolution during the injection period and 100 years post injection in *perp* models is the same as for the *para* models (Figure *3.27* and Figure *3.28*). However, amplitude has a slight effect on the amount of $CO_2$ dissolution in *perp* models whereas this was negligible in *para* models.

**Effect of amplitude:**

By increasing amplitude from 0 to 9 m the amount of dissolved $CO_2$ falls to around 1% (Figure *3.29*). This is because of the structural trapping that occurs in perp models. The bigger the amplitude, the more $CO_2$ is trapped structurally, and therefore less $CO_2$ migrates along the tilt direction, resulting in less $CO_2$ dissolution.

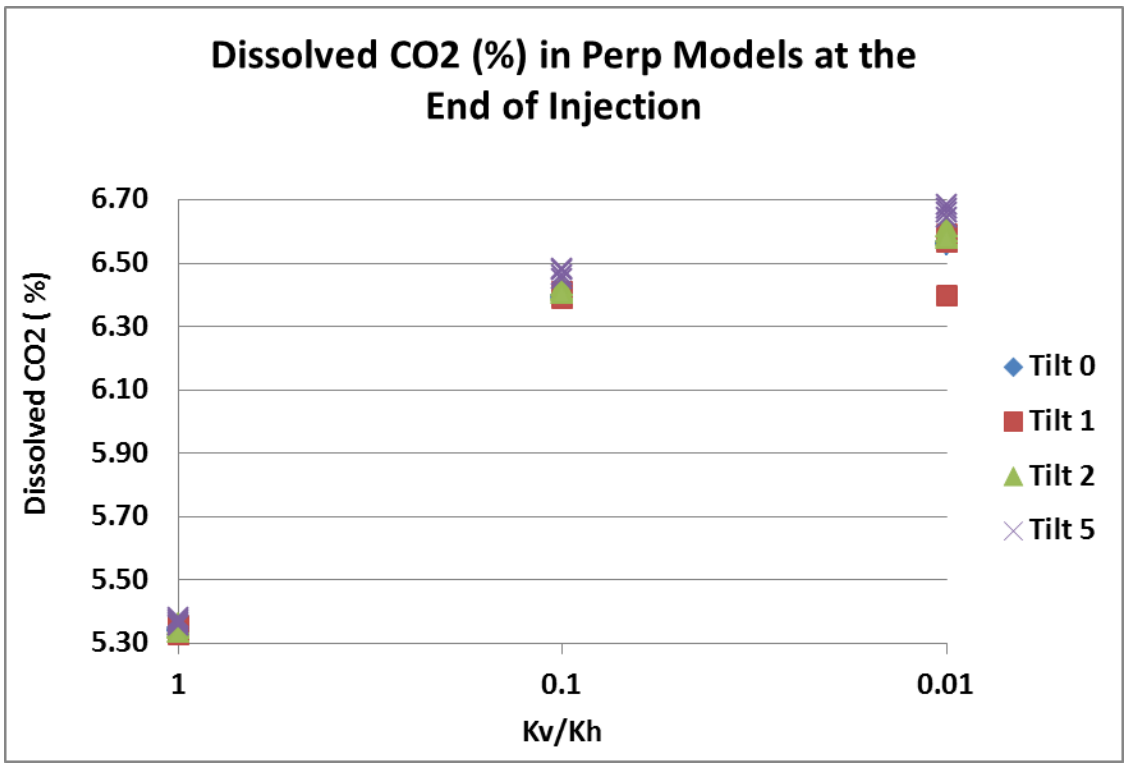


*Figure 3.27 The amount of dissolved $CO_2$ in the perp models at the end of injection comparing $k_V/k_H$ ratio and tilt.*

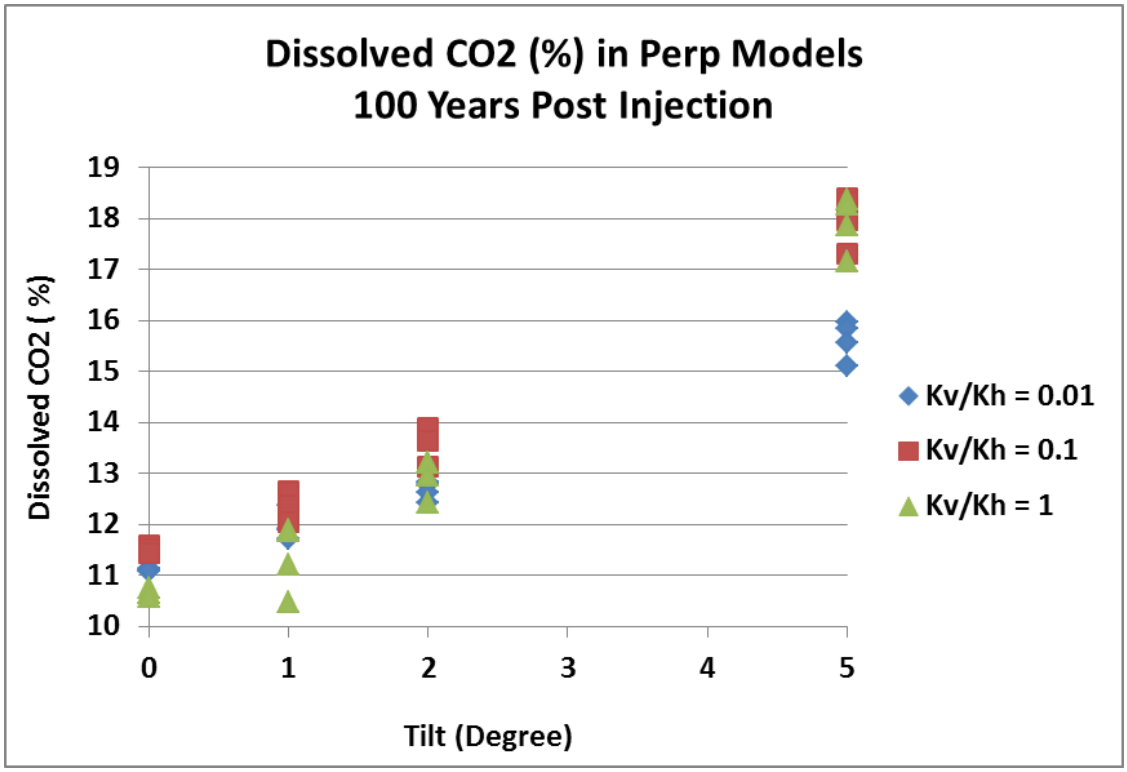


*Figure 3.28 The amount of dissolved $CO_2$ in the perp models at the end of injection comparing tilt and $k_V/k_H$ ratio.*

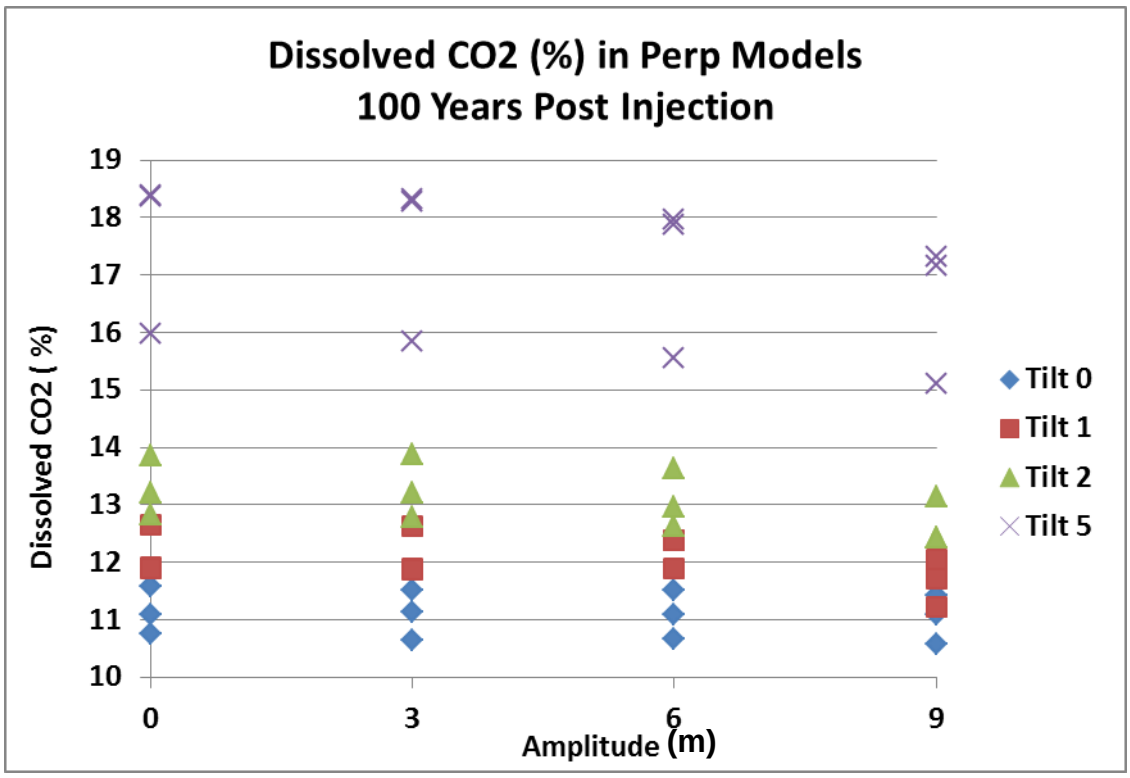


*Figure 3.29 The amount of dissolved $CO_2$ in the perp models 100 years post injection period comparing amplitude and tilt.*

***Plume Migration in para and perp Models***

In this section the plume migration for the *para* and *perp* models at the end of injection and 100 years post injection period is studied. The length and the width of the plume (where $CO_2$ saturation is more than 0.1) were examined to study the effect of $k_V/k_H$ ratio, tilt and amplitude on plume migration. Length refers to the distance where $CO_2$ migrates parallel to the tilt and width refers to the distance where $CO_2$ moves perpendicular to the tilt direction. In this study, "width" refers to half the width of the plume, i.e. the lateral distance moved from the injector. This is to be consistent with the length (because the injection is at the edge of the model).

***Para Models, End of Injection***

Figure *3.30*, Figure *3.31* and Figure *3.32* demonstrate the length and the width of the plume for *para* models at the end of injection with respect to the effect of $k_V/k_H$ ratio, tilt and amplitude respectively. The most sensitive parameter during the injection amongst these three is $k_V/k_H$ ratio.

**Effect of $k_V/k_H$ Ratio:**

The higher the $k_V/k_H$ ratio the greater are the width and the length of the plume. When the $k_V/k_H$ ratio is higher the vertical transmissibility is higher. Thus, more $CO_2$ reaches

the top of the storage formation and more $CO_2$ spreads out at the top of storage formation (Figure *3.30*). There is not a significant difference between width and length of plume during the injection.

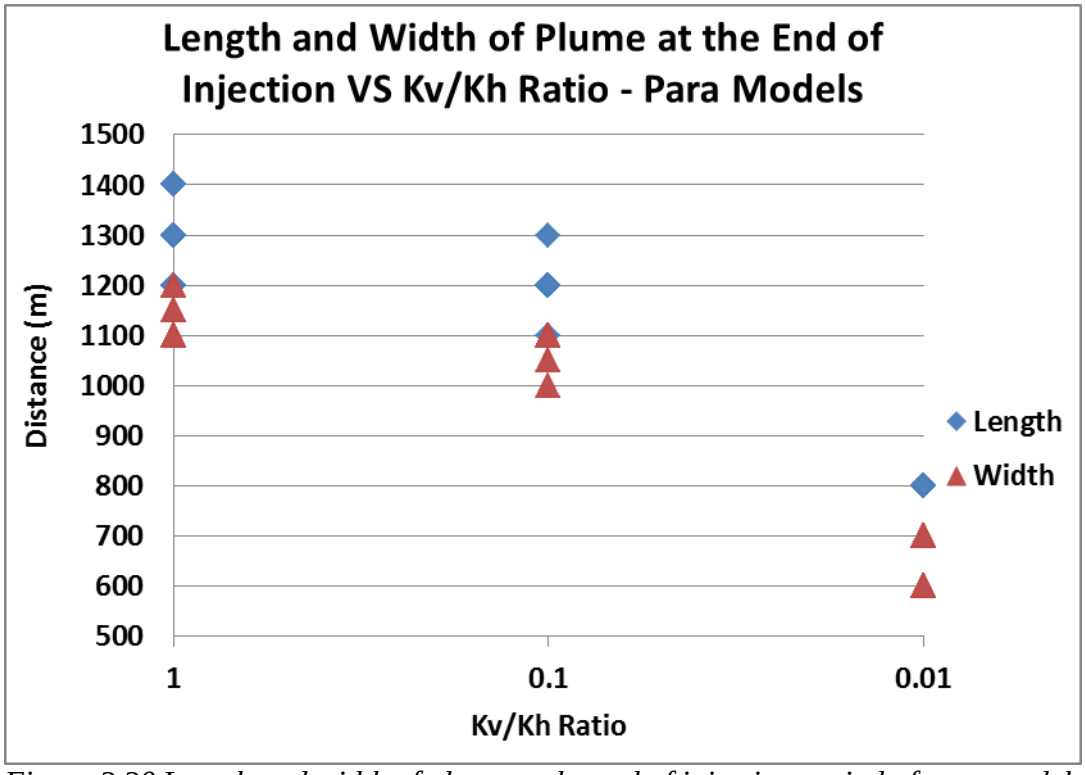


*Figure 3.30 Length and width of plume at the end of injection period of para models with $k_V/k_H$ ratio.*

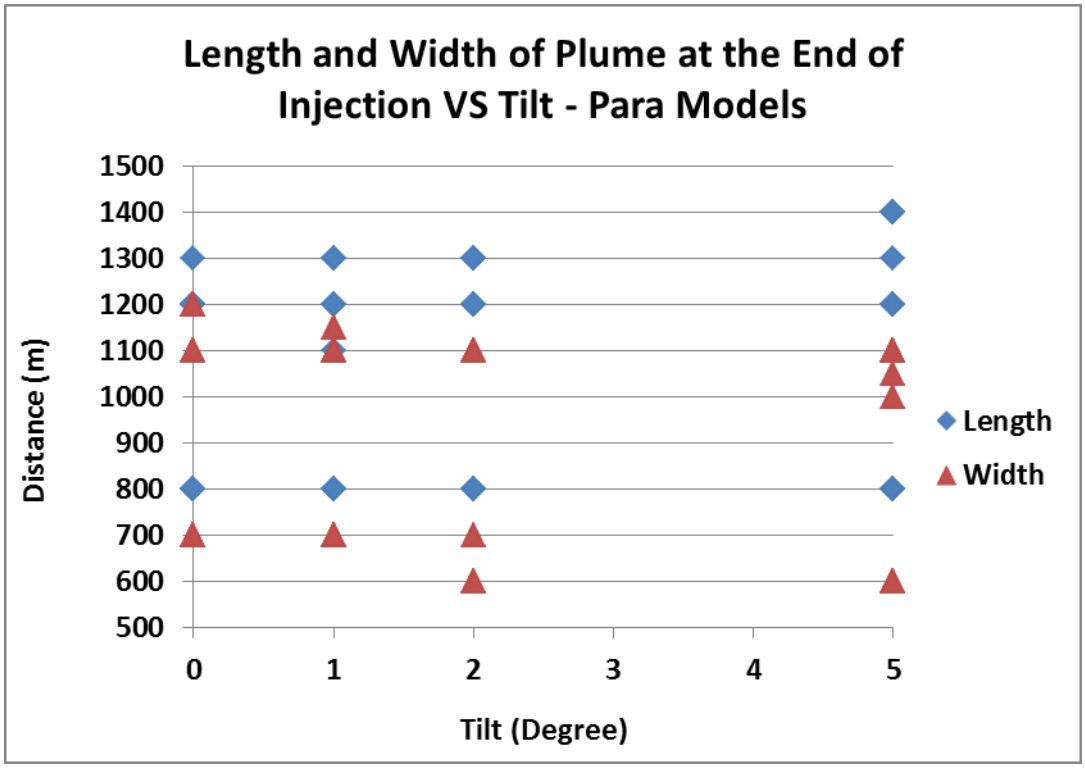


*Figure 3.31 Length and width of plume at the end of injection period of para models with tilt.*

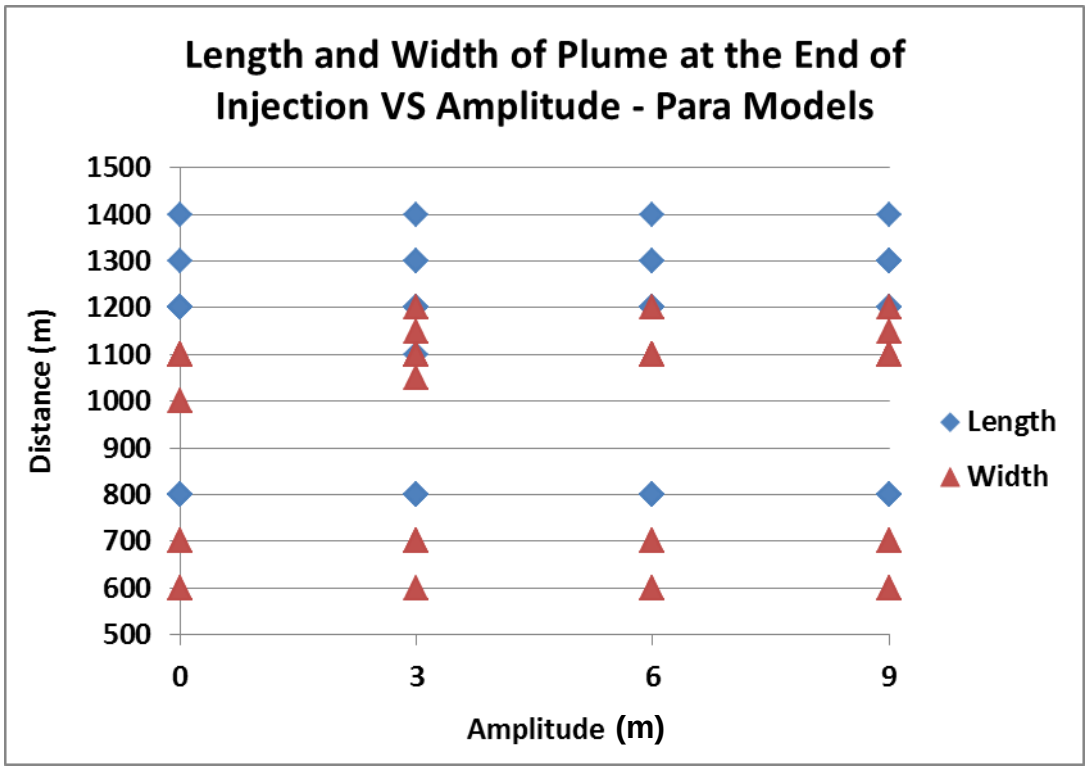


*Figure 3.32 Length and width of plume at the end of injection period of para models with $k_V/k_H$ ratio.*

***100 Years Post Injection***

Figure ***3.33***, *Figure 3.34*, and *Figure 3.35* shows width and length of plume 100 years post injection period verses $k_V/k_H$ ratio, tilt, and amplitude respectively.

**Effect of $k_V/k_H$ ratio:**

The effect of $k_V/k_H$ ratio on width is not very significant whereas it has a significant effect on the length of the plume (Figure ***3.33***).

**Effect of Tilt:**

This effect on the width of the plume is not significant; however, the width of the plume becomes shorter with increasing tilt. By increasing the tilt from 0 to 2 degrees the length of the plume does not change significantly; however, by increasing it to 5 degrees there is a significant change in the length of the plume. This is due to the fact that $CO_2$ tends to migrate up-dip under buoyancy.

**Effect of Amplitude:**

The width of the plume decreases with the amplitude (Figure *3.36*). The length of the plume increases with the amplitude (Figure *3.36*).

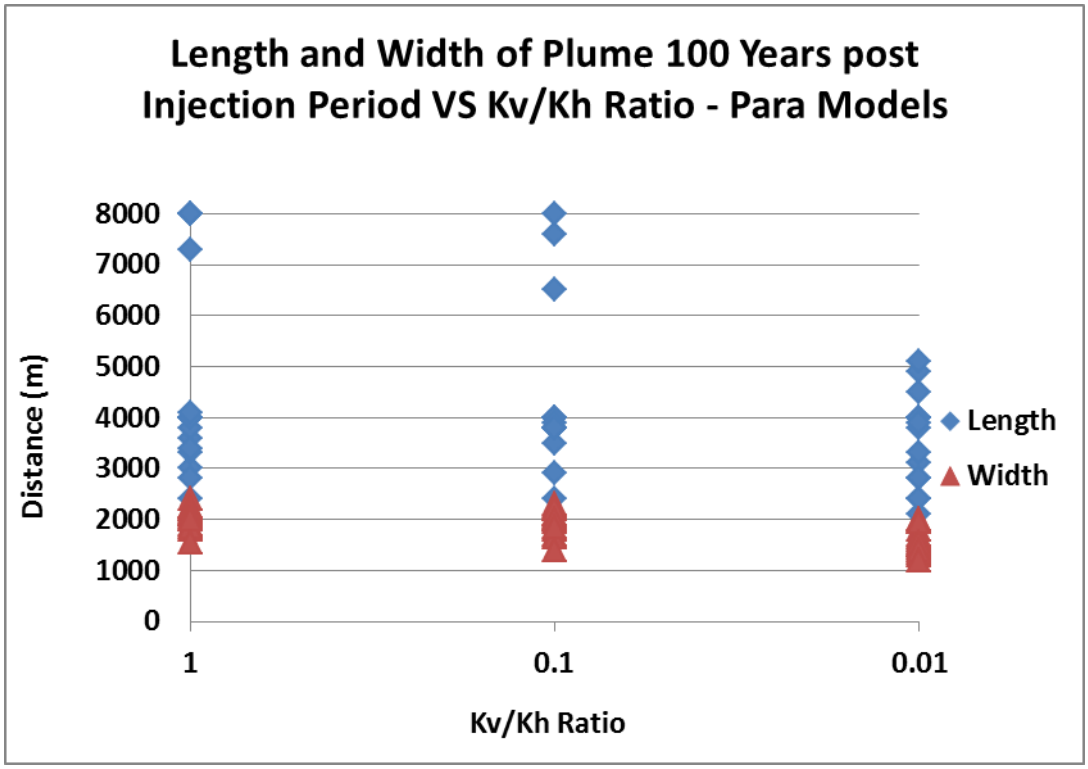


*Figure 3.33 Length and width of plume of para models with $k_V/k_H$ ratio100 years post injection.*

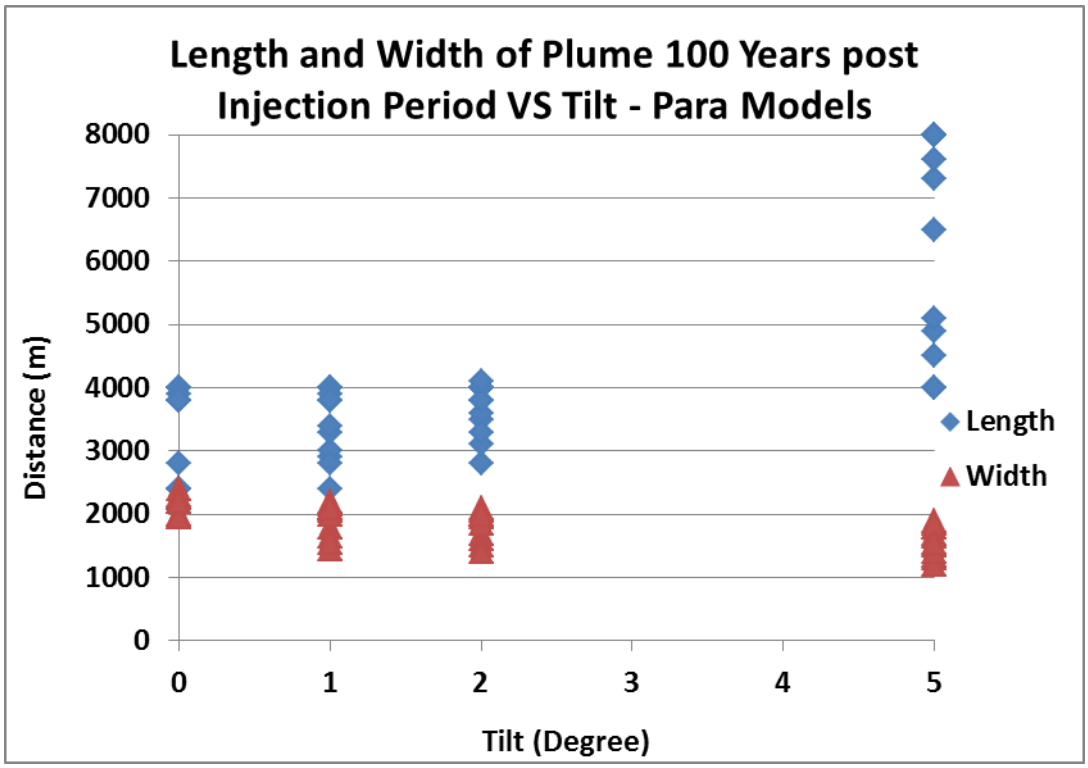


*Figure 3.34 Length and width of plume of para models with tilt 100 years post injection.*

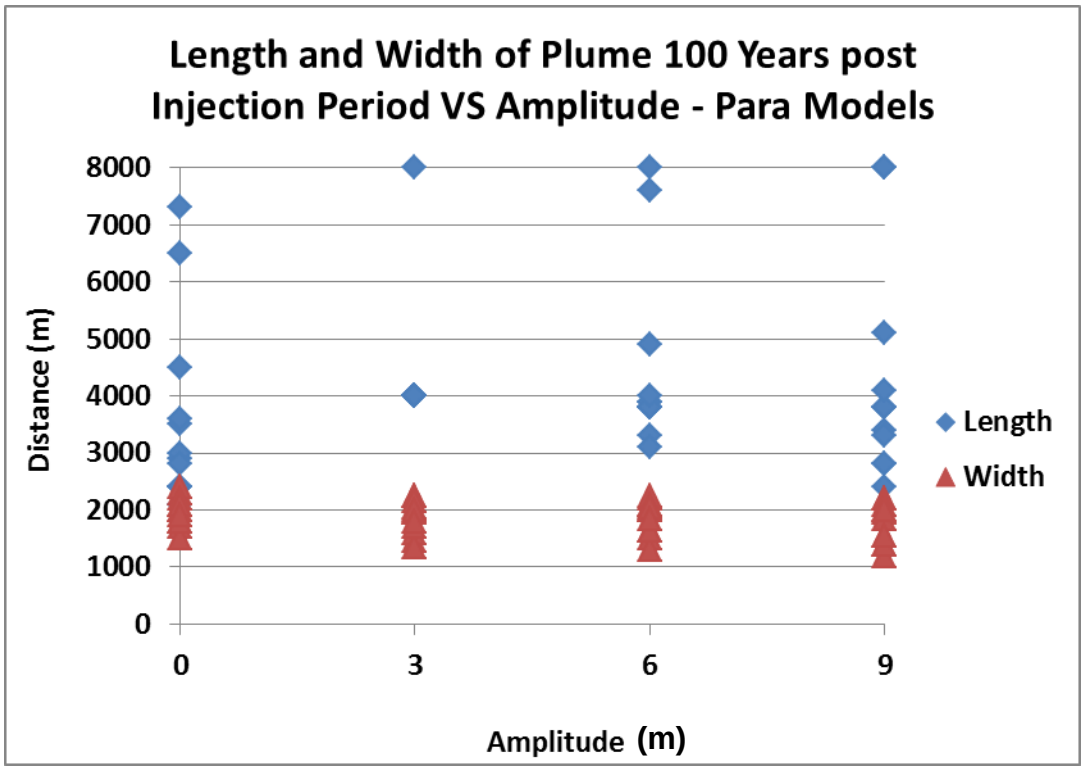


*Figure 3.35 Length and width of plume of para models with amplitude100 years post injection.*

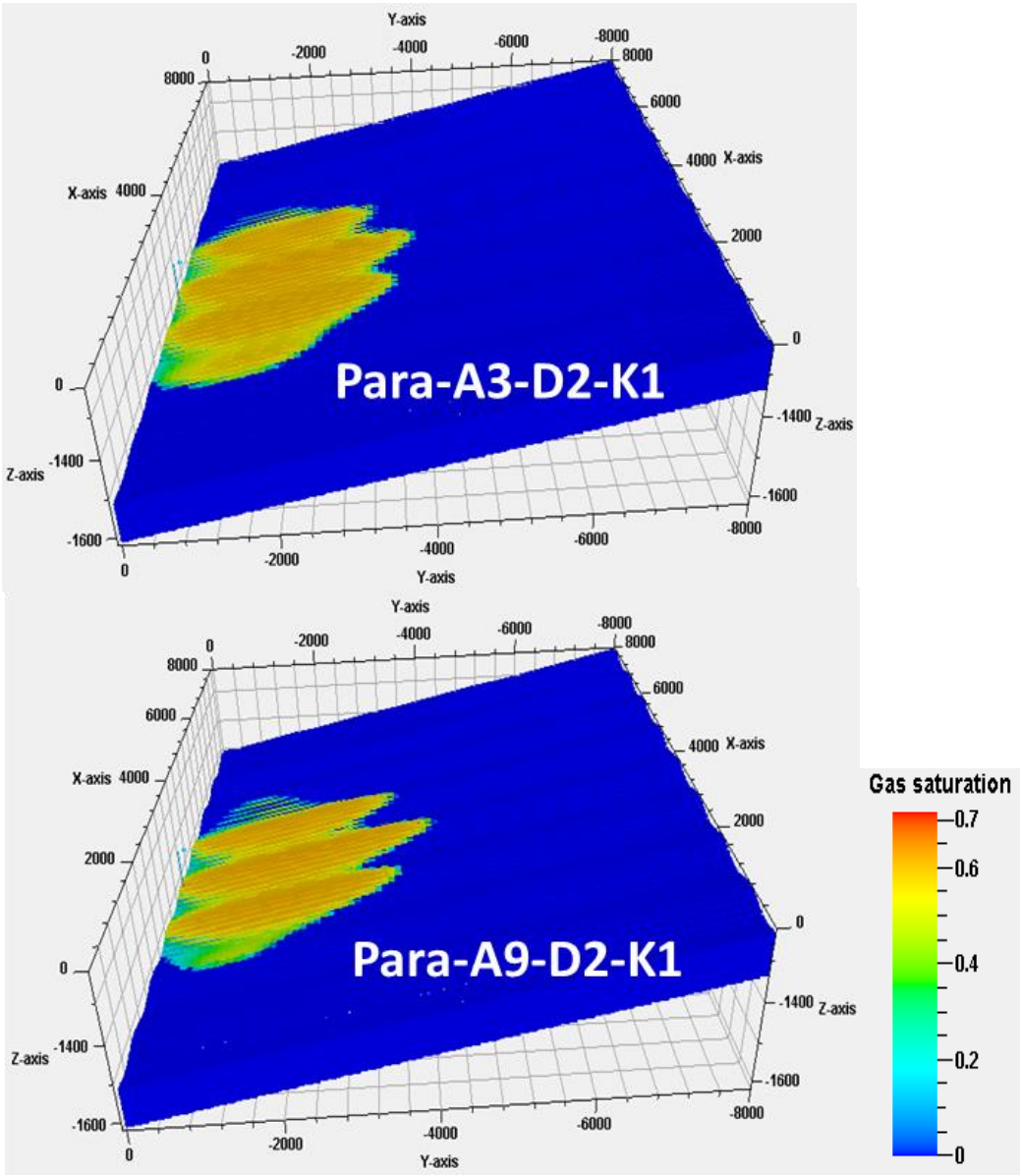


*Figure 3.36 Gas saturation 100 years post injection in two para models with the same tilt and $k_V/k_H$ ratio and different amplitudes. Top picture with the smaller amplitude (3 m) and bottom one with bigger amplitude (9 m).*

***Perp Models, End of Injection:***

Figure *3.37*, Figure *3.38*, and Figure *3.39* illustrate the length and the width of the plume at the end of the injection period versus $k_V/k_H$ ratio, tilt, and amplitude in *perp* models, respectively. Results show that all three factors have some effect on the length and width of the plume.

**Effect of $k_V/k_H$ Ratio:**

The width and length of the plume decrease with decreasing $k_V/k_H$ ratio (Figure *3.37* and Figure *3.40*). The width and length of the plume are similar at the low $k_V/k_H$ ratio (Figure *3.37* and Figure *3.40*).

**Effect of Tilt:**

The width of the plume does not change significantly with tilt. The length of plume increases with tilt for some models (high $k_V/k_H$ ratio and low amplitude) (Figure *3.38* and Figure *3.39*).

**Effect of Amplitude:**

The width of the plume increases with amplitude. By increasing amplitude more $CO_2$ needs to fill the ridge to migrate to the next ridges and meanwhile more $CO_2$ migrates laterally. Thus the width of the plume is bigger in the high amplitude models than in the low amplitude models. The length of the plume decreases with amplitude as more $CO_2$ is trapped structurally under ridges with bigger amplitude.

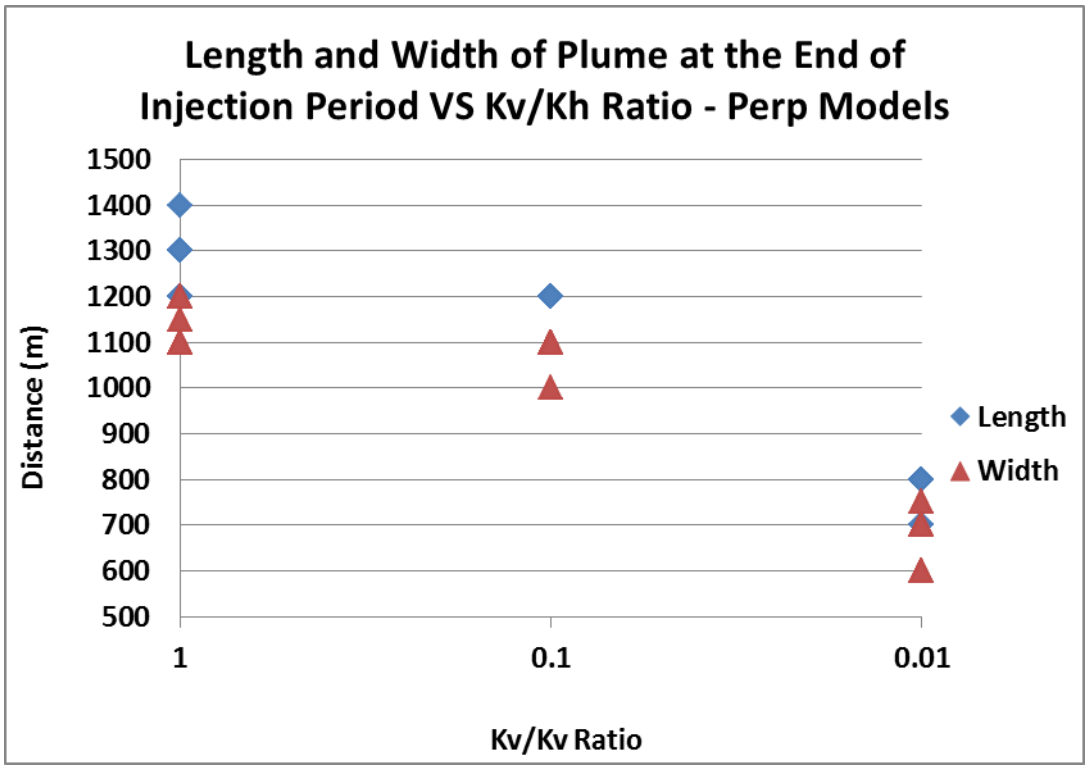


*Figure 3.37 Length and width of plume of perp models with $k_V/k_H$ ratio, at the end of injection.*

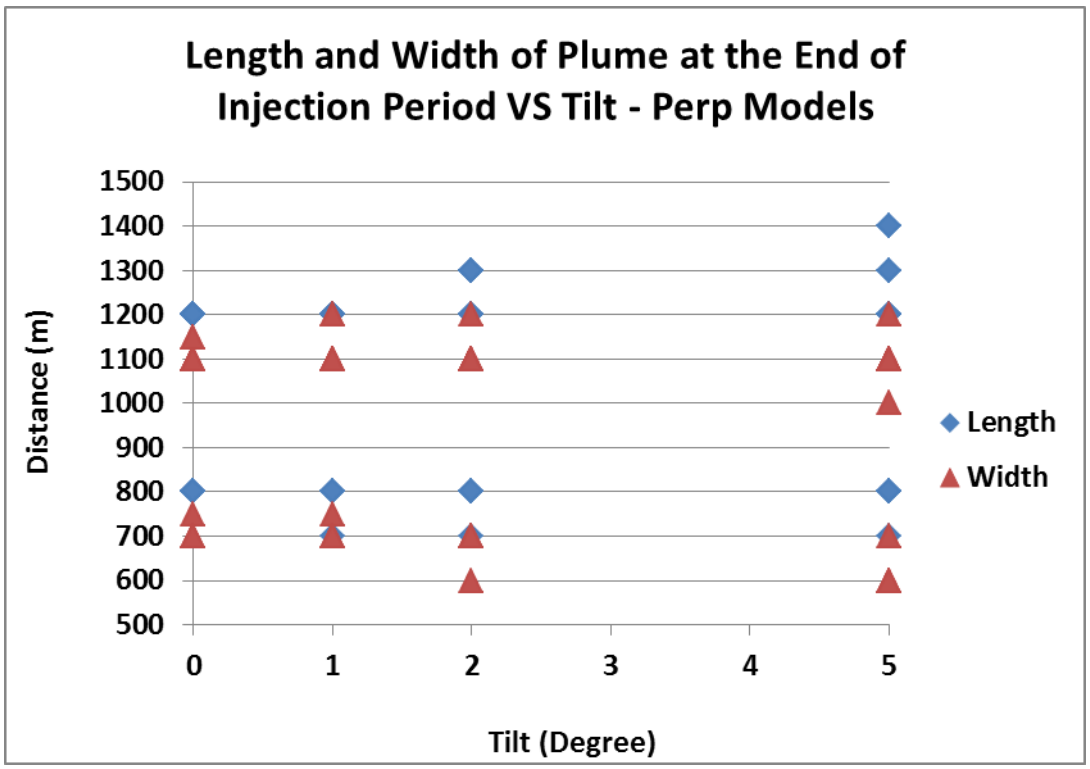


*Figure 3.38 Length and width of plume of perp models with tilt, at the end of injection.*

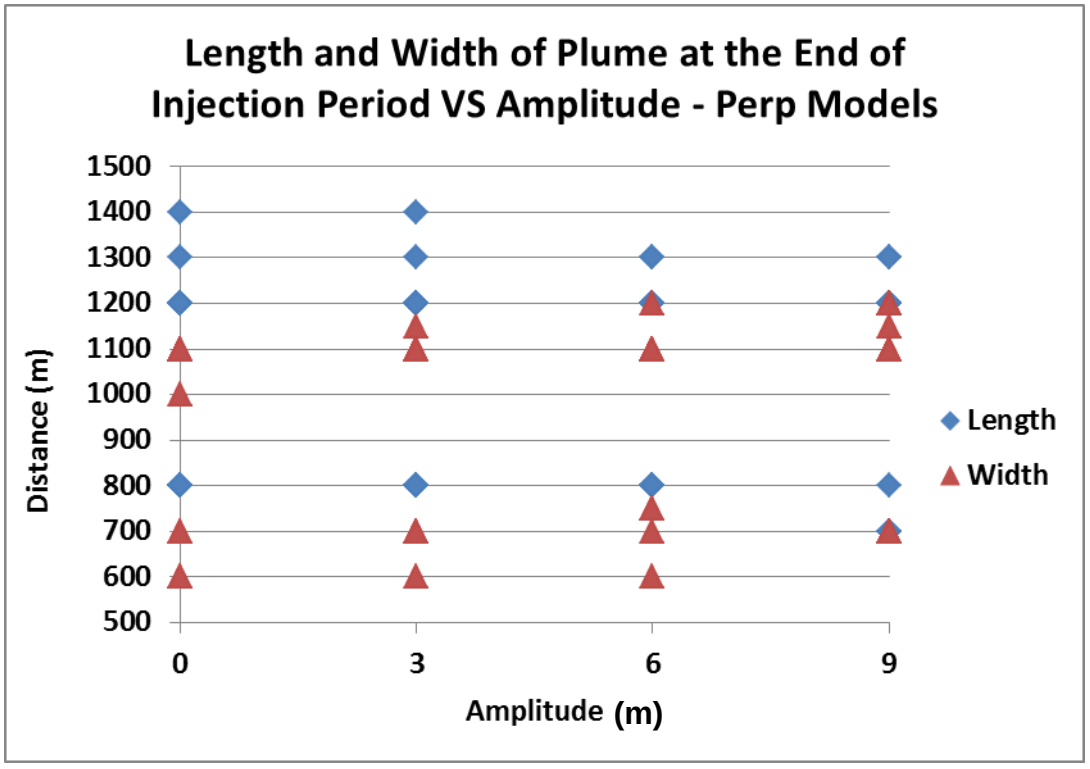


*Figure 3.39 Length and width of plume of perp models with amplitude, at the end of injection.*

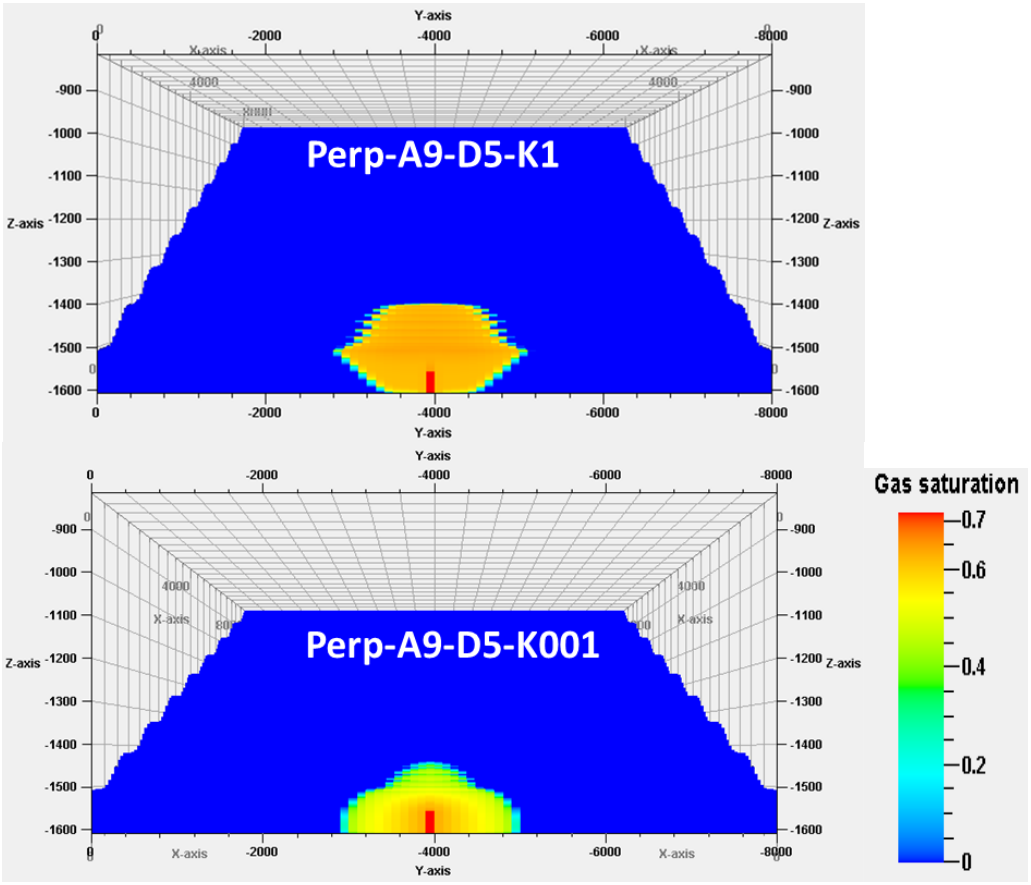


*Figure 3.40 Gas saturation at the end of injection in two perp models with the same amplitude (9m) and tilt (5) but different $k_V/k_H$ ratio, the top picture has higher $k_V/k_H$ ratio (1) and the bottom one has smaller $k_V/k_H$ ratio (0.01).*

***100 Years post Injection***

**Effect of $k_V/k_H$ Ratio:**

The width and the length of the plume decrease with decreasing $k_V/k_H$ ratio. However, the length is more sensitive. The difference between the lengths of the plume in some models (high $k_V/k_H$ and low $k_V/k_H$) is around 2.5 km (Figure *3.41* and Figure *3.44*). The plume shape is more symmetrical for low $k_V/k_H$ ratios (Figure *3.41* and Figure *3.44*).

**Effect of Tilt:**

The width of the plume decreases slightly with tilt. The length of the plume increases with tilt and there is more segregation between results for highest tilt angle (Figure *3.42* and Figure *3.45*).

**Effect of Amplitude:**

The width of the plume slightly increases with the amplitude. The length of the plume decreases with amplitude as some $CO_2$ is trapped under the ridges structurally (Figure *3.43* and Figure *3.46*).

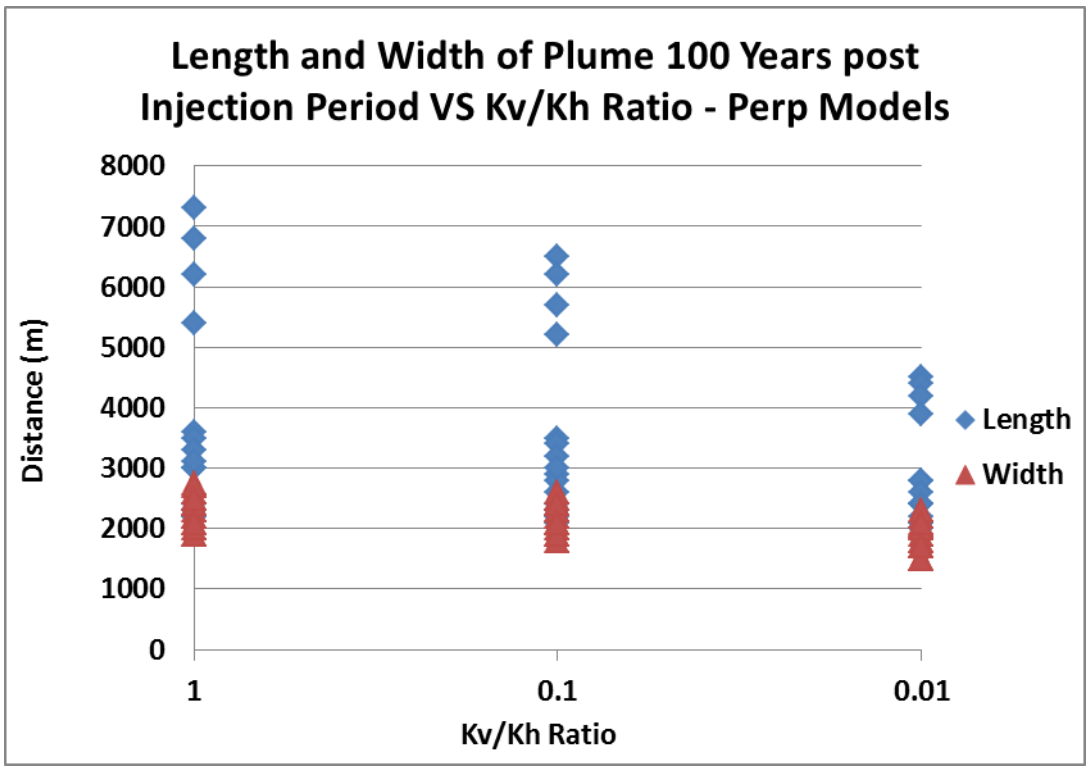


*Figure 3.41 Length and width of plume of perp models with $k_V/k_H$ ratio, 100 years post injection.*

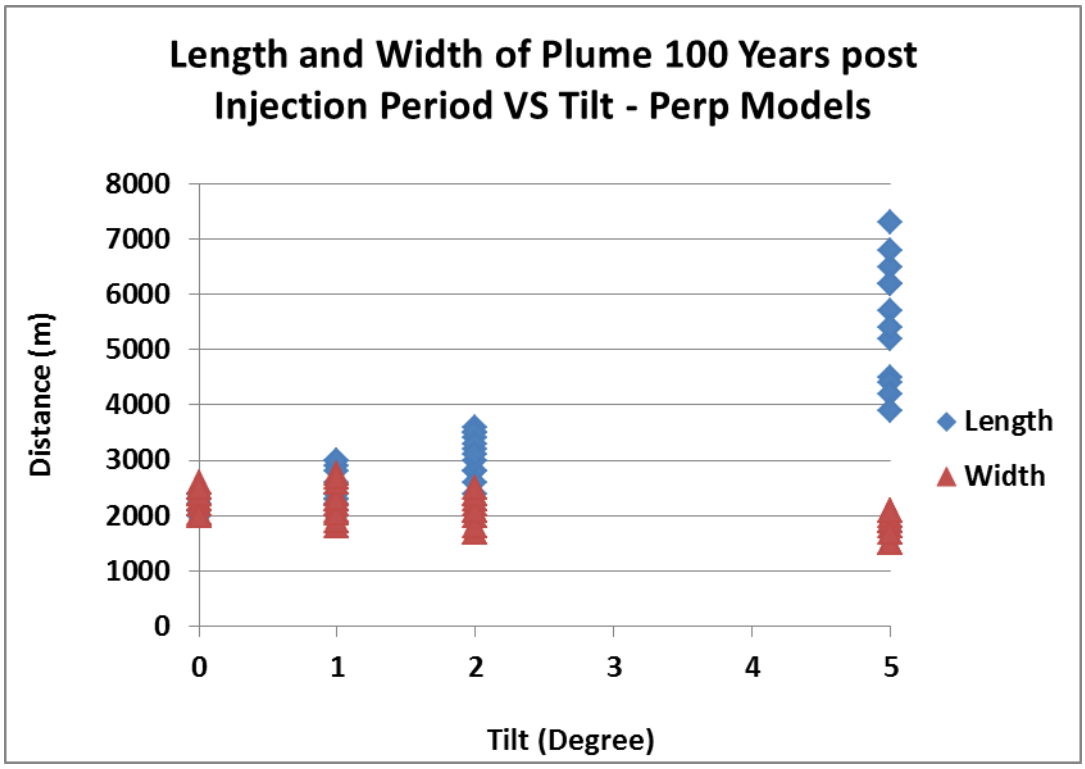


*Figure 3.42 Length and width of plume of perp models with tilt, 100 years post injection.*

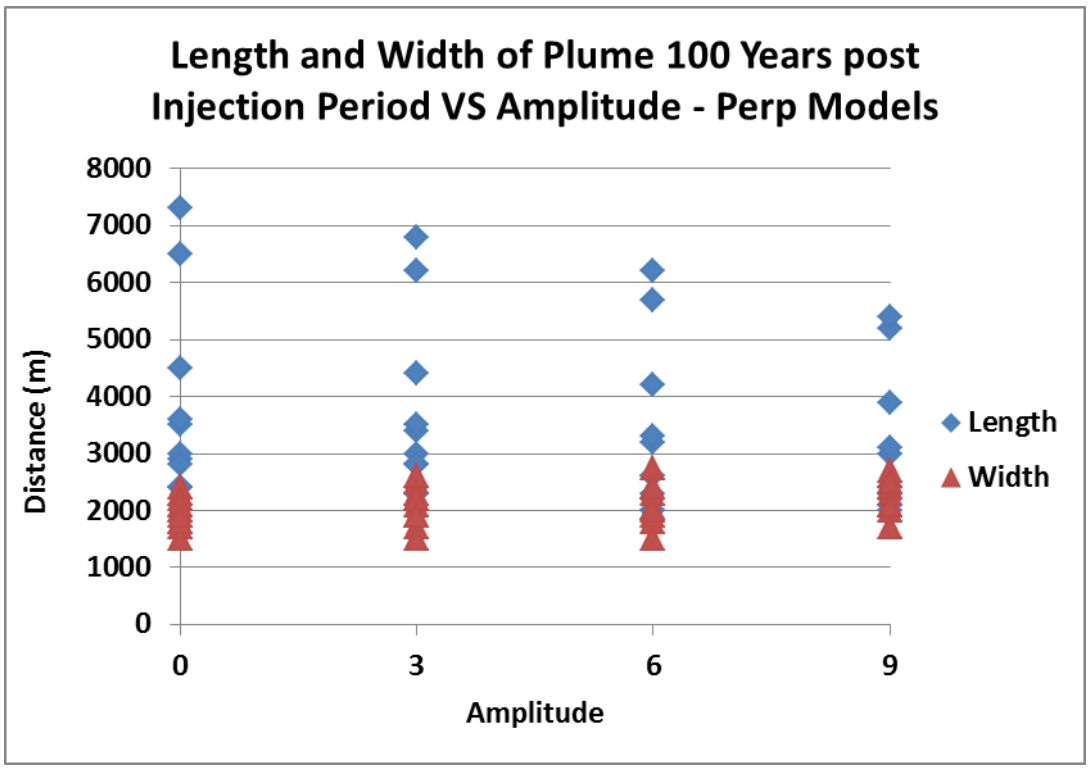


*Figure 3.43 Length and width of plume of perp models with amplitude, 100 years post injection.*

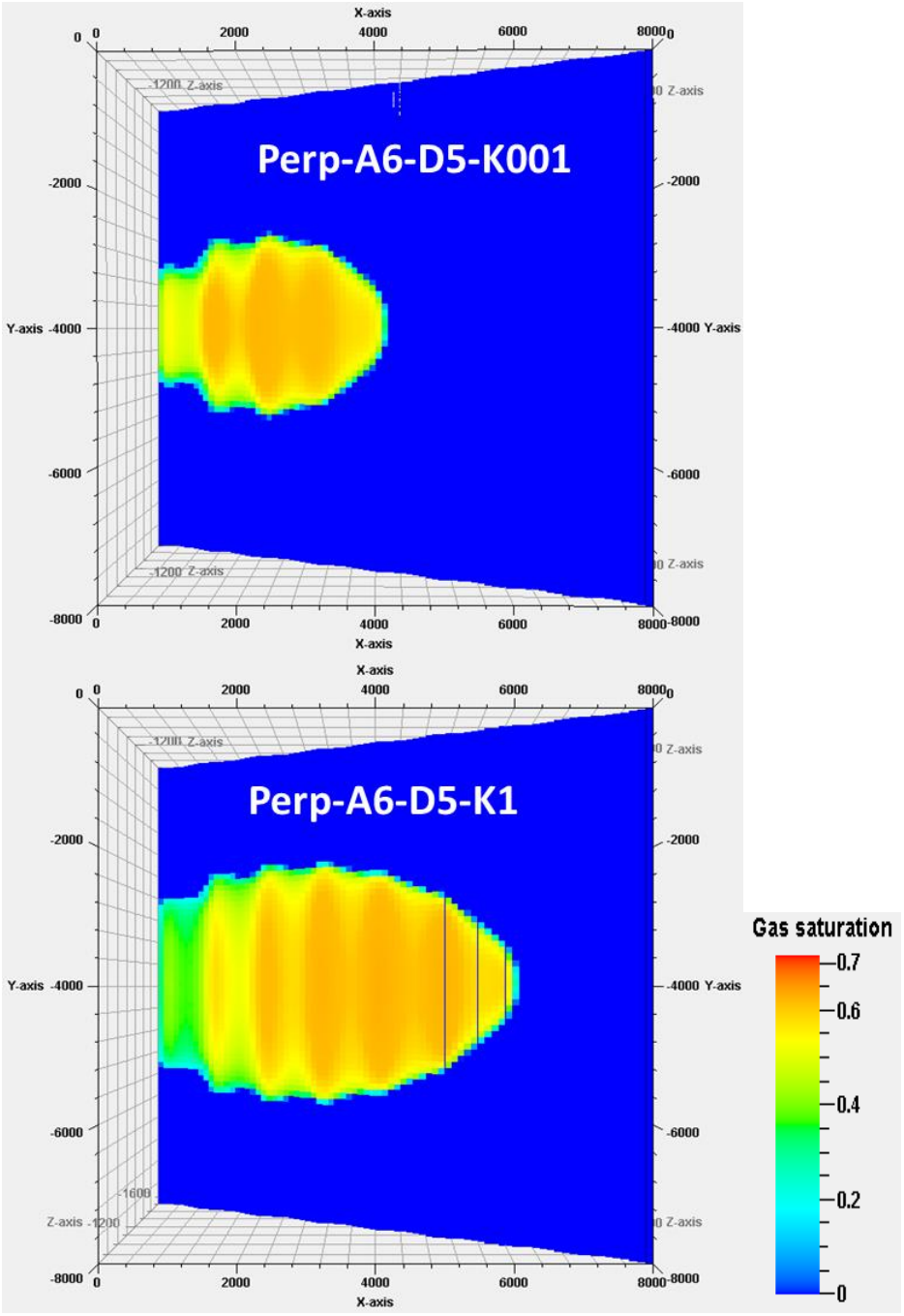


*Figure 3.44 Gas saturation 100 years post injection period in two perp models with the same amplitude and tilt and different $k_V/k_H$ ratios: top picture shows a model with a $k_V/k_H$ ratio of 0.01, whereas the bottom picture shows a model with $k_V/k_H$ ratio of 1. More $CO_2$ migrated along the direction of the tilt in the model with higher $k_V/k_H$ ratio (bottom picture).*

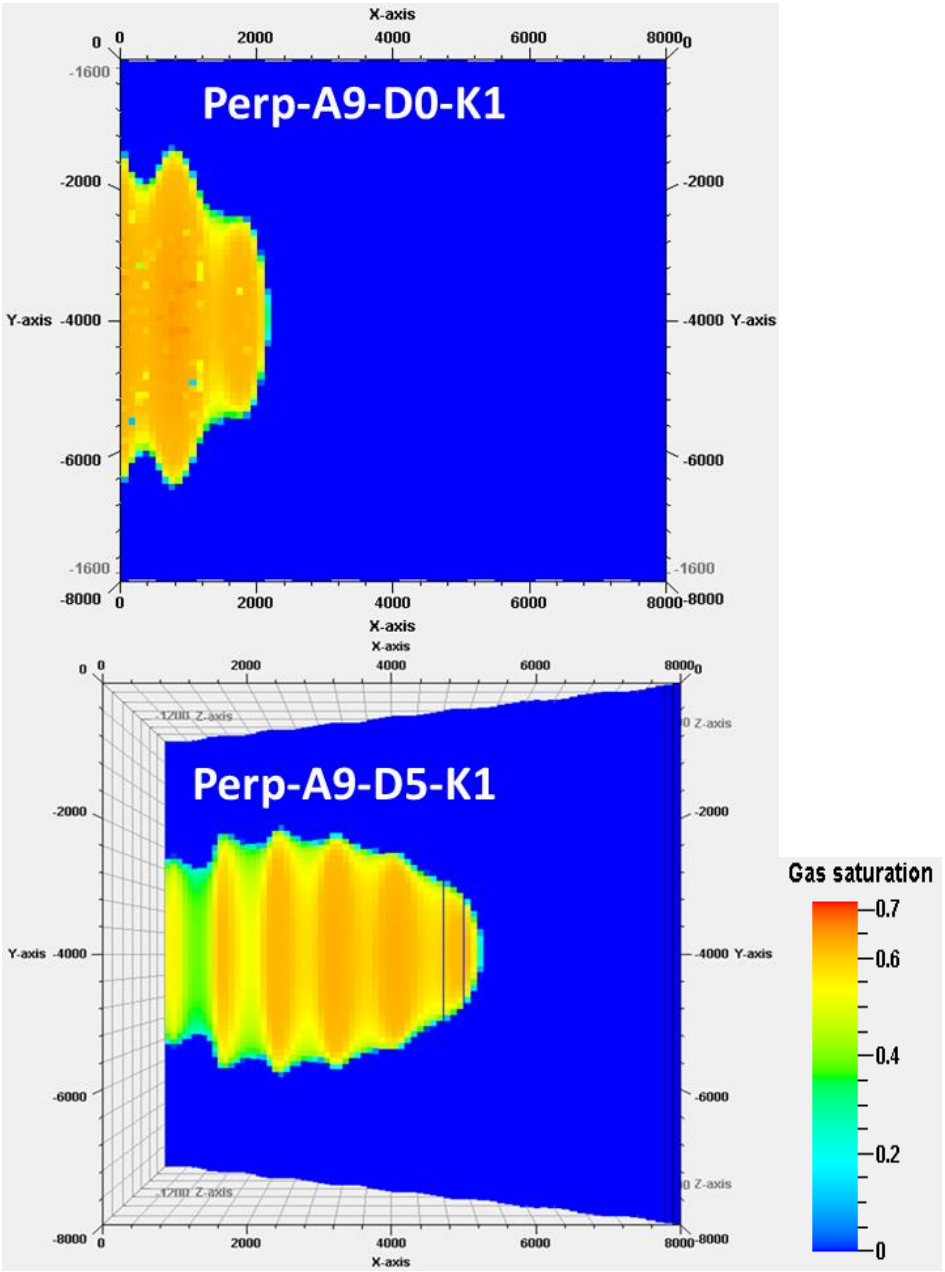


*Figure 3.45 Gas saturation 100 years post injection period in two perp models with the same amplitude and $k_V/k_H$ ratio and different tilt: top picture has zero tilt, whereas bottom picture shows a 5 degree tilted model. More $CO_2$ migrated perpendicular to the ridges in the tilted model (bottom picture), whereas the width of plume is bigger in the flat model (top picture) than in the tilted model.*

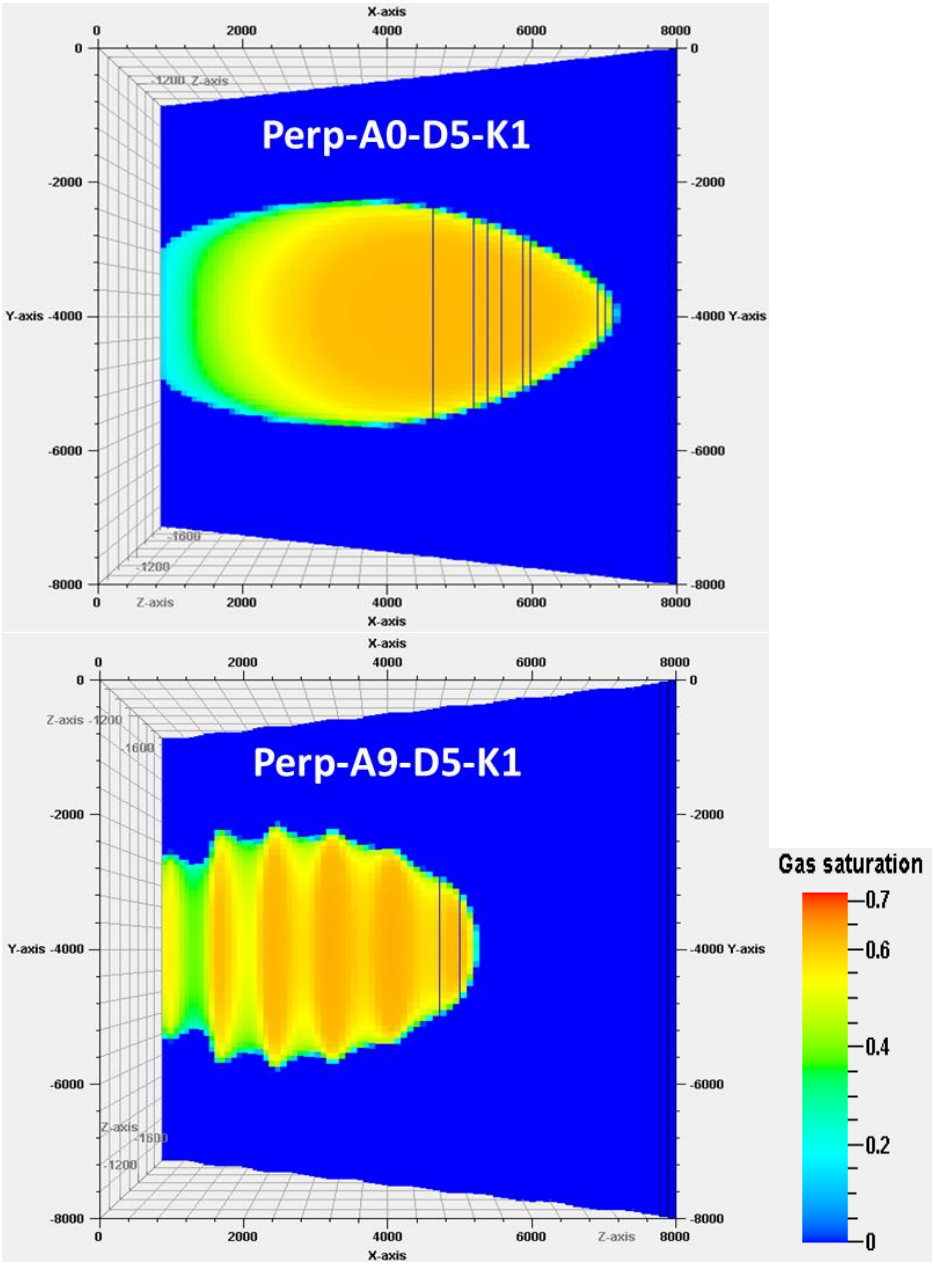


*Figure 3.46 Gas saturation 100 years post injection period in two perp models with the same tilt angle and $k_V/k_H$ ratio and different amplitude: model with amplitude equals zero (top picture) and model with amplitude equals 9m (bottom picture). More $CO_2$ migrated alongside the tilt in the model with zero amplitude tilted (top picture) because there is no obstacle to prevent of $CO_2$ migration up-dip than model with amplitude equals 9m (top picture).*

### *3.3.4 Sensitivity Study on the Effect of Tilt on the Plume Migration*

In order to investigate the relation between the tilt and the plume migration, some additional tilted models with 3 and 4 degree tilts were constructed. Results show that the length of the plume increases with tilt angle linearly from 0 to 4 degrees. However, after 4 degrees it increases more rapidly (Figure ***3.47***).

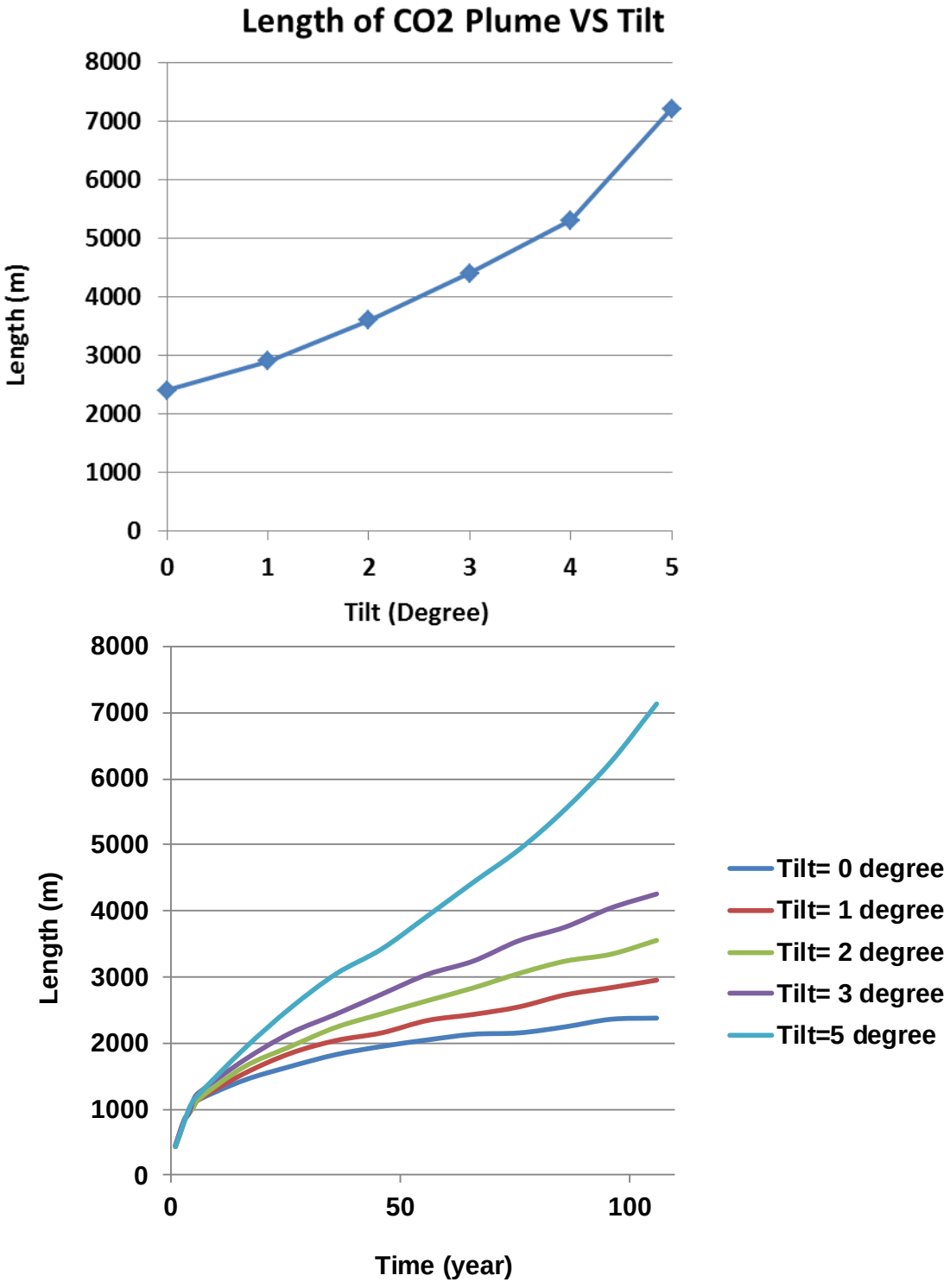


*Figure 3.47 The length of plume in models with zero amplitude with tilt (top picture) and with time (bottom picture).*

### *3.3.5 Effect of Transition Zone*

***Trans Models, End of Injection***

Figure *3.48*, Figure *3.49* and *Figure 3.50* demonstrate the effect of $k_V/k_H$ ratio, tilt and thickness of transition zone at the end of the injection period on the *trans* models respectively.

**Effect of $k_V/k_H$ Ratio**

Similar to the *para* and *perp* models, the $k_V/k_H$ ratio is the most sensitive factor. The amount of dissolved $CO_2$ increases with decreasing $k_V/k_H$ ratio.

**Effect of Tilt:**

Tilt is the second most sensitive factor. The amount of dissolved $CO_2$ slightly increases by tilt.

**Effect of Amplitude (Thickness of Transition Zone here)**

The effect of amplitude is negligible during injection period.

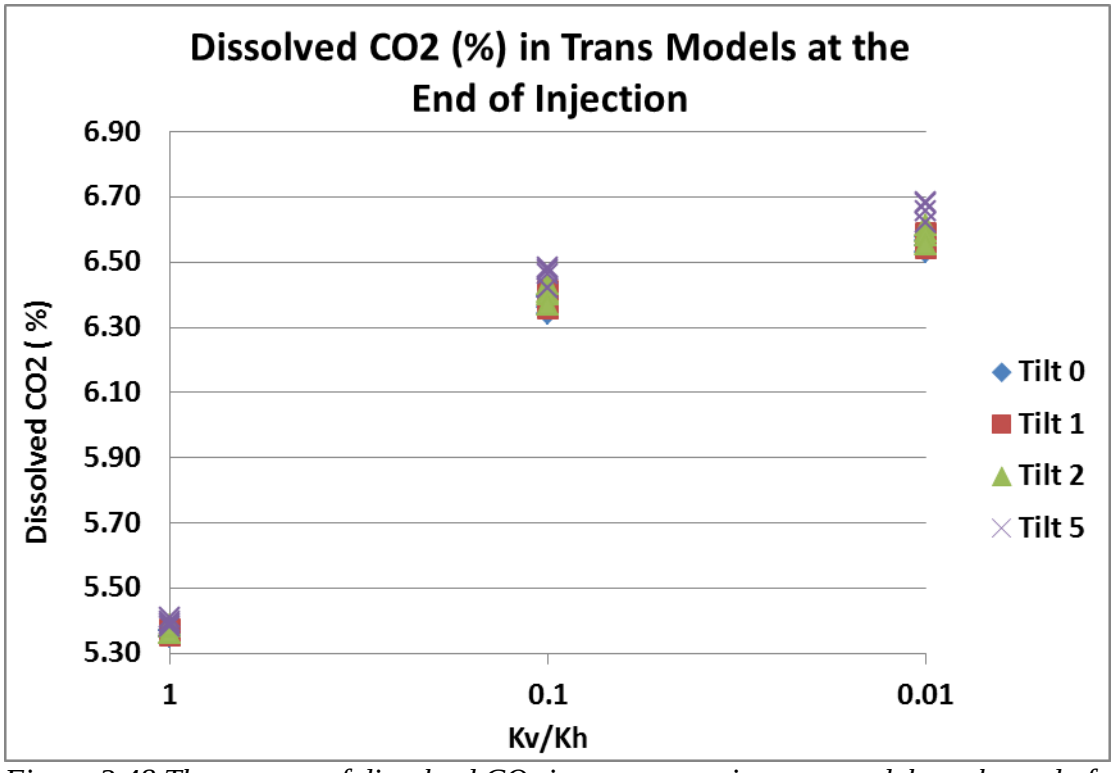


*Figure 3.48 The amount of dissolved $CO_2$ in percentage in trans models at the end of injection with $k_V/k_H$ ratio and tilt.*

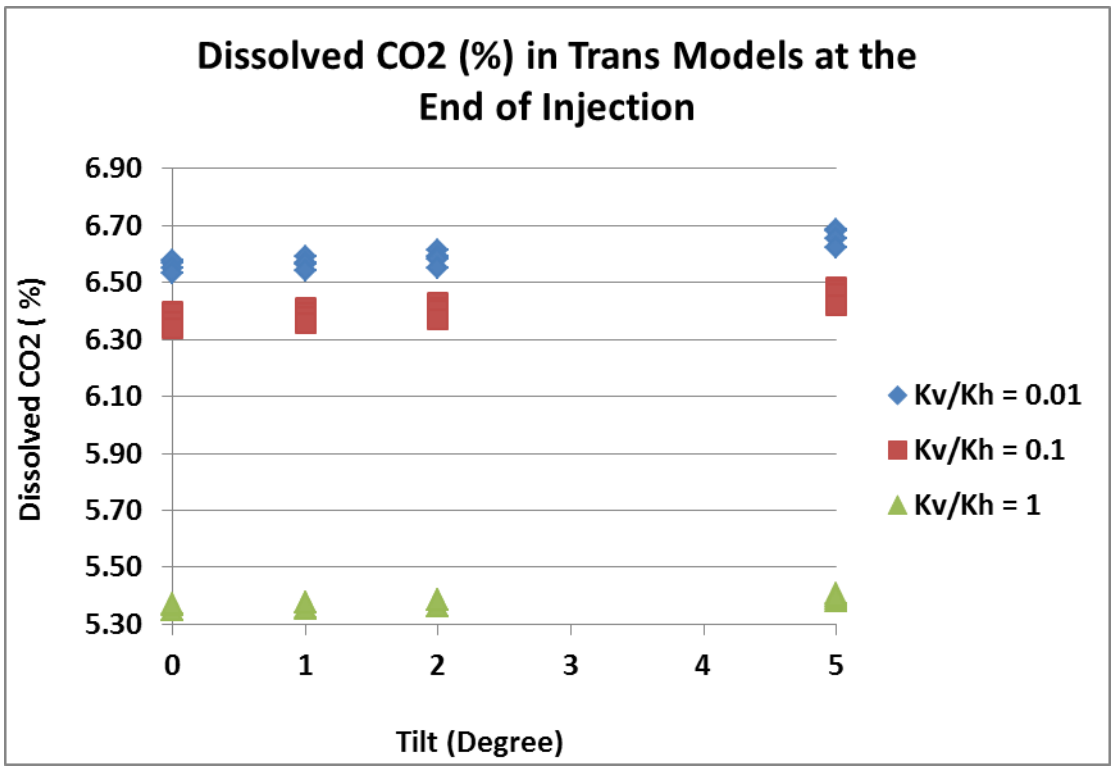


*Figure 3.49 The amount of dissolved $CO_2$ in percentage in trans models at the end of injection with tilt and $k_V/k_H$ ratio.*

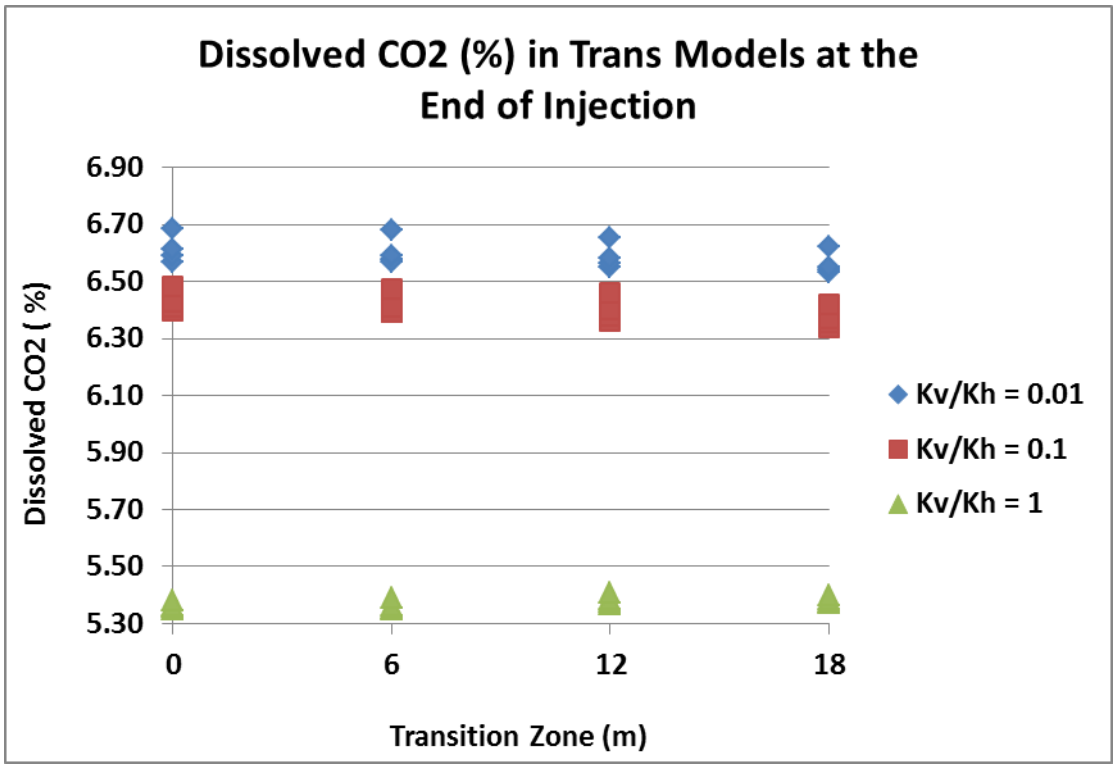


*Figure 3.50 The amount of dissolved $CO_2$ in percentage in trans models at the end of injection with thickness of transition zone and $k_V/k_H$ ratio.*

***Trans Models, 100 Years Post Injection Period***

Figure *3.51*, Figure *3.52* and Figure *3.53* show the effect of $k_V/k_H$ ratio, tilt and thickness of transition zone 100 years post injection period on tranz models respectively.

**Effect of $k_V/k_H$ Ratio**

Similar to the *para* and *perp* models, the $k_V/k_H$ ratio is the second most sensitive factor (Figure *3.51*). The amount of dissolved $CO_2$ increases with $k_V/k_H$ ratio for the largest tilt angle (5). However, for the flat models and tilted models up to 2 degrees the intermediate $k_V/k_H$ ratio gives the highest dissolved $CO_2$.

**Effect of Tilt**

Tilt is the most sensitive factor (Figure *3.52*) and the amount of dissolved $CO_2$ increases with tilt. At higher tilts, the effect of $k_V/k_H$ ratio is greater.

**Effect of Amplitude (Thickness of Transition Zone here)**

By increasing the thickness of transition zone the amount of dissolved $CO_2$ increases. However this increase is not significant.

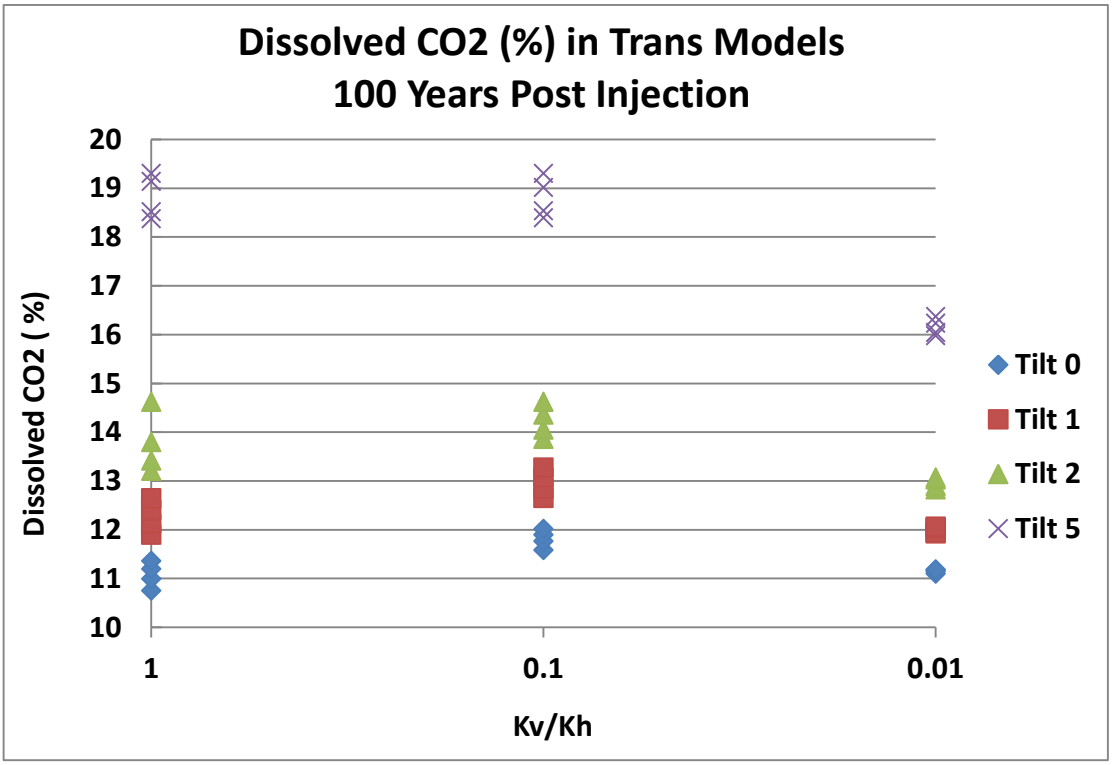


*Figure 3.51 The amount of dissolved $CO_2$ in percentage in trans models 100 years post injection with $k_V/k_H$ ratio and tilt.*

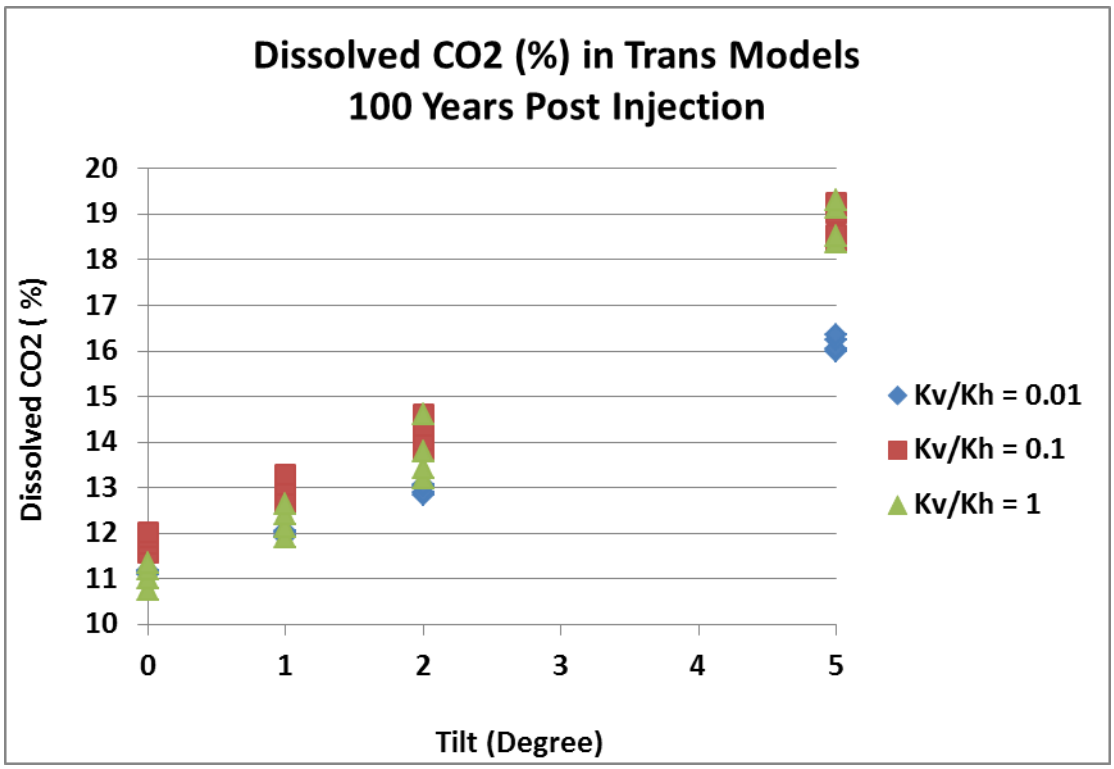


*Figure 3.52 The amount of dissolved $CO_2$ in percentage in trans models 100 years post injection with tilt and $k_V/k_H$ ratio.*

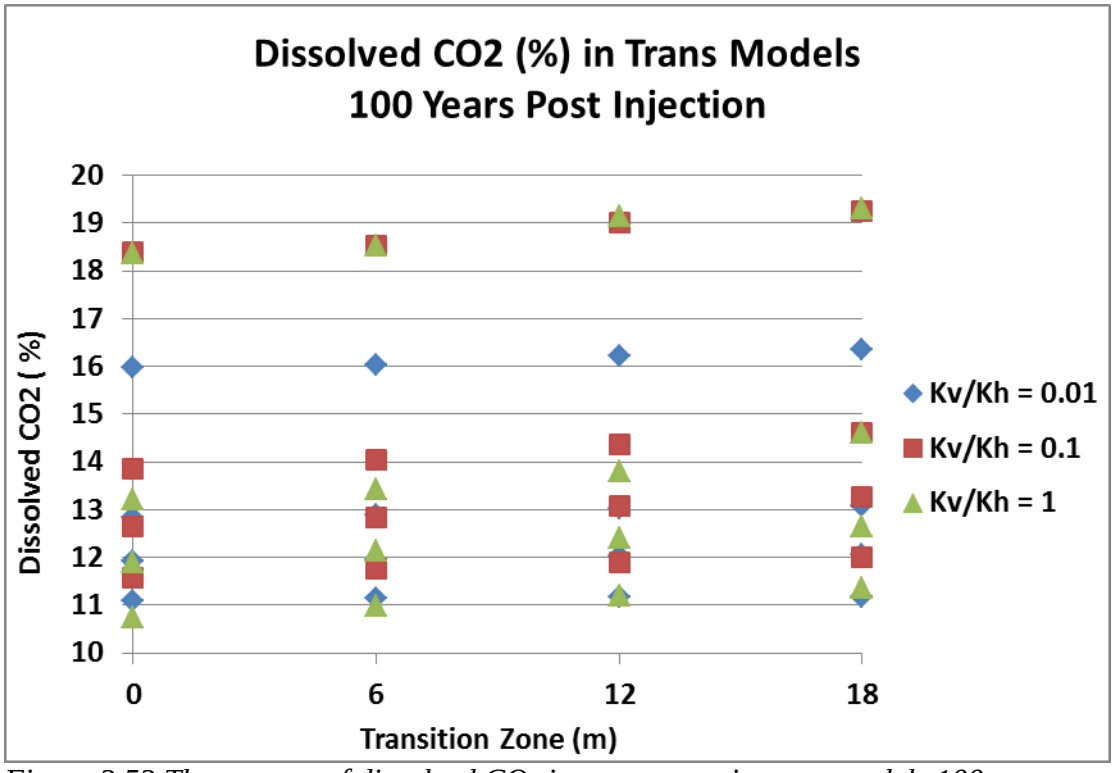


*Figure 3.53 The amount of dissolved $CO_2$ in percentage in trans models 100 years post injection with thickness of transition zone and $k_V/k_H$ ratio.*

### *3.3.6 Plume Migration in trans Models*

Three models were chosen to investigate plume migration in the *trans* models with respect to tilt and $k_V/k_H$ ratio. Figure *3.54* shows plume migration in 3 *trans* models (Trans-A6-D5-K1, Trans-A6-D1-K1, Trans-A6-D1-K001) 100 years after post injection period. Pictures on the left demonstrate the $CO_2$ plume in the top-most layer and pictures in right show the length and the width of migrated $CO_2$ through different layers.

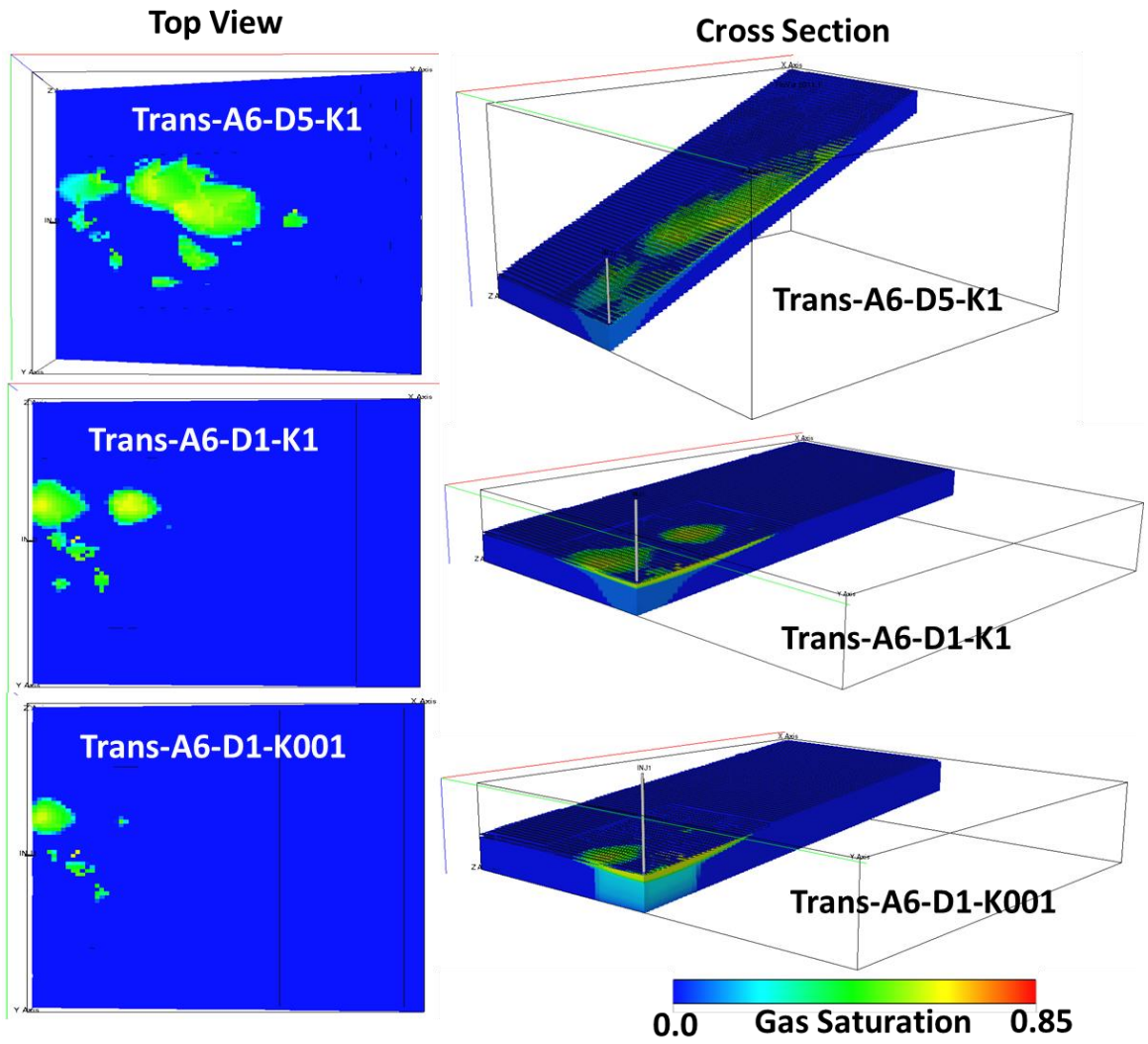


*Figure 3.54 Gas saturation 100 years post injection period in three trans models. All three models have the same amplitude. However, top one and middle one have the same $k_V/k_H$ ratio but the former one is tilted and the later one is flat. The bottom one which also is flat however has a low $k_V/k_H$ ratio (o.o1). More $CO_2$ reaches the top layer due to higher tilt angle and higher $k_V/k_H$ ratio (top picture) whereas the least upwards migration happened in the model with lower tilit angle and lower $k_V/k_H$ ratio (bottom picture).*

Figure *3.54* shows that more $CO_2$ can reach the top of the storage formation by increasing tilt and $k_V/k_H$ ratio. The plume at the top of the aquifer will have a patchy form depending on the permeability distribution. In addition, it can be concluded that

the length of the plume is sensitive to the tilt and then $k_V/k_H$ ratio. By increasing these two factors more $CO_2$ migrates up-dip resulting in the plume having a smaller width. On the other hand, more $CO_2$ spreads out laterally at the lower tilt angle and higher $k_V/k_H$ ratio (Trans-A6-D1-K1). In the model with the small tilt and low $k_V/k_H$ ratio (Trans-A6-D1-K001) more $CO_2$ accumulates above the injector and gives the highest thickness of $CO_2$ amongst these models. Therefore less $CO_2$ migrates resulting in having the smallest length.

Figure 3.55 shows that less $CO_2$ can reach the top of the formation storage by increasing the thickness of transition zone.

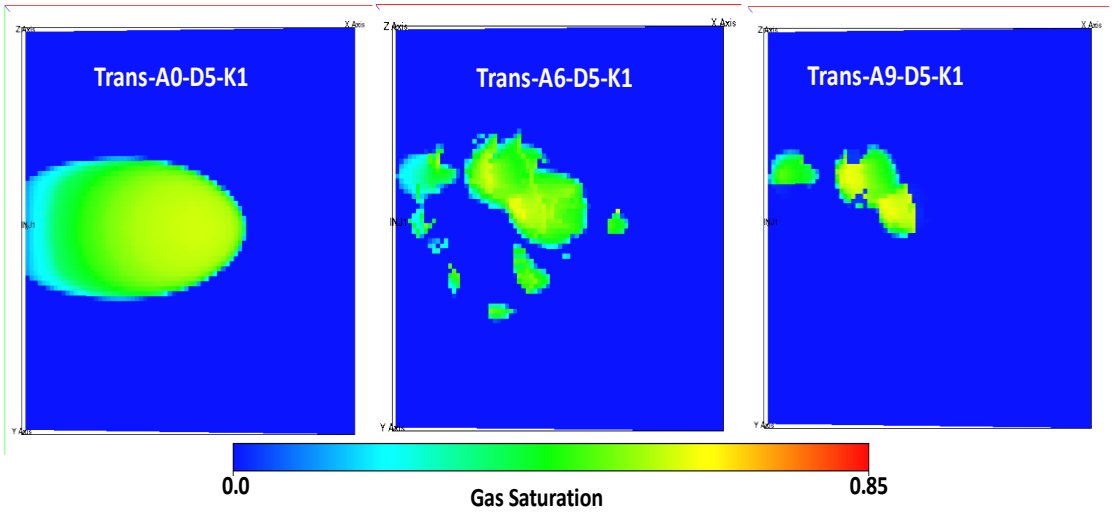


*Figure 3.55 Gas saturation 100 years post injection period in trans models*

### *3.3.7 Discussion on numerical simulation results*

Results of all 144 models can be divided into two sections:

a) The effect of top morphology and transition zone on the amount of $CO_2$ dissolved

b) The effect of top morphology and transition zone on plume migration

***a) The effect of top morphology and transition zone on the amount of $CO_2$ dissolved***

The amount of $CO_2$ dissolved at the end of the injection period and 100 years post injection period in all trans, *para* and *perp* models was chosen to investigate the effect of amplitude of ridges (thickness of transition zone in *trans* models), tilt and $k_V/k_H$ ratio. Figure *3.56* and Figure *3.57* demonstrate amount of dissolved $CO_2$ in percentage at the end of injection and 100 years post injection with $k_V/k_H$ ratio (Z axis), tilt (X axis), and amplitude (Y axis) for *trans* models (top values), *para* models (middle values) and *perp* models (bottom values) respectively.

**End of Injection**

Results show that the most sensitive parameter at the end of the injection period is $k_V/k_H$ ratio (Figure *3.56*).

The lower the $k_V/k_H$ ratio the more $CO_2$ is dissolved. This is due the fact that more $CO_2$ spreads out when the $k_V/k_H$ ratio is low therefore more $CO_2$ will be in contact with fresh brine resulting in more $CO_2$ dissolution (Figure *3.56*). In other words, in models with high $k_V/k_H$ ratio the effect of viscous force on the lateral migration is less than the model with low $k_V/k_H$ ratio.

**100 Years Post Injection Period**

Results show that the most sensitive parameter is tilt (Figure *3.57*). As the tilt increases from the left hand side of graph to the right side of the graph from 0 to 5 degrees more $CO_2$ dissolved in the models regardless the amplitude of the model.

The second most sensitive parameter is $k_V/k_H$ ratio. The gas migration during post injection period is governed by buoyancy therefore the higher the $k_V/k_H$ ratio the more $CO_2$ migrated upwards. Thus more $CO_2$ in contact with fresh brine the more $CO_2$ dissolution in brine (Figure *3.57*).

The effect of amplitude is not significant in *para* models due the fact that there is no obstacle for $CO_2$ migration. However, in *perp* models by increasing the amplitude,

especially for the high $k_V/k_H$ and high tilt models, the amount of dissolved $CO_2$ falls (Figure *3.57*).

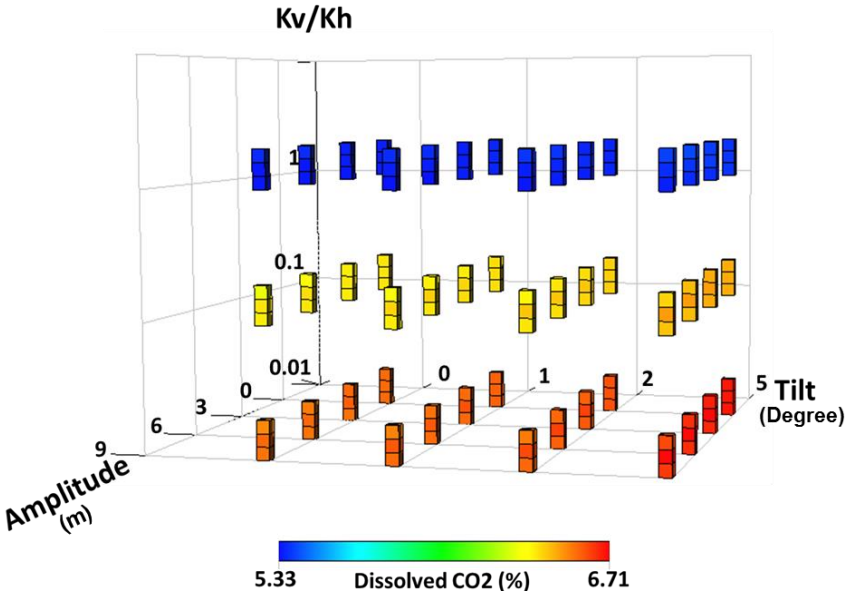


*Figure 3.56 Dissolved $CO_2$ at the end of injection period for Trans, para and perp models. The top value at each point refers to Trans Model, the middle one refers to the Para Model and the bottom one refers to the Perp Model. Models with lowest $k_V/k_H$ ratio have the highest amount of dissolved $CO_2$ at the end of injection period.*

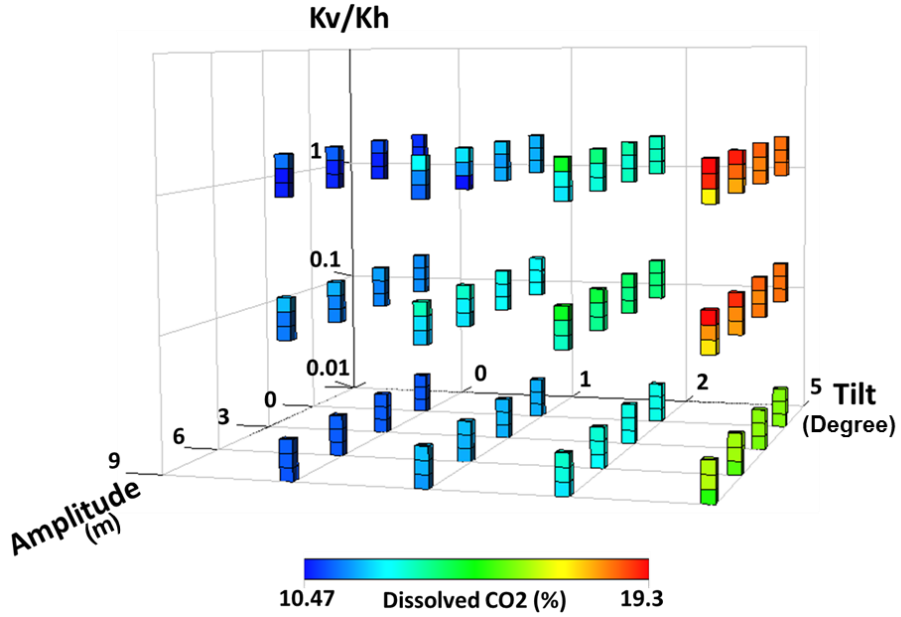


*Figure 3.57 Dissolved $CO_2$ 100 years post injection period for Trans, para and perp models. The top value at each point refers to Trans Model, the middle one refers to the Para Model and the bottom one refers to the Perp Model.*

***b) Effect of top morphology and transition zone on plume migration***

Figure *3.58* and Figure *3.59* show length of plume for *para* and *perp* models at the end of injection and 100 years post injection period respectively.

It can be concluded that the length of plume at the top surface is more sensitive to the $k_V/k_H$ ratio during the injection period. Because the lower the $k_V/k_H$ ratio the lesser the $CO_2$ reached to the top of storage formation therefore the smaller the size of plume would be.

In addition, the length of plume is more sensitive to the tilt after 100 years post injection period.

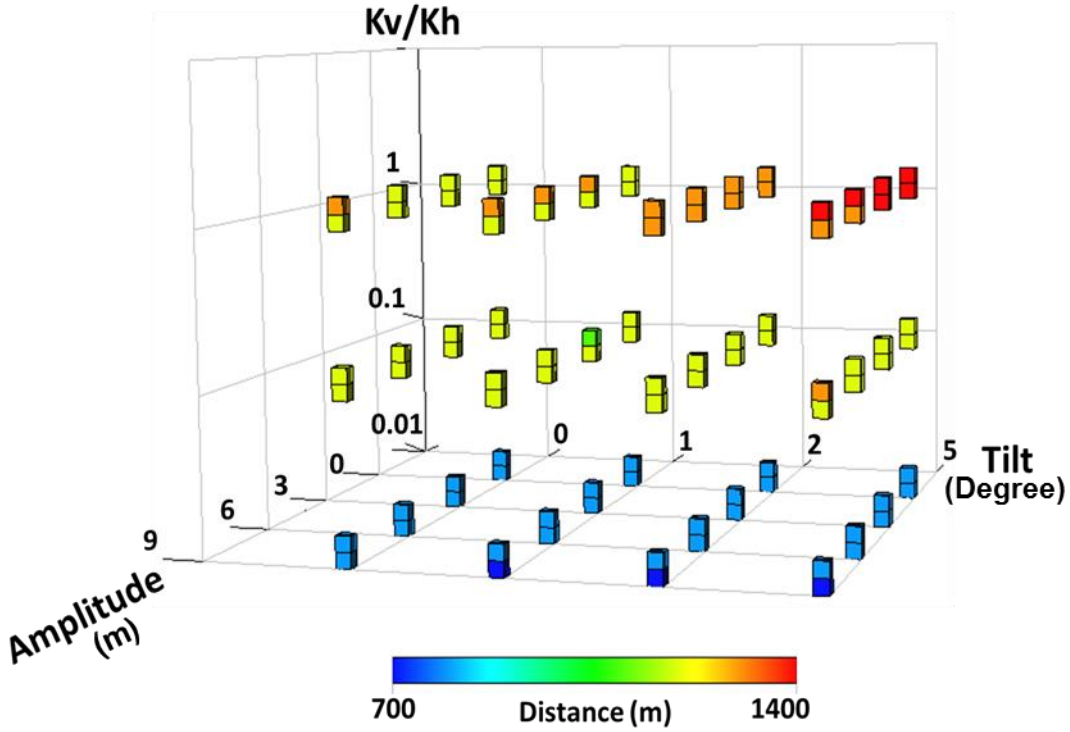


*Figure 3.58 Length of plume at the end of injection for para models (upper values at each point) and perp models (lower values at each point).*

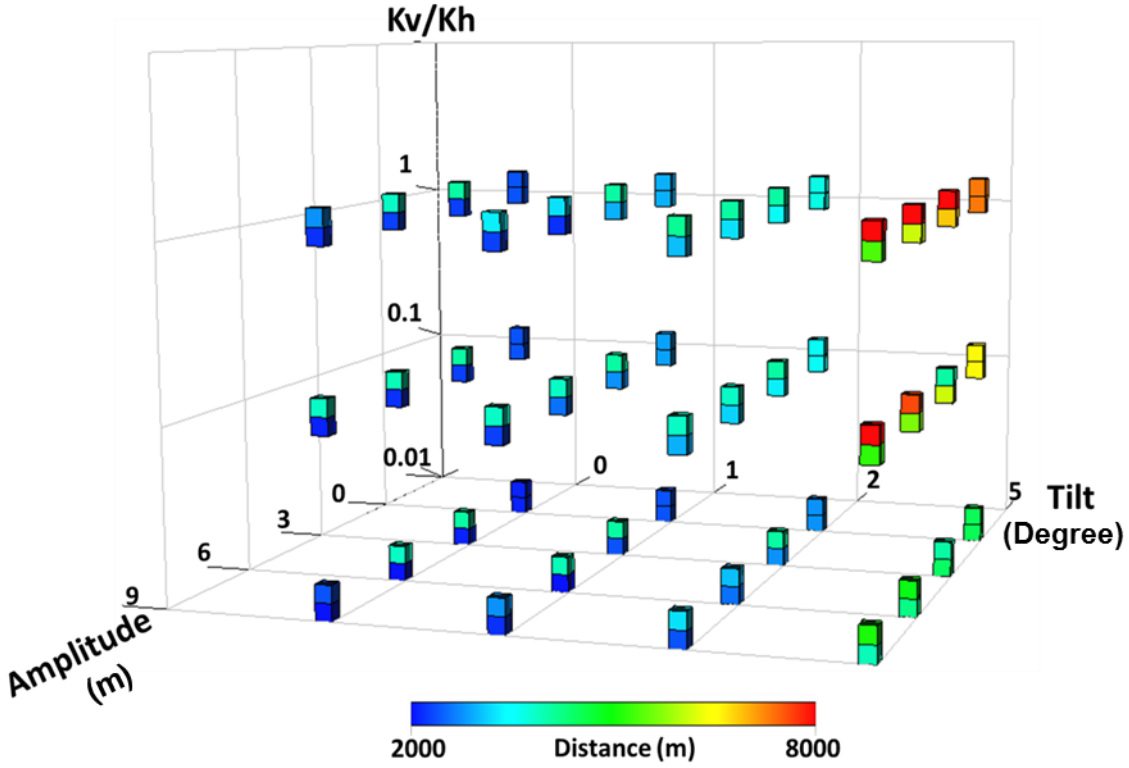


*Figure 3.59 Length of plume 100 years post injection for para models (upper values at each point) and perp models (lower values at each point).*

### *3.3.8 Discussion on analytical calculations*

Up-dip (0.1 – 1 degree) plume migration during the injection phase was studied by Gasda et al., 2008 (see section 2.4.2). However, they did not consider the effect of $k_V/k_H$ ratio, morphology of caprock (amplitude), and higher tilt angle. In this study, plume migration both during injection period and 100 years post injection period were investigated and the impacts of the aforementioned parameters were tested.

Nordbotten et al., (2005) presented an equation for the extent of plume migration in flat models (tilt equals zero) and $k_V/k_H = 1$, as follows:

$$d = \sqrt{\frac{\lambda_c Q t}{\phi \lambda_w B \pi}} \tag{3.2}$$

where

d is the length of plume

$\lambda_c$ denotes for $CO_2$ mobility

$\lambda_w$ denotes for water mobility

$\phi$ refers to porosity

B is the reservoir thickness

$Q$ is the flow rate

t refers to time

When the flow of $CO_2$ is dominated by the injection rate Equation 3.2 can be written in the form of equation 3.3 (Okwen et al., 2010).

$$d = \sqrt{\frac{\lambda Q t}{\phi B \pi (1 - S_r)}} \tag{3.3}$$

Where $\lambda$ denotes the ratio of motilities of two fluids ($\frac{\lambda_c}{\lambda_w}$). The length of the plume was calculated based on above equation for the PERP-A0-D0-K1 Model, at which amplitude and tilt are zero and $k_V/k_H$ ratio equals 1. Table 3.5 shows properties of the model that were used to calculate length of plume (d), which equals 1207 m. This validates numerical results for this case (see Figure 3.58).

*Table 3.5 values used to calculate length of plume in PERP-A0-D0-K1 Model*

| $\lambda$ | $Q$ $(m^3/day)$ | t (day) | $S_r$ | $\phi$ | B (m) | Length from Okwen (m) | Length from simulation (m) |
|---|---|---|---|---|---|---|---|
| 4 | 6638 | 2190 | 0.364 | 0.2 | 100 | 1207 | 1200 |

Numerical results show that the plume migration increases linearly with tilt (Figure 3.47). However, the changes in $k_V/k_H$ ratio are more influential during the injection period. In the 100 years post injection period, the effect of tilt is more important than $k_V/k_H$ ratio. The plume migrates linearly with tilt up to 4 degrees; however, this is not the case for 5 degrees. This is due to the fall in $CO_2$ density as a result of faster up dip migration under tilt.

The effects of small scale amplitudes on the plume migration and $CO_2$ dissolution are diminished when the tilt increases. This is due to the fact that less $CO_2$ will trap locally under ridges. For instance in sine wave models, the amount of $CO_2$ that can be trapped under each wavelength decreases around 2/3$^{rd}$ by increasing tilt from 0 to 1 (see below calculations and Figure 3.60 ).

Using equation (3.1) and tilt $\theta = 0$, the area under any flat sine wave model (e.g. A1 in Figure 3.60 ) can be calculated.

$$Z = Z_0 + A(Sin(\frac{2\pi x}{\lambda})) + x(\tan\theta)$$

where $\lambda$ is wavelength.

Substituting $\theta = 0$,

Thus,

$$Z = Z_0 + A(Sin(\frac{2\pi x}{\lambda})) \qquad (3.4)$$

Assuming $Z_0 = 0$ and take integral from equation 3.4 for one wavelength (i.e. $x = 3\lambda/4$ to $x = 7\lambda/4$),

$$Area = \int A(sin(\frac{2\pi x}{\lambda}))dx = A\lambda$$

For models with $\theta = 1^o$, the same set of calculation can be written to calculate the area under one wavelength, which is approximately $A\lambda/3$.

As shown in Figure 3.60 below, at a certain tilt, the amount of trapping will be approximately equal to the area under the top half of a sine wave, i.e. the integral under the sine wave between angles of $0$ and $\pi/2$. The resulting area is equal to $A\lambda/\pi$, which is approximately equal to $A\lambda/3$. This occurs when the average height of the sine wave increases by approximately one amplitude over a distance of $\lambda/2$. In other words $\theta = \tan^{-1}(9/500) = 1^o$.

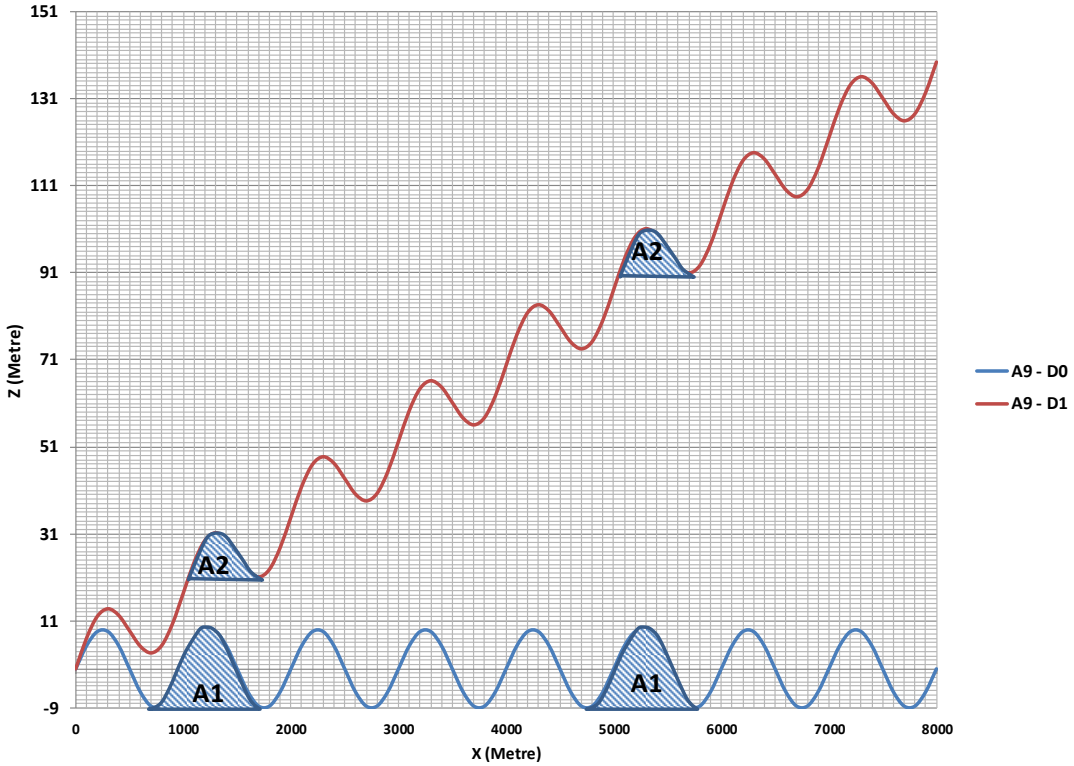


*Figure 3.60 Decrease in local structural trapping due to increase in tilt angle, A1 shows the area under a wavelength in a flat perp model with amplitude of 9 metres and A2 shows the area under a wavelength in a 1 degree tilted perp model, also with amplitude of 9 metres.*

In this section an equation is presented to show whether or not $CO_2$ will be trapped under the ridges. Differentiating from equation (3.1),

$$\frac{dz}{dx} = \tan(\theta) + \frac{2\pi A}{\lambda}\cos(\frac{2\pi x}{\lambda}) \tag{3.5}$$

For trapping, this must be always negative for some angle. But, for no trapping, this must always be non-negative $(dz/dx \geq 0)$. The minimum of a cosine is -1, so the minimum gradient is

$$\frac{dz}{dx} = \tan(\theta) - \frac{2\pi A}{\lambda} \geq 0$$

Thus;

$$\tan(\theta) \geq \frac{2\pi A}{\lambda} \tag{3.6}$$

If the minimum gradient is zero, then

$$\tan(\theta) = \frac{2\pi A}{\lambda}$$

Therefore theta is given by:

$$\theta = \tan^{-1}(\frac{2\pi A}{\lambda}). \quad (3.7)$$

Obviously this calculation does not take account of the amount of trapping, or whether it is significant (i.e. the volume trapped under the tilted sine wave is large compared with the thickness of the plume). However, it gives a guideline on what kind of topography could make a significant difference, and what will never have an effect, due to the fact that the slope is always positive. For *perp* models studied in this chapter, Figure 3.61 and

***Table 3.6*** can be generated based on this equation. Results show that for models with tilt more than 1 degree, and amplitude less than 3 metres, morphology cannot make a significant effect on the $CO_2$ trapping.

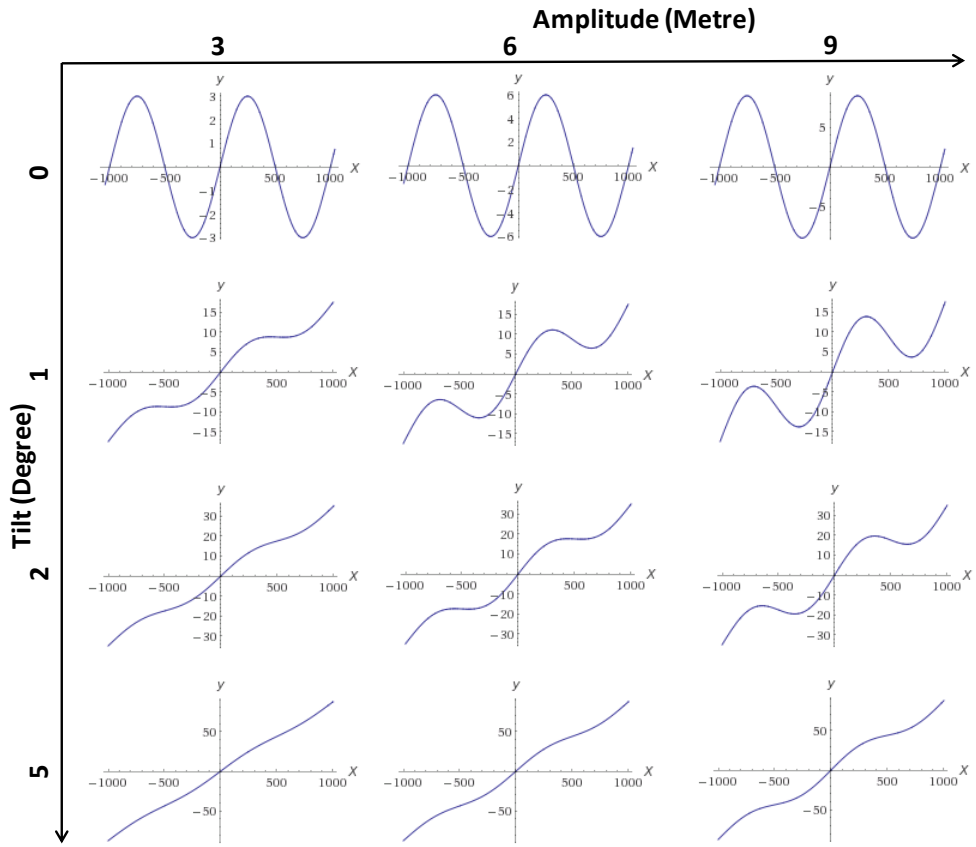


*Figure 3.61 Relationship between Tilt and Amplitude and trapping when Lambda equals 1000 metres in a period from (-1000 m to 1000 m). By increasing tilt top morphology gets closer to tilted flat surface where no $CO_2$ will be trapped (in this figure, y refer to vertical axis z ).*

*Table 3.6 Relationship between Tilt and Amplitude and trapping when $\lambda$ equals 1000 metres (T = trapping and NT = no trapping).*

| **Tilt** $(\theta)$ **\ Amplitude (A)** | **3** | **6** | **9** |
|---|---|---|---|
| **0** | T | T | T |
| **1** | T | T | T |
| **2** | NT | T | T |
| **5** | NT | NT | NT |

## 3.4 Summary and Concluding Remarks

Firstly, the nature of the interface can influence estimates of storage capacity. A transition zone between the aquifer and the caprock leads to uncertainty in the effective aquifer volume. As discussed in section (3.1.2) this may overestimate or underestimate the storage capacity. It can be concluded that the impact of this uncertainty on the storage capacity depends on the thickness of the transition zone compared to the thickness of the aquifer. Irregularity of the interface may also increase uncertainty in the storage capacity either by providing extra local structural traps or by re-directing the $CO_2$ migration.

Secondly, the aquifer/caprock interface can affect the security of $CO_2$ storage. A transition zone can increase the security by providing partial baffles to hinder $CO_2$ migration towards the caprock and lowering pressure build up at the base of the caprock. Also, the slower the migration the longer the time for interaction of the $CO_2$ with the brine and minerals, which assists $CO_2$ trapping. Irregularity at the aquifer-caprock interface may assist structural trapping by providing extra storage volume. On the other hand, topographical highs may provide pathways for rapid migration of $CO_2$ from the injector, especially where such highs serve to focus subsequent tectonic deformation.

Thirdly, the results of the detailed simulations show that the amount of dissolved $CO_2$ in the storage formation 100 years post injection period is more sensitive to the tilt than to the anisotropy ratio for permeability ($k_V/k_H$) and amplitude or thickness of transition zone.

In this study the effect of some petrophysical properties such as $k_V/k_H$ were also considered. One noticeable result during injection was the importance of the $k_V/k_H$ ratio. In other words, it was not just the caprock morphology that was affecting the results (dissolution and plume migration), it was the structure of the aquifer as a whole (The $k_V/k_H$ ratio is used to take account of small-scale structure, which tends to be approximately horizontal). Lateral plume migration has been extensively studied (e.g. Gasda et al 2008, Gasda and Celia 2005). However, the effect of the combination of tilt, $k_V/k_H$ ratio, and amplitude during injection and post injection period was not addressed. Regarding the length of the plume, one interesting result was a change in the length of the plume when the tilt of the aquifer changed from 4 to 5 degrees. This is

due to the increase in the density difference between $CO_2$ and brine. However, in models with lower $k_V/k_H$ ratio this is not the case. The effects of amplitude, $k_V/k_H$ ratio and tilt on the width of the plume in *perp* models are similar. In some works such as Nilsen et al. (2012), the main focus was on the morphology of the top surface of storage formation.

In addition, the transition zone has a positive effect on the $CO_2$ storage as more $CO_2$ dissolved and the $CO_2$ vertical migration is limited too. In order to study the effect of top morphology on the $CO_2$ storage the amplitude of ridges and the orientations of ridges to the tilt varied systematically which, has not been addressed in any work previously. Ridges with higher amplitude (bigger than plume thickness) provided more structural trapping if they are perpendicular to the tilt. However, ridges parallel to the tilt provide a pathway for rapid $CO_2$ upwards migration. Although this may increase the risk of $CO_2$ leakage as it migrates further away from the injection point, more $CO_2$ is dissolved due to more migration.

An equation for the relationship between tilt $(\theta)$, amplitude $(A)$, and wavelength $(\lambda)$ is presented (equation 3.6) that can be deployed to find out under what conditions the morphology of top surface could make a significant difference, and what will never have an effect. It can be concluded that as long as $\tan(\theta) \prec (2\pi A/\lambda)$ a percentage of $CO_2$ will be trapped under ridges. Therefore, this could be a simple important measurement tool to identify whether the topography of top surface has an important role in $CO_2$ trapping or not.

In general, it could be concluded that the amount of $CO_2$ dissolution in saline aquifers is not dependent on the direction of the ridges at the top of aquifer or thickness of the transition zone (allowing a few percent differences). However, these have a significant effect on the plume migration and specially the amount of $CO_2$ which could reach at the top of the aquifer. The effect of amplitude on plume migration is more important for the cases with small tilt angle than large tilt angle models.

These results suggest that good reservoir characterization is required for planned $CO_2$ storage sites. In conclusion, this work shows the importance of characterising the interface in terms of the size (amplitude and lateral extent) of irregularities and also in terms of the existence of any transition zone which has not been addressed in previous works.

# Chapter 4

# The Role of Unconformable Surfaces as an Interface between Caprock and Storage Formation

## 4.1 Introduction

A structural trap is an essential prerequisite for $CO_2$ sequestration. In Chapter 3 the importance of characterisation of the interface between the caprock and the aquifer was shown. This work follows on from Shariatipour et al. (2012), and investigates the effect of unconformities, which is one type of interface, on the storage capacity and security.

Unconformities have been studied extensively, especially because of the types of trap they provide for oil and gas in the geological formations. There are four types of unconformity: angular unconformity, disconformity, paraconformity and non-conformity (Dunbar and Rogers 1957). In this study the focus is on angular unconformities. An angular unconformity is caused by erosion of underlying sediments that have been previously folded or tilted.

In this study, the term "unconformity surface" is used. Just above the unconformity surface or just below that, there could be a high permeability or low permeability layer. The high permeability layer could be the result of weathering and erosion of the older layer at the unconformity surface or deposition of the coarse-grained sediments on top of unconformity surface (Swierczek 2012). Besly et al. (1993) and Swierczek (2012) studied the base Permian Unconformity in the Southern North Sea and they analysed the petrophysical properties of some wells logs (Cygnus field, UKCS Quadrant 44). They presented a theory that a zone just beneath the Permian unconformity had been weathered, and consequently the permeability and the porosity of this zone have increased dramatically (average porosity changed from 0.1 to 0.2 and average permeability changed from 0.1-10 mD to 500 mD). In this work, the effect such a structure has on $CO_2$ storage has been studied.

## 4.2 Methodology

A number of 2D and 3D numerical simulations were conducted to study the impact of unconformities on $CO_2$ storage. All models were constructed in Petrel (Schlumberger, 2011a). The reservoir models were input to the ECLIPSE reservoir simulator (Schlumberger, 2011b).

Due to the slope of the layers in an angular unconformity, an investigation on the effect of type of gridding on $CO_2$ storage needs to be carried out before modelling the unconformity.

### *4.2.1 An Investigation on the Effect of Type of Gridding on $CO_2$ Storage*

Spatial discretisation is used to perform the numerical block to block flow calculation. In Geo-Modelling software such as Petrel there are different options to grid the models. During model construction, when dividing the zones into different layers, the layers can be proportional to the top and bottom horizon of the zone, or fractional, or follow top or base of the model. When simulating the $CO_2$ storage in an aquifer the result of $CO_2$ migration may depend on the type of gridding used.

In this study the effects of different gridding techniques were investigated. Two sets of grids were examined, the first one corresponding to a regular 100×1×71 flat grid (Figure ***4.1***), and the second one corresponding to a 50×1×131 tilted grid (corner point geometry) (Figure ***4.2***).

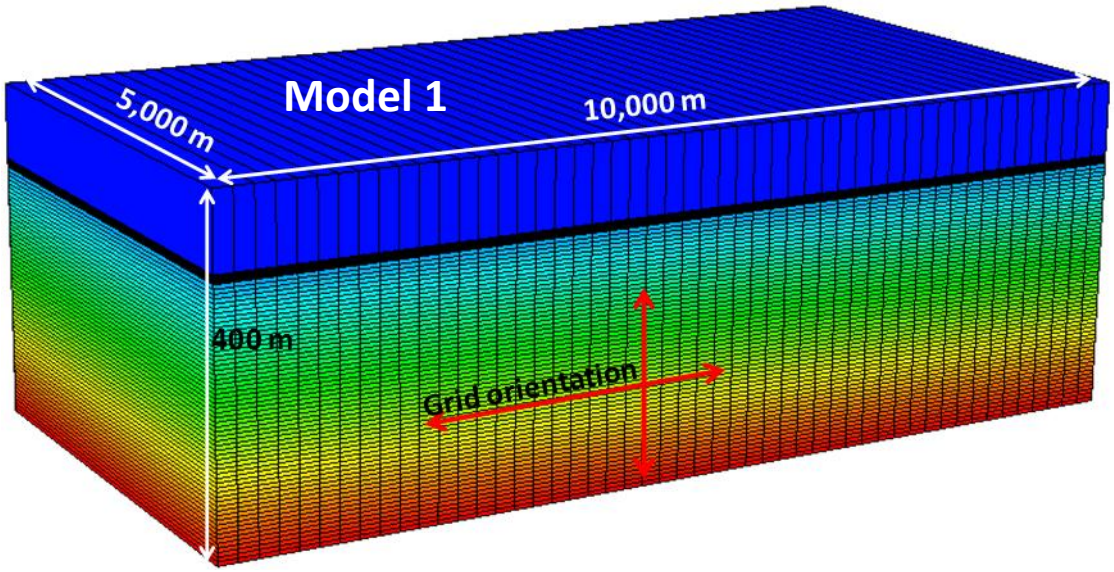


*Figure 4.1 Regular flat Cartesian grid*

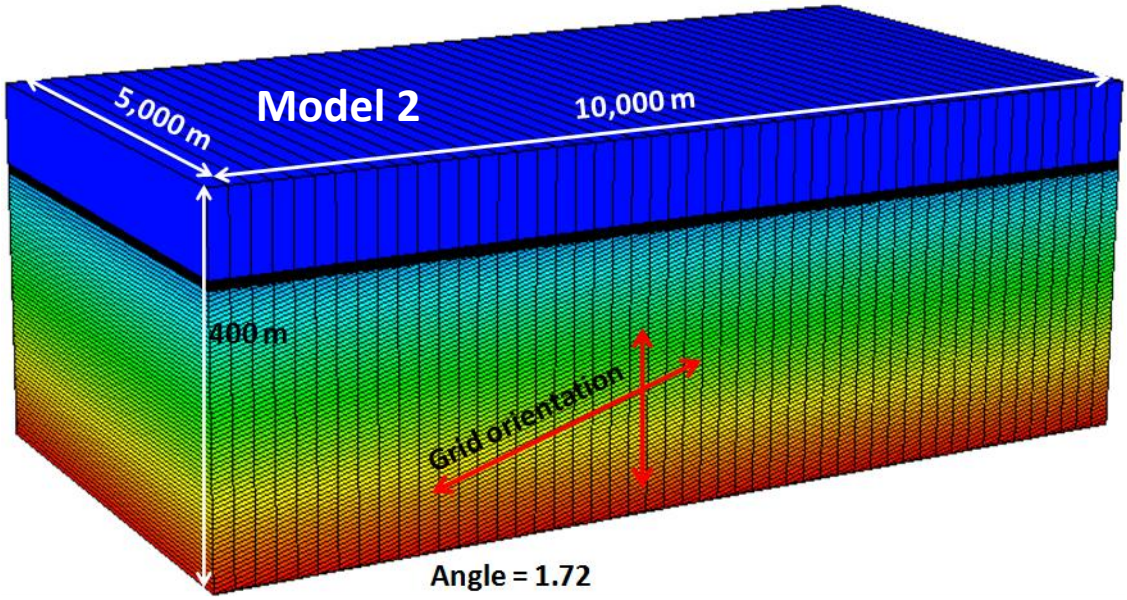


*Figure 4.2 Tilted grid*

Both models have the same pore volume and each model is divided into three sections. The top part of the models, which consists of one layer, corresponds to the caprock. The second part, referred to as the interface between caprock and storage formation consists of ten layers in the z direction. These are regular Cartesian grid cells in both models. The third part which is assumed to be the aquifer is different in terms of types of grid. In Model 1, a regular Cartesian grid was used and the aquifer was discretised into 50 layers in the z direction, 5 meters thick each. For Model 2, although the thickness of each layer is the same as in the Model 1, the numbers of layers (120) is greater, as they are diagonally elongated.

When $CO_2$ is injected into an aquifer, it rises up under buoyancy, reaches the caprock, and then starts to migrate laterally. In the Model 2, at the top of the storage formation where the tilted grid cells meet the regular grid cells, all of the tilted grid cells pinch out.

The aquifer was assumed to be homogeneous: the aquifer (sand) was assigned a permeability of 1000 mD and a porosity of 0.25, and the other reservoir lithologies a permeability of 1E-6 mD and a porosity of 0.1. An injector was placed on the left hand side of both 2D models. The wells were controlled by the surface injection rate which was 1,000,000 cubic metres per day with a maximum pressure limit of 600 bars. The injectors were shut in after 50 years and the simulations were continued for 1000 years. Zero-flow boundaries were assumed to be present at all edges of the models. The same properties were used for both models. The initial pore fluid pressure was assumed to be hydrostatic, around 90 bar at the top of the storage structure.

Figure ***4.3*** shows lateral migration of $CO_2$ at the top of the aquifer in Models 1 and 2 at different time steps. At the very top of the aquifer in Model 1, $CO_2$ migrates laterally away from the injector. In Model 2, the $CO_2$ cannot migrate laterally by moving horizontally from one cell to the next, due to the cells pinching out. $CO_2$ must move to a lower (deeper) cell before migration laterally (Figure ***4.3***). Therefore, in Model 2 there is a thicker plume whereas in Model 1 there is a thinner plume which migrates further. The difference in $CO_2$ migration in these models can be observed from Figure ***4.3*** where in Model 1 at the $11^{th}$ time step $CO_2$ reached the $6^{th}$ cell in the right hand side of injector (top picture) whereas in Model 2 at the same time step $CO_2$ reached the $4^{th}$ cell in the right hand side of the injector (bottom picture).

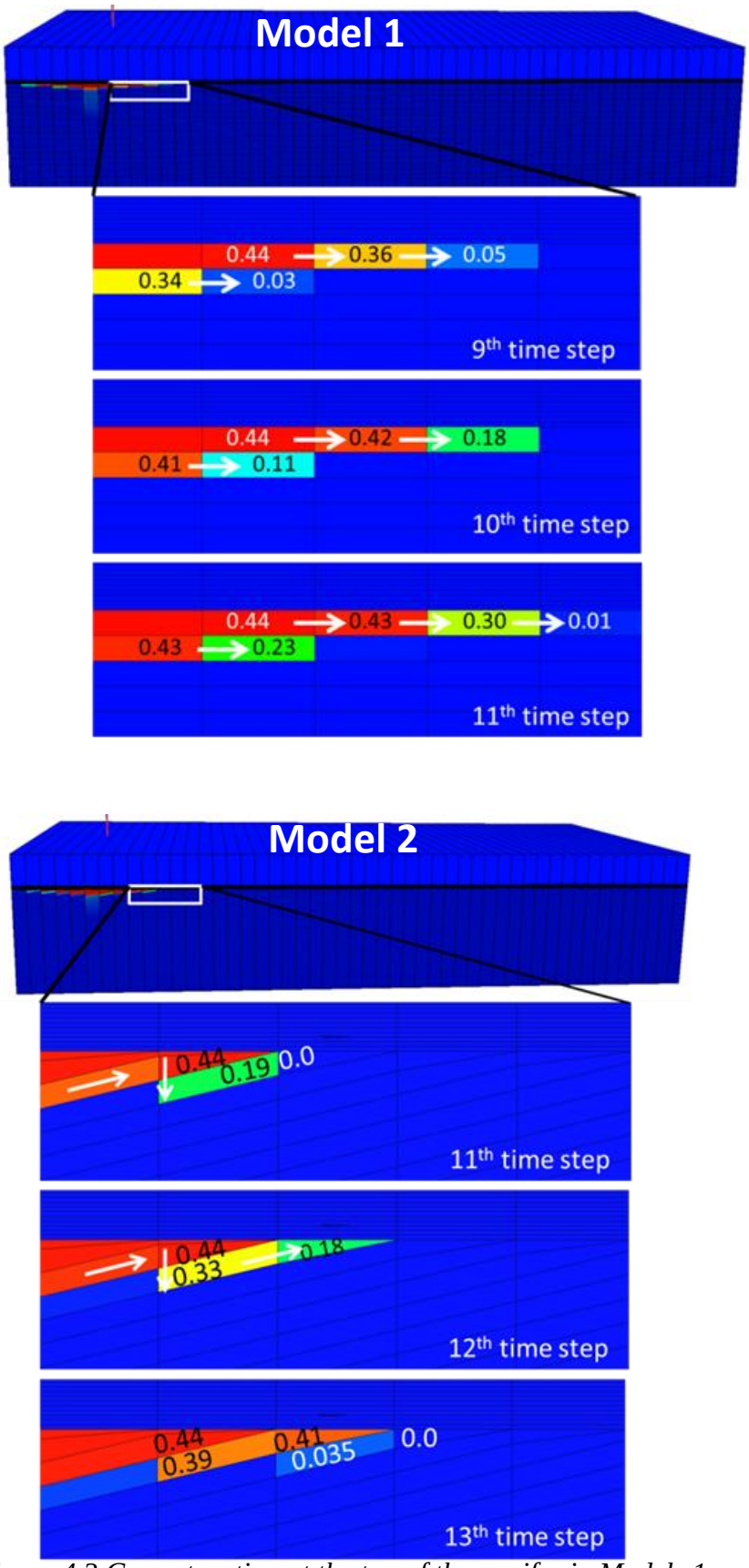


*Figure 4.3 Gas saturation at the top of the aquifer in Models 1 and 2. Model 1, top picture (Cartesian grid) and Model 2, bottom picture (Tilted grid). White arrows show $CO_2$ migration direction and the values written in the grid cells are gas saturation values.*

Figure ***4.4*** demonstrates the distribution of the $CO_2$ plume in Models 1 and 2 at the end of post injection period. It is clear that the plume migrates further in Model 1 than Model 2. However, the thickness of the plume in Model 2 is greater than that in Model 1. This is because of the way that cells are oriented at the top of the aquifer in Model 2; subsequently there is more accumulation of $CO_2$ at the top of the aquifer.

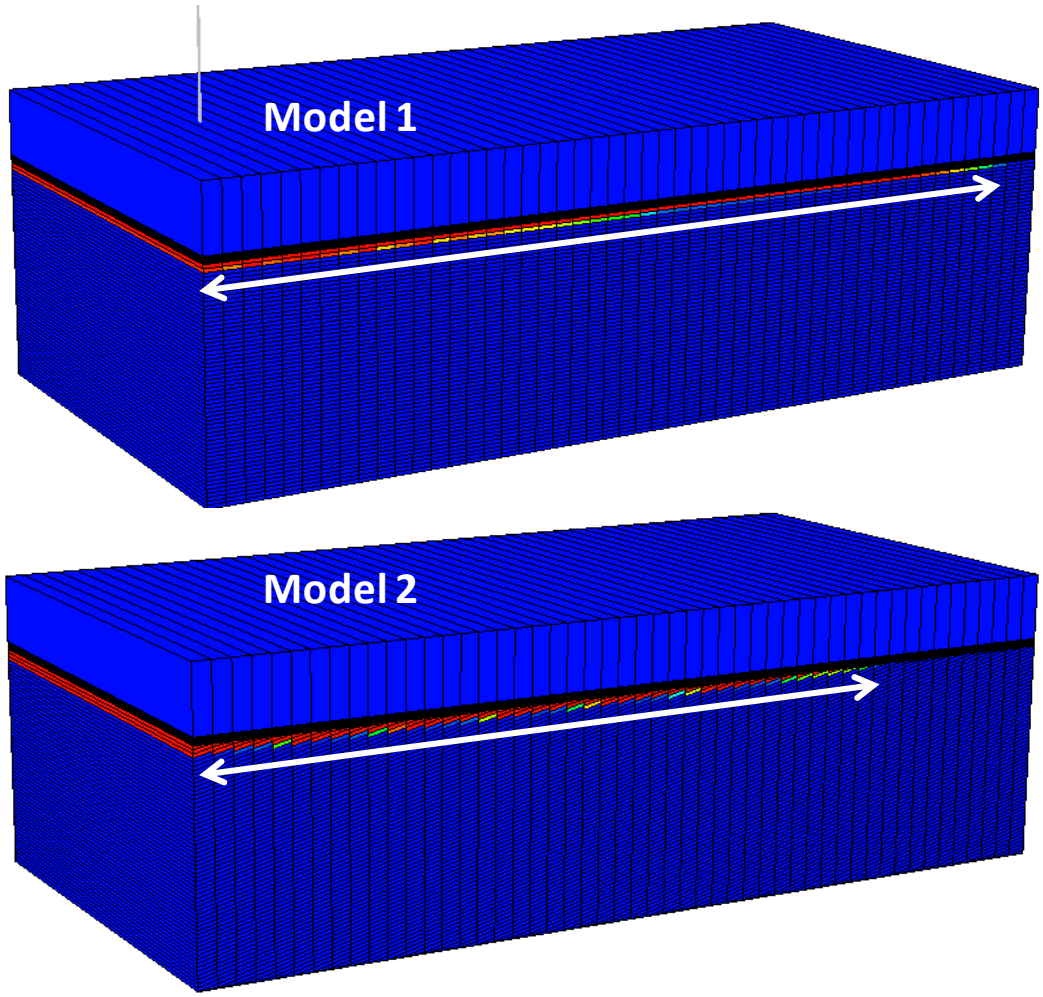


*Figure 4.4 $CO_2$ Gas saturation at the end of post injection period (White array shows length of plume).*

Regarding the amount of $CO_2$ dissolved in brine, in Model 1 (regular Cartesian grids), $CO_2$ migrates laterally more at the top of the aquifer than Model 1, and so more free $CO_2$ phase is in contact with the fresh brine resulting in more $CO_2$ dissolution (10%) in Model 1 than Model 2 (Figure ***4.5***). Since there is more dissolution in Model 1, there is less free $CO_2$ and therefore the average field pressure is lower.

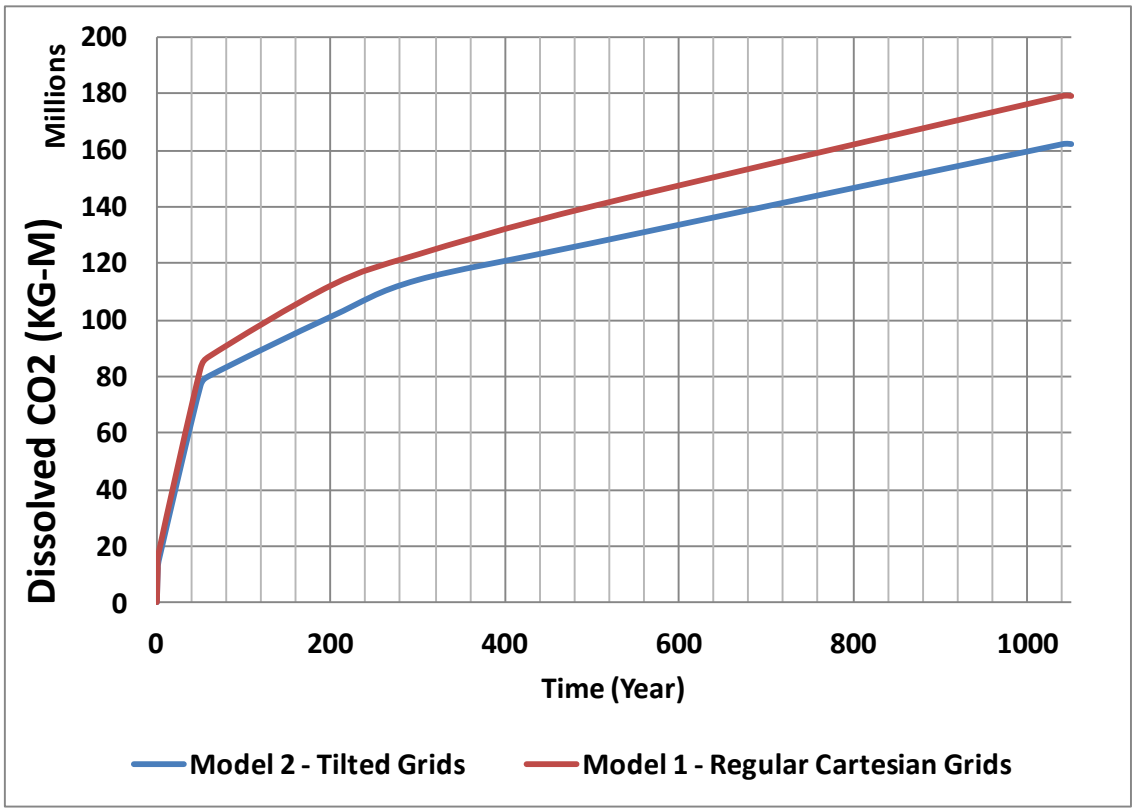


*Figure 4.5 $CO_2$ dissolved in Water Phase in Both Models.*

***Discussions***

This part of the study is only aimed at comparing the effect of different gridding techniques available in the reservoir simulator for the simulation of $CO_2$ storage in aquifers. The results reveal that when the models are gridded extra consideration needs to be carried out. Specifically, where there are some tilted layers and we may need to use a tilted grid for some of these layers. However, the current study shows that an increase in inclination of the aquifer cells leads to a decrease in the distance migrated by the $CO_2$, both during the injection and post injection period. This effect is more significant where these inclined grids pinch out (e.g. in Model 2 at the top of the aquifer).

The results demonstrate that the way in which the model is gridded affects the results, both in terms of the distance migrated and the amount of dissolution.

Although the findings of this study are very important in modelling of $CO_2$ storage as they show that different types of gridding lead to overestimation or underestimation of the amount of dissolved $CO_2$ in aquifer. However, this fact does not affect our modelling results in the next section, because all the models will be constructed in the same way (regular flat Cartesian grid) and then the results are compared.

## 4.3 2D Model

This is an analysis of the effect of a thin conductive layer (as a result of weathering at the unconformity surface) at the aquifer-caprock interface. A 2D model with a length of 10 km, thickness of 400 m, and a width of 100 metres was used (Figure ***4.6***). This model was devised to check seepage out of Aquifer 1, which was assumed to be the storage formation.

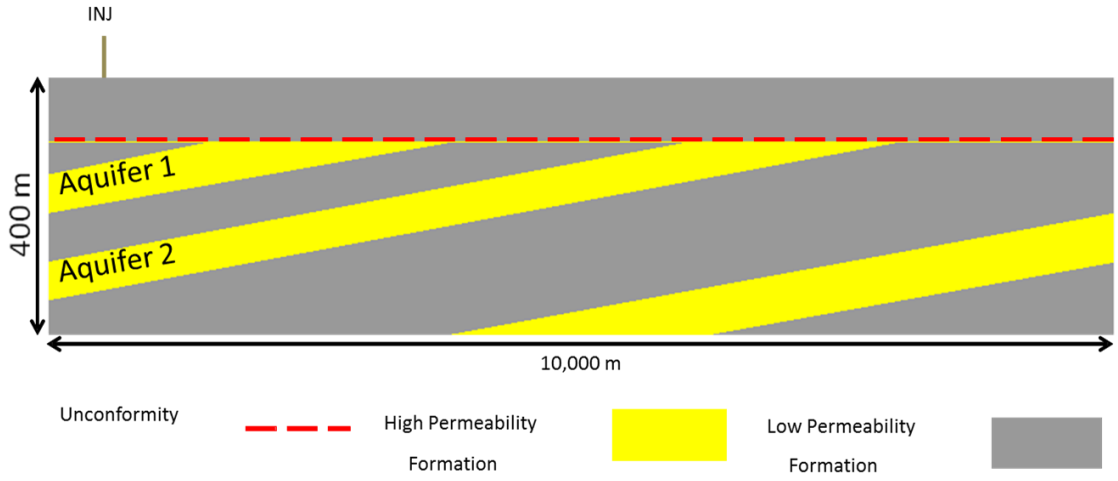


*Figure 4.6 Angular Unconformity 2D Model.*

Seven Models were considered (Table ***4.1***), the only difference between Model 1, Model 2, and Model 3 being the thickness of the high permeability layer beneath the caprock. The thickness of the high permeability layer in Model 1, Model 2, and Model 3 is 100 cm, 10 cm, and 1 cm respectively. The aquifers were assumed to be homogeneous. The aquifers and the thin layer below the caprock were assigned a permeability of one Darcy and a porosity of 0.25, and the other reservoir lithologies were assigned a permeability of 1E-6 mD and a porosity of 0.1.

To investigate the effect of grid refinement, Model 1 was modified to Model 4 by refining the high permeable layer below the caprock from one layer to ten layers.

Model 5 is based on Model 4, but the perforations in the injector well were at the bottom of Aquifer 2 while the location of the injector was the same as in Model 4. Models 6 and 7 are the same as Models 4 and 5 respectively apart from the properties of the layer below caprock. In these cases, the high permeability layer was replaced with low permeability, equal to the permeability of the caprock, and the interface region (R2) was assumed to be part of R1 (caprock).

*Table 4.1Models details*

| Model | Thickness of conductive layer (cm) | Number of layers (Refinement) | Primary storage target | Perforations | Permeability |
|---|---|---|---|---|---|
| 1 | 100 | 1 | Aquifer 1 | Aquifer 1 | HP |
| 2 | 10 | 1 | Aquifer 1 | Aquifer 1 | HP |
| 3 | 1 | 1 | Aquifer 1 | Aquifer 1 | HP |
| 4 | 100 | 10 | Aquifer 1 | Aquifer 1 | HP |
| 5 | 100 | 10 | Aquifer 2 | Aquifer 2 | HP |
| 6 | 100 | 10 | Aquifer 1 | Aquifer 1 | LP |
| 7 | 100 | 10 | Aquifer 2 | Aquifer 2 | LP |

To gain a better understanding of changes in the models after $CO_2$ was injected into them, the models were divided into seven regions (Figure ***4.7***).

Region 1 - caprock
Region 2 - high permeability layer
Region 3 - low permeable layer above Aquifer 1
Region 4 - Aquifer 1
Region 5 - low permeable layer between Aquifer 1 and Aquifer 2
Region 6 - Aquifer 2
Region 7 - low permeable layer below Aquifer 2

One injector was placed on the left hand side of model and $CO_2$ injected through perforations at the bottom of Aquifer 1 (R4). The well was controlled by surface rate (20,000 cubic metres per day) with a maximum pressure limit of 229 bars. However, in all models studied here the same amount of $CO_2$ was injected into the models, as the pressure did not reach the maximum bottom-hole pressure. The injector was shut in after 50 years and the simulation was continued for 200 years.

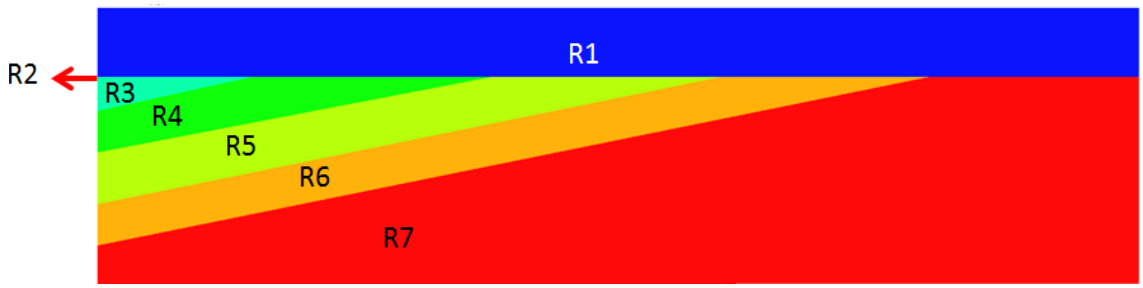


*Figure 4.7 Model regions, R stands for Region.*

### *4.3.1 Results and Discussions*

In Model 1 (which had the thickest high permeable layers) the free $CO_2$ phase migrates more easily through the high permeability layer than in Model 3, consequently there is more $CO_2$ dissolved in Aquifer 2 in Model 1 than Model 3 (Figure ***4.8*** and Figure *4.9*). However, more $CO_2$ dissolved in Model 3 overall due to higher pressure in Aquifer 1.

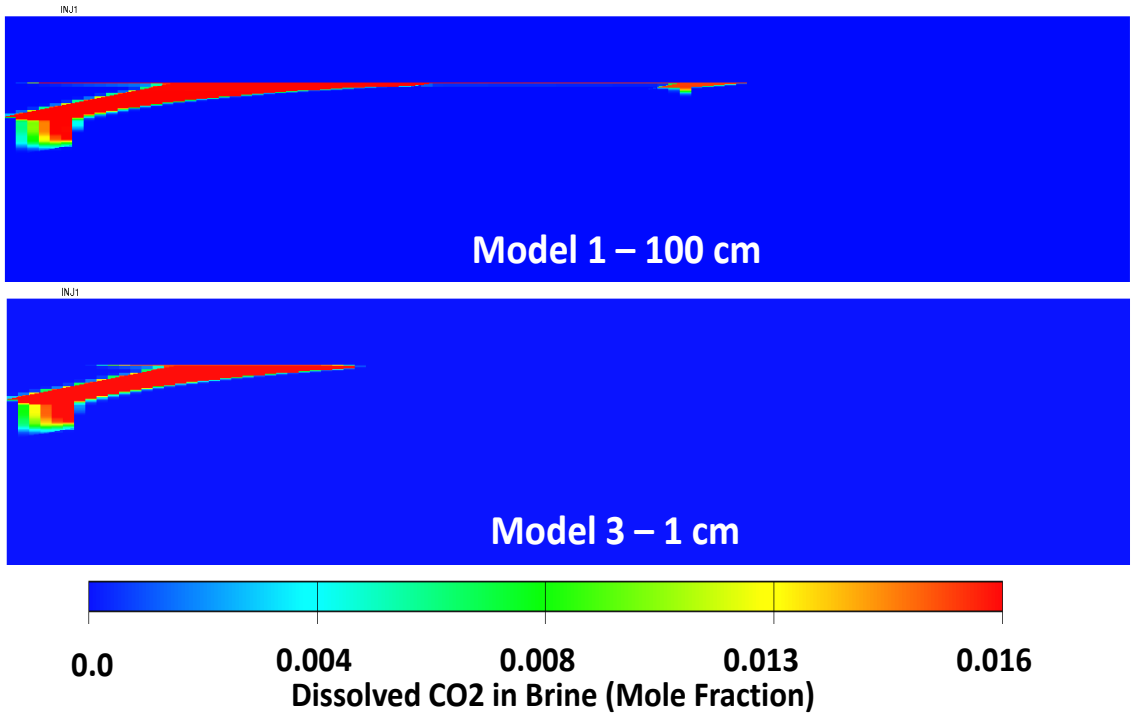


*Figure 4.8 Mole fraction of $CO_2$ dissolved in brine at the end of injection period (50 years) Models 1 and 3.*

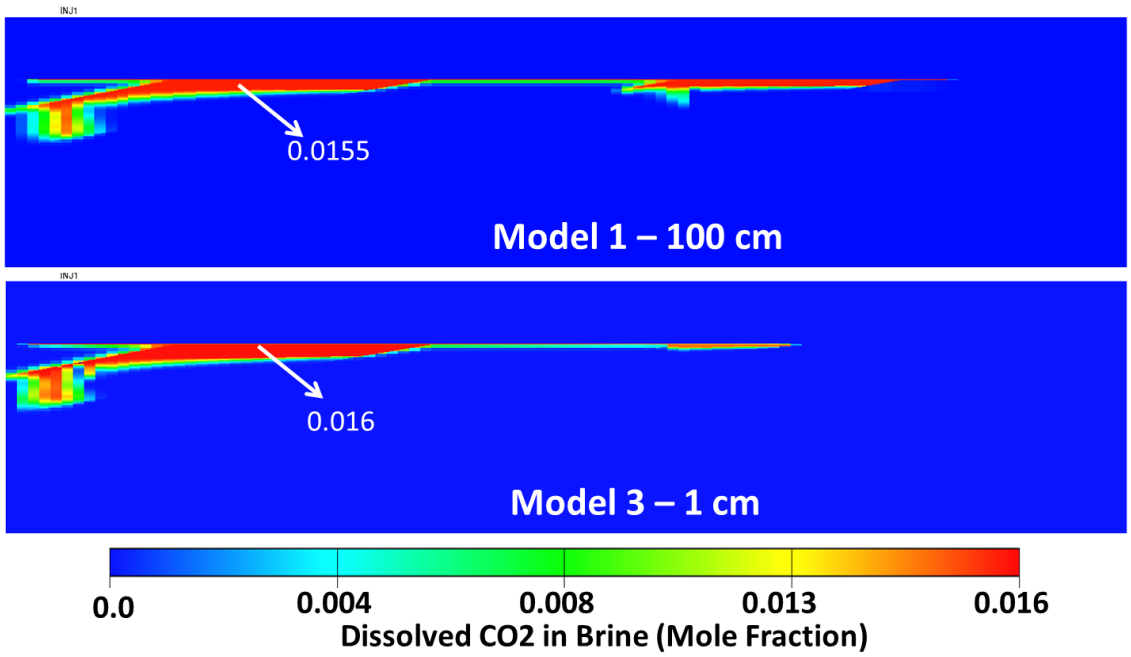


*Figure 4.9 Mole fraction of CO2 dissolved in brine 200 Years after well shut in Models 1 and 3.*

Figure ***4.10*** illustrates pressure increase in Models 1, 2, and 3 (effect of hydrostatic pressure excluded in the models). The high permeability layer beneath the caprock has a strong contribution to the pressure diffusion from Aquifer 1 to Aquifer 2 in Model 1 at the end of injection period whereas in Model 3 this is not the case (Figure ***4.10***). Interestingly, 200 years after well shut in, the average pressure in Aquifer 2 in Model 1

exceeded the average pressure in Aquifer 1 whereas in Model 3 the average pressure in Aquifer 1 has not changed significantly from the average pressure at the end of injection.

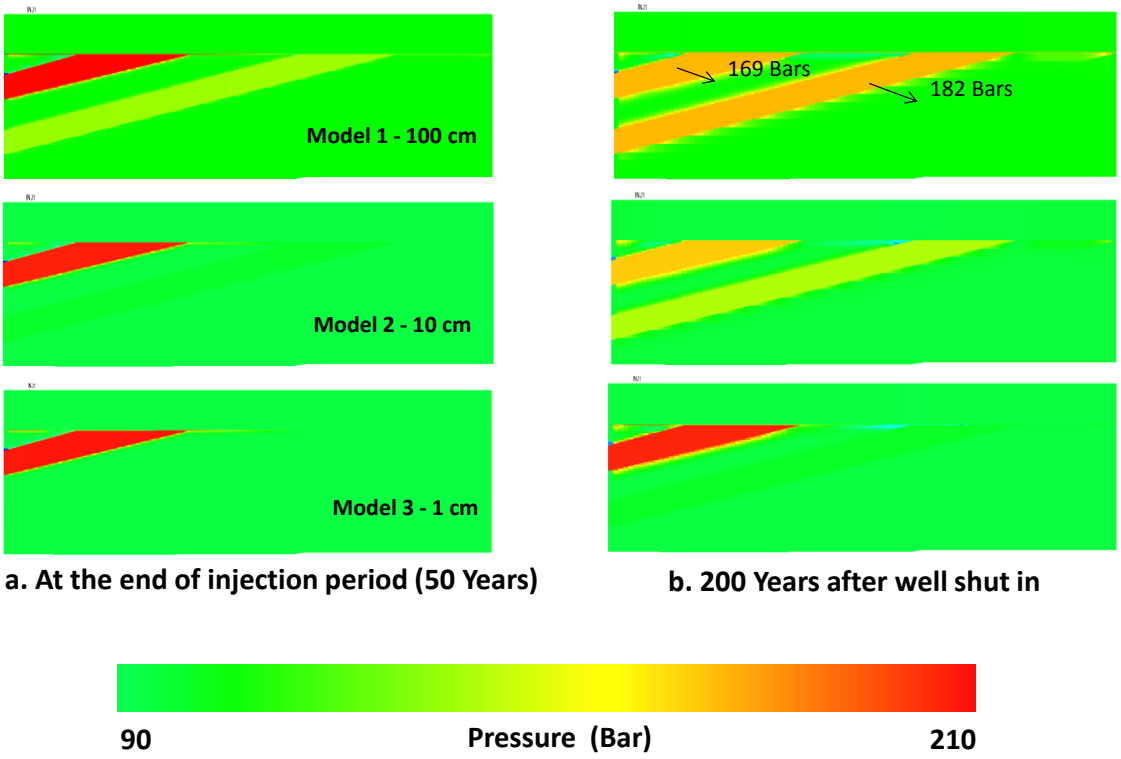


*Figure 4.10 Pressure increase (hydrostatic pressure excluded) in Models 1, 2, and 3.*

Figure ***4.11*** compares the average pressure in each region in Models 1 and 3. The average pressures in low permeability layers are the same both at the end of the injection period and the post injection period. However, the pressure in the high permeability layers (Region 2) increases due to the gas migration through them (Figure ***4.11***). In Model 3 average pressure in Aquifer 2 (R6) is lower than Aquifer 1 (R4) even 200 years after well shut in due to lower $CO_2$ migration into it.

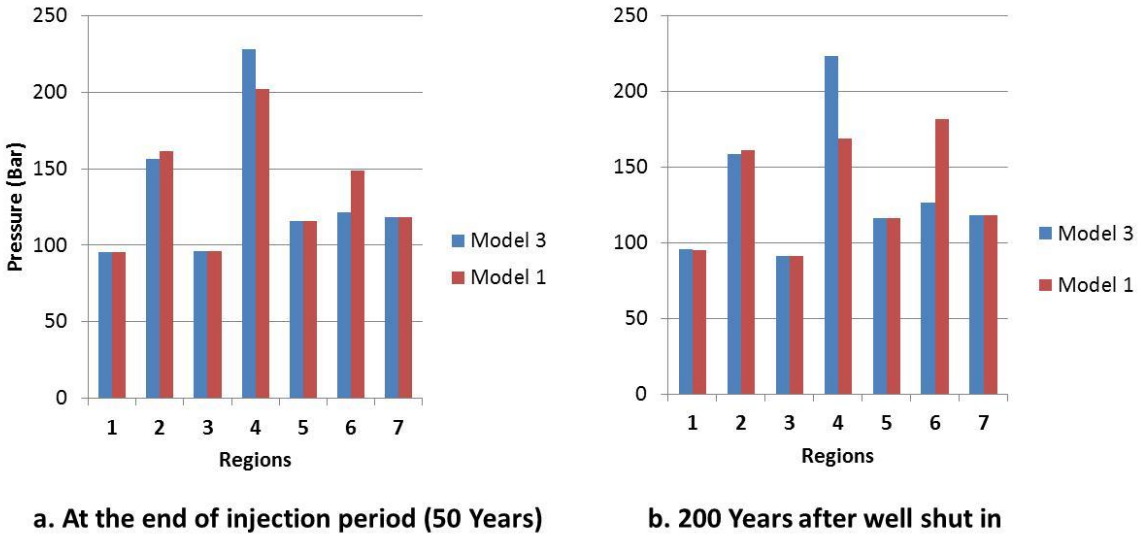

*Figure 4.11 Average pressure in regions 1 to 7.*

In Model 3, compared to Model 1, more $CO_2$ dissolved in brine in Aquifer 1 (R4) because of higher pressure (e.g. Spycher and Pruess, 2005). However, more $CO_2$ dissolved in Aquifer 2 (R6) in Model 1 than Model 3 (Figure ***4.12***) due to more $CO_2$ migration through the 1 metre high permeability layer into that aquifer.

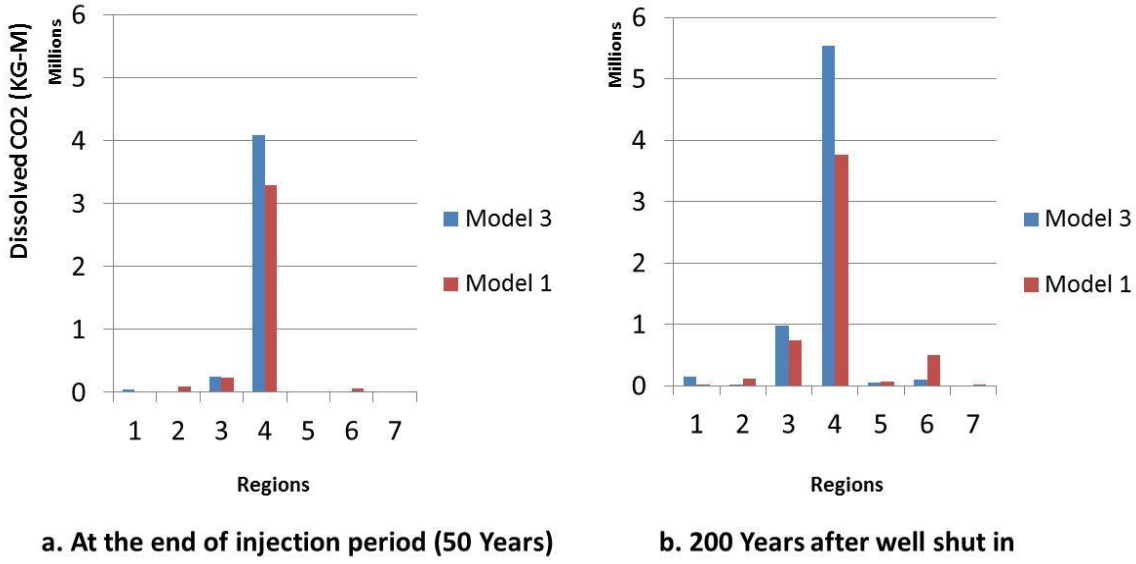


**a. At the end of injection period (50 Years)** **b. 200 Years after well shut in**

*Figure 4.12 The amount of $CO_2$ dissolved in Models 1 and 3.*

There is slightly more free $CO_2$ in Model 4 at the end of post injection period than Model 1(Figure ***4.13***), this is due to less numerical dispersion error in refined region in Model 4.

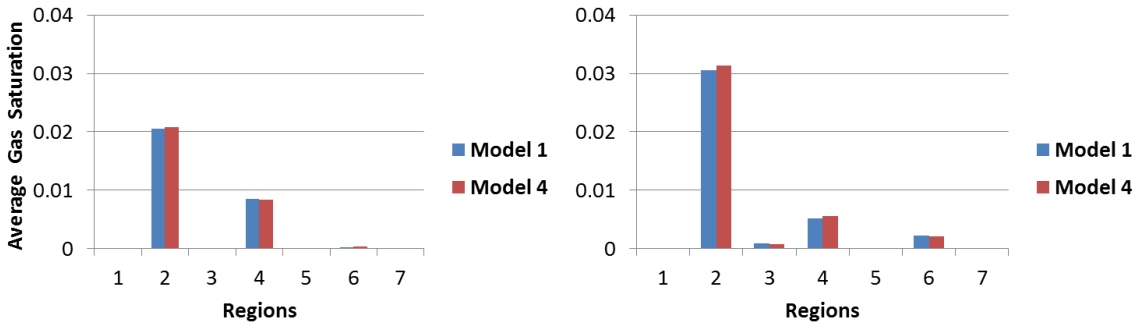


a. At the end of injection period (50 Years) b. 200 Years after well shut in

*Figure 4.13 Average free $CO_2$ Saturation in Models 1 and 4.*

Figure ***4.14*** compares the amount of $CO_2$ dissolution in Models 4 through 7. Firstly, comparing models 4 and 5 and 6 and 7, more dissolution of $CO_2$ takes place when the well is perforated in Aquifer 2. This is because the $CO_2$ migration path is longer in Aquifer 2, which encourages more dissolution. Comparing Models 4 and 6 and 5 and

7, there is more dissolution when there is no high permeability layer at the unconformity. This means that the $CO_2$ is confined to one aquifer, so the pressure increases, giving rise to more dissolution.

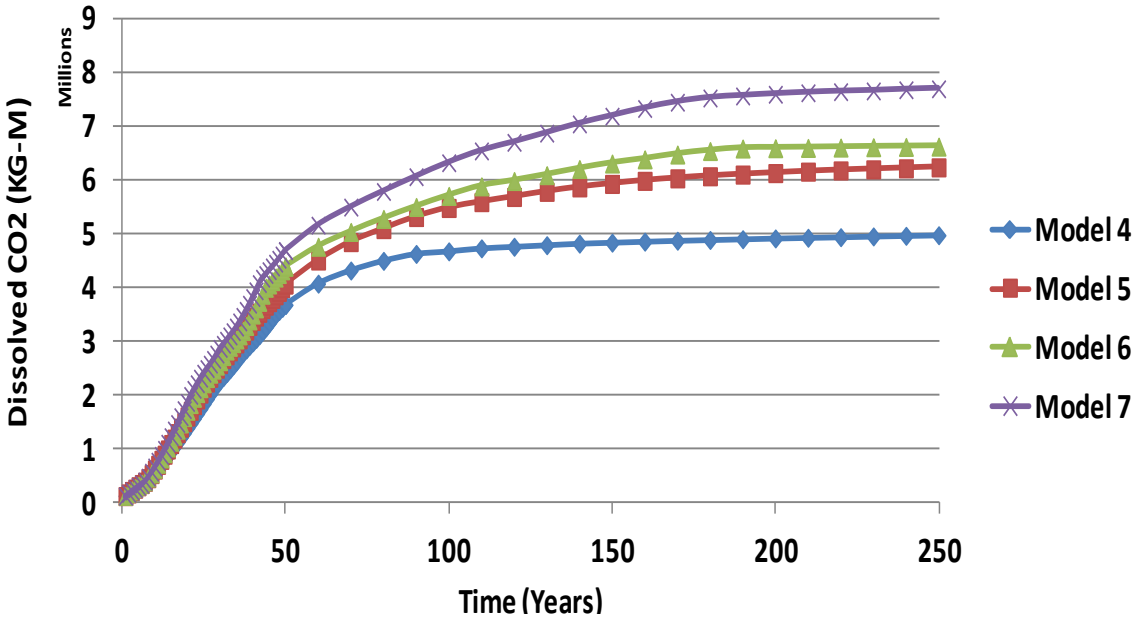


*Figure 4.14 Total amount of $CO_2$ dissolved in Models 4, 5, 6, and 7.*

### *4.3.2 Conclusions:*

The results reveal that migration of $CO_2$ is influenced by the type of sediment deposited just over or below the unconformity surface. This can have both positive and negative effects on $CO_2$ storage capacity and security.

The results indicate that unconformities could improve $CO_2$ sequestration by providing path ways for $CO_2$ migration to access other storage formations.

In the absence of a high permeability layer either above or below an unconformity, lateral migration of $CO_2$ is limited. Pressure builds up, but the amount of dissolution increases.

A very thin weathered zone (10 cm – 1m) can contribute significantly to pressure diffusion across the model, which can reduce the pressure in the reservoir as a result of $CO_2$ injection.

With appropriate placement of the well in a case where there are parallel aquifers, it is possible to maximize $CO_2$ storage.

## 4.4 3D Models

Here two Models for angular unconformity are presented (Figure ***4.15***). The diagram on the top (Model 1) shows that a group of dipped layers which lies beneath the unconformity (red line) prior to the deposition of shale (cap rock). Model 2 (bottom picture) shows an anticline whose crest was eroded (red line) prior to the deposition of the upper sediments (shale).

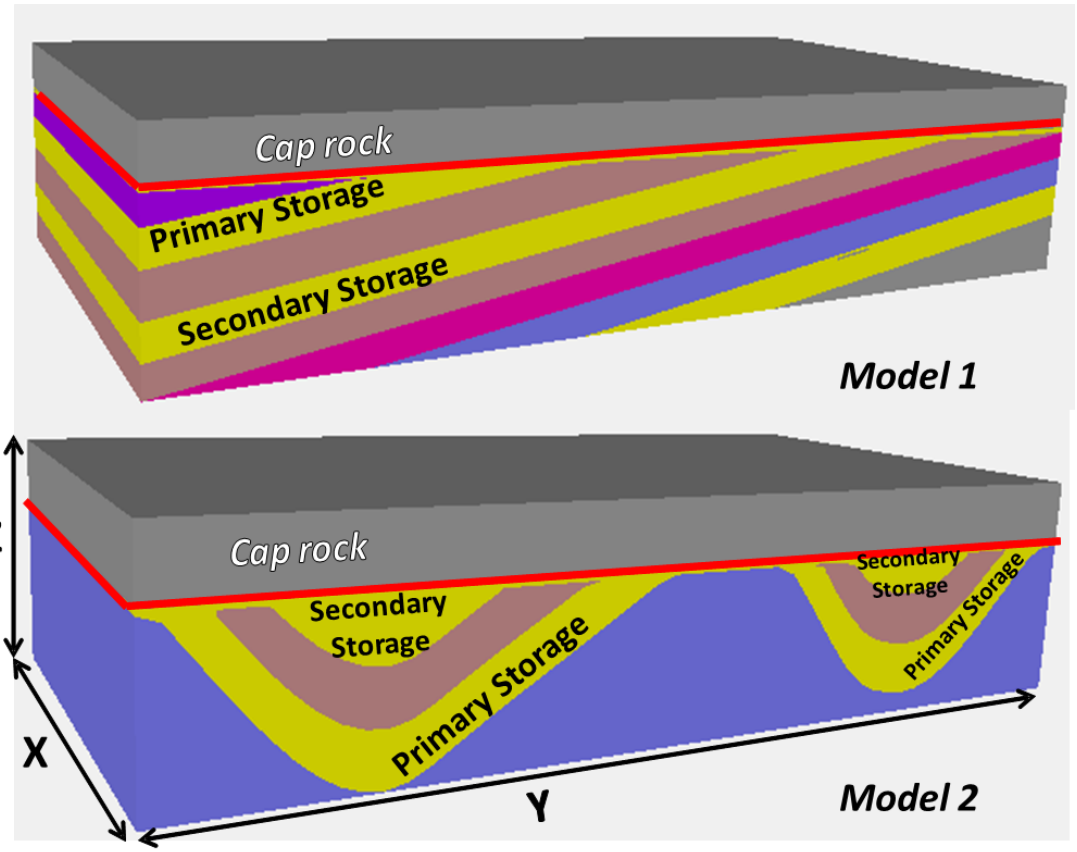


*Figure 4.15 Angular Unconformity, top picture (Model 1) illustrates a group of tilted layers that lie beneath the unconformity (red line) prior to the deposition of shale (cap rock) and bottom picture (Model 2) shows an anticline the crest of which was eroded beneath the unconformity (red line) prior to the deposition of shale.*

The models all have dimensions of 5000 m × 10000 m × 400 m. The properties for the models were taken from Smith et al. (2012) (Lincolnshire model) and are listed in Table ***4.2***.

*Table 4.2 Model's properties*

| ***Formation*** | ***Geometric Ave. Perm (mD)*** | ***Std Dev ln(Perm)*** | ***Ave. Porosity*** | ***Std. Dev. Porosity*** | ***Min Porosity*** | ***Max Porosity*** |
|---|---|---|---|---|---|---|
| ***Sandstone (storage formation)*** | 500 | 0.5 | 0.2 | 0.02 | 0.16 | 0.25 |
| ***Mudstone (Cap rock)*** | 0.006 | 0.1 | 0.1 | 0.03 | 0.06 | 0.20 |
| ***Layer between two storage formations in Model 2*** | 5 | 0.1 | 0.15 | 0.02 | 0.10 | 0.20 |
| ***Bottom layer in Model 2*** | 0.05 | 0.1 | 0.15 | 0.03 | 0.10 | 0.20 |

Models 1 and 2 were discretized into 25×50×131 cells and 25×50×77 cells respectively. Ten vertical wells were placed across the x direction on the left side of Model 1 (Figure ***4.16***). In Model 2, five vertical wells were placed on the left side of the model and five more vertical wells on the right side (Figure ***4.17***). ECLIPSE 300 with the CO2STORE module (Schlumberger, 2011) was used for all the simulations which were carried out for a period of 250 years. Three components ($CO_2$, Water and Salt) were considered. The models initially consisted of 100% brine and 100% supercritical $CO_2$ was injected during the injection period. All injectors were shut after 50 years and simulations were continued for 200 years. The same amount of $CO_2$ injected was into all cases.

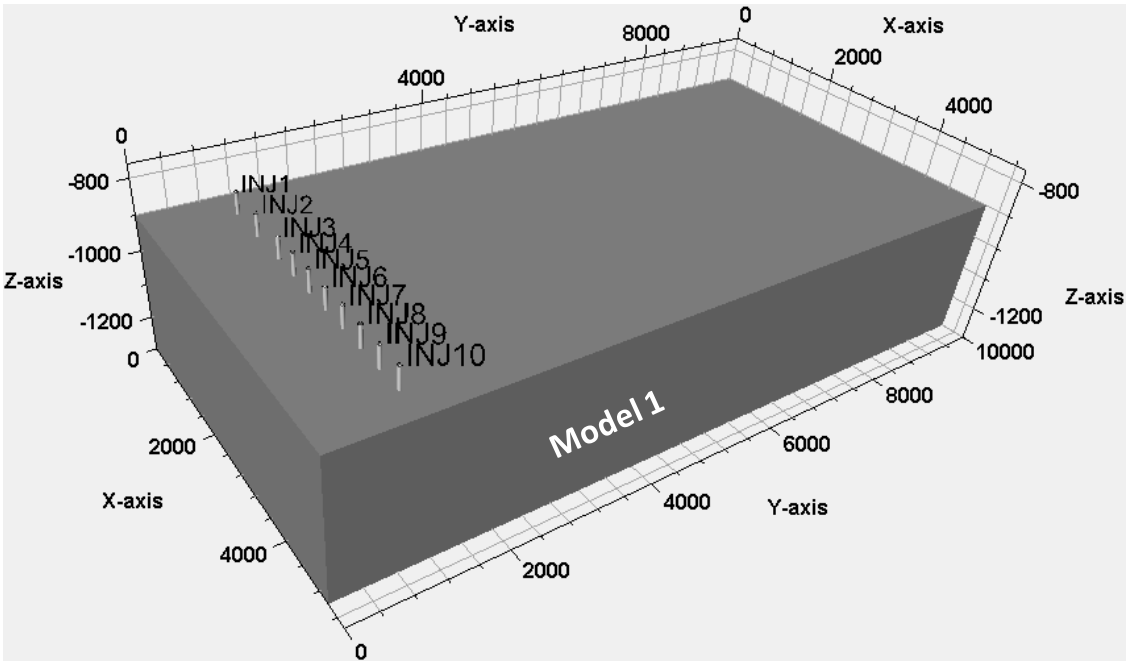


*Figure 4.16 Model 1, well locations and dimensions.*

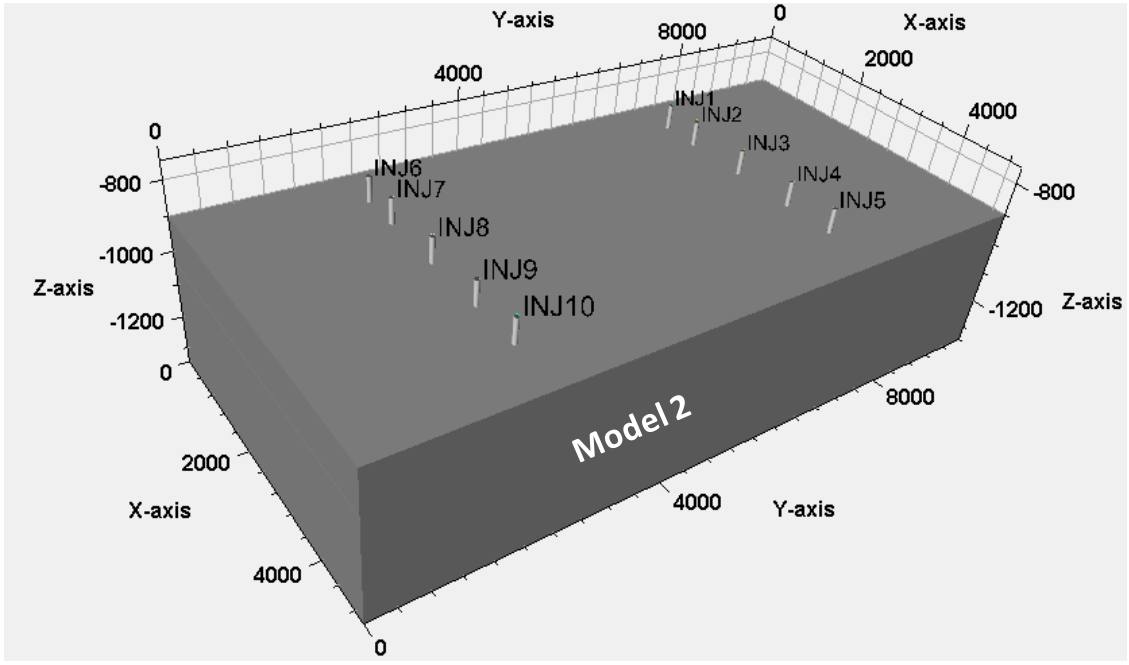


*Figure 4.17 Model 2, well locations and dimensions*

The primary and the secondary storage formations on the right side of the Model 2 did not connect with the edge of the model. This side of the model was therefore assumed closed. On the other hand, both storage formations (Figure ***4.15***) contact the left side of the model. Therefore this side of the model was assumed open, and a porosity multiplier of 1000 was applied to the left column to represent additional aquifer pore volume.

To study the effect of the unconformity surface on the $CO_2$ storage for each of these two Models, three cases (A, B and C) are made by changing the properties of the one metre thick layer just above the unconformity surface. The values of permeabilities and the porosities of that layer from high values (Sandstone) to low values (Mudstone) were changed to investigate the $CO_2$ migration beneath the caprock. Case A, could be the result of material with high permeability being deposited in the valleys (Figure ***4.18*** and Figure ***4.21***). Case B (patchy interface), could be the result of material with low permeability being deposited in the valleys (Figure ***4.19*** and Figure ***4.22***). In case C there is no difference between the properties of this layer and the layers above it, in another word, this layer has the same properties as caprock (Figure ***4.20*** and Figure ***4.23***). Table ***4.3*** shows total pore volume in these models.

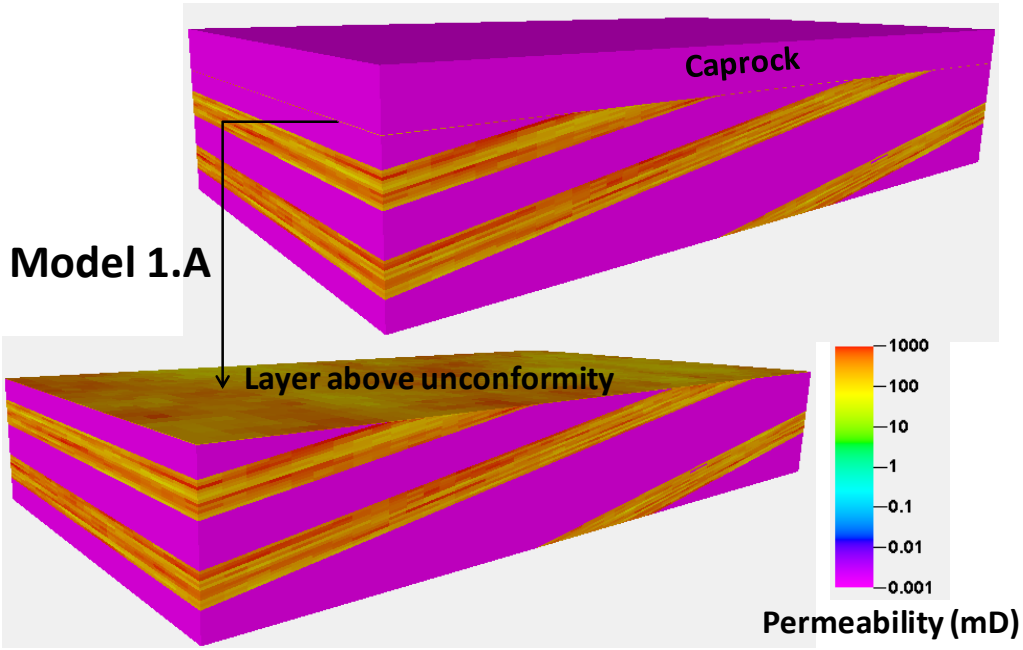


*Figure 4.18 Model 1.A permeability distributions. Top diagram shows the whole model, including the caprock. Bottom diagram shows the model, excluding caprock.*

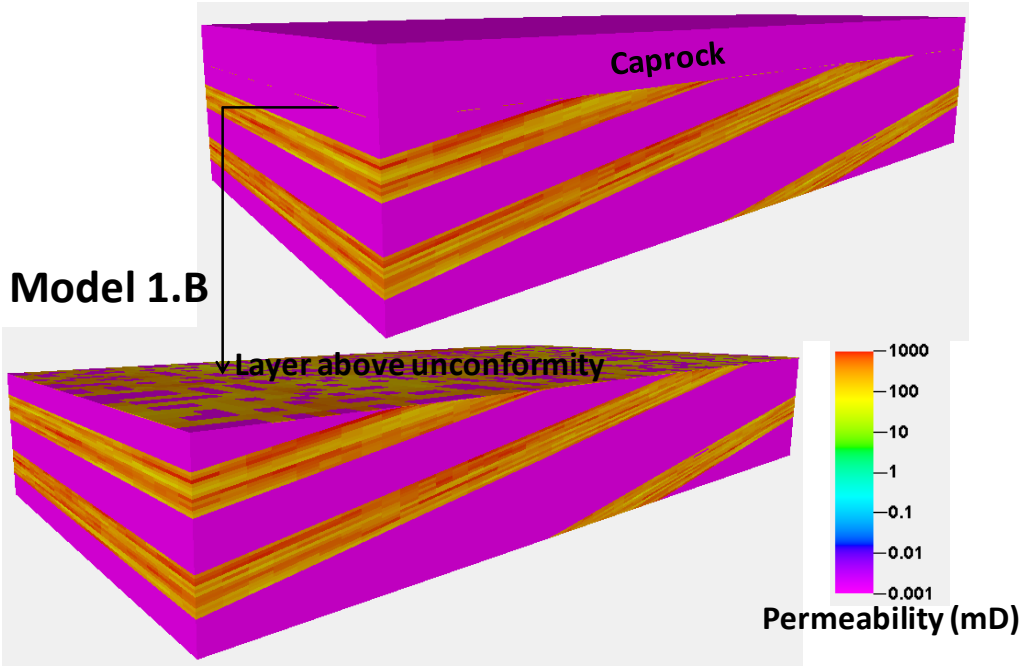


*Figure 4.19 Model 1.B permeability distributions. Top diagram shows the whole model, including the caprock. Bottom diagram shows the model, excluding caprock.*

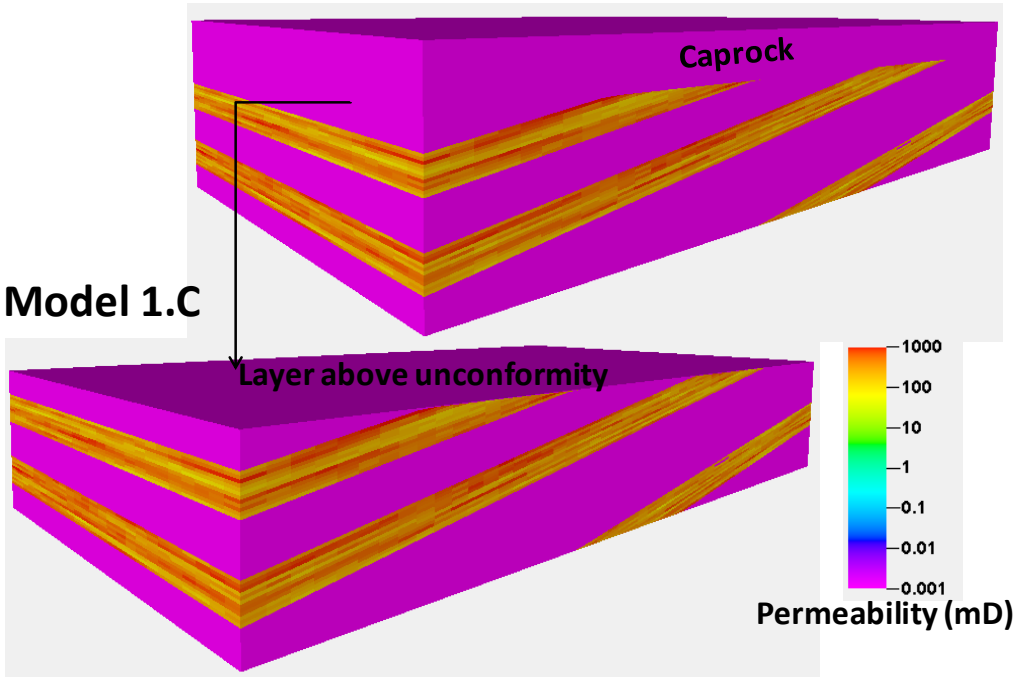


*Figure 4.20 Model 1.C permeability distributions. Top diagram shows the whole model, including the caprock. Bottom diagram shows the model, excluding caprock.*

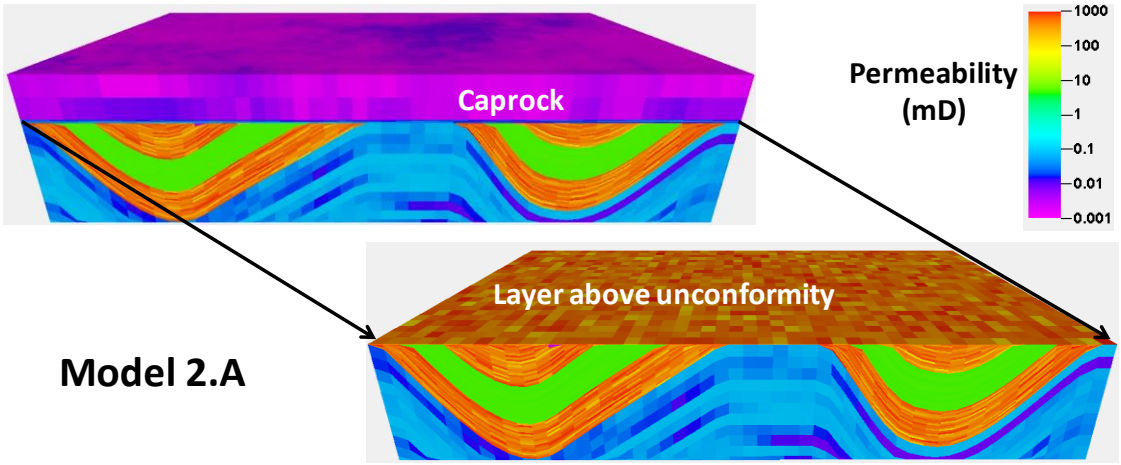


*Figure 4.21 Model 1.A permeability distributions. Top diagram shows the whole model, including the caprock. Bottom diagram shows the model, excluding caprock.*

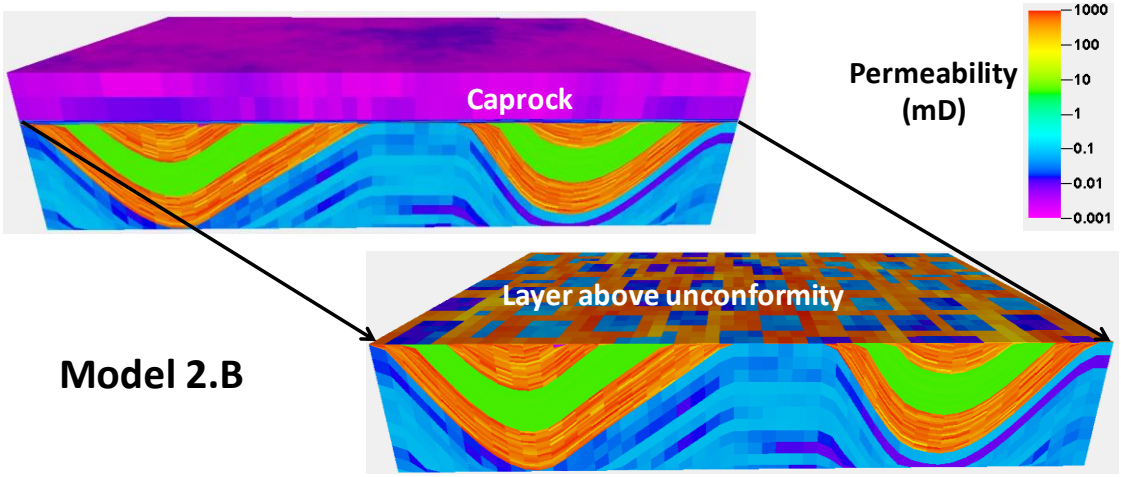


*Figure 4.22 Model 2.B permeability distributions. Top diagram shows the whole model, including the caprock. Bottom diagram shows the model, excluding caprock.*

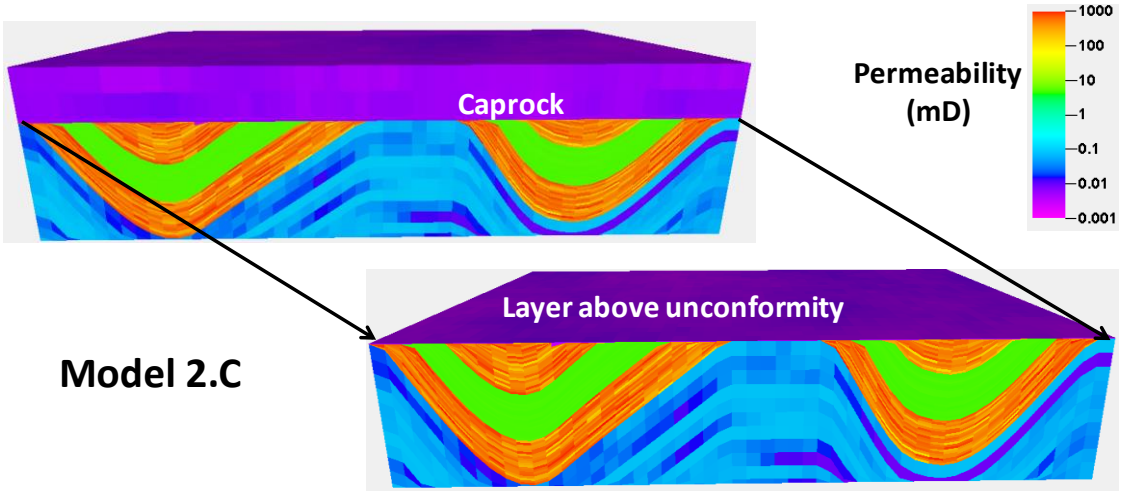

*Figure 4.23 Model 2.C permeability distributions. Top diagram shows the whole model, including the caprock. Bottom diagram shows the model, excluding caprock.*

*Table 4.3 Total pore volume (in $m^3$) in Models 1 and 2.*

| Total Pore Volume | Model 1 | Model 2 |
|---|---|---|
| **A** | 4.187334E+10 | 5.35051E+10 |
| **B** | 4.183907E+10 | 5.347378E+10 |
| **C** | 4.175741E+10 | 5.311618E+10 |

| Pore Volume | Primary Storage | Secondary Storage | Both Storage | Intermediate Layer | Sum |
|---|---|---|---|---|---|
| **Model 1.C** | 4.92E+09 | 5.32E+09 | 10.23E+09 | NA | 10.23E+09 |
| **Model 2.C** | 1.40E+09 | 3.44E+08 | 1.74E+09 | 6.52E+08 | 2.39E+09 |

### *4.4.1 Results for Section Two:*

Figure ***4.24*** to Figure ***4.29*** show the $CO_2$ gas saturation in brine for all cases of Model 1 and 2 at the end of injection period (50 years) and 200 years post injection. They illustrate how the unconformity surface affects the $CO_2$ migration beneath the cap rock. After $CO_2$ is injected into an aquifer (Primary storage in both models) near the lowest point of each aquifer, it migrates up dip under buoyancy until it reaches the caprock. Then, depending on the nature of the layer above the unconformity surface between the caprock and the storage formation, $CO_2$ migrates laterally.

If the unconformity surface has high permeability (e.g. Model 1.A and Model 2.A) the plume can easily migrate in all directions, away from injectors, under the caprock (Figure ***4.24*** and Figure ***4.27***). There are advantages and disadvantages associated with this. Regarding the advantages, $CO_2$ migrates laterally until it reaches another high permeability formation (e.g. secondary storage in Model 1 and both storage formations in the right side of Model 2). The more that $CO_2$ is in contact with brine, the more $CO_2$ dissolves, thus increasing storage capacity and security. On the other hand, $CO_2$ escapes from the primary storage and therefore the structural trapping is not very effective.

Models 1.C and 2.C demonstrate the importance of layers underlying an aquifer when there is an unconformity. In Model 1.C the properties of both layers below and above primary storage are the same as cap rock properties and it acts as a seal thus is not allowing $CO_2$ to communicate to the bottom aquifer (secondary storage) (Figure ***4.26***). However, in Model 2.C, $CO_2$ migrates through the high permeable layer and reaches the upper aquifer (secondary storage) and starts to fill it from top of aquifer (Figure ***4.29***).

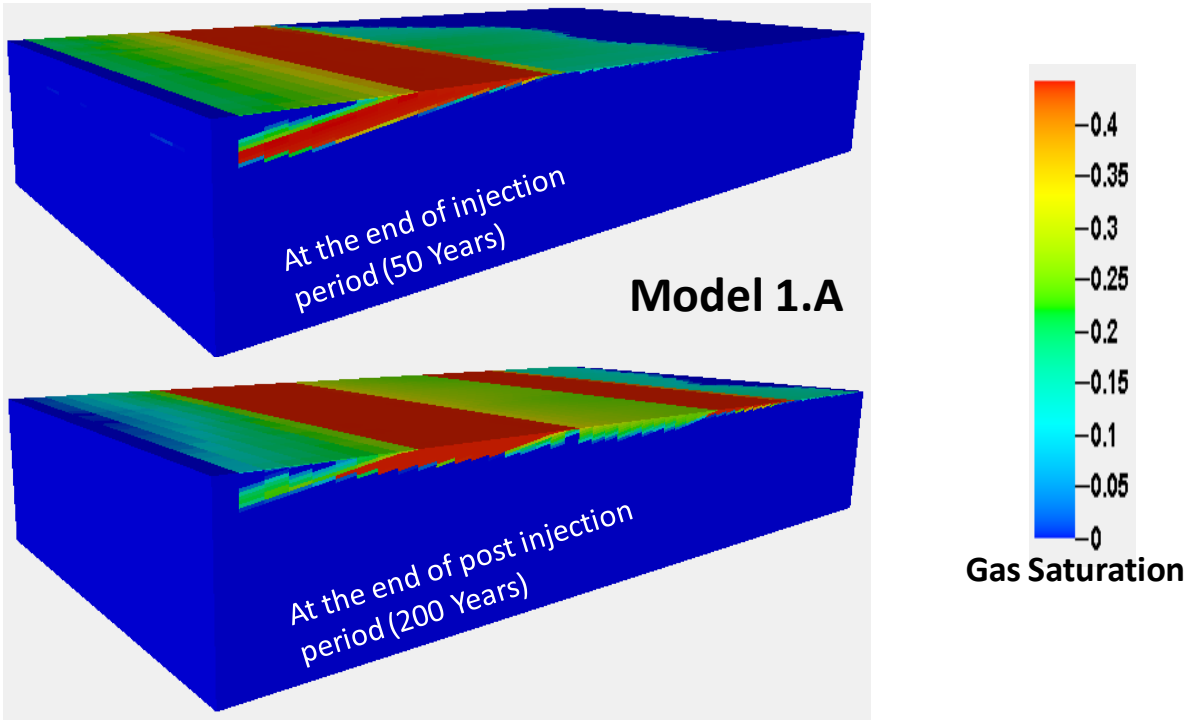


*Figure 4.24 Top picture shows $CO_2$ gas saturation in the Model 1.A at the end of injection period (50 years), bottom picture illustrates $CO_2$ gas saturation in the Model 1.A after 200 years post injection.*

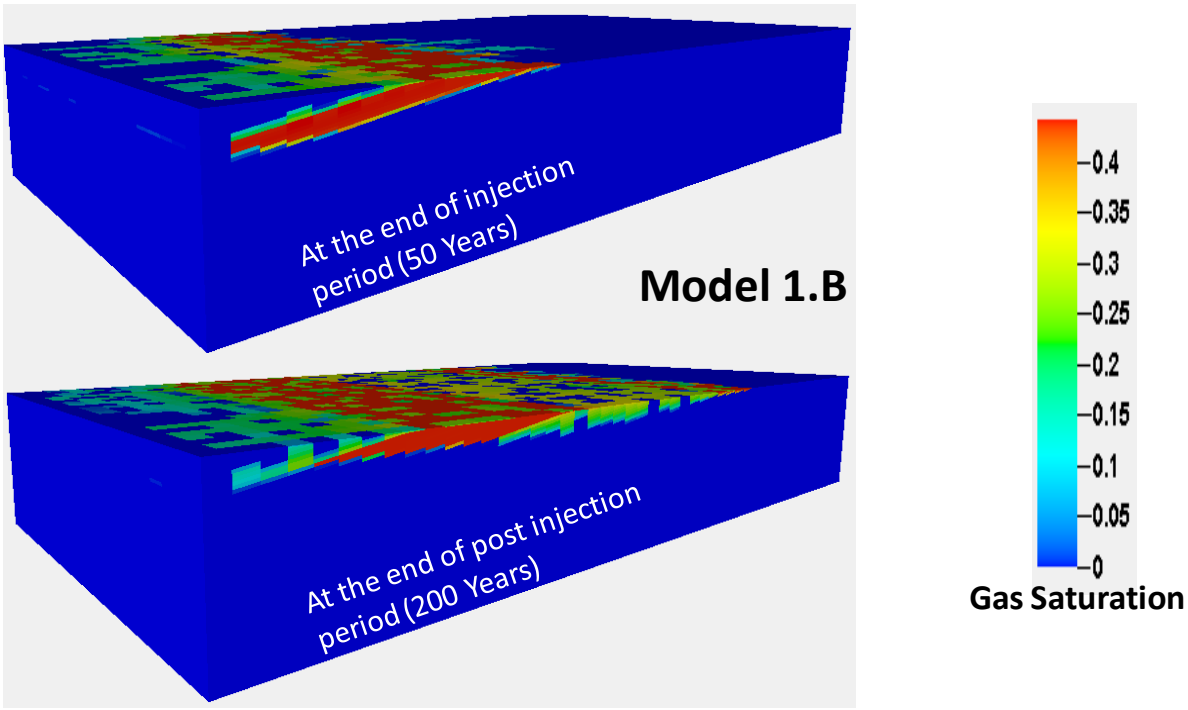


*Figure 4.25 Top picture shows $CO_2$ gas saturation in the Model 1.B at the end of injection period (50 years), bottom picture illustrates $CO_2$ gas saturation in the Model 1.B after 200 years post injection.*

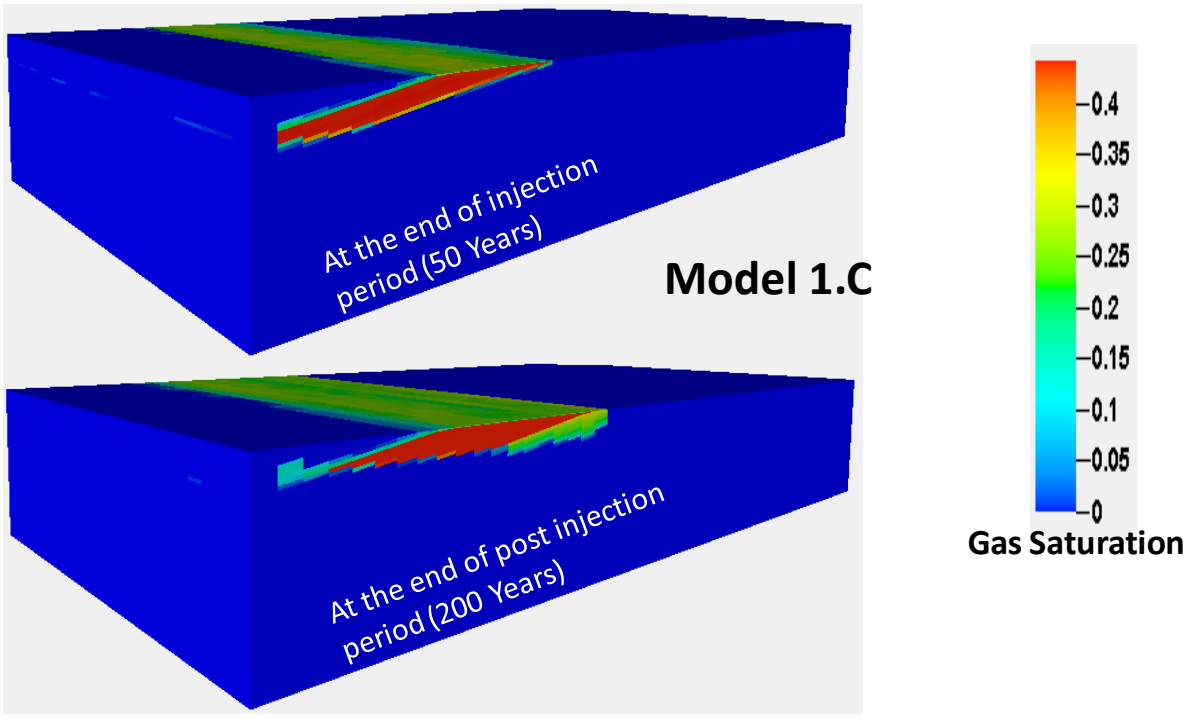


*Figure 4.26 Top picture shows $CO_2$ gas saturation in the Model 1.C at the end of injection period (50 years), bottom picture illustrates $CO_2$ gas saturation in the Model 1.C after 200 years post injection.*

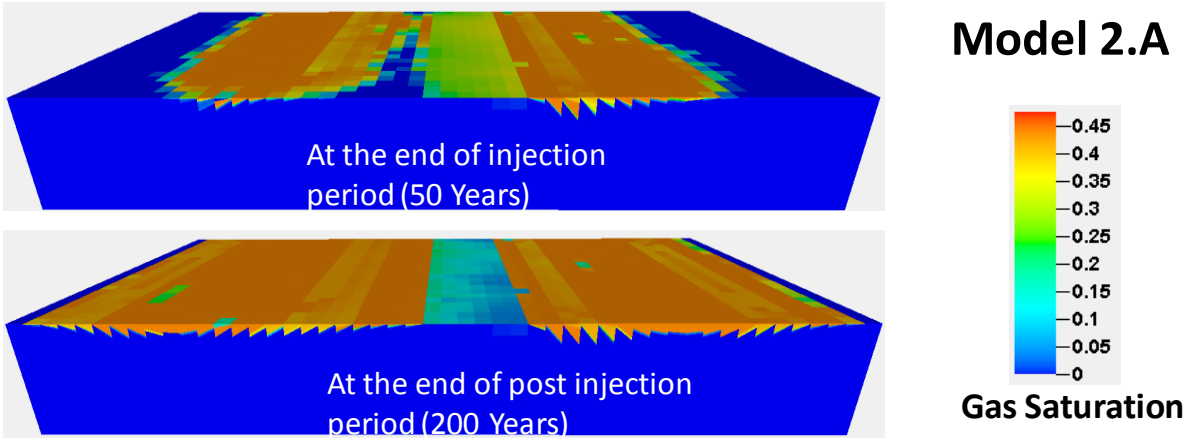


*Figure 4.27 Top picture shows $CO_2$ gas saturation in the Model 2.A at the end of injection period (50 years), bottom picture illustrates $CO_2$ gas saturation in the Model 2.A after 200 years post injection.*

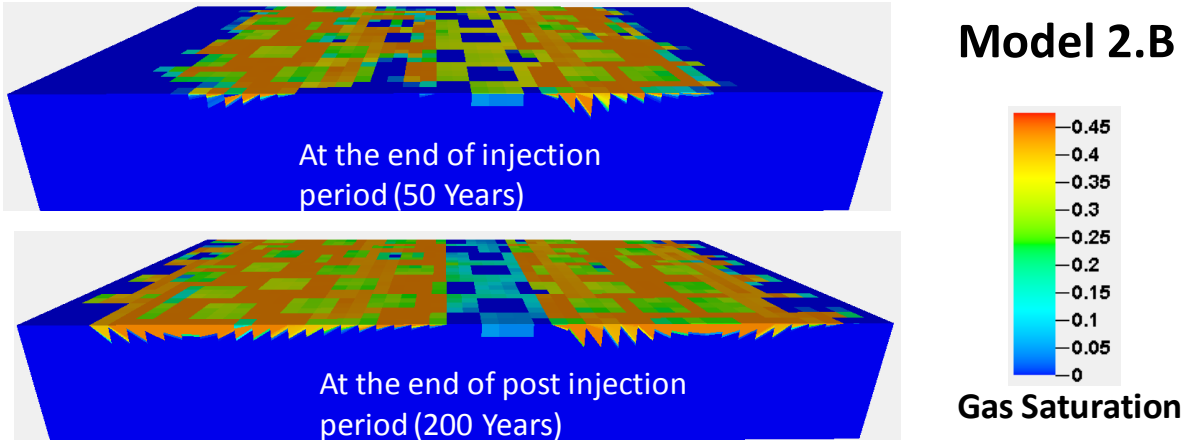


*Figure 4.28 Top picture shows $CO_2$ gas saturation in the Model 2.B at the end of injection period (50 years), bottom picture illustrates $CO_2$ gas saturation in the Model 2.B after 200 years post injection.*

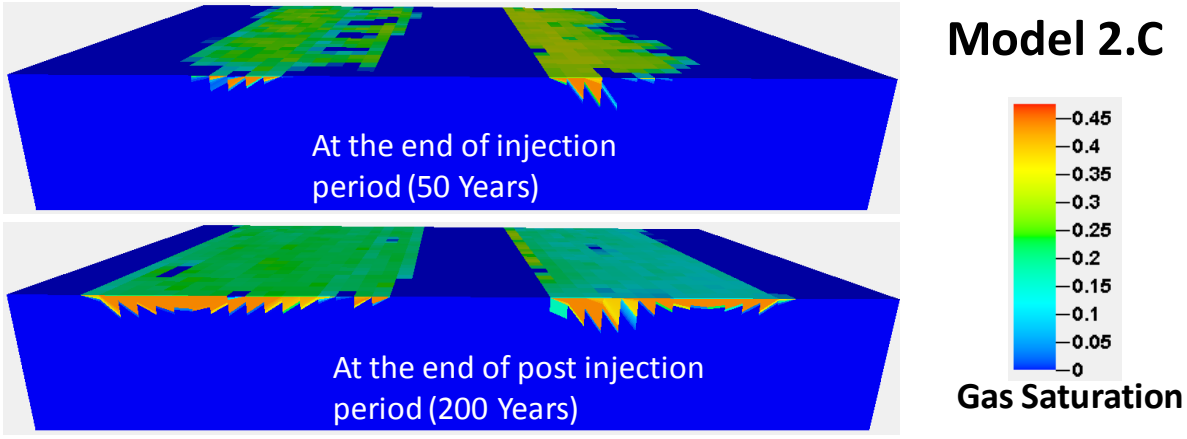


*Figure 4.29 Top picture shows $CO_2$ gas saturation in the Model 2.C at the end of injection period (50 years), bottom picture illustrates $CO_2$ gas saturation in the Model 2.C after 200 years post injection.*

The amount of $CO_2$ that dissolved in all models vs time (Figure ***4.30***) illustrates that there are two stages of dissolution of $CO_2$ in brine corresponding to the injection and the post injection period. During the injection period the rate of $CO_2$ dissolution in brine is higher than in the post injection period, and therefore the slope of dissolved $CO_2$ in brine line is higher than the one during the post injection period. The slope of the line in the post-injection phase depends on the amount of $CO_2$ migration, laterally and up-dip.

It should be noted that the amount of $CO_2$ is dissolved in Model 1 is slightly more that Model 2. This is due the fact that in Model 1 $CO_2$ reaches the boundary of model from the bottom of primary storage where a very high pore volume was assigned in the edge of the model. Therefore more $CO_2$ can be dissolved in Model 1 due to the access of $CO_2$ to this extra high pore volume of brine.

In addition, in Model 1.C the amount of $CO_2$ dissolved in brine during the injection period and post injection period (200 years) is more that Model 1.A and Model 1.B although this trend changes at later times. In Models 1.A and 1.B, $CO_2$ tends to migrated laterally through the high permeable layer above the unconformity surface under viscous forces, whereas in Model 1.C, when the $CO_2$ reaches the top of primary storage, it starts to fill this aquifer and then it has a downward migration.

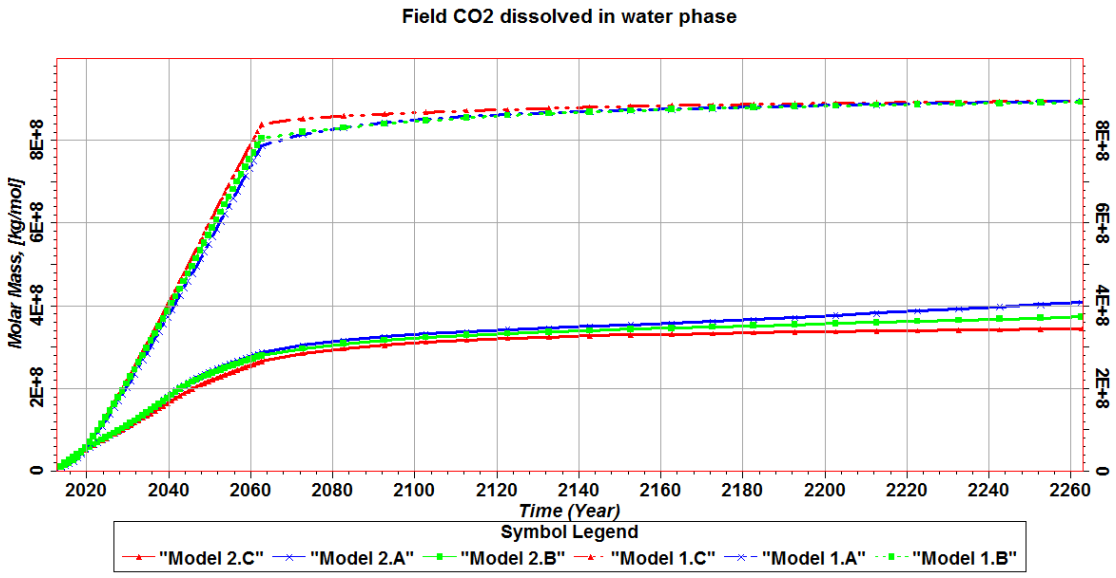


*Figure 4.30 The amount of $CO_2$ dissolved in water phase. Solid lines are for the cases of Model 2 and dashed line for the cases of model 1.*

As discussed earlier, the left leg of primary storage in Model 2.C is semi closed and the right leg of it is closed. Thus pressure distributions compartmentalize the model into two sections. The pressure difference between the two sections is around 60 bars (Figure ***4.31***).

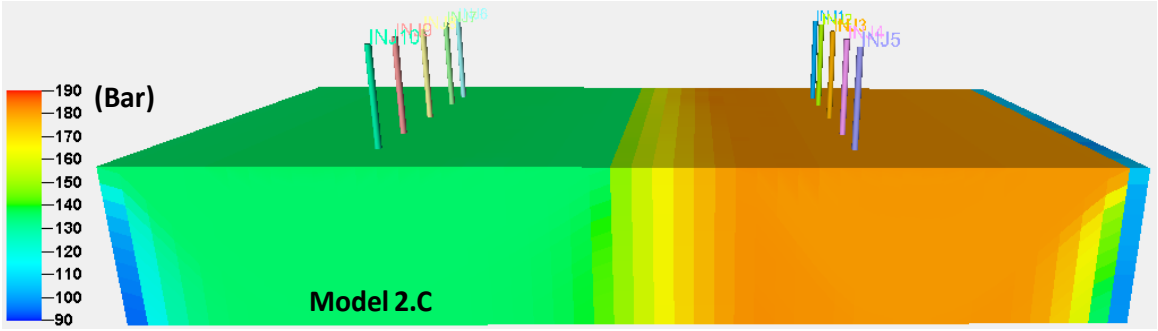


*Figure 4.31 Pressure in Model 2 C at the end of post injection period (200 Years).*


*Figure 4.32 Pressure in Model 1 C at the end of post injection period (200 Years).*

### *4.4.2 Sensitivity Analysis*

***Sensitivity on Thickness of High Permeable Layer above Unconformity***

The thickness of the layer above the unconformity surface was initially one metre, in Model 1.A. In Model 1.D it is changed to ten metres. In Model 1.A we have a one meter high permeable layer whereas in Model 1.D have a ten metre high permeable layer just above the unconformity surface. Figure ***4.33*** reveals the $CO_2$ mole fraction in these two Models after 50 years injection period (left pictures) and after 200 years post injection (right pictures).

The results show that the thinner the high permeable layer the slower the lateral $CO_2$ migration hence more $CO_2$ dissolved near the injectors. During the post injection period, $CO_2$ migrates slower in Model 1.A than Model 1.D however; it reaches the boundary of the model at the end of post injection period. In addition, $CO_2$ in Model 1.D has a downward migration when it reaches the top of secondary storage on the right

side of the model. This downward migration is controlled by the height of the $CO_2$ column on the primary storage (on the left side of the model).

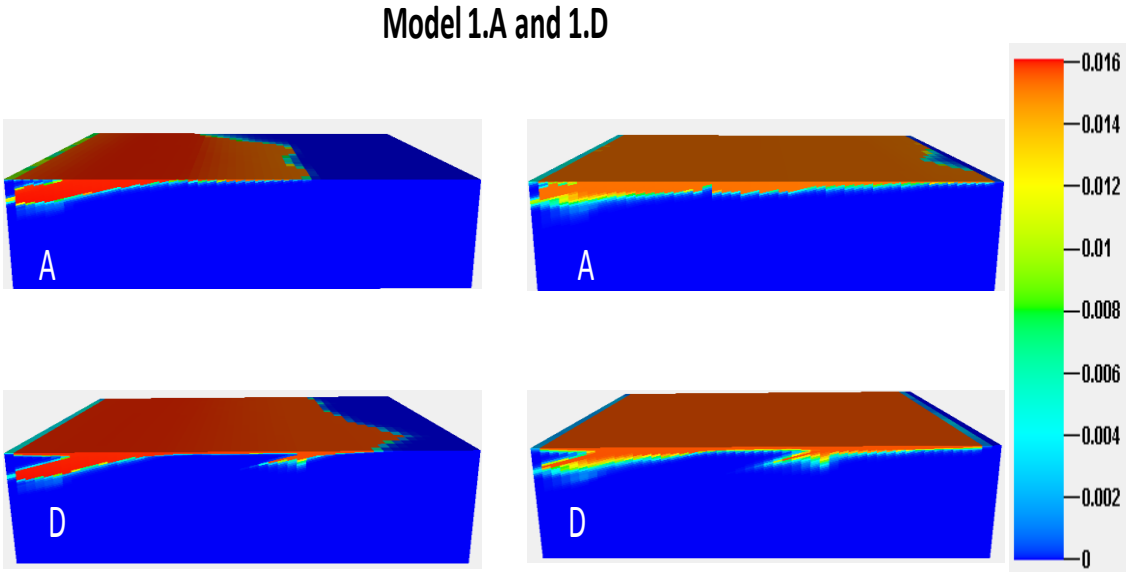


*Figure 4.33 Model 1.A with a 1m thick high permeability unconformity zone. Model 1.D has a 10-m thick high permeability layer. Left pictures show mole fraction at the end of injection period (50 years) and the right pictures show the $CO_2$ mole fraction at the end of post injection period (200 years).*

## 4.5 Conclusions

In this study, the effects of the most common type of unconformity (angular unconformity) on $CO_2$ storage were demonstrated. The results reveal that migration of $CO_2$ is influenced by the type of sediment deposited just over the unconformity surface. This can has positive effects on $CO_2$ storage capacity and security.

Regarding the negative effects, $CO_2$ can access other storage formations through that high permeable layer just over the unconformity surface and increase the risk of $CO_2$ migration out of primary storage. On the other hand, $CO_2$ can access other storage formation through that high permeable layer and increases storage capacity.

When the crest of an anticline is eroded and there is low permeability layer above the unconformity surface, an aquifer could be compartmentalised and this could be an advantage for $CO_2$ storage due to limitation of $CO_2$ migration and pressure compartmentalization after $CO_2$ is injected into aquifer.

# Chapter 5

# A Novel Method for $CO_2$ Injection that Enhances Storage Capacity and Security

## 5.1 Introduction

There are examples of industrial scale planned and active $CO_2$ storage projects around the world. This provides strong empirical support that geological storage of $CO_2$ can be employed in a safe manner (Leonenko and Keith 2008). However, there are uncertainties regarding the risks for this technology to play an important role in managing anthropogenic $CO_2$ emissions (Leonenko and Keith 2008).

In the long term, several trapping mechanisms can be used to sequester supercritical $CO_2$ into aquifers and depleted reservoirs. Understanding each of those mechanisms is not easy: for example, mineral trapping takes thousands of years. Investigation and monitoring of some of those processes, such as migration of plume is complex and costly as it takes hundreds of years. Structural trapping to prevent upward migration of $CO_2$ is provided by a finite non-zero permeable layer, which is mainly clay or shale layer, at the top of the storage formation (Figure ***5.1***).

Safe long-term $CO_2$ storage has been one of the most important issues, in terms of environmental damage that can be caused by leakage, public concerns, and technical matters, as long-term monitoring needs to be done. Considering safety issues; therefore, more cost would be expected for the $CO_2$ storage projects ($CO_2$ storage enhancement).

Different methods have been proposed to increase the security of geological storage of $CO_2$. Ozah et al. (2005) proposed "inject low and let rise" strategy, Anchliya and Economides (2009) suggested an engineering system to accelerate $CO_2$ dissolution in aquifers using horizontal brine injection well placed above the horizontal $CO_2$ injection well. Burton and Bryant (2009) and Eke et al. (2011) suggested $CO_2$/brine surface mixing strategy. They believed these methods could improve the effectiveness of $CO_2$ storage.

In this chapter, a novel method for $CO_2$ injection at which $CO_2$ dissolved in brine down-hole is presented. If we can minimize the vertical migration of $CO_2$ in the reservoir then it increases the safety in terms of any possible leakage through existing or pre-existing fractures and faults. Therefore, providing dissolved $CO_2$ at the bottom hole of injectors could not only prevent buoyant vertical migration of $CO_2$, but it could also lead to dissolved $CO_2$ sinking in the reservoir, as brine with dissolved $CO_2$ is denser (around 1%) than brine with no $CO_2$ (Lindeberg and Bermo, 2003, Ennis-King and Paterson, 2003, Ennis-King et al., 2005, Riaz et al. 2006).

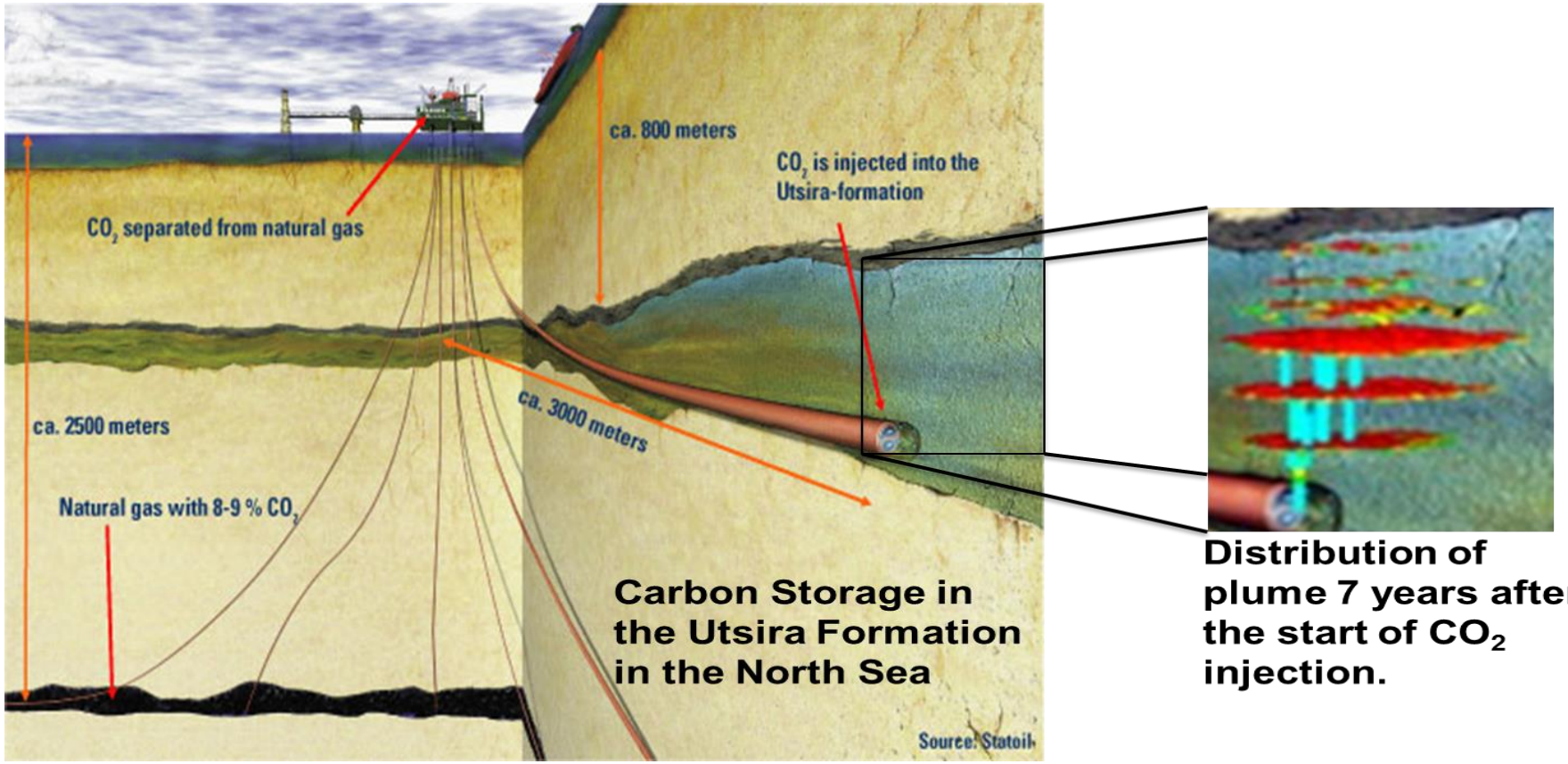


*Figure 5.1. The picture above illustrates standard method of $CO_2$ injection into a real field (Sleipner, North Sea). When $CO_2$ is injected into the aquifer, it migrates upward under buoyancy until it reaches the low permeability layers. Thereafter it migrates beneath these layers laterally (structural trapping), with this migration also being governed by gravity. Thus $CO_2$ tends to move up dip.*

## 5.2 Background

In many carbon capture and storage (CCS) research projects that have been published (Kumar et al. (2004), Burton and Bryant (2009), Anchliya and Economides (2009) and more), one of the main concerns the authors addressed is security of $CO_2$ storage. They have suggested different methods to reduce this risk. The "inject low and let rise" strategy was proposed by Ozah et al. (2005). Anchliya and Economides (2009) suggested an engineering system to accelerate $CO_2$ dissolution in aquifers. They proposed a system where a horizontal brine injection well placed above the horizontal $CO_2$ injection well.

A study was conducted by Burton and Bryant (2009) to investigate a $CO_2$/brine surface mixing strategy (Figure ***5.2***). They believed this method could improve the effectiveness of $CO_2$ storage. Firstly, injecting dissolved $CO_2$ eliminates free $CO_2$ in the aquifer, so there is no buoyant rise of $CO_2$ towards the caprock. However, they admit that the surface dissolution method has some disadvantages in comparison to the standard method for example: many more injection wells and extraction wells are needed which raises the storage cost. In addition, as the $CO_2$ saturated brine is acidic, the surface facilities and injection wells need to be resistant to corrosion. Furthermore, the cost of surface mixing equipment and related operations need to be considered.

Following Burton and Bryant (2009), Eke et al. (2011) conducted some studies to investigate $CO_2$/brine surface mixing strategy. They showed that the surface dissolution facilities enhance $CO_2$/brine solubility. Hence, the $CO_2$-saturated brine stream could eliminate the buoyancy force. Bergmo et al. (2011) showed that producing water from the aquifer while injecting $CO_2$ leads to a reduction in pressure both in the near well bore and throughout the field.

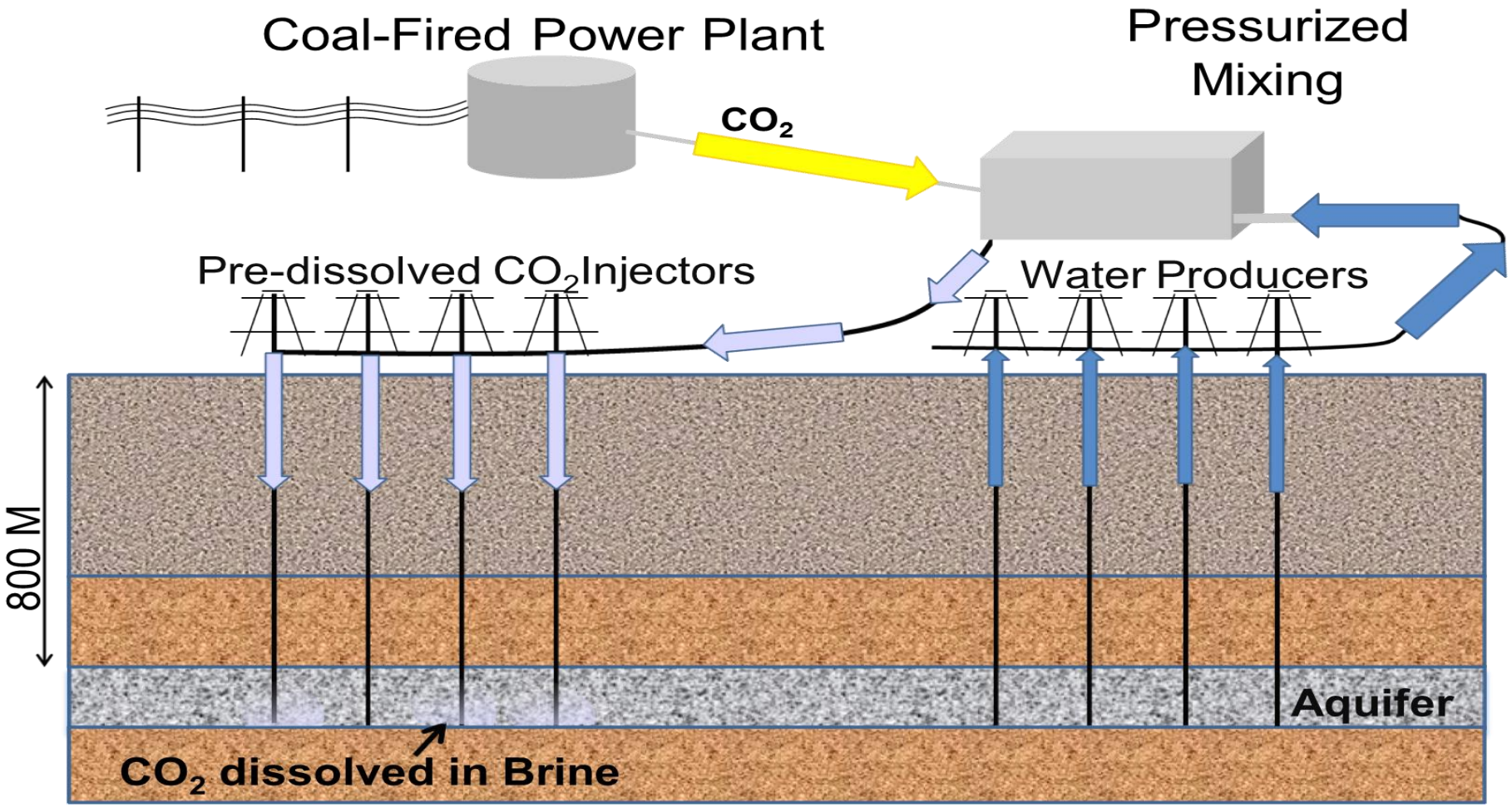


*Figure 5.2 $CO_2$/brine Surface Mixing Strategy.*

## 5.3 Methodology

The aim of this work is to investigate the potential to increase storage security by use of a novel method for $CO_2$ injection in which $CO_2$ is dissolved in brine down-hole. The advantage of injecting $CO_2$ dissolved in brine is that it is denser than unsaturated in-situ formation brine, and so will not migrate towards the surface as free phase $CO_2$ would. Therefore, in this approach, retention of $CO_2$ within a formation does not rely on the presence of a finite non-zero permeable seal. Instead, all $CO_2$ injected as a dissolved phase will migrate downwards. This has three consequences. Firstly, the entire rock pore volume becomes available for storage, and not just that part of the rock that is shallower than the spill point. Secondly, there is no longer a requirement for injection into formations deeper than 800 m, since the injected $CO_2$ need not be supercritical. Thirdly, there are no concerns around the integrity of the caprock. Indeed, there is no requirement for a caprock to prevent vertical migration of $CO_2$ due to buoyancy. This means that many additional formations may become available as potential storage sites.

$CO_2$ dissolution in brine at the surface prior to injection has been considered previously. However, this postulated method of injection suffers from serious technical limitations that make it unfeasible. The solubility of $CO_2$ in brine is limited at standard conditions, and thus energy would be required to pressurise brine and $CO_2$ at surface prior to mixing to enhance solubility. The cost of such equipment, which would have to have an appropriate pressure rating, be made of corrosion resistant material, and have capacity for dissolving in the order of thousands of tonnes of $CO_2$ per day, would be prohibitive. Also, the volume of brine that would have to be injected in addition to the $CO_2$ would increase the reservoir pressure much more rapidly than during pure $CO_2$ injection, very severely restricting storage capacity.

### *5.3.1 Equation of state and mixing rules*

Solubility of $CO_2$ in brine is discussed in section 2.2.3, therefore it is not repeated here. For saline system, the $CO_2$ mole fractions in the aqueous phase ( $x_{CO_2}$ ) can be expressed as:

$$x_{CO_2} = B\left(1 - y_{H_2O}\right) \tag{5.1}$$

where,

$$B = \frac{\Phi_{CO_2} P_{tot}}{55.508 a_{CO_2} K^0_{CO_2}} \exp\left( - \frac{\left(P - P^0\right)\overline{V}_{CO_2}}{RT} \right)$$

As it stated in Equation 5.1, in order to calculate $x_{CO_2}$, the water mole fraction in the $CO_2$ rich phase ( $y_{H_2O}$ ) must be known. Following equation express these calculations:

$$y_{H_2O} = A\left(1 - x_{CO_2} - x_{salt}\right) \tag{5.2}$$

where,

$$A = \frac{K^0_{H_2O}}{\Phi_{H_2O} P_{tot}} \exp\left(\frac{\left(P - P^0\right)\overline{V}_{H_2O}}{RT}\right)$$

and $x_{salt}$ can be calculated from:

$$x_{salt} = \frac{\upsilon m_{salt}}{55.508 + \upsilon m_{salt} + m_{CO_2(aq)}} \tag{5.3}$$

and,

$$m_{CO_2} = \frac{x_{CO_2} 55.508}{x_{H_2O}} \tag{5.4}$$

where,

$$x_{H_2O} = 1 - x_{_{CO_2}} - x_{salt} \tag{5.5}$$

$\upsilon$ is the stoichiometric number of ions contained in the dissolved salt (i.e., 2 for NaCl, 3 for CaCl, etc.).

$$m_{CO_2} = \frac{x_{CO_2}\left(\upsilon m_{salt} + 55.508\right)}{\left(1 - x_{CO_2}\right)} \tag{5.6}$$

Equations (5.5) and (5.6) are solved by substitution,

Thus:

$$y_{H_2O} = \frac{\left(1 - B\right)55.508}{\left(1/A - B\right)\left(\upsilon m_{salt} + 55.508\right) + \upsilon m_{salt} B} \tag{5.7}$$

$CO_2$ solubility in brine, at constant temperature and salinity, increases with increasing pressure (Spycher and Pruess (2005), Figure ***5.3***). With increasing temperature, the solubility of $CO_2$ decreases. Thus, the best conditions for having a higher $CO_2$ dissolution in brine are higher pressure and lower temperature. Computed data shows that the optimum depth of $CO_2$ storage has to be just below 800 meters. On the one hand, pressure and temperature meet $CO_2$ supercritical conditions at that depth. On the other hand, if $CO_2$ is stored at greater depth, the temperature and salinity will rise, so the amount of dissolutions will decrease.

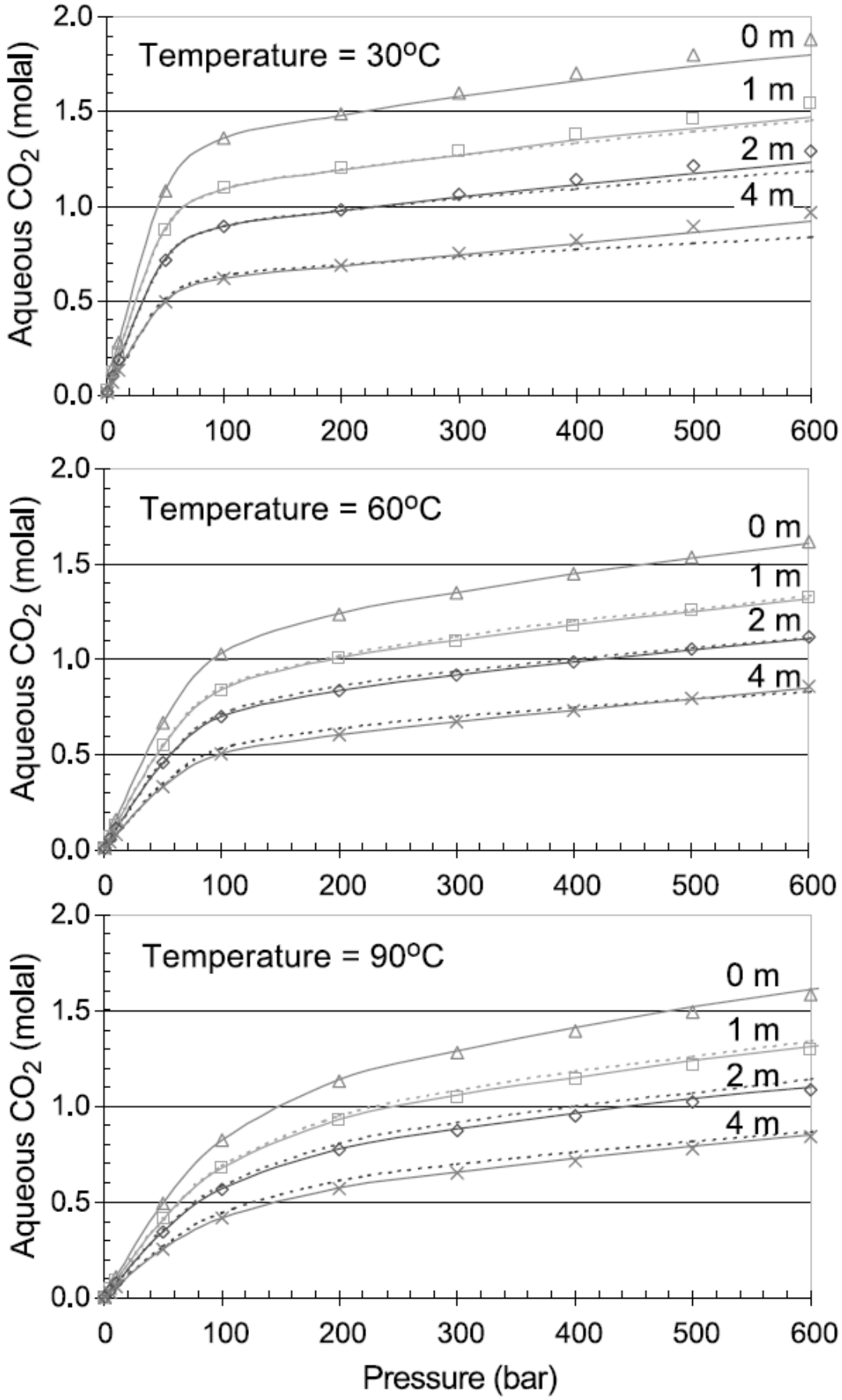


*Figure 5.3 predicted solubilities of $CO_2$ in brine (0 m – 4 m) using two types of activity coefficients (solid and dashed lines) Spycher and Pruess (2005).*

### *5.3.2 Amount of $CO_2$ Which Can Be Stored by this Method:*

Table *5.1* shows the amount of $CO_2$ can be dissolved in water with 3 different salinities (35000 mg/l, 100000 mg/l and 200000 mg/l) at depths of 1000 m and 2000 m. This analytical calculation is made based on Spycher and Pruess (2005).

*Table 5.1: Amount of $CO_2$ can be dissolved in brine at different conditions*

| **Amount of $CO_2$ (kg) Dissolved in 1 $m^3$ brine** | | | | | |
|---|---|---|---|---|---|
| **Depth** | Pressure | Temperature | Salinity (mg/l) | | |
| **(m)** | (bar) | (C) | 35000 | 100000 | 200000 |
| **1000** | 100 | 35 | 50.583 | 39.34 | 29.067 |
| **2000** | 200 | 70 | 46.667 | 37.616 | 28.67 |
| **Amount of $CO_2$ (Million Tonne per Year) dissolved - Reservoir Inj. Rate is 4000 $m^3$/day** | | | | | |
| **Depth** | Pressure | Temperature | Salinity (mg/l) | | |
| **(m)** | (bar) | (C) | 35000 | 35000 | 35000 |
| **1000** | 100 | 35 | 0.074 | 0.057 | 0.043 |
| **2000** | 200 | 70 | 0.068 | 0.055 | 0.042 |

In this novel proposed injection system (Shariatipour et al 2012; 2013), brine is extracted from the target aquifer by means of a lateral horizontal completion located near the top of the formation (Figure 5.4 and Figure *5.5*). An Electrical Submersible Pump (ESP) is used to extract the brine and boost its pressure, before it mixes with $CO_2$ that is being injected down the vertical section of the well. The mixing takes place in the vertical section of the well below the upper lateral. The $CO_2$ – brine mix is then injected into the same formation in a lower lateral. A down-hole mixing chamber (Zirrahi et al. 2013) would be used to maximise agitation and contact area between $CO_2$ and brine in the mixing section of the well, which may be 10s to 100s of metres long.

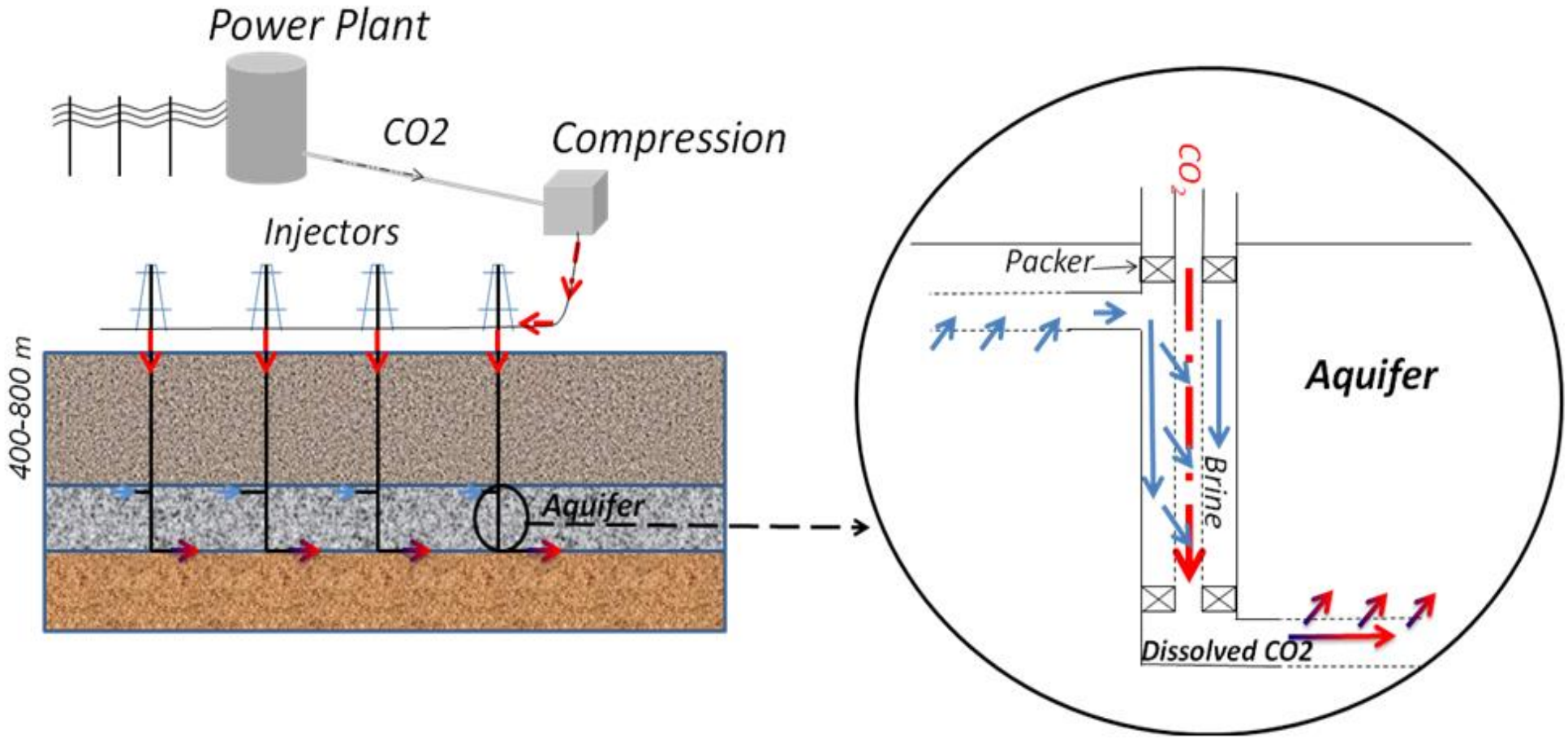


*Figure 5.4 Schematic process of CO2/brine down-hole mixing*

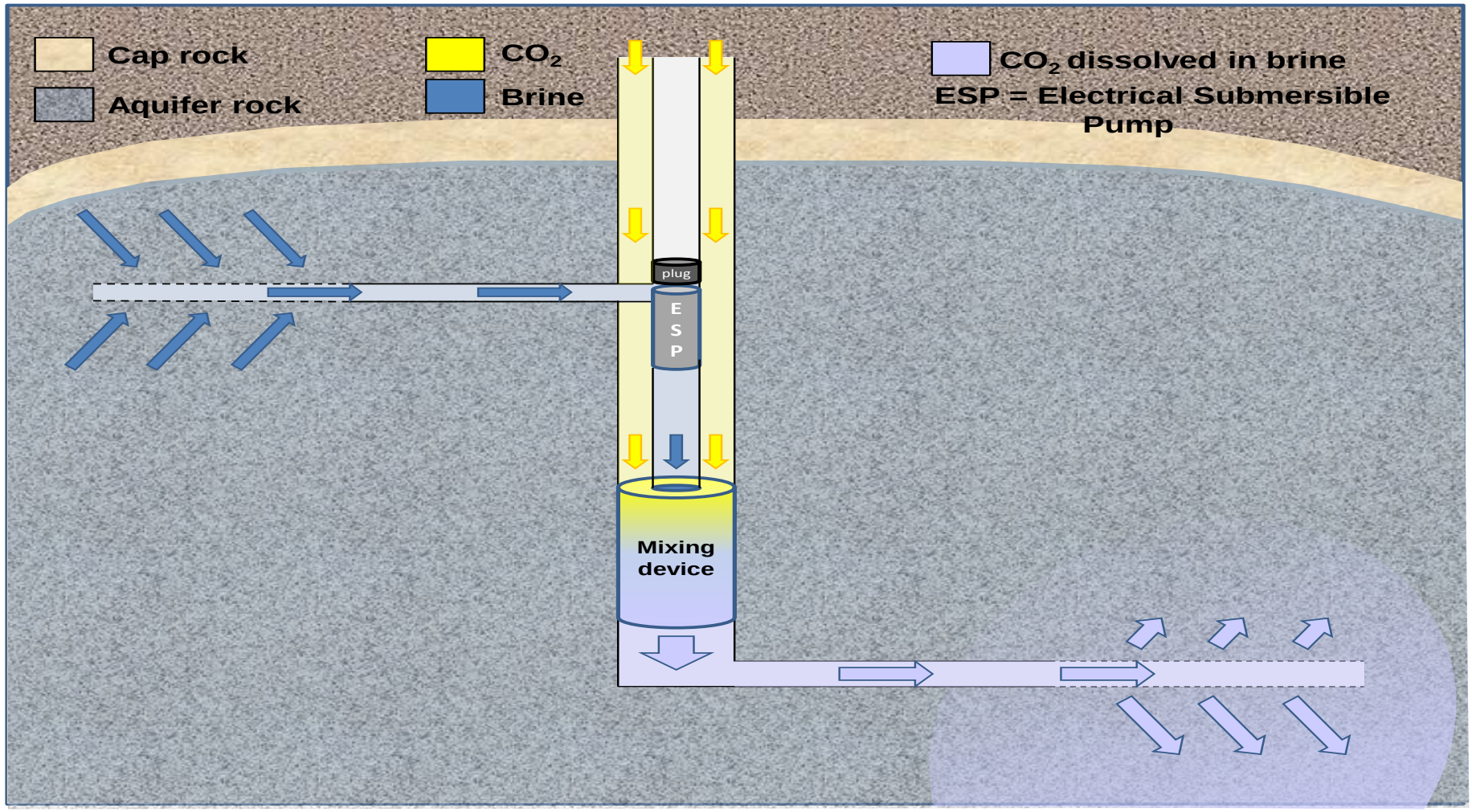


*Figure 5.5: Schematic process of $CO_2$/brine down-hole mixing.*

A range of numerical simulations on a variety of heterogeneous and homogeneous models to investigate the impact of the $CO_2$/brine down-hole mixing injection strategy was conducted.

The models all have dimensions of 10000 m × 500 m × 134 m and were discretized into 200×50×80 cells. The porosity and the permeability values in the homogeneous models were assigned values of 0.2 and 1000 mD respectively in all directions. For the heterogeneous models the average porosity and average permeability values were the same as the homogeneous one. The correlation length was 100 m in the horizontal and 1 m in the vertical, and the standard deviation was 0.5. In the simulations, the pump for extracting the brine was modelled as a producer in one branch of a well. The down-hole dissolution was not modelled explicitly. Instead, in the simulation, a solution of $CO_2$ in dissolved brine through the lower branch of the well is injected. In the subsequent description, it is referred to these branches of the well as the producer and the injector.

In all cases, a single production/injection well was placed in the centre of the model. The control mode for both production and injection was reservoir fluid volume rate and the rates were 1000 $rm^3$/day and 941$rm^3$/day for the injector and the producer respectively. Both producer and injector were shut after 20 years and the simulation was continued for 100 years. The composition of the injected fluid, in terms of mole fractions was 0.015, 0.9556 and 0.0294 for dissolved $CO_2$, water and NaCl respectively. These values correspond to thermodynamic equilibrium at down hole conditions. Conversation for salinity units is presented in Appendix C.

Figure *5.6* demonstrates the well location and connections. Water is extracted from the top of the reservoir and pumped into the bottom hole while the supercritical $CO_2$ is injected into the well. Supercritical $CO_2$ is dissolved in the extracted brine at the bottom hole. It is assumed that this process can be managed by a specific $CO_2$/brine down-hole mixing tool.

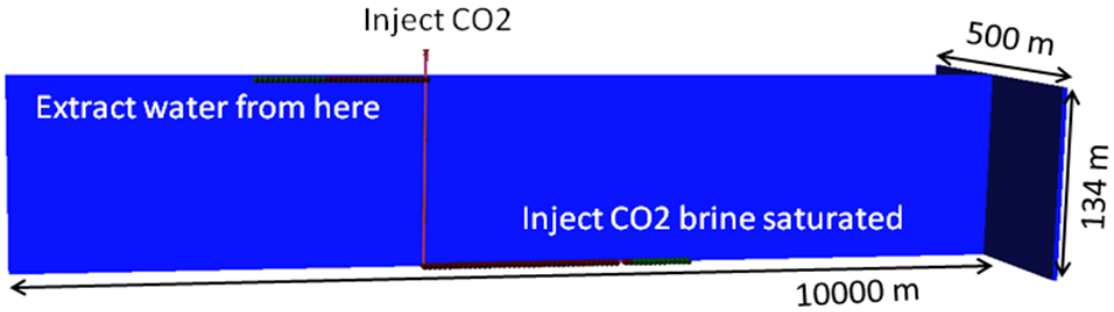


*Figure 5.6: Well location and Connections.*

This work does not consider the design of such a tool, but is purely concerned with the question of whether such a tool, if it could be appropriately designed, would provide a benefit for CCS.

## 5.4 Results and Discussion:

Figure *5.7* demonstrates the $CO_2$ mole fraction at the end of the 20 year injection period and 100 years after shut-in, for the 3-D homogeneous and heterogeneous models. Note that, because $CO_2$ was dissolved in brine in the well, there was no free injected $CO_2$ in the model, nor did any exsolve from solution during the period of the calculation.

As the dissolved $CO_2$ is injected into the aquifer it moves in all directions. This migration is mainly governed by the injection rate, permeability, production rate and gravity forces during the injection period. When both producer and injector were shut, gravity is dominant. The $CO_2$-saturated region tends to be skewed towards the producer where the pressure is lower, but the dissolved $CO_2$ does not reach the extraction region.

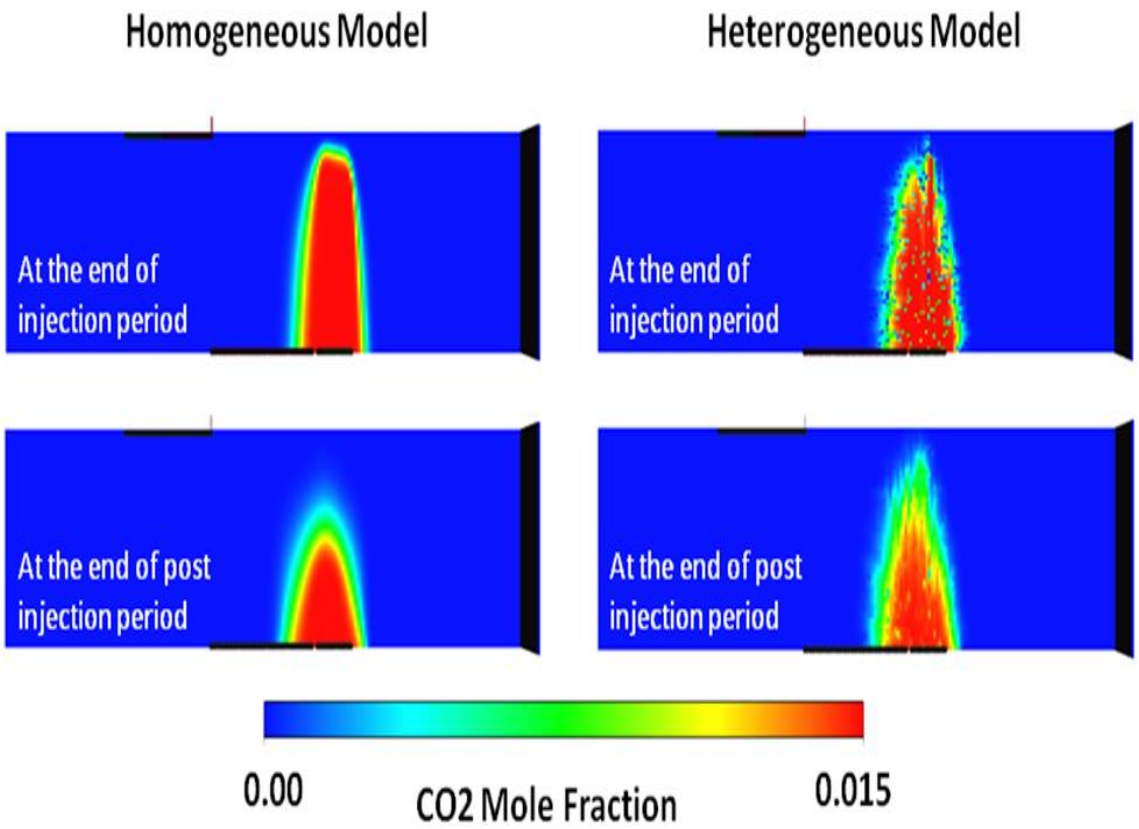


*Figure 5.7: $CO_2$ mole fractions dissolved in brine in the X-Z plane for the homogeneous model (left) and heterogeneous model (right).*

Figure *5.8* shows the average pressure in the heterogeneous and homogeneous 3-D models and Figure *5.9* shows pressure changes across the aquifer in a cross section of the heterogeneous model. As can be seen the rise in average pressure does not even reach 0.3 bar. The time to establish a steady state pressure field is determined by the magnitude of the diffusivity constant. Once the transient period is completed (after 25 days), the subsequent pressure trends are determined by mass balance in the field, that is the difference between the down-hole injection and production rate.

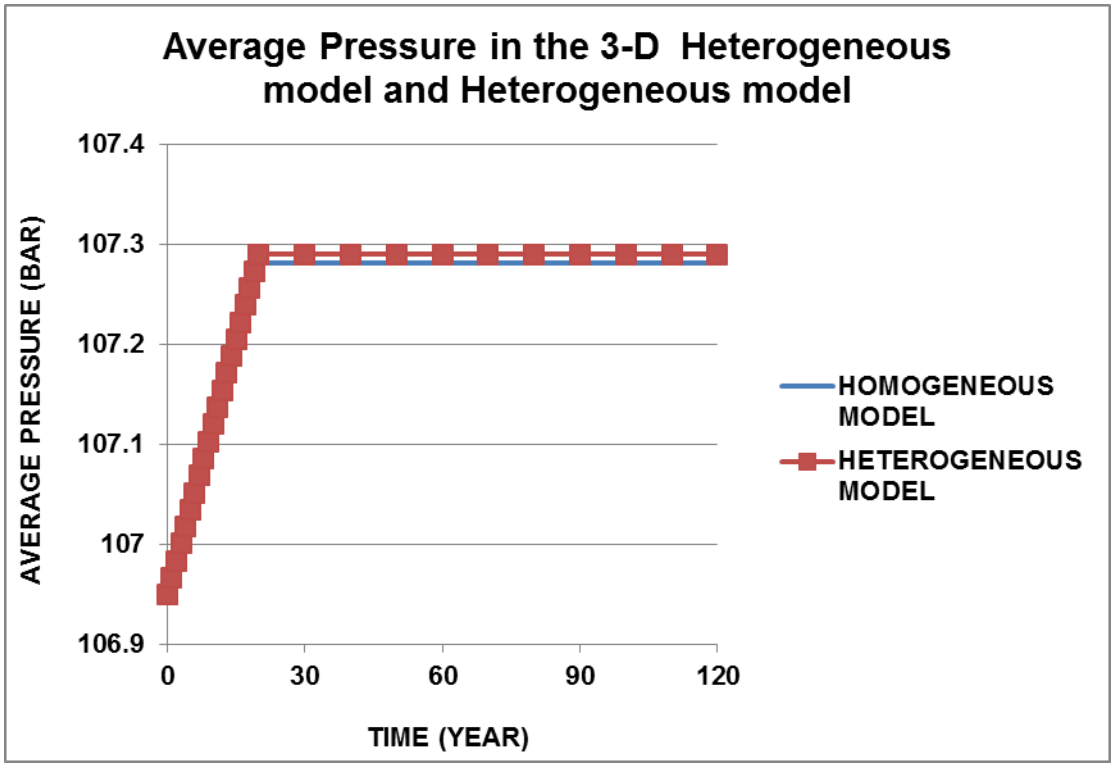


*Figure 5.8: Average pressure in the heterogeneous and homogeneous 3-D models.*

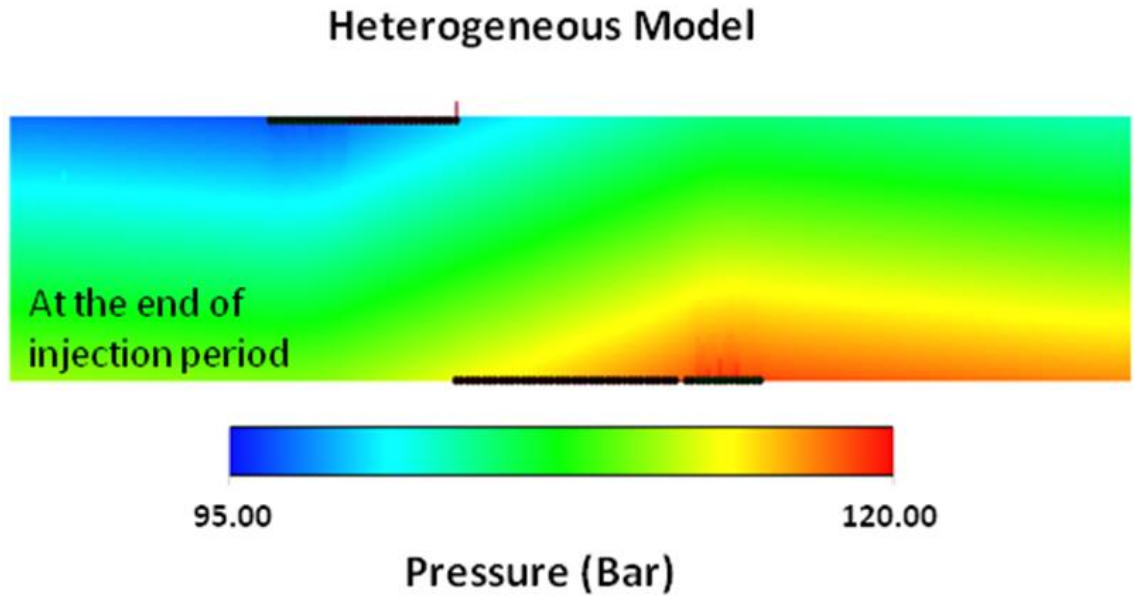


*Figure 5.9: Pressure distributions in the X-Z plane at the end of injection period in the heterogeneous model.*

## 5.5 Conclusions and Recommendations:

The results indicate that $CO_2$/brine down-hole mixing could improve $CO_2$ sequestration. This reservoir simulation study demonstrates that the vertical migration of $CO_2$ in the reservoir can be limited to viscous effects during the injection period, and that during the subsequent shut-in period gravity segregation displaces the $CO_2$ saturated brine downwards, thereby increasing the storage safety. With appropriate placement of the laterals in the well, it is possible to prevent migration of $CO_2$ saturated brine towards the brine production lateral, this will be demonstrated in Chapter 6.

The problem with this proposed method of injection is that it will restrict the amount of $CO_2$ can be injected in one well. Therefore, it requires more well in comparison to the standard $CO_2$ injection method. Injecting at a much higher total volume rate will increase the BHP. As a result, there will be concerns about integrity as injecting incompressible fluid has risks. On the other hand, it will be single phase injection, and the acid brine may stimulate the formation. The BHP will certainly be much higher for this method than if the $CO_2$ were injected without brine, but the increase will be somewhat mitigated by the aforementioned factor. Also, the overall field average pressure will be the same as if the $CO_2$ were injected without brine, as the overall material balance is the same.

# Chapter 6

# Application of Transition Zone and Down-Hole Mixing Method to a Real Field

## 6.1 Introduction

In Chapter 3 a transition zone was introduced, based on the observations of an outcrop in Devon, South England, where Sidmouth outcrop was used, consisting of the Triassic Sherwood Sandstone Group and Mercia Mudstone Group. Some numerical simulations were conducted to study the effect on $CO_2$ storage of a gradual transition from the sand-rich facies in the aquifer to the mud-rich facies in the caprock.

In this chapter a model of an analogue to a potential offshore storage site in Lincolnshire (Smith et al. 2012) with the same formation as described in Chapter 3 is used to model $CO_2$ behaviour at the interface between the storage formation and the caprock (Transition Zone). In this model it was originally assumed that there is a sharp boundary between the aquifer and the caprock. However, as it discussed in Chapter 3, this is not always the case. For example at the Sidmouth outcrop it was estimated that the transition zone may be up to 10 m in places. Therefore, the base case model was modified by adding some mud layers in the top sand layer (10 m) to investigate the effect of the transition zone.

In addition, the application of down-hole mixing in this model was also examined. Calculations will be performed to identify the best scenario for the position of the water extractor and the brine injector with dissolved $CO_2$.

## 6.2 The CASSEM Lincolnshire Site

The British Geological Survey (BGS) identified an onshore site in Lincolnshire as an analogue to a hypothetical large offshore aquifer to be used for storing captured $CO_2$ from the Ferrybridge Power Station (Figure ***6.1***). The criteria for this selection were as follows. First of all, the formation has fairly uniform sandstone of high porosity (20%) and permeability (500mD), overlain by a thick caprock at a depth below 800 m (Table 6.1), to meet the supercritical conditions for $CO_2$. In addition, BGS had access to 3D seismic data with uniform coverage. The geology and stratigraphy of the hypothetical Lincolnshire site is presented in Table ***6.1***. Figure ***6.2*** shows a West to East schematic geological cross-section of the Lincolnshire study area.

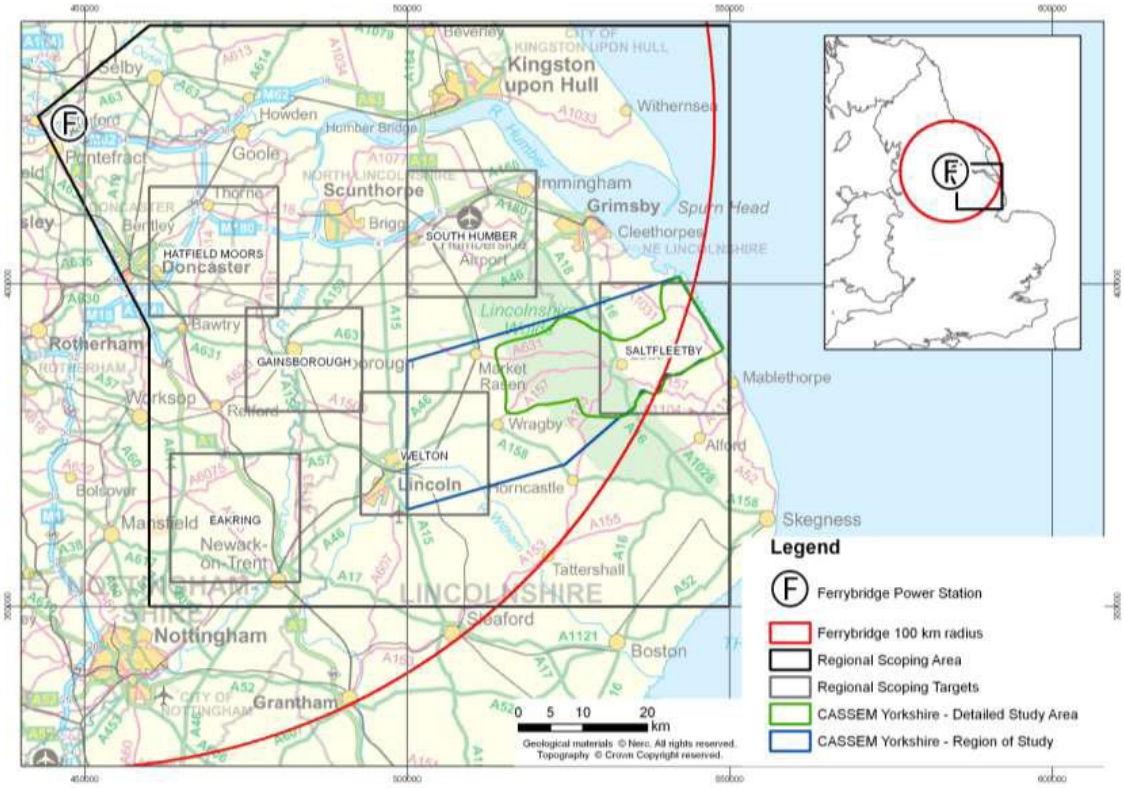


*Figure 6.1 Location Map of Ferrybridge Power Station, which is shown by (F).*

*Table 6.1 Geology and stratigraphy of the Lincolnshire Area. The geology of the target analogue aquifer for $CO_2$ storage is the Sherwood sandstone group classified in the Triassic period overlain by the Mercia Mudstone as the primary seal (after Smith et al. 2012).*

| Period | Geological Unit | Age (Ma) | Aquifer/seal/ overburden classification | Approximate depth below ground level at Saltfleetby |
|---|---|---|---|---|
| Cretaceous | Upper Cretaceous (Chalk Group) | 90 | Primary overburden | Base = 180 m (not modelled) |
| | Lower Cretaceous | 100 | Primary overburden | Base = 200 m (not modelled) |
| Jurassic | Upper Jurassic | 151 | Primary overburden | Base = 560 m (not modelled) |
| | Middle Jurassic (inc. Lincolnshire Limestone Fm) | 164 | Primary overburden | Base = 600 m (Top Lincolnshire Limestone modelled) |
| | Lower Jurassic (Lias Group) | 179 | Primary overburden | Base = 860 m (not modelled) |
| Triassic | Penarth Group | 200 | Primary overburden / seal | Base = 870 m |
| | Mercia Mudstone Group | 204 | Primary seal | Base = 1160 m |
| | Sherwood Sandstone Group | 242 | Primary aquifer | Base = 1490 m |

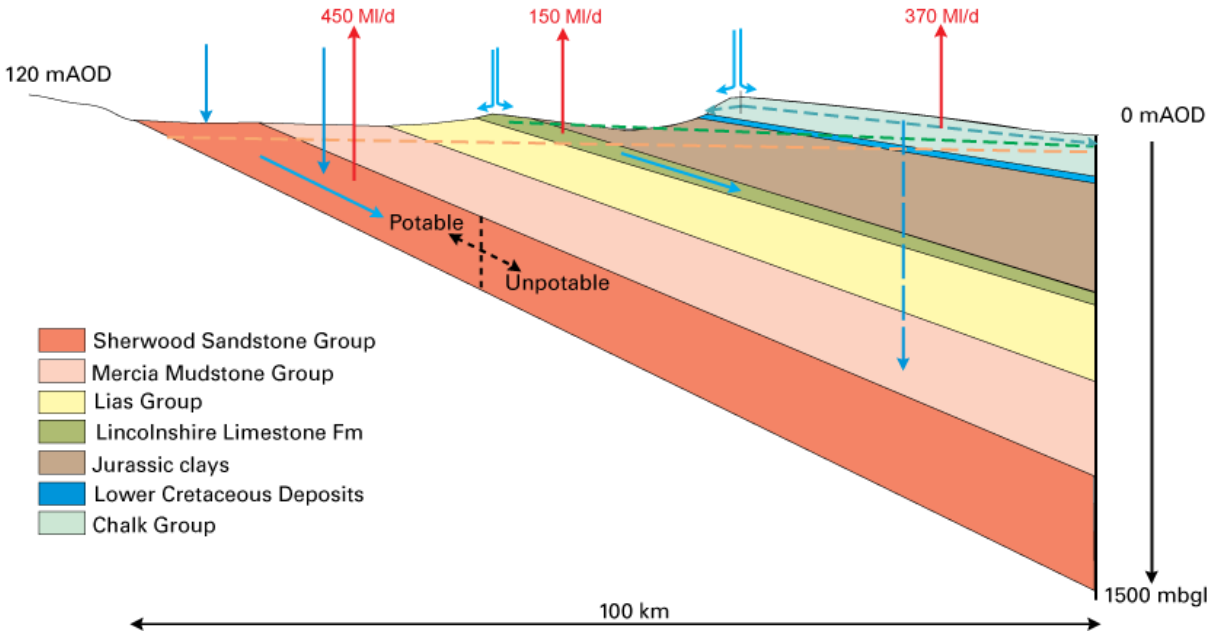


*Figure 6.2 Schematic geological cross-section (west to east) of the Lincolnshire study area along with regional groundwater flow and abstraction. mbgl stands for metres below ground level. Abstraction from the Sherwood Sandstone Group is approximately 85% unconfined, 15% confined. Blue arrows represent the flow of recharge, red arrows are abstraction (Smith et al. 2012).*

## 6.3 The Lincolnshire Model

Figure ***6.3*** shows the geological framework of the Lincolnshire model. The reservoir model was developed through the CASSEM ($CO_2$ Aquifer Storage Site Evaluation and Monitoring) Project (Olden et al. 2012). The model has dimensions of 43 km × 33 km × 600 m and was discretized into 96×67×15 cells. An isotropic range of 2000m in the horizontal was used for the correlation in the distributions of properties. The ratio of vertical permeability to horizontal permeability (Kv/Kh) was assumed to be 0.1 due the layered types of sediments which were deposited in this region (Ford and Monaghan, 2009). Table ***6.2*** shows permeability and standard deviation used in the Lincolnshire Model (Jin et al. 2012), and the relationship between permeability and porosity for core plugs in the Petrel model is illustrated in Figure ***6.4***. It is referred to this model as the base case Model (BC) in this chapter. In order to consider the effect of the transition zone, the facies in the top aquifer layer were changed from 100% sandstone to 60% mudstone and 40% sandstone and it was divided into 10 layers.

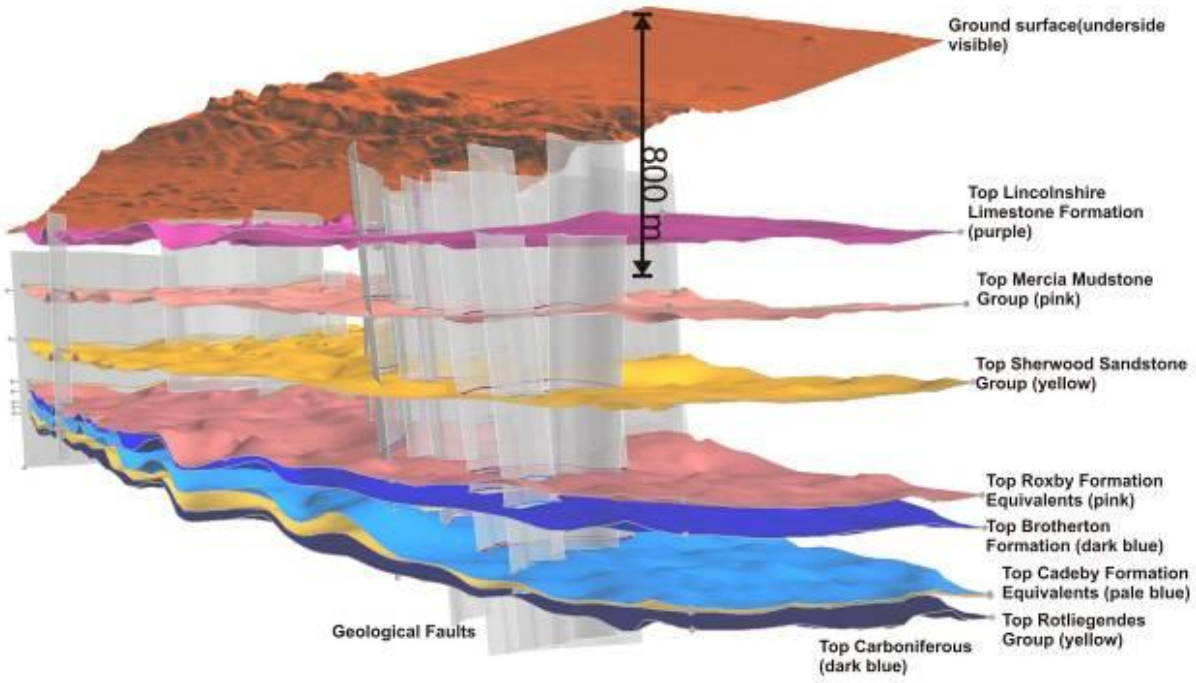


*Figure 6.3 The Geological Framework of Lincolnshire Model (10X vertical exaggeration).*

*Table 6.2 Permeability and Standard Deviation used in the Lincolnshire Model.*

| Formation | Geometric Average (mD) | Standard Deviation from plugs (ln(mD)) | Standard Deviation used |
|---|---|---|---|
| **Mercia Mudstone Group (MMG)** | 0.005 | 1.0 | 0.1 |
| **Sherwood Sandstone Group(SSG)** | 500 | 3.5 | 0.5 |

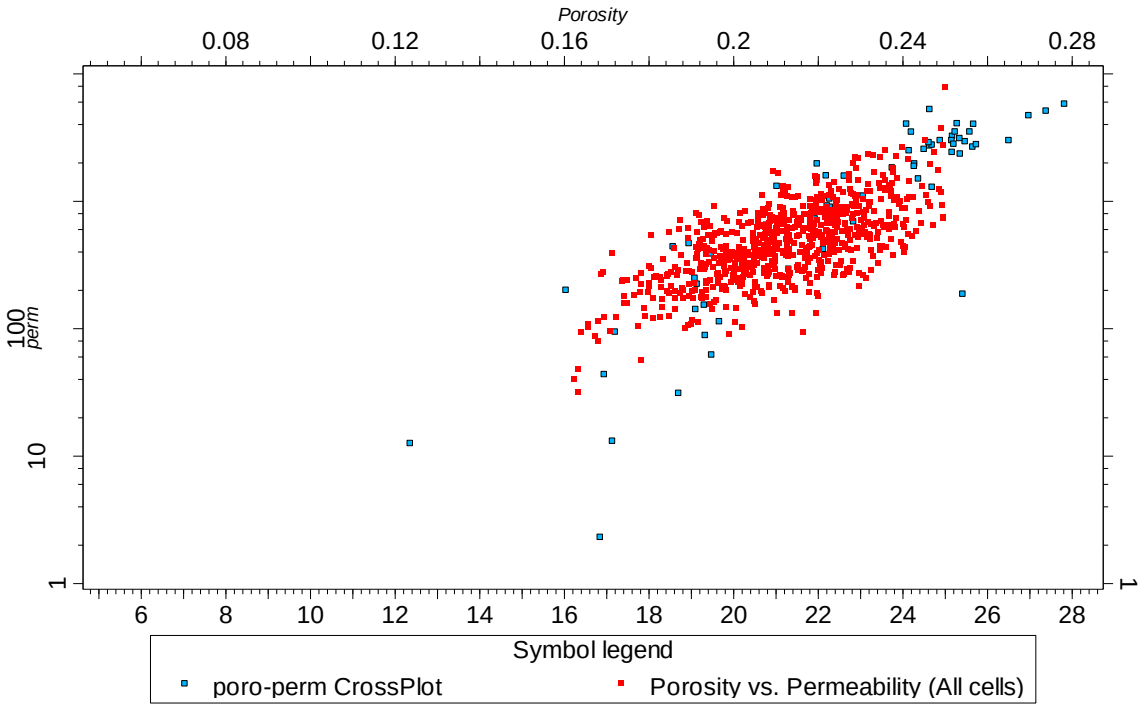


*Figure 6.4 shows porosity- permeability (perm) relationship for core plug (blue squares) and the Petrel model (red dots) (Smith et al. 2012).*

Based on rock mechanics data, rock compressibilities for the aquifer and the caprock were assigned as $5\times10^{-5}bar^{-1}$ and $10\times10^{-5}bar^{-1}$ respectively.

The relative permeability curves which were used in this model were obtained from a sample of Sherwood Sandstone at (Sohrabi et al. 2010) (Figure ***6.5***). The relative permeability to water is denoted by $K_{rw}$, and $K_{rg}$ denotes the relative permeability to $CO_2$. Imb and Dr are representative of the imbibition process when water saturation increased and drainage when water saturation decreases, respectively. The irreducible water saturation ($Sw_{ir}$) is 0.36; this means the maximum gas saturation in the model will be 0.64. During the imbibition process where water replaces migrated $CO_2$, residual trapping will be occur, which in this case is 0.27.

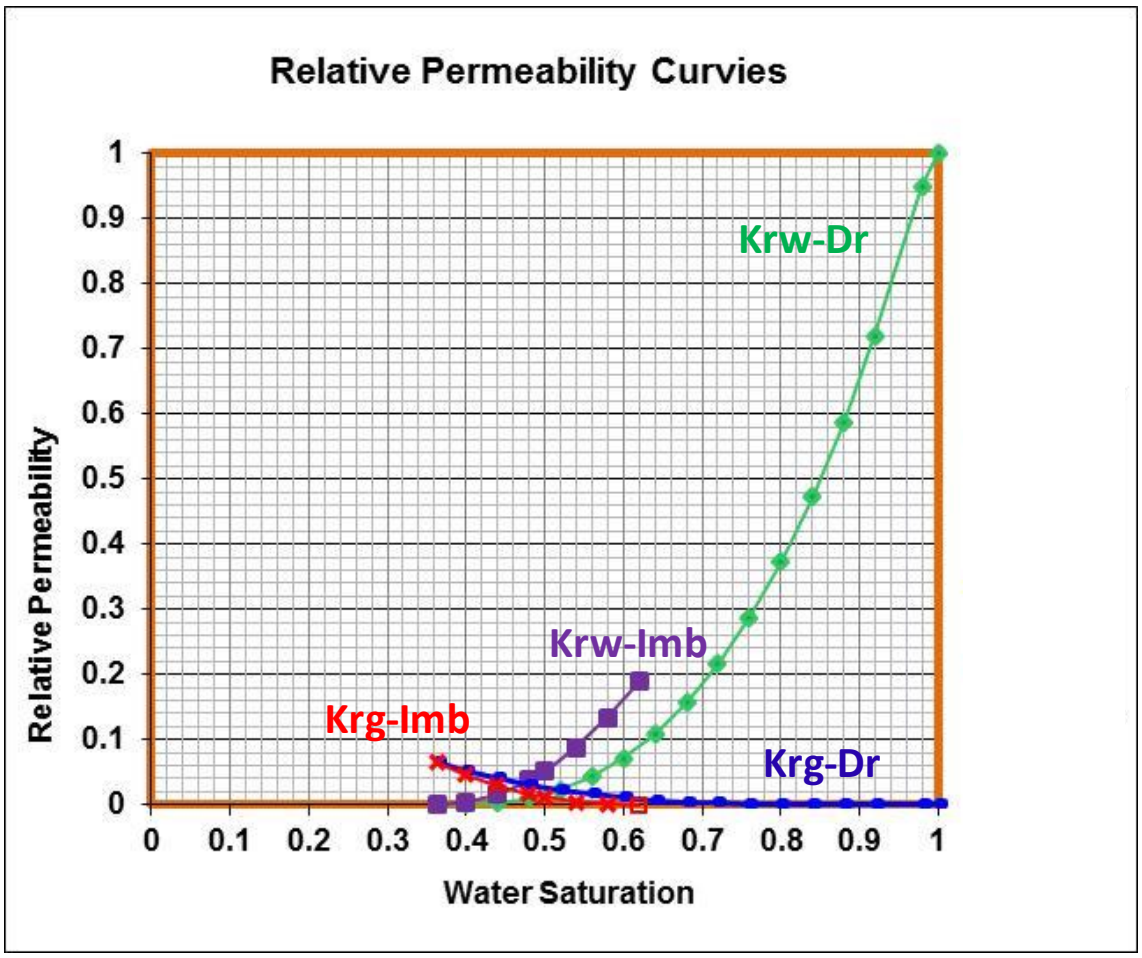


*Figure 6.5 Relative permeability curves used in this study, obtained from a Sherwood Sandstone sample (Smith et al. 2012).*

### 6.4 Impact of the transition zone on the $CO_2$ storage in the Lincolnshire Model

As discussed in Chapter 3, there could be a transition zone at the interface between the aquifer and the caprock. The Petrel model was used to divide the top aquifer layer into 10 layers and to change the facies in the top aquifer layer from 100% sandstone to 60% mudstone and 40% sandstone. Sequential Gaussian simulation was used to generate the porosity distribution, and the permeability was correlated with porosity. The correlation length was 1 km in the horizontal and 0.5 m in the vertical. Figure ***6.6*** shows a Simbox view (visualization of a propertiy as a regular box in XYZ) of permeability distributions in the initial top aquifer layer before and after modification. Figure ***6.7*** shows a histogram of the new permeability distribution in the X direction for Sandstone and Mudstone in the top 10 layers in the modified model. It was assumed that the models represented part of a larger aquifer, and the pore volume of the first outer cell on each side was multiplied by a factor of 10E+9, to take account of this.

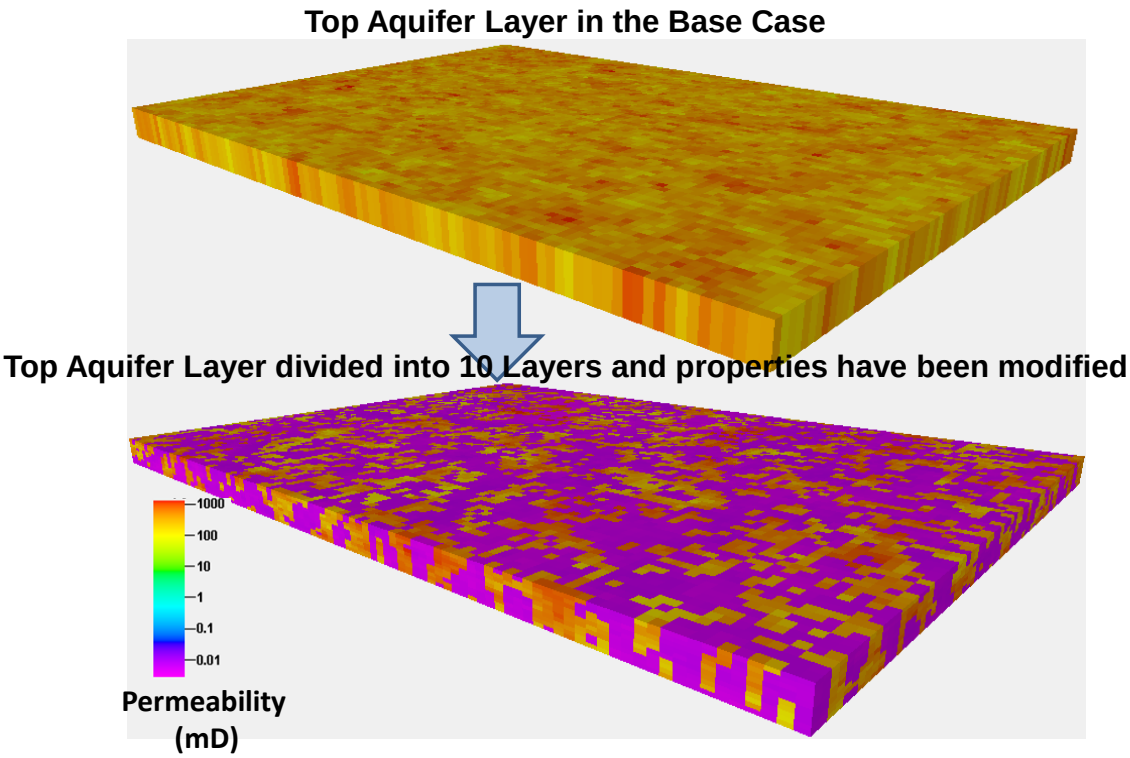


*Figure 6.6 Simbox view (model visualized as a regular box in XYZ) of permeability distributions in the initial top aquifer layer before (top picture) and after modification (bottom picture).*

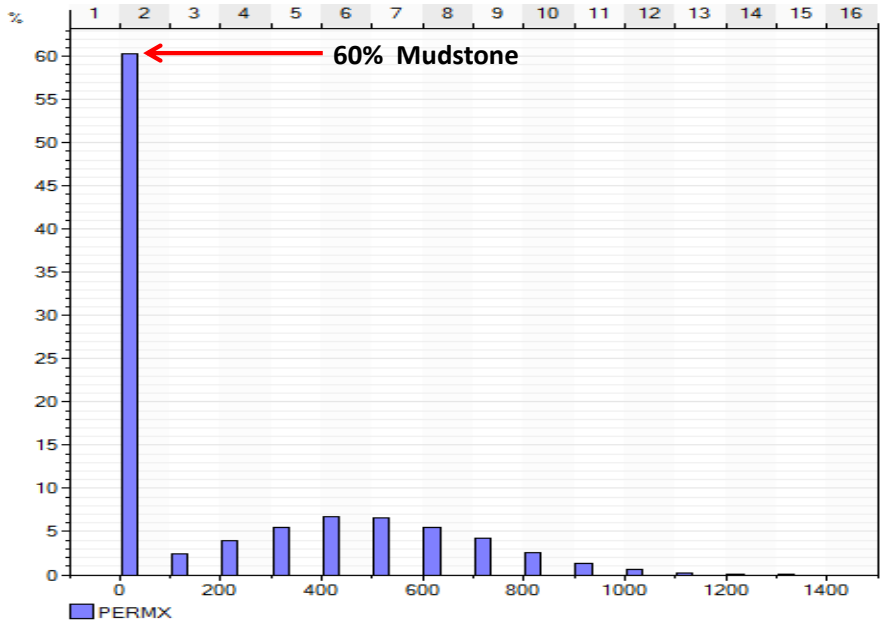


*Figure 6.7 Histogram of permeability in the X direction for Sandstone and Mudstone in the 10 top layers in the modified model (Transition Zone). The red arrow shows that 60% of these layers consist of Mudstone.*

### *6.4.1 Area of Interest*

A series of numerical simulations were conducted to investigate the plume migration in the base case model (BC). 2.8 $M_T$ $CO_2$ per year was injected for 30 years through one vertical injector and the well was completed in the bottom 4 layers of the aquifer. Simulation was continued for 1000 years after well shut in to predict the extent of $CO_2$ migration at the top of the aquifer. The base case model is large, covering an area of 1419 $km^2$ (top surface) and also has a large cell size 0.2 $km^2$ (450m×450m, in the X and Y direction). In order to cut down on simulation time, and to improve the accuracy of the simulations, a sector of this model was used with a finer resolution. There are different ways of conducting this such as using Flux option in ECLIPSE or deactivating all the cells in the area which are not of interest using the ACTNUM keyword. Both methods were tested and the latter method was selected. Figure ***6.8*** demonstrates the area of interest for further study in this model. The deactivated pore volumes were added to the edges of the sub model by using PORO MULTIPLY keywords in ECLIPSE.

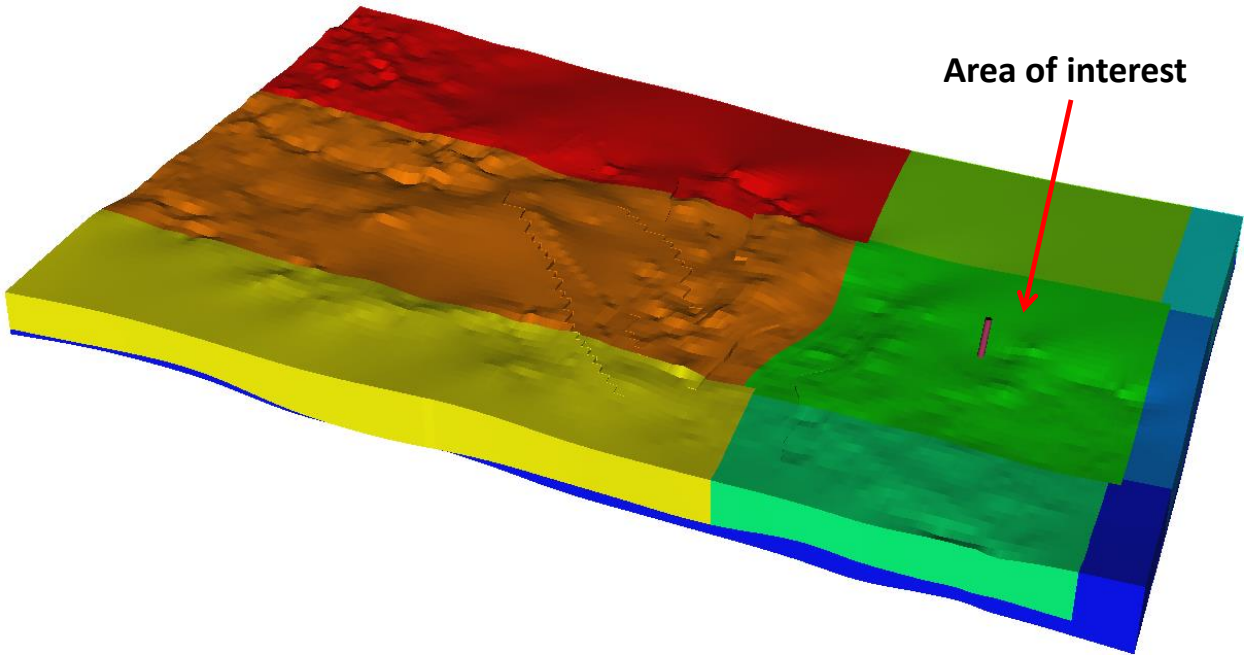


*Figure 6.8 The red Arrow indicates the green section in the middle of the model which is the area of interest. The injector is located at the centre of this section.*

### *6.4.2 Models Studied and Grid Refinements*

Six models have been considered in this chapter (Table **Error! Reference source not found.**). The first one is the base case (BC) Model, as discussed in the previous section. The second model is the sub-model of the base case model, which is the area of interest. Model 1 refers to the modified BC Model where the top aquifer layer was divided into 10 layers and the new properties were distributed in order to investigate the effect the transition zone on $CO_2$ storage. Model 2 is the sub-model of Model 1 (area of interest).

In order to investigate the grid refinement effect, Model 2 was modified to Model 3 by refining the area where $CO_2$ migrated in the top ten layers of Model 2 (see LGR1 section in Figure ***6.9***). Model 3 was modified to Model 4 by refining the 7 cells around the well in the X and Y directions by a factor of 5 for further reduction in numerical dispersion errors. Numerical dispersion causes an artificial spreading of the CO2 front in a coarse grid model. In addition, numerical dispersion artificially increases the amount of dissolution in a coarse scale model (Green and Ennis-King 2012).

Figure ***6.9*** shows a cross section of Model 4 to clarify the initial cell size, the refinement areas and the size of refined grids. Petrel was used to add all modification to the base case model and then the grids and properties were exported to ECLIPSE 300 to study the flow simulation, using the CO2STORE module. In all figures presented in this section, the caprock is excluded for a better visualization of the top of the aquifer.

*Table 6.3 Models used in this section*

| Model | Descriptions |
|---|---|
| Base case (BC) | Initial Lincolnshire Model |
| Sub-BC | Area of interest |
| Model 1 | Modified BC Model (transition zone is added) |
| Model 2 | Sub model of Model 1 (area of interest) |
| Model 3 | Top 10 layers of Model 2 were refined (LGR1) |
| Model 4 | Seven cells around the well of Model 3 were refined (LGR2) |

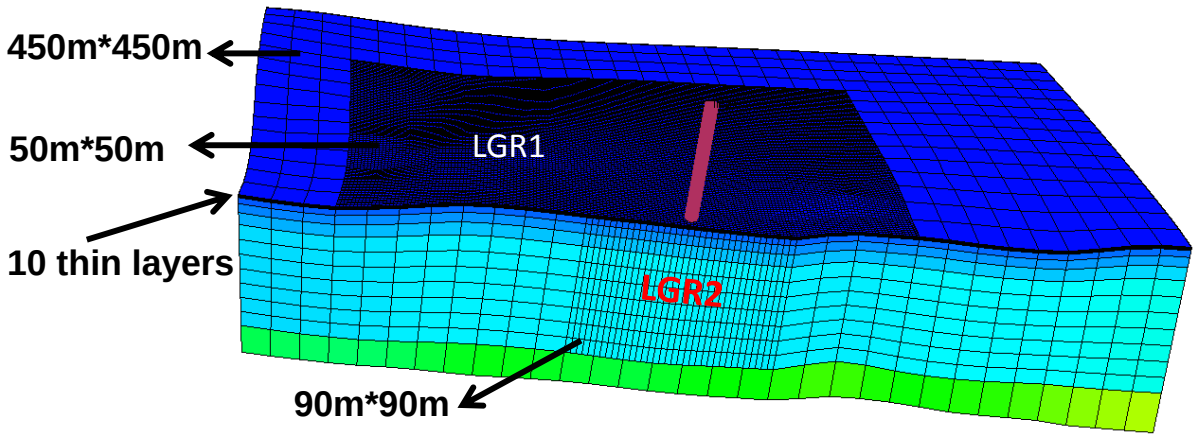


*Figure 6.9 A cross section of Model 4 without caprock. The initial cell size was 450m × 450m, the cell sizes in the local grid refinement 1 (LGR1) and LGR2 are 50m × 50m and 90m × 90m respectively. All cells are just refined in the X and the Y directions, not in the Z direction.*

### *6.4.3 Results and discussion*

Figure ***6.10*** shows gas saturation 1000 years into the post injection period. The top two pictures show plume migration at the top of aquifer in the base case Model and the bottom two pictures show gas migration at the top of the aquifer where it contains the transition zone. This figure shows the results were not affected by focussing only on a sector model. In addition, it shows the effect of the transition zone on $CO_2$ migration beneath the caprock. The heterogeneous permeability distribution obviously influences the amount of $CO_2$ which reaches the top layer of the aquifer and this affects the direction of $CO_2$ migration at the top of the aquifer and local trapping of $CO_2$. Mud layers in the transition zone act as partial baffles to hinder plume migration towards the caprock, and therefore, slowdown the vertical migration. This has significant effects on the storage capacity and security:

- Increases the lateral migration in the layers below the caprock.
- $CO_2$ will come into contact with more brine due to two effects: first is the lateral migration and secondly the buoyancy effect.

The latter effect causes more interactions between $CO_2$, and new fresh brine, resulting in slightly more $CO_2$ dissolution in the aquifer (Figure ***6.11***).

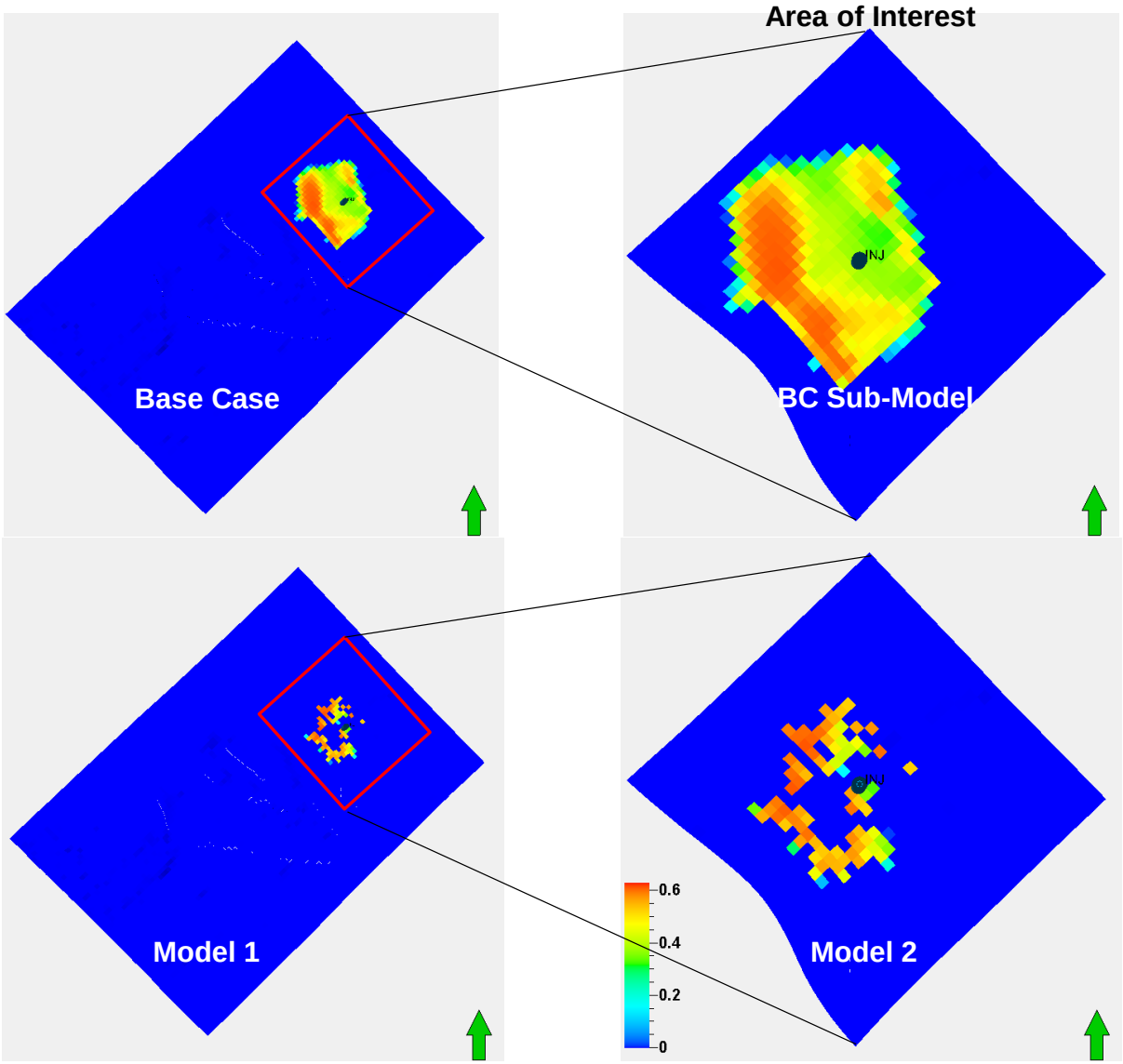


*Figure 6.10 Gas saturation 1000 years after well shut-in, all models. Models on the right side are sub-models of the models in the left side. Bottom two models demonstrate the effect of transition zone on $CO_2$ migration at the top of aquifer whereas in the top two models this effect is not considered.*

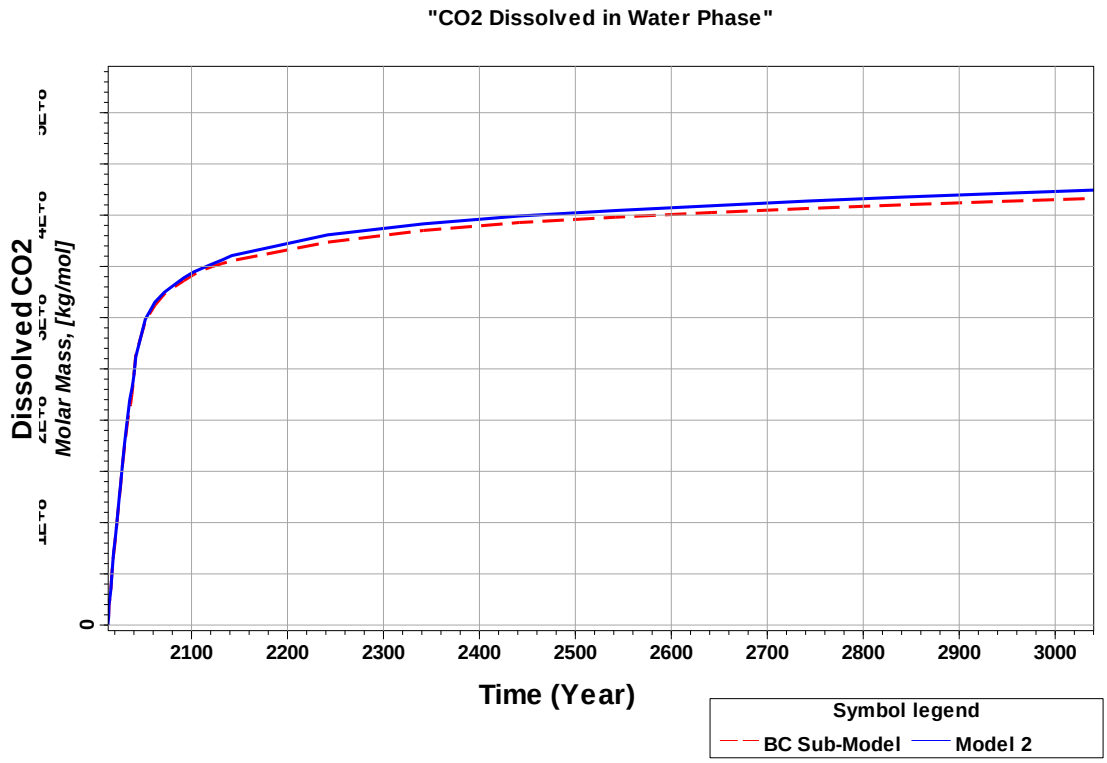


*Figure 6.11 CO2 dissolved in Brine, solid line refers to Model 2 and red dashed line refers to BC Sub-Model.*

Figure ***6.12*** and Figure ***6.13*** show the effect of grid refinement on the $CO_2$ storage in the Lincolnshire Model with the transition zone. There was effectively no change going from Model 2 to Model 3 by using LGR at the top of the model. In addition, it can be concluded that this effect is more severe when we refine grids around the well (Model 4) rather than just refining grids beneath the caprock (Model 3). This is because less numerical dispersion in the horizontal direction, so the plume does not spread out so far and a narrower plume reaches the top of the aquifer sooner. However, less $CO_2$ will be dissolved.

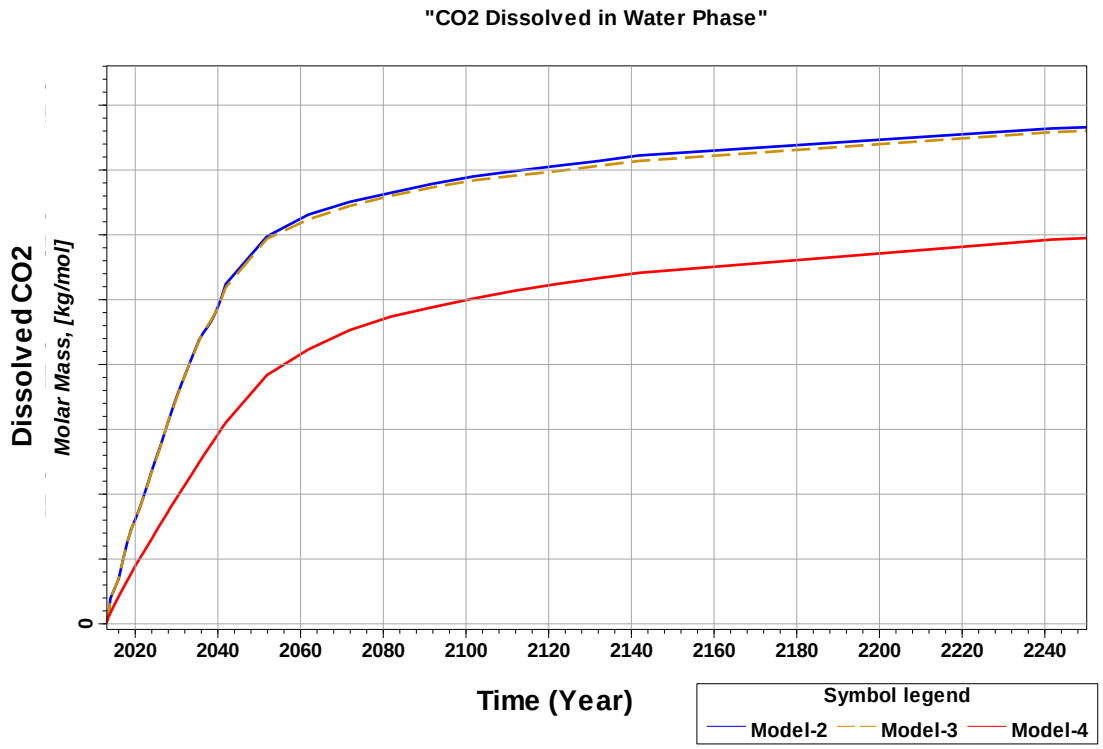


*Figure 6.12 CO2 dissolved in brine in Models 2, 3, and 4.*

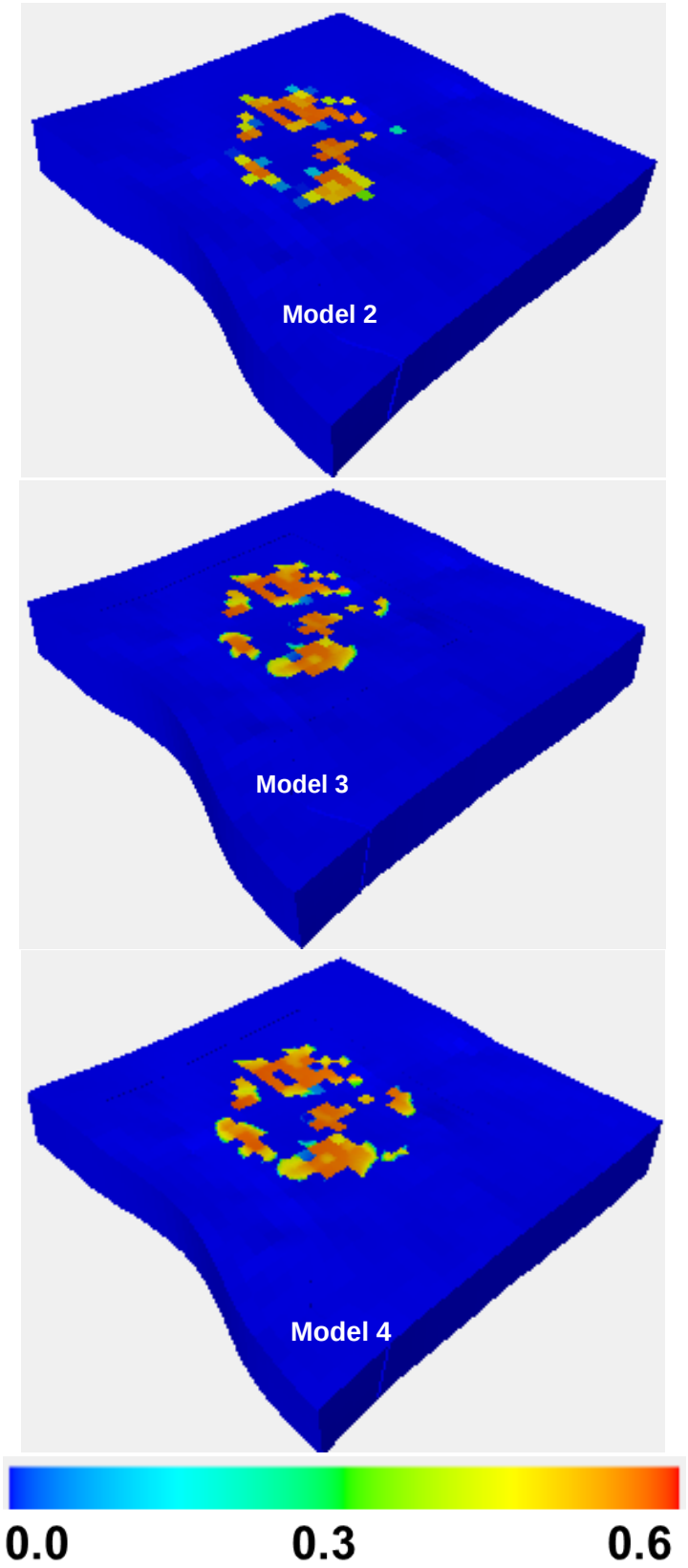


*Figure 6.13 Gas saturation 200 years after well shut in, in all models. The most $CO_2$ reached the top of the aquifer in Model 4.*

### *6.4.4 Regional $CO_2$ dissolution*

The models were divided into four regions vertically in order to gain a better understanding of the changes in the models after $CO_2$ was injected into them (Figure ***6.14***). Region 1 is the caprock. Region 2 is the transition zone, (Region 2 in base case models is the top sand layer in the aquifer). Region 3 is the aquifer excluding the transition zone. Region 4 is a low permeability layer (under burden).

The results show that all of the free $CO_2$ phase is either in the aquifer (Region 3) or in the transition zone (Regions 2).

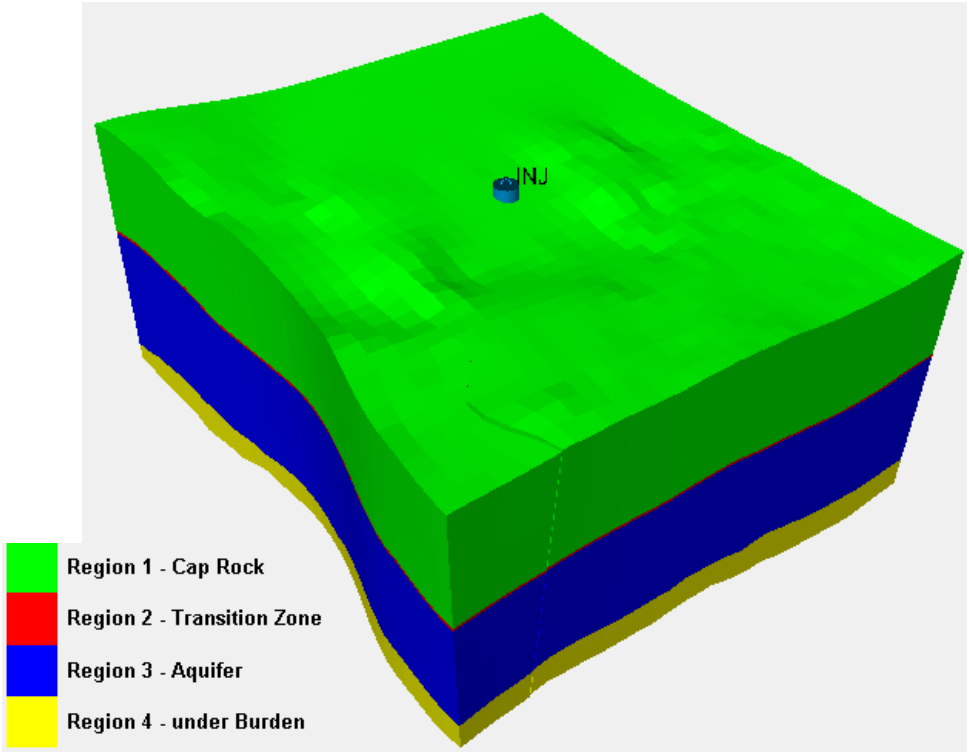


*Figure 6.14 Model regions.*

After $CO_2$ is injected into the aquifer it is expected to be either in the aqueous phase (dissolved) or in the gas phase (mobile and immobile). Figure ***6.15*** shows that around 20 % of $CO_2$ is modelled to be dissolved in brine by 200 years post-injection in both the BC Sub-Model and Model 2. However, as discussed in the previous section, the amount of dissolved $CO_2$ in Model 2 is a little more than in the BC Sub-Model.

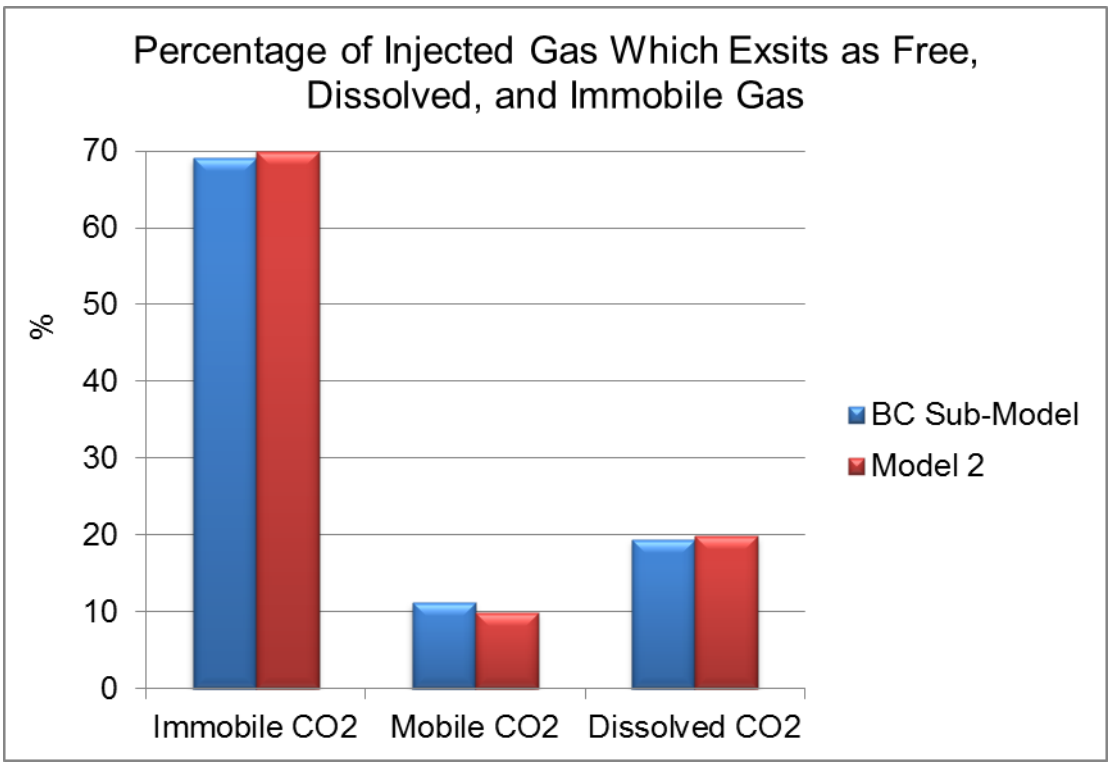


*Figure 6.15 Free, dissolved, and immobile $CO_2$ on percentages in Model 2 and in the BC Sub-Model 200 years into the post-injection period. Around 20% of the injected $CO_2$ is dissolved in brine, 10% is in the free $CO_2$ phase and 70% is immobile.*

Figure ***6.16*** shows that in Region 2 in Model 2, 4.5% of the injected $CO_2$ exists as free $CO_2$ phase, whereas in the BC Sub-Model this amount is double by 200 years post-injection. This shows that less $CO_2$ reaches the zone beneath the caprock in Model 2 in comparison to the BC Sub-Model due to the effect of the low permeability mudstone layers in the transition zone.

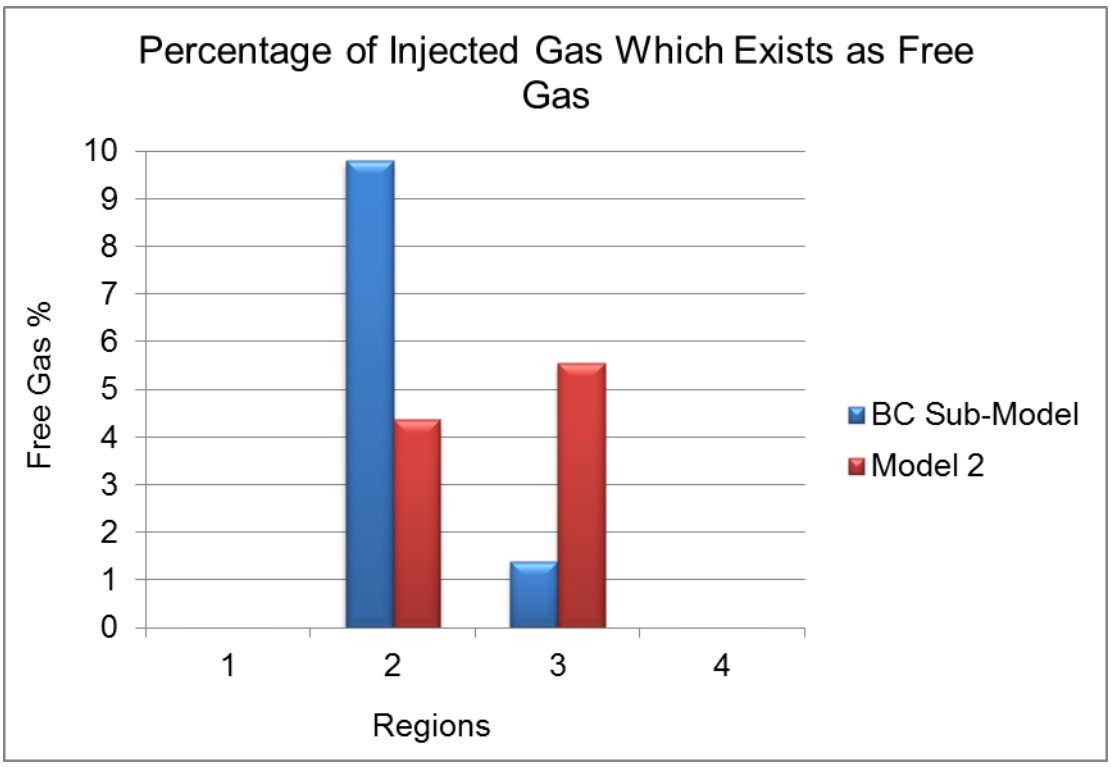


*Figure 6.16 Free $CO_2$ phase in percentage in Regions 1 to 4 in the BC Sub-Model and Model 2. (Region 2 is the transition zone, and Region 3 the main part of the aquifer.)*

Figure ***6.17*** shows that most of the injected $CO_2$ is in the immobile state by 200 years post-injection period. A very large proportion of this occurs in Region 3. More $CO_2$ is in the immobile state in Region 3 in Model 2 than in the BC Sub-Model. This is due to lower $CO_2$ migration to the transition zone, and thus more $CO_2$ will be in contact with fresh brine and this increases the opportunity for $CO_2$ to become trapped. However, in the BC Sub-Model more $CO_2$ reaches the zone just beneath the caprock (Region 2), and therefore more $CO_2$ is in an immobile state than in Model 2.

Although the amount of dissolved $CO_2$ in brine in both models is almost the same (Figure ***6.18***), more $CO_2$ dissolves in Model 2 in Region 3 in comparison to the BC Sub-Model and in the transition zone this is the other way round. This is because of lower permeability resistance to $CO_2$ vertical migration in the BC Sub-Model, and therefore more $CO_2$ reached the zone beneath the caprock resulting in more dissolution in brine, due to further $CO_2$ migration, than in Model 2.

Figure ***6.19*** shows that in Model 2 around 10% less $CO_2$ can reach Region 2 (transition zone in this model) than in the BC Sub-Model 200 years after well shut-in.

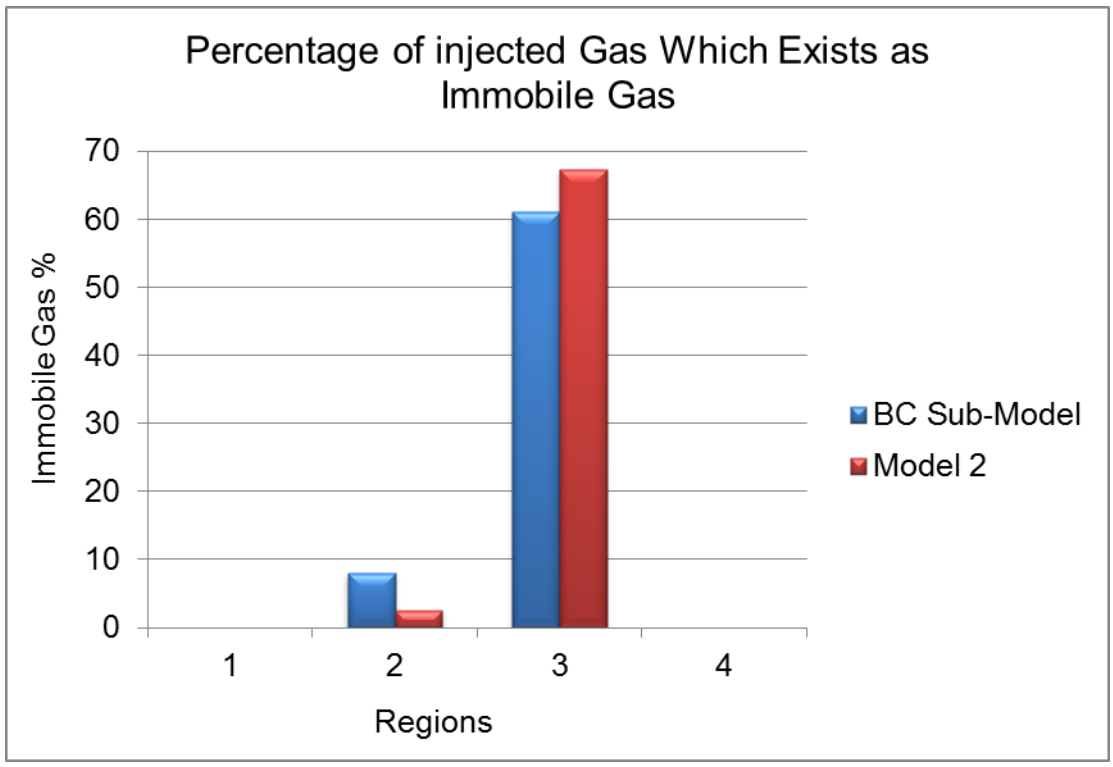


*Figure 6.17 Percentage of immobile $CO_2$ in Regions 1 to 4 in the BC Sub-Model and Model 2.*

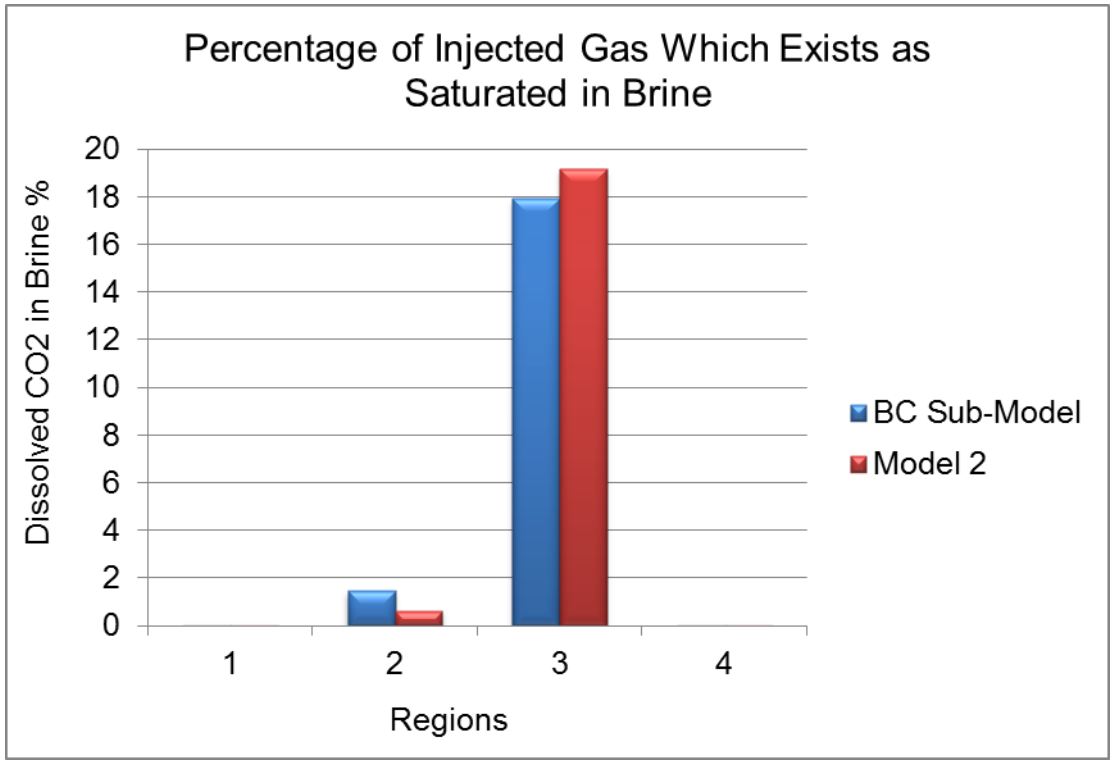


*Figure 6.18 Dissolved $CO_2$ in brine (%) in Regions 1 to 4 in the BC Sub-Model and Model 2.*

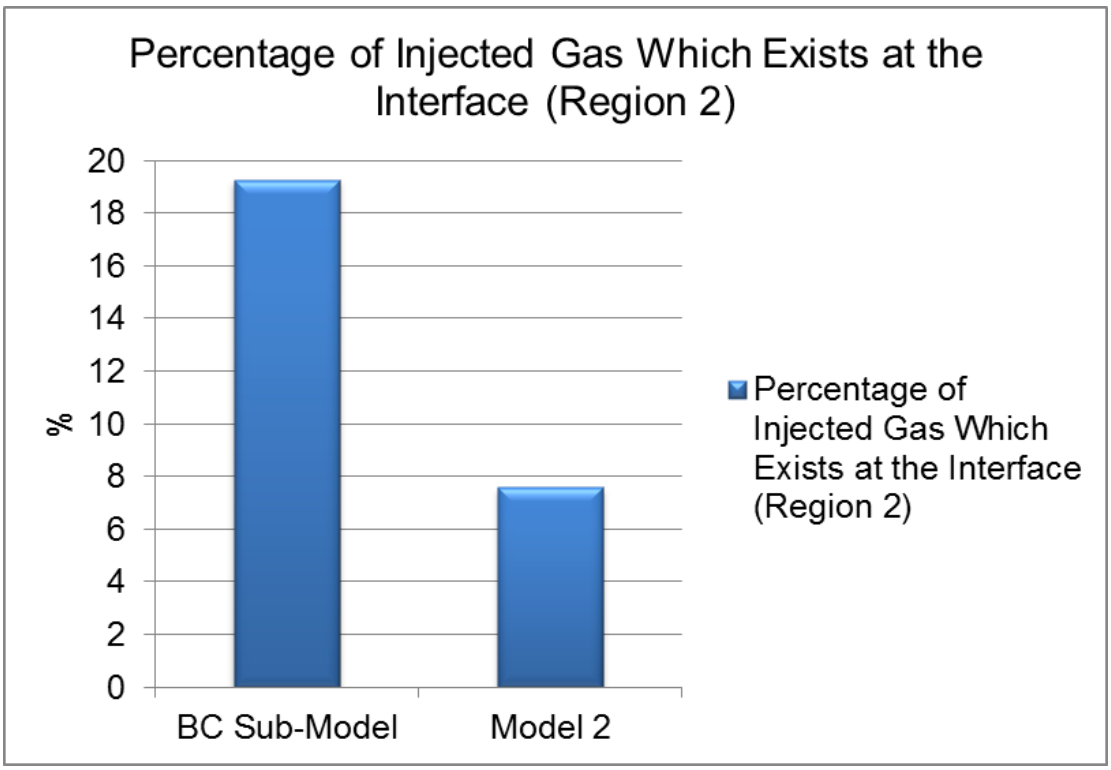


*Figure 6.19 The proportion of injected $CO_2$ which exists in all states at the transition zone (Region 2).*

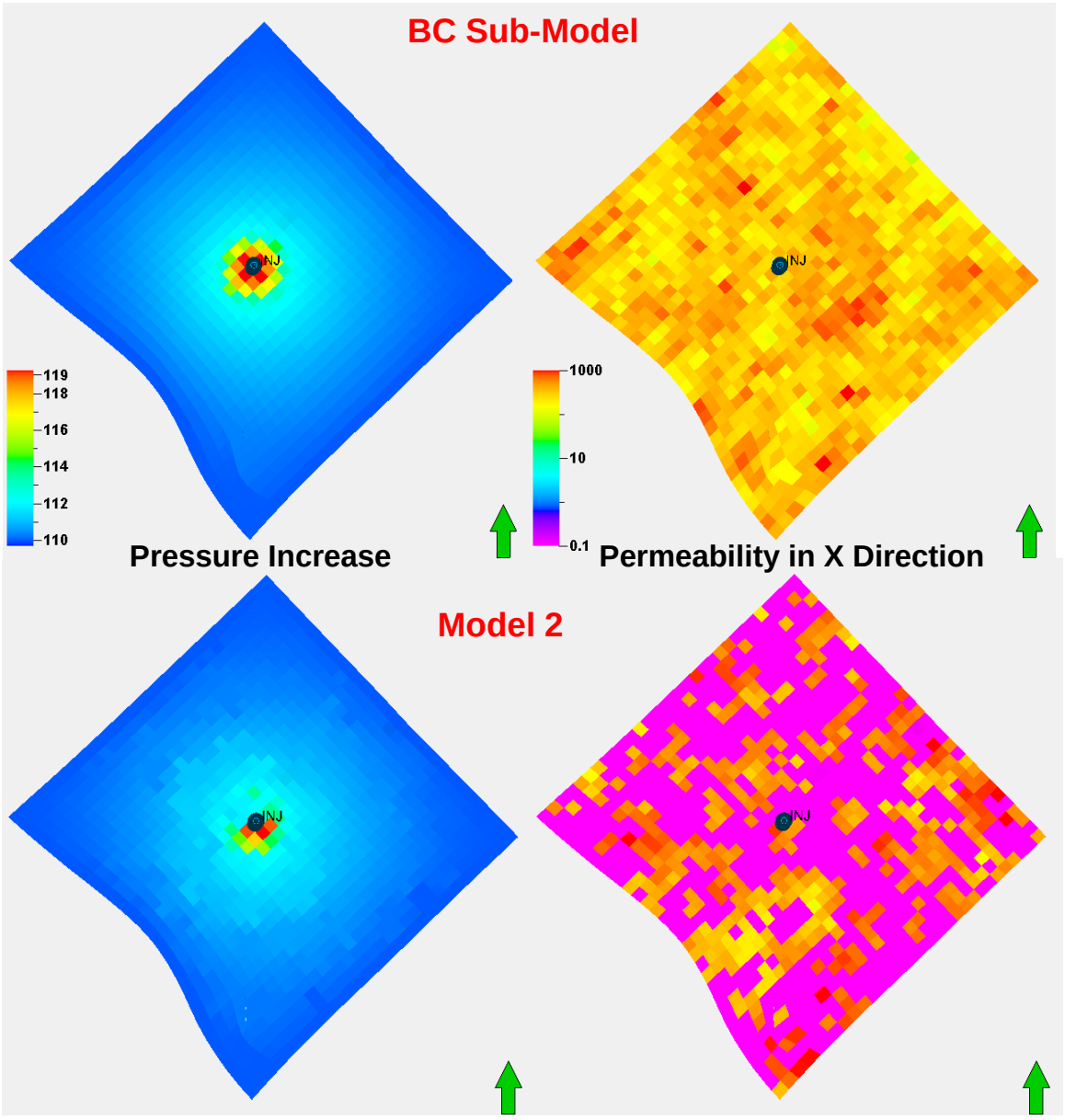


*Figure 6.20 Pressure increase (in bar) (left pictures) in the layer just beneath the caprock by the end of injection (30 years) and the top aquifer layer's permeability distribution (right pictures). Top two refer to the BC Sub-Model and the bottom two refer to Model 2.*

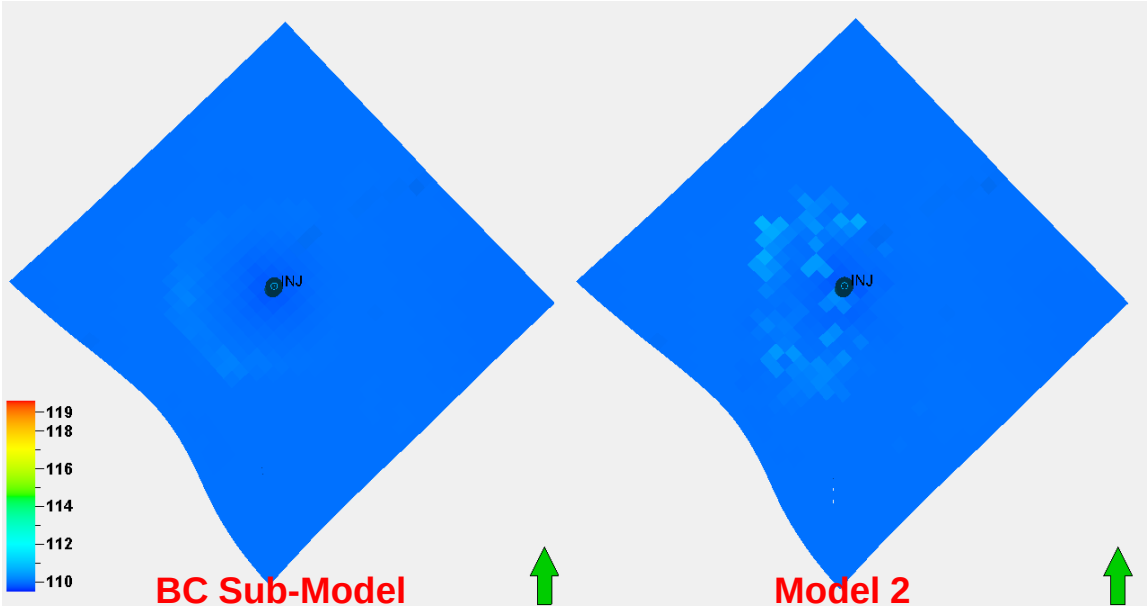


*Figure 6.21 Pressure increase (in bar) in the layer just beneath the caprock, 200 years after wells shut-in.*

### *6.4.5 Conclusions*

As discussed earlier, the boundary between the aquifer and the caprock could contain a transition zone where there is a gradual change from sand-rich facies at the top of the aquifer to the mud-rich facies in the caprock. It can be concluded that the transition zone can increase the security of the $CO_2$ storage. The reasons for this are outlined below:

- Vertical migration decreases at the transition zone due to the presence of partial baffles.

- Lateral $CO_2$ migration increases due to the effect of baffles, and therefore more $CO_2$ will be in contact with fresh brine resulting in more $CO_2$ residual trapping and also more $CO_2$ dissolution in brine.

- The less $CO_2$ reaches the caprock the lower the pressure builds up at the base of caprock due to thickness of $CO_2$ column (Figure ***6.21***).

These results show the importance of characterisation of the interface between the caprock and the aquifer formation.

In addition, the transition zone can have an effect on the storage capacity. Including the transition zone as a part of the caprock or the aquifer causes an underestimation or the overestimation of the effective storage capacity. Based on a conclusion made in Chapter 3, assuming that the transition zone is 10 metres thick and consists of 60% mud and 40% sand, results in less than 5% uncertainty in the storage capacity due the fact that aquifer is quite thick in Lincolnshire model.

## 6.5 Application of Down-Hole Mixing Method in a Real Field

In Chapter 5 $CO_2$/brine down-hole mixing method (DHM) was presented and it was concluded that this method could be an engineering solution to tackle the leakage risk of free $CO_2$ phase through the caprock. In this section the application of down-hole mixing in a real field model is examined.

Suppose that engineers are concerned about $CO_2$ leakage through the faults which are present in the formations in the hypothetical Lincolnshire storage site. In this case, using the conventional $CO_2$ storage method incurs risk if $CO_2$ could reach the non-sealing faults. In this section, the application of DHM in the Lincolnshire Model is tested. Calculations are performed to identify the optimum level of water extraction and injection of dissolved $CO_2$ in brine. In addition, simulations will be presented to show the other advantages of using DHM on $CO_2$ storage (e.g. $CO_2$ injection for much longer period).

### *6.5.1 Methodology*

#### *Well types and Drilling Scenarios*

There are three scenarios in terms of well types which can be considered when planning DHM (Figure ***6.22***). The first scenario (A) uses a vertical well. Water is extracted near the top of the aquifer, $CO_2$ is mixed with water in the intermediate section of this well, and then water with dissolved $CO_2$ is injected at the bottom of the formation. The advantages associated with this scenario are outlined below:

- Lower cost for vertical drilling
- It is a good method for the low injectivity $CO_2$ injection plans

In the second scenario (B) is using a horizontal well. Injectivity (which depends on the length of the completion interval) is greater if a horizontal injection well is used. Extracting brine, dissolving $CO_2$ into brine, and injecting dissolved $CO_2$ in brine would

be the same as discussed for case A. The advantage of this scenario over the previous one is that we can inject $CO_2$ with a higher rate into the storage formation.

In the third scenario (C), a multi-lateral well, which uses two or more branches joined to a main or mother well bore can increase contact length with the formation. Brine is extracted from one lateral and then re-injected into the aquifer through another lateral using multiple tubing after it was saturated with $CO_2$ in the down-hole mixing tool.

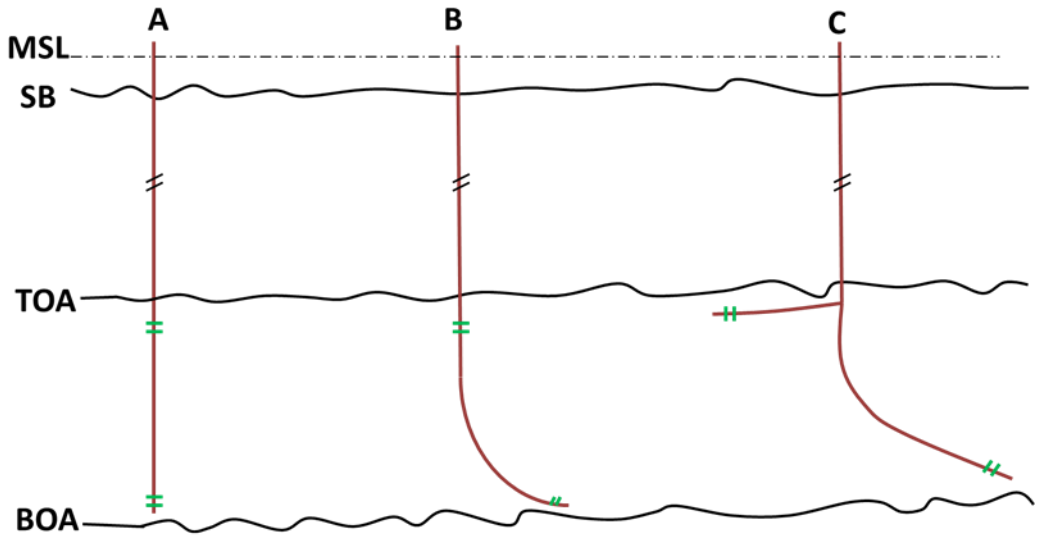


*Figure 6.22 Schematic cross section of different well scenarios. A denotes a vertical well, B refers to a deviated well, and C denotes a multi-lateral well. Green lines refer to the perforations for the water extraction at the upper section and for the injection points at the bottom of the storage formation. MSL (dashed lines) refer to the mean sea level and TOA refer to the top of the aquifer. BOA and SB refer to the bottom of aquifer and the sea bed respectively.*

The first scenario would be the lowest cost option where a vertical well is available and there is only a limited $CO_2$ supply available in terms of quantity for a limited $CO_2$ injection scenario. In the oil and gas industry where produced gas contains $CO_2$ then this option can be considered if separation takes place at the facility. The maximum injection rate would be limited by the flow rate that could be achieved between the point of mixing and the completion where $CO_2$ saturated brine is injected. The thickness of the aquifer controls the maximum allowable distance between injection and the extraction.

The second and the third scenarios can be considered when a large $CO_2$ storage site is planned. In these scenarios there is a possibility of drilling the wells laterally to ensure

sufficient distance between extraction and injection points to avoid the injected dissolved $CO_2$ reaching the brine extraction point. Producing brine which is already saturated with some $CO_2$ will decrease the $CO_2$ storage performance and increase the corrosion risk. In this study, we focus on the scenario C.

Model 2 will be used to conduct a series of numerical simulations on the application of DHM in the Lincolnshire Model. The grid cells in the aquifer have been refined in X and Y direction by factor of 9, however the grid cells where wells have been drilled remain unchanged.

In terms of modelling this can be modelled using separate producer and injector wells. However, this may cause some error in the results (e.g. pressure distribution around the wells). Therefore, in this study, one well was used to model this scenario. This is designed by having two horizontal branches in one well. In the simulations, a pre-determined volume of brine required for the planned $CO_2$ injection rate (Spycher and Pruess 2005) is extracted from the top lateral. The pump for extracting the brine was modelled as a producer in the top branch of a well. The extracted brine is assumed to be used for dissolving $CO_2$ in it based on Spycher and Pruess (2005). The down-hole dissolution was not modelled explicitly. Instead, in the simulation, a solution of $CO_2$ dissolved in brine was injected through the lower branch of the well. It is assumed that the fluid mixing is achieved based on Spycher and Pruess (2005). This can also be tested by checking the amount of free $CO_2$ phase in the aquifer that has to be zero. In the subsequent description, these branches of the well are referred to as the producer and the injector.

In all cases, a single well was placed in the centre of the model. The control mode for both production and injection was reservoir fluid volume rate and the rates were 6500 $rm^3$/day and 6175 $rm^3$/day for the injector and the producer, respectively. Both producer and injector were shut after 100 years and the simulation was continued for 1000 years.

### *6.5.2 Results*

Figure *6.23* demonstrates the well location and connections. Water is extracted from the top of the reservoir and pumped into the bottom hole and the supercritical $CO_2$ is injected into the well simultaneously. The dissolution of supercritical $CO_2$ in the

extracted brine takes place at the bottom hole. It is assumed that dissolution process can be managed by a specific $CO_2$/brine down-hole mixing tool.

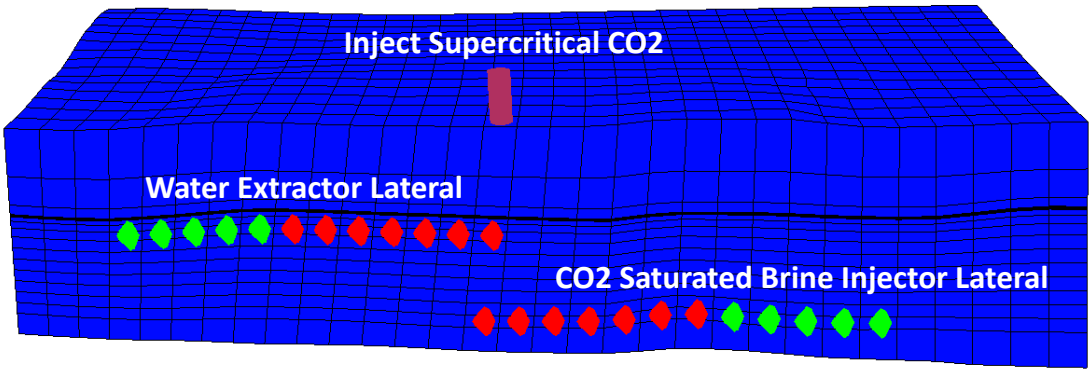


*Figure 6.23 Well location and connections, Green dots in the laterals show the locations of perforations.*

Figure ***6.24*** demonstrates the $CO_2$ mole fraction at the end of the 100 year injection period and 1000 years after well is shut-in, in the Lincolnshire Model 2. Note that, because $CO_2$ was dissolved in brine in the well, there was no free injected $CO_2$ phase in the model, nor did any exsolve from solution during the period of the calculation. $CO_2$ saturated brine is denser than in situ brine. Therefore, it should go downwards. However, it goes upwards due to injection pressure gradient and then subsequently sinks down again due to gravity.

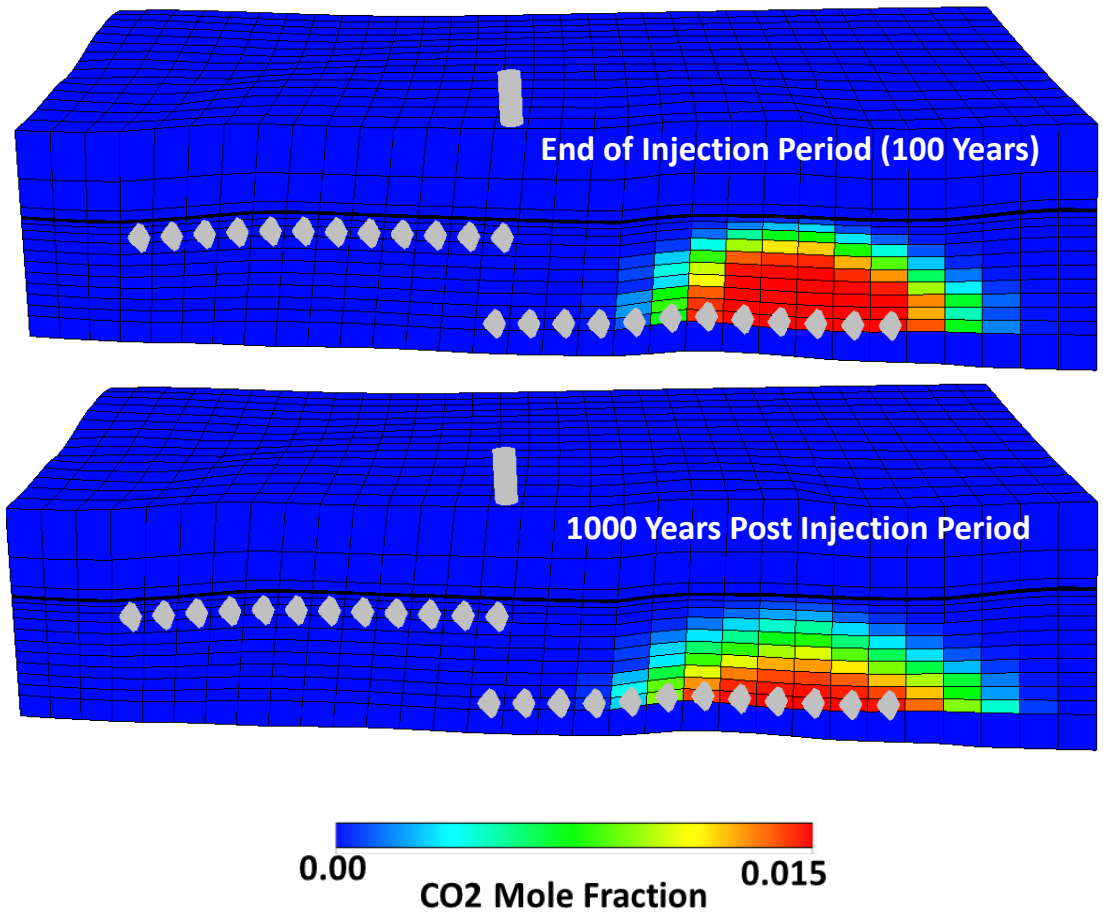


*Figure 6.24 Cross sections of Lincolnshire Model 2 show $CO_2$ mole fraction dissolved in brine at the end of injection period (top) and by the 1000 years post injection period.*

***The amount of $CO_2$ can be stored by this method***

One mole $CO_2$ equals 44 gm so one tonne contains 22727 moles of $CO_2$ (1,000,000gm/44 gm/mole) and one mole is 24.47 litres thus, one tonne $CO_2$ equals 556.13 cubic metres at standard conditions.

The density of $CO_2$ at 100 bars and 35 C equals 713.68 kg/m$^3$ and at the standard conditions (15 C and 1 bar) equals 1.85 kg/m$^3$ (MIT Calculator). In our calculation 39.34 kg $CO_2$ can be dissolved in 1 m$^3$ brine (NaCl, 100,000mg/l). Thus, the amount of $CO_2$ can be dissolved at this reservoir condition in 6175 m$^3$ brine equals:

$$39.34 \times 6175 = 242924.5(kg)$$

Assuming mass conservation, then 0.088 Mt $CO_2$/year per well can be dissolved down-hole and injected into the aquifer at the aforementioned condition. The target of injecting 1 MT $CO_2$/year can be achieved by drilling 11 wells. This calculation depends on the P, T, salinity, and the reservoir volume injection rate. For a reservoir with lower salinity (e.g. 35,000 ppm at the brine extractor points) with the same T, P, and reservoir

volume injection rate just 8 wells need to inject 1 MT dissolved $CO_2$ in brine/year. Drilling engineering enables us to use dual completion and multi-lateral well techniques to have more laterals for brine extractor and $CO_2$ saturated brine injector. This results in reducing the number of required wells for $CO_2$ injection as mentioned earlier.

Figure ***6.25*** shows brine density verses depth used in the Lincolnshire Model for the DHM study. As a result of dissolving $CO_2$ in brine the density of brine increases (Duan and Sun 2003, Spycher et al. 2005). This increase for the extracted brine at the depth of 1000 m in this model equals 7.8 kg/m$^3$ which is equal to the density of fresh brine at the depth of 2557 m. The difference in density of brine with and without $CO_2$, for most of suitable storage aquifer roughly is the same. However, the salinity gradient may vary therefore blue line may moves upwards to downwards.

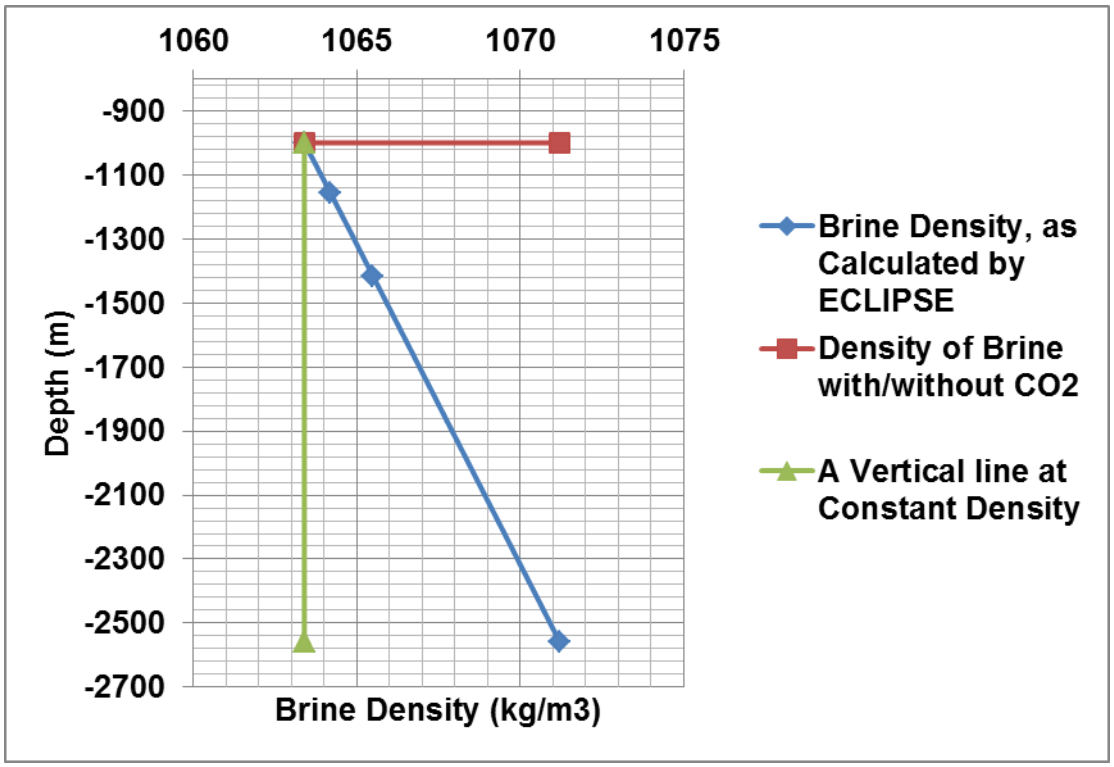


*Figure 6.25 Brine density verses depth, red dots show density of brine without $CO_2$ (1063.4 kg/m$^3$) and with $CO_2$ (1071.2 kg/m$^3$) at the depth of 1000 m. Blue line refers to the brine density extracted from ECLIPSE for the Lincolnshire Model. Geothermal gradient is set at 20 C/km.*

***Optimisation***

In this section the position of the laterals in terms of depths and lengths is investigated. Figure ***6.26*** shows all scenarios studied here. The area around the injection lateral into which the dissolved $CO_2$ is displaced was refined by factor of 9×9×9 in X, Y, and Z

directions, except for the layers where the laterals were located. The best scenario will be screened based on the following criteria:

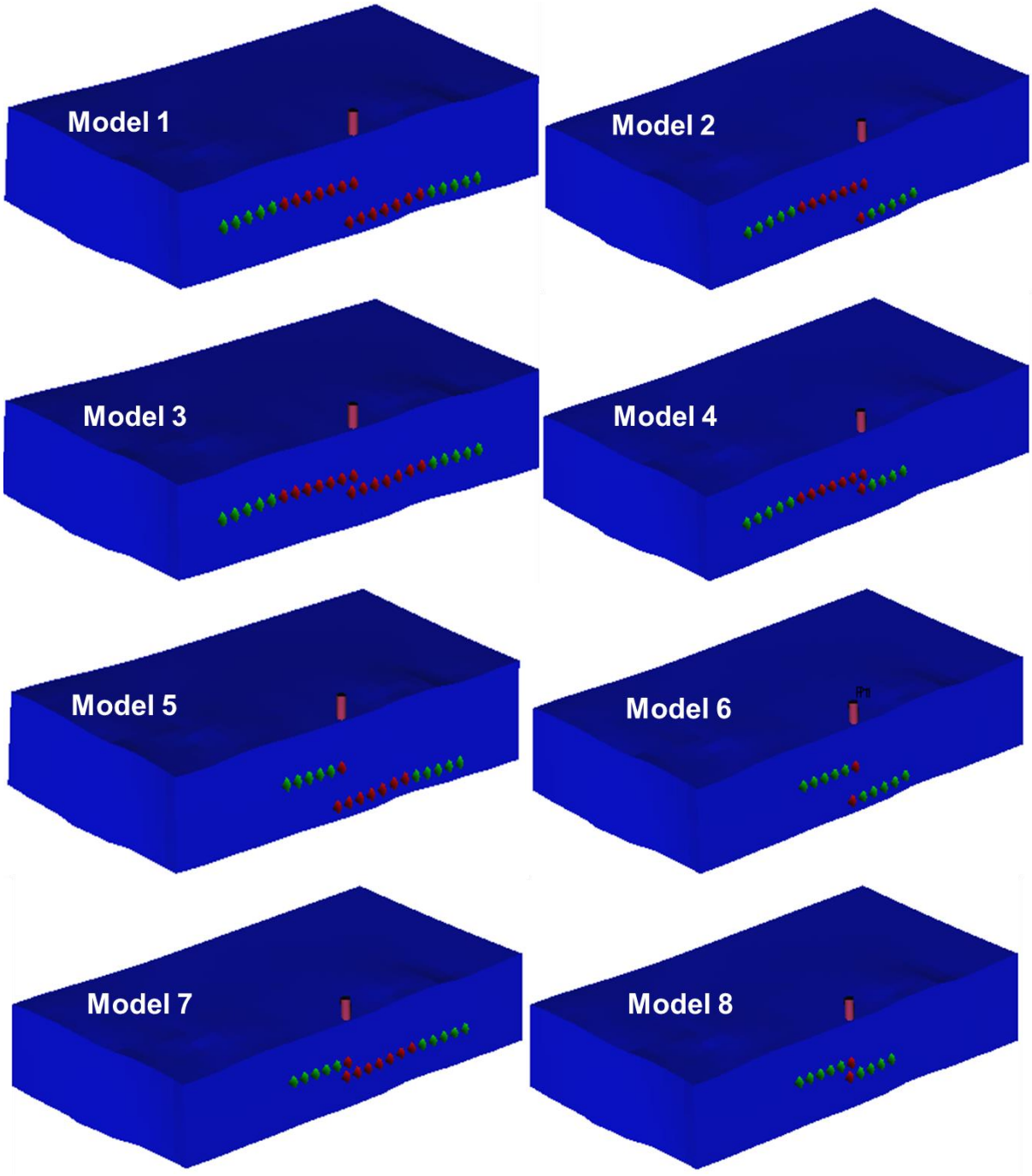


*Figure 6.26 Cross sections of Models 1 to 8 show the brine extractor laterals at the top of the storage formation and the injector laterals at the either bottom of the aquifer (Models 1,2,5, and 6) or at the Middle of the aquifer (Models 3,4,7, and 8). Brine is extracted 2.7 km away from the well bore in top four Models (1, 2, 3 and 4) whereas is extracted at adjacent to the well bore in Model 5, 6, 7 , and 8(bottom four). Dissolved $CO_2$ in brine is injected into the storage formation 2.7 km away and at adjacent to the well bore in the four left Models (1, 3, 5, and 7) and the four right Models (2, 4, 6, and 8) respectively.*

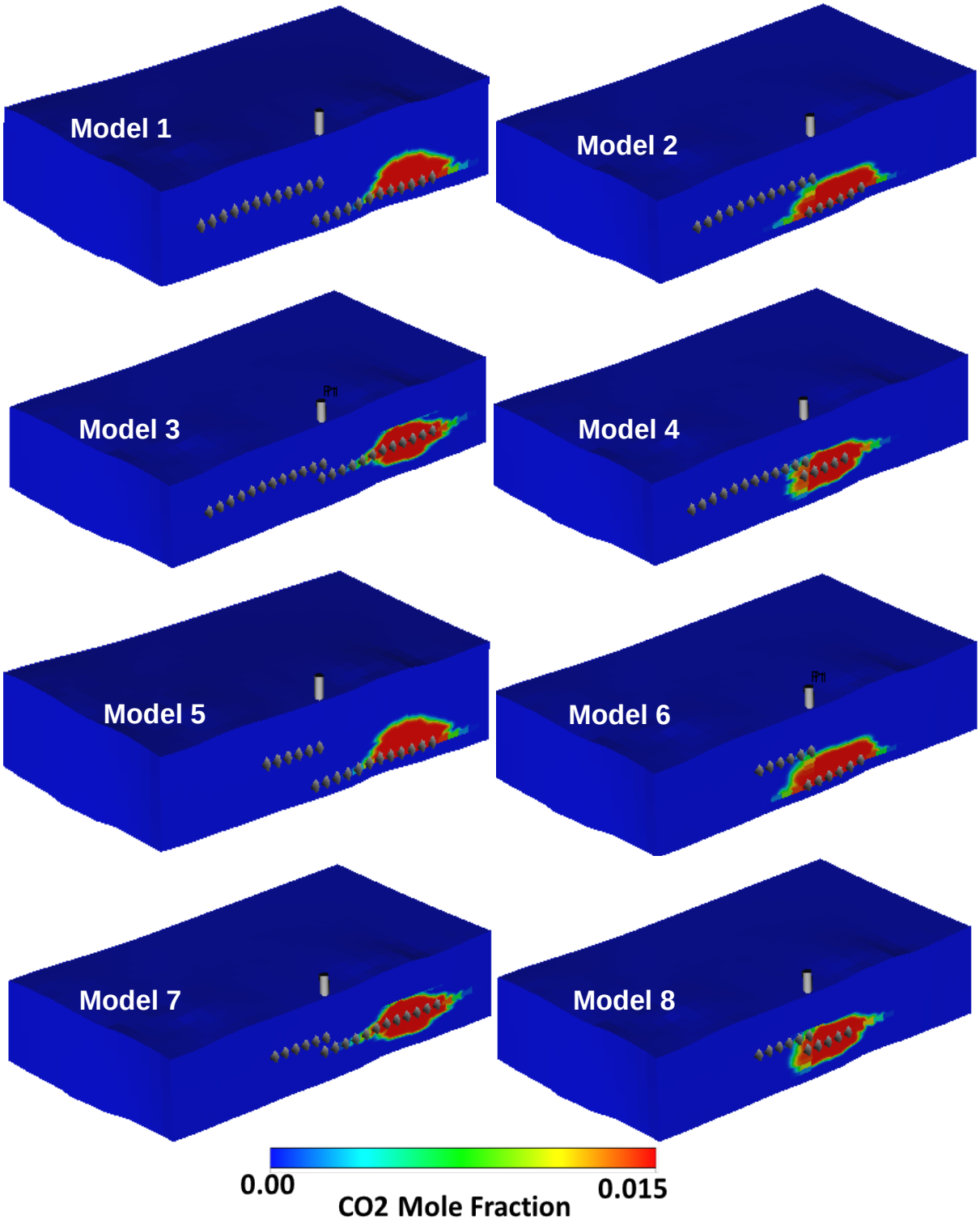


*Figure 6.27 $CO_2$ mole fractions dissolved at the end of injection period (100 years).*

The viscous force is the main driving force when dissolved $CO_2$ is injected into the aquifer. The injected fluid tends to migrate towards the brine extractor lateral where the pressure is lower. However, even after 100 years of dissolved $CO_2$ injection into the storage formation, the dissolved $CO_2$ does not reach the brine extractor perforations except in Models 6 and 8 due to shorter distance between injection and producer points that in other models (Figure ***6.27***).

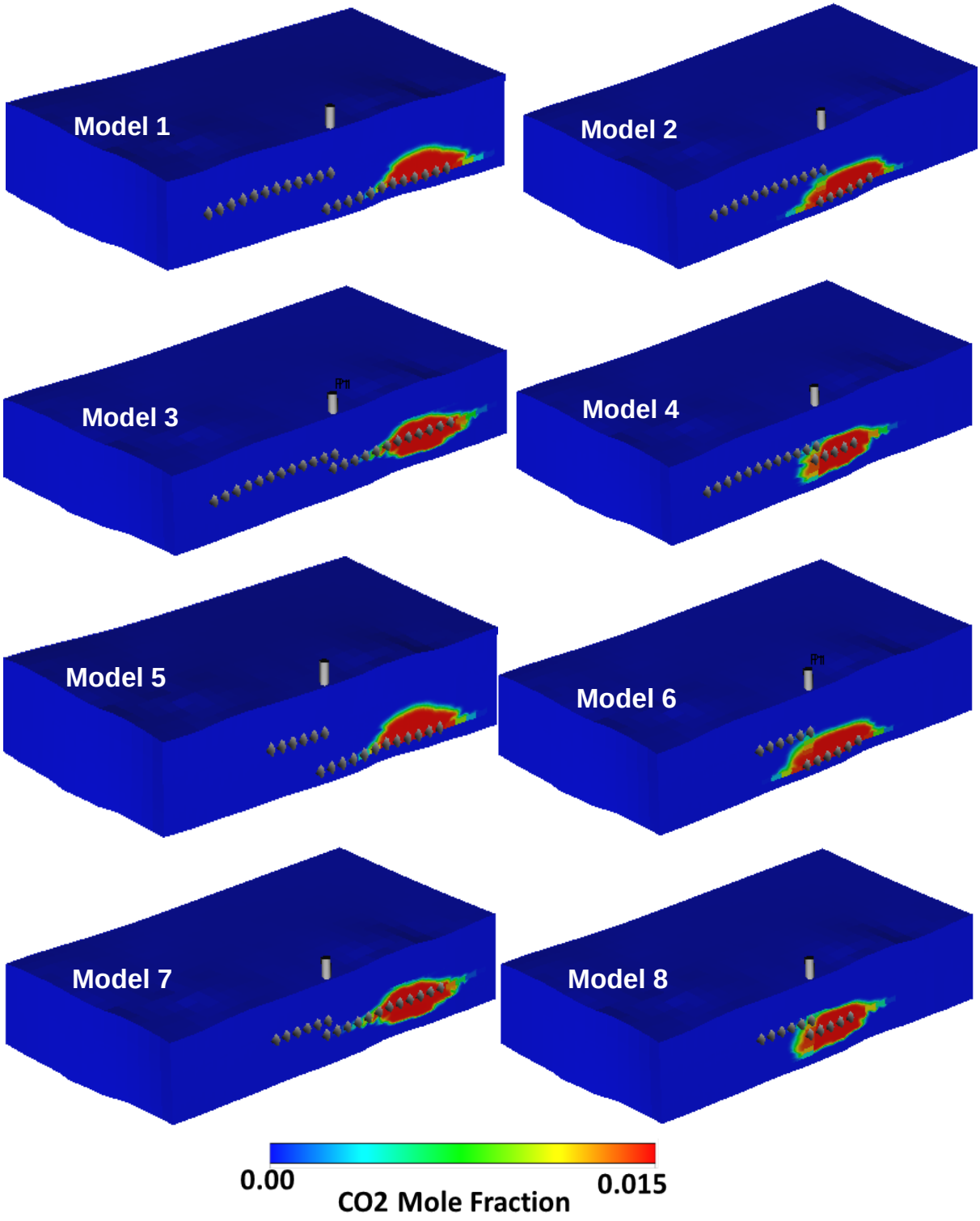


*Figure 6.28 $CO_2$ mole fractions dissolved in brine 200 years post injection period.*

Figure ***6.28*** shows $CO_2$ mole fraction dissolved in brine 200 years after wells shut-in. All the free phase $CO_2$ was dissolved prior to injection into the storage formation. Dissolved $CO_2$ in brine is heavier than fresh brine and thus the $CO_2$ saturated brine tends to sink in the aquifer under gravity.

Models 6 and 8 are not of further interest due to the small distance between the perforation at the injector lateral and extractor lateral that could allow dissolved $CO_2$ to reach the extraction region. In all other models (1, 2, 3, 4, 5, 7) dissolved $CO_2$ does not reach the perforations at the extractor lateral. Therefore, all these models are acceptable to be used. However, to screen these models cost (shortest length) and pressure loss were used as new criteria. Model 1 provides the biggest distance between the extraction region and the injection region among all models, therefore it can be considered as the safest scenario. Thus, Model 4 would be the best option because of:

1. The lowest frictional pressure loss in the wellbore.
2. The minimum length of high chromium steel needed.

***Conclusion:***

As discussed in Chapter 5, using $CO_2$/brine down-hole mixing could improve $CO_2$ sequestration in the geological formations by switching free phase $CO_2$ migration upwards under buoyancy to dissolved $CO_2$ migration downward. In this study the placement of the laterals was studied. It was concluded that the most efficient model is the one where the brine extraction lateral is at a large distance from the $CO_2$ saturated injection lateral is close to the bore hole. The former is to maximize the distance between extraction and injection and the latter is to minimize the need for having high chromium steel.

In addition, calculations were performed to determine the amount of $CO_2$ that can be stored by this method. It can be concluded that 1 MT $CO_2$ can be dissolved in brine down hole through five dual completion and mutli-laterals wells, where there are two brine extraction laterals and two dissolved $CO_2$ injection laterals.

A proper economical calculation needs to be carried out to evaluate the use of a dual completion, instead of a new well.

***Economic Evaluation***

Delays in tackling climate change could result in increasing potential costs. Apart from the technical aspect, economic evaluation should be considered as part of a CCS analysis to encourage the acceptance and allow increased benefit from carbon capture and storage. Economic evaluation is crucial to allow decision-makers involved in CCS projects, regulators, and other stakeholders, such as environmental organisations and the general public. Indeed, more secure storage of $CO_2$ at lower cost will be of interest to any member of these groups.

## 6.6 Concluding remarks

This chapter presents the impact of transition zone on a real field model for $CO_2$ sequestration, followed by the application of a novel approach for $CO_2$ injection at the same field. Seismic data and well data are used to construct the geological models. During the well logs interpretation people might ignore a narrow mudstone layer just beneath the caprock if it was not missed while the well had been drilled. In addition, depending on the seismic survey and the seismic interpreter a thin mudstone layer might not be detected or might be ignored.

For $CO_2$ storage purposes in the geological formations these layers might be important because they might lessen the amount of $CO_2$ accumulating underneath the caprock or they might lead the $CO_2$ migration in different direction. Therefore it can be concluded that the transition zone could increase the security of $CO_2$ storage. The security of $CO_2$ storage increases because less $CO_2$ reaches beneath the caprock resulting in less pressure build up beneath the caprock. Therefore less $CO_2$ migrates underneath the caprock. This could result in more lateral plume migration in the transition zone beneath the low permeable layers, thus more $CO_2$ can be dissolved.

A fully comprehensive storage formation/caprock characterization can lead towards a better anticipation of the migration of the free phase $CO_2$ in the geological storage formation. However, the risk of leaking of $CO_2$ from the storage formation for any possible reason (e.g. through faults, etc) would remain there.

The presented novel engineering solution for minimizing the $CO_2$ vertical migration could increase storage security. The advantages of this method are outlined below:

- There is no free phase $CO_2$ in the storage formation.
- Dissolved $CO_2$ in brine is heavier than fresh brine therefore it is not governed by the buoyance resulting in no $CO_2$ migration towards the surface.
- Using drilling techniques such as multi-lateral wells with a dual completion would increase the amount of $CO_2$ that can be dissolved per well.
- Long-term $CO_2$ storage (e.g. 100 years $CO_2$ injection) is possible.

An effective long-term monitoring of geological $CO_2$ storage sites involves monitoring and sampling to identify and measure the $CO_2$ leakage (Darby et al. 2009). In the In Salah $CO_2$ project, monitoring techniques were set to be production, geophysical, and

geochemical techniques in 2005 (Mathieson et al. 2011). DHM could reduce the level of monitoring of $CO_2$ migration and sampling of the soil in the geological formation than the standard method because all the $CO_2$ is dissolved resulting in reduction on the cost of geological $CO_2$ storage projects.

The problem with this proposed method of injection is that it will restrict the amount of $CO_2$ can be injected in one well. Therefore, it is required more wells in comparison to the standard $CO_2$ injection method. Injecting at a much higher total volume rate will increase the BHP. On the other hand, it will be single phase injection, and the acid brine may stimulate the formation. The BHP will certainly be much higher for this method than if the $CO_2$ were injected without brine, but the increase will be somewhat mitigated by the aforementioned factor.

# Chapter 7

# Conclusions and Discussion

## 7.1 Overview

There are concerns about safe long-term storage of $CO_2$ in aquifers, due to the high uncertainty in their structure. The work described in this thesis investigates the effects of some of these uncertainties. Calculations have been performed to identify the impact of structure, irregularity, dip angle, on dissolution and migration of $CO_2$. Different types of interface between caprock and storage formation were studied. Modelling of $CO_2$ behaviour in some types of interface such as tilted beds, interbedded sandstone and mudstone, and unconformities has been performed. Furthermore, due to complexity of fully understanding the interface between caprock/aquifer, and the risk of $CO_2$ leakage through caprock as a result of pressure build-up at the interface between aquifer/caprock (Shariatipour et al. 2012), a novel method has been proposed in which injected $CO_2$ into aquifers does not migrate toward interface and it could maximise storage capacity and security.

In this chapter a summary of the results and the main findings of this thesis are presented. Recommendations for further research topics of this work are also outlined.

## 7.2 Conclusions

In Chapter 3, firstly, the interface between caprock and storage formation has been studied. Some studies assume a smooth interface or a sharp boundary between sealing formation and storage formation, whereas typically the surface is irregular, due to sedimentological and stratigraphic effects or structural deformation.

Calculations were performed to identify the impact of structure and rugosity on the migration of $CO_2$. Both storage capacity and security of $CO_2$ storage have been studied. After $CO_2$ is injected into an aquifer, it eventually reaches the caprock and will migrate beneath the caprock.

The result for the model studied shows that assuming that a transition zone is part of the reservoir could lead to overestimation of the storage capacity by up to 6% compared to the actual model. However, including the transition zone as a part of caprock could underestimate the storage capacity by up to 29%. In addition, results show that a transition zone can increase the security by providing a partial baffle to hinder $CO_2$ migration towards the caprock and lowering pressure build up at the base of the caprock. Also, the slower the migration the longer the time for interaction of the $CO_2$ with the brine and minerals, which assists $CO_2$ trapping. Furthermore, irregularity at the aquifer-caprock interface may assist structural trapping by providing extra storage volume. On the other hand, topographical highs may provide pathways for rapid migration of $CO_2$ from the injector, especially where such highs serve to focus subsequent tectonic deformation.

Secondly, having discussed the transition zone in the first section, different types of caprock/aquifer interface were investigated to determine how these affect the pressure build-up under the caprock and the amount of $CO_2$ which is dissolved in brine. Depending on the nature of the interface between the caprock and the storage formation (which is governed by sedimentological and stratigraphic effects or structural deformation), the plume spreads laterally. The results indicate that depending on the depositional setting between the aquifer and the caprock, the amplitude of the irregularities can limit the migration of the $CO_2$ plume, and this has an effect on the amount of $CO_2$ dissolution. In addition, a tilted interface leads $CO_2$ to migrate up dip, therefore more $CO_2$ comes into contact with more fresh brine. This increases $CO_2$ dissolution in the aquifer. Furthermore, in domed shaped interfaces, $CO_2$ fills the domes so there is lower area of interface between $CO_2$ and brine and the security of $CO_2$

storage could be increased by limiting the $CO_2$ migration. Moreover, migration of $CO_2$ beneath the caprock is controlled by the morphology of the bottom of the caprock specially, after the injection period when the viscous force is negligible. We might have good knowledge of low permeability zones near a well beneath the caprock from well logs or cores but, in order to have a best anticipation on $CO_2$ migration, the rugosity of the interface between the caprock and the storage formation need to be very well characterised even away from the injector.

Thirdly, having discussed the morphology and transition zone a set of numerical simulations was conducted (144 models) to study the effect of anisotropic ratio for permeability ($k_V/k_H$), tilt, amplitude of ridges and thickness of transition zone on the amount of dissolved $CO_2$ in storage formation and also $CO_2$ plume migration. Results show that a transition zone has a positive effect on the $CO_2$ storage as more $CO_2$ is dissolved and $CO_2$ vertical migration is limited.

Ridges with higher amplitude (larger than the plume thickness) provided more structural trapping if they are perpendicular to the tilt. However, ridges parallel to the tilt provide a pathway for rapid $CO_2$ upwards migration. Although this may increases the risk of $CO_2$ leakage as it migrates further away from the injection point, more $CO_2$ is dissolved due to greater contact with brine.

The impact of the anisotropy ratio for permeability ($k_V/k_H$) on the $CO_2$ storage shows that this parameter is the most sensitive factor during the injection period and the second most sensitive factor at post injection period in *perp*, *para* and *trans* models. This has a direct relation with $CO_2$ upwards migration and an indirect relation with the amount of $CO_2$ dissolution in brine. Thus, the lower the $k_V/k_H$ the more $CO_2$ dissolves in the aquifer. This is because the low permeability causes more $CO_2$ to migrate laterally while moving upwards. In addition, this effect increases with increasing tilt angle.

It is concluded that tilt is the most sensitive parameter to the amount of $CO_2$ dissolution and plume migration 100 years post injection period. The higher the tilt the more $CO_2$ moves up-dip therefore free $CO_2$ phase migrates further away from injector and more $CO_2$ is in contact with unsaturated brine resulting in more $CO_2$ dissolution and thinner plume. Furthermore, the length of the plume migration increases linearly with tilt from 0 to 4 degrees. However, after 4 degrees it increases rapidly. This indicates that the length of plume migration may be predicted when the tilt is small (e.g. less than 4

degrees). However, at the higher dip angle the spread of plume migration is changing. This is due to the increase in the density difference between $CO_2$ and brine.

In order to find the relationship between tilt $(\theta)$, amplitude $(A)$, and wavelength $(\lambda)$ an equation is presented (equation 3.6) that can be deployed to find out under what conditions the morphology of top surface could make a significant difference, and what will never have an effect. It can be concluded that if $\tan(\theta) \prec (2\pi A/\lambda)$ then always a fraction of $CO_2$ will be trapped.

Finally, this study shows that it is important to investigate reservoir characterization regarding the size (amplitude and lateral extent) of irregularities at the interface of caprock/aquifer very carefully for any planned $CO_2$ storage sites.

The role of an unconformity surface as an interface between caprock and storage formation has been studied in chapter 4. Prior to this study, the effect of type of gridding on $CO_2$ storage was investigated due to the slope of layers in an angular unconformity model. The results show that an increase in inclination of the aquifer cells leads to a decrease in the distance migrated by the $CO_2$, both during the injection and post injection periods. This effect is more significant where these inclined cells pinch out. The findings of this study are very important in modelling of $CO_2$ storage as they show that choosing different types of gridding leads to overestimate or underestimate of the amount of dissolved $CO_2$ in aquifer. However, this fact does not affect our modelling results in the next section, because all the models were constructed in the same way and then the results were compared.

The results show that an unconformity model which has a layer of high permeability at the interface between the aquifer and the caprock, as a result of weathering, can contribute to pressure diffusion across the reservoir. This could improve $CO_2$ sequestration by providing pathways for $CO_2$ migration to access other storage formations (provided $CO_2$ did not migrate out of the storage complex). Therefore, with appropriate placement of the well in a case where there are parallel aquifers, it is possible to maximize $CO_2$ storage. In the absence of a high permeability layer either above or below an unconformity, lateral migration of $CO_2$ is limited. Pressure builds up, but the amount of dissolution increases. On the other hand, if the pressure builds up too much, the formation or caprock could fracture.

In addition, the existence of a high permeability layer at the unconformity surface could have a negative effect on the security of $CO_2$ storage by providing path ways for $CO_2$ to migrate out of the storage formation and increase the risk of $CO_2$ migration.

In Chapter 5 a novel approach for $CO_2$ injection is presented. The main idea behind this method is to minimize vertical migration of $CO_2$ in storage formations by down-hole mixing of $CO_2$. This technique provides the opportunity for much more secure storage of $CO_2$ than is currently envisaged by conventional injection of $CO_2$ alone. Some of the advantages of this method are:

- Store $CO_2$ for thousands of years with lower risk of leakage, as dissolved $CO_2$ is denser than fresh brine and sinks into reservoir.
- Capacity could be improved because rocks shallower than 800 m could be used for storage available as $CO_2$ no longer need to be supercritical.
- Extent of monitoring of migration of free $CO_2$, which is costly, is decreased because all the $CO_2$ is dissolved.
- More secure storage of $CO_2$ will be of interest to organisations involved in CCS projects, regulators, and other stakeholders, such as environmental organisations and the general public.

The application of a transition zone on a real field (Lincolnshire Model) was studied in Chapter 6. The British Geological Survey (BGS) highlighted a near shore formation in Lincolnshire as a large analogue of an optional offshore storage site for captured $CO_2$ from potential onshore capture projects. The actual model was modified to study the effect of transition zone by adding some mud layers just beneath the caprock. In order to improve the accuracy of the simulations, a sector of this model was used with a finer resolution. It was concluded that transition zone could significantly reduce the amount of $CO_2$ reaching the caprock (in this study, 50% less than the model without considering the transition zone). Thus, it is very important to characterise the interface between the caprock and the aquifer formation for $CO_2$ storage projects.

The application of the down-hole mixing method to the same field was also studied. Three scenarios were presented in terms of well type (vertical, deviated, and multi-lateral well (Figure ***6.22***)) which can be considered when planning DHM depending on the $CO_2$ supply and the scale of the planed $CO_2$ storage site. Calculations were performed to identify the optimum level and length of water extraction and injection of dissolved $CO_2$ in brine. In terms of the minimum length of corrosion-resistance tools

and frictional pressure loss, the most efficient model is the one where the brine extraction lateral is completed away from the bore hole whereas the $CO_2$ saturated injection lateral is close to the bore hole. The former is to maximize the distance between extraction and injection and the latter is to minimize the need for having high chromium steel. In addition, it was suggested that the use of dual completion could double the amount of $CO_2$ that can be dissolved by DHM method.

## 7.3 Future Work

Last, but by no means least, after considering all discussions throughout Chapter 2 to Chapter 6 there are some interesting subjects that can be studied as further research topics. There are two main research areas can be recommended for future work. Firstly, topics around the interface between caprock and storage formation. Secondly, development of the down-hole mixing method as a novel method to eliminate the vertical migration of $CO_2$ towards the caprock hence, increase security and capacity of $CO_2$ storage in saline aquifers.

### *7.3.1 Further Work on the Interface between Caprock and Storage Formation*

Regarding modelling of $CO_2$ behaviour at the interface between the storage formation and the caprock, the impact of capillary trapping and dissolution on the migration of $CO_2$ on the interface could be studied in more detail. The positive and negative impacts of possible mobilisation of hydrocarbons trapped locally beneath the caprock may also be important and should be considered. In this thesis the effect of angular unconformity has been studied. However, other types of unconformities also can be investigated. The effects of pressure and saturation dependent properties of the reservoir fluids and rocks can be considered by having a more complex model with different rock compressibilities, etc.

### *7.3.2 Further Work on the Novel Down-Hole Mixing (DHM) Method*

This novel method needs to be studied more in detail and it does need some more work on the mixing process. In addition, more numerical simulation needs to be carried out to investigate different scenarios of mixing $CO_2$/brine down-hole and inject it into the reservoir. The effect of groundwater flow in the vicinity of the injection well on the DHM can be studied. A feasibility study of the pumping system also needs to be considered. A feasibility study of using the advantage of the existence of the vertical

wells in the depleted oil and gas reservoirs to examine down-hole mixing method should also be considered.

The applications of this novel method for different types of enhanced oil and gas recovery methods such as EOR, water-alternative-gas (WAG), and carbonated- water-injection (CWI) is worth investigating.

# References


ABANADES, J.C., RUBIN E.S., AND ANTHONY E.J., (2004), Sorbent cost and performance in CO2 capture system. Ind. Eng. Chem. Res., 43, pp. 3462-3466.

ANCHLIYA, A., & EHLIG-ECONOMIDES, C. (2009). Aquifer management to accelerate CO2 dissolution and trapping. In SPE International Conference on CO2 Capture, Storage, and Utilization.

ANDERSON G.K. (2002) Solubility of carbon dioxide in water under incipient clathrate formation conditions, J. Chem. Eng. Data 47, pp. 219–222.

ARTS, R. J., CHADWICK, A., EIKEN, O., THIBEAU, S., & NOONER, S. (2008). Ten years' experience of monitoring $CO_2$ injection in the Utsira Sand at Sleipner, offshore Norway. First Break, 26(1).

BACHU, S., ADAMS, J. J. (2003). Sequestration of $CO_2$ in geological media in response to climate change: capacity of deep saline aquifers to sequester $CO_2$ in solution. Energy Conversion and Management, 44(20), 3151-3175.

BACHU, S. (2008) $CO_2$ storage in geological media: Role, means, status and barriers to deployment. *Progress in Energy and Combustion Science*, 34**,** 254-273.

BACHU, S. (2010) Screening and selection criteria, and characterisation for CO2 storage. *Developments and Innovation in Carbon Dioxide (CO2) Capture And Storage Technology*, 2**,** 27-56.

BESLY, B. M., BURLEY, S. D. & TURNER, P. (1993) The late carboniferous barren red bed play of the silver pit area, southern north sea, Vol. 4, Geological Society of London, p. 727.

BERGMO, P. E. S., GRIMSTAD, A. A., & LINDEBERG, E. (2011). Simultaneous CO2 injection and water production to optimise aquifer storage capacity. International Journal of Greenhouse Gas Control, 5(3), 555-564.

BIRKHOLZER T.J., ZHOU Q., TSANG CH-F., (2008) Large – scale impact of CO2 storage in deep saline aquifers, Earth Sciences Division Lawrence Berkeley National Laboratory, pp. 182-194.

BJORLYKKE K., (2010). Petroleum Geoscience From Sedimentary Environment to Rock Physics, 508 pp.

BURTON, M & BRYANT, S. (2009) Eliminating Buoyant Migration of Sequestered CO2 Through Surface Dissolution: Implementation Costs And Technical Challenges. SPEREE, 12: 399-407.

BUTLER, M., (1998). The geological history and the southern Wessex Basin – a review of new information from oil exploration. In: Underhill, J.R. (Ed.), Development, evolution and petroleum geology of the Wessex Basin. Geological Society London Special Publication 133, pp. 67–86.

BOAIT, F., WHITE. N., CHADWICH. A., NOY. D., BICKLE. M., (2011) Layer spreading and dimming within the CO2 plume at the Sleipner Field in Noth sea, Energy Procedia 4, 3254–3261.

BOWMAN, M. B. J., McCLURE, N. M. & WILKINSON, D. W. (1993). Wytch Farm Oilfield: deterministic reservoir description of the Triassic Sherwood Sandstone. In: PARKER, J. R. (ed.) Petroleum Geology of Northwest Europe." Proceedings of the 4th Conference. Geological Society, London, 1513-1517.

CAVANAGH, A., & RINGROSE, P. (2011). Simulation of CO2distribution at the In Salah storage site using high-resolution field-scale models. Energy Procedia, 4, 3730-3737.

CASABIANCA, D., & COSGROVE, J. (2012). A new method for top seals predictions in high-pressure hydrocarbon plays. Petroleum Geoscience, 18(1), 43-57.

CHADWICK, R.A., NOY, D., (2010) History-matching flow simulations and time-lapseseismic data from the Sleipner CO2 plume, 7th Petroleum Geology Conference, London, pp. 1171-1182.

CHADWICK, R. A., NOY, D., ARTS, R. & EIKEN, O. (2009) Latest time-lapse seismic data from Sleipner yield new insights into CO2 plume development. Energy Procedia, 1, 2103-2110.

CHIQUET, P., DARIDON, J. L., BROSETA, D., & THIBEAU, S. (2007). CO2/water interfacial tensions under pressure and temperature conditions of CO2 geological storage. Energy Conversion and Management, 48(3), 736-744.

CO2CARE (2011), CO2 Site Closure Assessment Research: D3.1 - Review of relevant trapping mechanisms based on site portfolio, Project Number 256625, FP7-Energy 2010.

CORCORAN, J. (2006) Application of a sealing surface classification for stratigraphic related traps in the UK Central North Sea. Geological Society, London, Special Publications, 254:207-223.

DARBY, E. B., BUMGARNER, J., & HOVORKA, S. D. (2009). Geochemical modeling of near-surface CO2 interactions: The critical element in cost-effective long-term monitoring. Energy Procedia, 1(1), 2389-2395.

DUAN Z., MØLLER N., AND WEARE J. H. (1992) An equation of state for the CH4-CO2-H2O system: II. Mixtures from 50 to 1000°C and 0 to 1000 bars. Geochim. Cosmochim. Acta 56, 2619–2631.

DUAN, Z., SUN R. (2003) An improved model calculating CO2 solubility in pure water and aqueous NaCl solutions from 273 to 533 K and from 0 to 2000 bar, Chem. Geol. 193 (3–4), pp. 257–271.

DUNBAR, C. O. & ROGERS, J. (1957). Principles of Stratigraphy, 356 pp.

FREEZE, R. A., & CHERRY, J. A. (1979). Groundwater, 604 pp.

Department of Energy and Climate Change (DECC) (2012), The Hydrocarbon Prospectivity Of Britain's Onshore Basins report. https://www.og.decc.gov.uk/UKpromote/onshore_paper/UK_onshore_prospectivity.pdf

EKE, P., NAYLOR, M., HASZELDINE, S., & CURTIS, A. (2011). CO2/Brine Surface Dissolution and Injection: CO2 Storage Enhancement. SPE Projects, Facilities & Construction, 6(1), 41-53.

EIKEN, O., RINGROSE, P., HERMANRUD, C., NAZARIAN, B., TORP, T. A., & HØIER, L. (2011). Lessons learned from 14 years of CCS operations: Sleipner, In Salah and Snøhvit. Energy Procedia, 4, 5541-5548.

ENICK R. M., AND KLARA S. M. (1990) CO2 solubility in water and brine under reservoir conditions. Chem. Eng. Comm. 90, 23–33.

ENNIS-KING, J. & PATERSON, L. (2003) Role of Convective Mixing in the Long-Term Storage of Carbon Dioxide in Deep Saline Formations. *SPE Annual Technical Conference and Exhibition.* Denver, Colorado: Society of Petroleum Engineers.

ENNIS-KING, J., PRESTON, I. & PATERSON, L. (2005) Onset of convection in anisotropic porous media subject to a rapid change in boundary conditions. *Physics of Fluids,* 17**,** 084107.

FORD, J.R., & MONAGHAN, A.A. (2009) Lithological Heterogeneity of the Mercia Mudstone and Sherwood Sandstone Groups in the Yorkshire-Lincolnshire Region, and Knox pulpit Sandstone, Kinnesswood and Ballagan Formations in the Forth Region - additional information for CASSEM work package one Responsive Surveys Scotland Programme (pp. 36) Edinburgh: British Geological Survey.

GASDA, S. E., CELIA, M. A., & NORDBOTTEN, J. M. (2008). Upslope plume migration and implications for geological CO2 sequestration in deep, saline aquifers. The IES Journal Part A: Civil & Structural Engineering, 1(1), 2-16.

GASDA, S. E., NORDBOTTEN, J. M., & CELIA, M. A. (2012). Application of simplified models to CO2 migration and immobilization in large-scale geological systems. International Journal of Greenhouse Gas Control, 9, 72-84.

GAMMER, D., GREEN, A., SMITH, G., HOLLOWAY, S., The, UKSAP., Consortium, (2011). Energy Technologies Institute's UK CO2 storage appraisal project (UKSAP). In: SPE-148426, SPE Offshore Europe Oil and Gas Conference and Exhibition, Aberdeen, UK.

GARCIA J.E., (2001) Density of Aqueous Solutions of CO2. Graduate Student Research Assistant Earth Sciences Division Lawrence Berkeley National Laboratory.

GHANBARI, S., AL-ZAABI, Y., PICKUP, G. E., MACKAY, E., GOZALPOUR, F., & TODD, A. C. (2006). Simulation of CO2 Storage In Saline Aquifers. Chemical Engineering Research and Design, 84(9), 764-775.

GLUYAS, J., & SWARBRICK, R. (2004). Petroleum Geoscience, 355 pp.

GOATER, A., BIJELJIC, B., AND BLUNT, M. J. (2011) The Effect of Top-Surface Structure Upon CO2 Storage Capacity in Open Aquifers. 1st Sustainable Earth Sciences Conference & Exhibition (SES). Valencia, Spain.

GOATER, A., BIJELJIC, B., AND BLUNT, M. J. (2013). Dipping open aquifers—The effect of top-surface topography and heterogeneity on $CO_2$ storage efficiency. *International Journal of Greenhouse Gas Control*, 17**,** 318-331.

GREEN, C. P., & ENNIS-KING, J. (2012). Spatial grid correction for short-term numerical simulation results of carbon dioxide dissolution in saline aquifers. Computational Geosciences, 16(4), 1153-1161.

GUNDOGAN, O. (2011). Geochemical modelling of CO2 storage (Doctoral dissertation, Heriot-Watt University).

GUNTER, W. D., PERKINS, E. H., & MCCANN, T. J. (1993). Aquifer disposal of CO2-rich gases: Reaction design for added capacity. Energy Conversion and Management, 34(9), 941-948.

HASANZADEH, H., POOLADI DARVISH, M. & KEITH, D. W. (2007). Scaling behavior of convective mixing, with application to geological storage of CO2. AIChE journal, 53, 1121-1131.

HASANZADEH H., POOLADI – DARVISH M., ELSHARKAWY A.L., KEITH D.W., LEONENKO Y., (2008) Predicting PVT data for CO2 – brine mixtures for black- oil simulation of CO2 geological storage, pp. 65- 77.

IEAGHG, (2005) IEAGHG Weyburn CO2 Monitoring and Storage Project. Public summary report. http://www.ieaghg.org/index.php?/General-Publications/.

IPCC, (2005) IPCC Special Report on Carbon Dioxide Capture and Storage. In: METZ, B., DAVIDSON, O., DE CONINCK H.C., LOOS, M., MEYER, L.A. (Eds.), Prepared by Working Group III of the Intergovernmental Panel on Climate Change. Cambridge University Press, Cambridge, UK/New York, NY, USA, 442 pp.

JIN, M., PICKUP, G., MACKAY, E., TODD, A., SOHRABI, M., MONAGHAN, A., & NAYLOR, M. (2012). Static and Dynamic Estimates of CO2-Storage Capacity in Two Saline Formations in the UK. SPE Journal, 17(4), 1108-1118.

JUANES, R., SPITERI, E. J., ORR, F. M., & BLUNT, M. J. (2006). Impact of relative permeability hysteresis on geological CO2 storage. Water Resources Research, 42(12).

KING M.B., MUBARAK A., KIM J.D. AND BOTT T.R. (1992) The mutual solubilities of water with supercritical and liquid carbon dioxide, J. Supercrit. Fluids 5, pp. 296–302.

KLAUS M, (2007) CO2 Storage into Dipped Saline Aquifers Including Ambient Water Flow, Diploma thesis, Universit¨at Stuttgart - Institut f¨ur Wasserbau Lehrstuhl f¨ur Hydromechanik und Hydrosystemmodellierung.

KNEAFSEY, T. J., & PRUESS, K. (2010). Laboratory flow experiments for visualizing carbon dioxide-induced, density-driven brine convection. Transport in porous media, 82(1), 123-139.
KNEAFSEY T. A., (2011) Laboratory and Numerical Simulation Studies of Convectively Enhanced Carbon Dioxide Dissolution, Paper presented at GHGT-10,Amsterdam, The Netherlands.

KUMAR, A., NOH, M., POPE, G. A., SEPEHRNOORI, K., BRYANT, S., & LAKE, L. W. (2004). Reservoir simulation of CO2 storage in deep saline aquifers. In SPE/DOE Symposium on Improved Oil Recovery.

LI, Z., DONG, M., LI, S., & HUANG, S. (2006). CO2 sequestration in depleted oil and gas reservoirs-caprock characterization and storage capacity. Energy Conversion and Management, 47(11), 1372-1382.

LI S, DONG M, LI Z, HUANG S, QING H, NICKEL E. Gas breakthrough pressure for hydrocarbon reservoir seal rocks: implications of the security of long-term CO2 storage in the Weyburn field. Geofluids 2005;5(4).

LINDEBERG, E., & BERGMO, P. (2003). The long-term fate of CO2 injected into an aquifer. Greenhouse Gas Control Technologies, 1, 489-494.

LEONENKO, Y., & KEITH, D. W. (2008). Reservoir engineering to accelerate the dissolution of CO2 stored in aquifers. Environmental science & technology, 42(8), 2742-2747.

LENGLER, U., DE LUCIA, M., KÜHN, M., (2010) The impact of heterogeneity on the distribution of CO2: Numerical simulation of CO2 storage at Ketzin. International Journal of Greenhouse Gas Control 4, 1016-1025.

LEVORSEN, A. I. (1967). Geology of petroleum (pp. 97-99). F. A. F. Berry (Ed.). San Francisco: WH Freeman.

LI, H., JAKOBSEN, P, J., WILHELMSEN, Q., AND YAN, J. (2011) PVTxy properties of CO2 mixtures relevant for CO2 capture, transport and storage: Review of available experimental data and theoretical models. Applied Energy. 88, PP. 3567–3579.

LI Y., AND NGHIEM L. X. (1986) Phase equilibria of oil, gas and water/brine mixtures from a cubic equation of state and Henry's law. Can. J. Chem. Eng. 64, 486–496.

MATHIESON, A., WRIGHT, I. ROBERTS, D. M. AND RINGROSE, P. S., (2009), Satellite Imaging to Monitor CO2 Movement at Krechba, Algeria. Energy Procedia, 1, 2201-2209.

MATHIESON, A., MIDGELY, J., WRIGHT, I., SAOULA, N., & RINGROSE, P. (2011). In Salah CO2 Storage JIP: CO2 sequestration monitoring and verification technologies applied at Krechba, Algeria. Energy Procedia, 4, 3596-3603.

MILLER, J.A. (1999) Ground Water Atlas of the United State, introduction and national summary, U.S. Geological Survey.

MILTON N. J. AND BERTRAM G. T., (1992). Trap styles; a new classification based on sealing surfaces, AAPG Bulletin, v. 76, p. 983-999.

NAYLOR, M., WILKINSON, M., & HASZELDINE, R. S. (2011). Calculation of CO2 column heights in depleted gas fields from known pre-production gas column heights. Marine and Petroleum Geology, 28(5), 1083-1093.

NILSEN, H. M., SYVERSVEEN, A. R., LIE, K.-A., TVERANGER, J. & NORDBOTTEN, J. M. (2012) Impact of top-surface morphology on CO2 storage capacity. *International Journal of Greenhouse Gas Control*, 11**,** 221-235.

NORDBOTTEN, J. M., & CELIA, M. A., 2006. Similarity solutions for fluid injection into confined aquifers. Journal of Fluid Mechanics, 561, 307-327.

NORDBOTTEN, J. M., CELIA, M. A., & BACHU, S., 2005. Injection and storage of CO2 in deep saline aquifers: Analytical solution for CO2 plume evolution during injection. Transport in Porous media, 58(3), 339-360.

NORDBOTTEN, JM, FLEMISCH, B, GASDA, S, NILSEN, H, FAN, Y, PICKUP, GE, WIESE, B, CELIA, M, DHALE, H, EIGESTAD, G & PRUESS, K (2012) 'Uncertainties in practical simulation of CO2 storage International Journal of Greenhouse Gas Control, vol 9, pp. 234-242.

OKWEN, R. T., STEWART, M. T., & CUNNINGHAM, J. A., 2010. Analytical solution for estimating storage efficiency of geologic sequestration of CO2. International Journal of Greenhouse Gas Control, 4(1), 102-107.

ORR JR, F. M. (2009). CO2 capture and storage: are we ready? Energy & Environmental Science, 2(5), 449-458.

OZAH, R., LAKSHMINARASIMHAN, S., POPE, G., SEPEHRNOORI, K., & BRYANT, S. (2005). Numerical simulation of the storage of pure CO2 and CO2-H2S gas mixtures in deep saline aquifers. In SPE Annual Technical Conference and Exhibition. Society of Petroleum Engineers.

PAU, G. S., BELL, J. B., PRUESS, K., ALMGREN, A. S., LIJEWSKI, M. J., & ZHANG, K. (2010). High-resolution simulation and characterization of density-driven flow in CO2 storage in saline aquifers. Advances in Water Resources, 33(4), 443-455.

OLDEN, P., PICKUP, G. E., JIN, M., MACKAY, E. J., HAMILTON, S. A., SOMERVILLE, J. M., & TODD, A. C. (2012). Use of rock mechanics laboratory data in geomechanical modelling to increase confidence in CO2 geological storage. *International Journal of Greenhouse Gas Control*, 11, 304-315.

PENG D.-Y. AND ROBINSON D. B. (1976) A new two-constant equation of state. Ind. Eng. Chem. Fundament. 15, 59–64.

PICKUP, G. E., JIN M., OLDEN P., MACKAY E. J., AND SOHRABI M. (2011) A Sensitivity Study on CO2 Storage in Saline Aquifers SPE 143054 SPE EUROPEC/EAGE Annual Conference and Exhibition, 23, Vienna, Austria.

PRESTON, C., WHITTAKER, S., ROSTRON, B., CHALATURNYK, R., WHITE, D., HAWKES, C., JOHNSON, W., WILKINSON, A., AND SACUTA, N. (2009) IEA GHG Weyburn-Midale CO2 monitoring and storage project–moving forward with the Final Phase. Energy Procedia, 1(1), 1743-1750.

PRUESS, K., C. OLDENBURG, AND G. MORIDIS (1999), TOUGH2 User's Guide, Version 2.0, Report LBNL-43134, Lawrence Berkeley National Laboratory, Berkeley, Calif.

PRUESS K. AND GARCIA J. (2002) Multiphase flow dynamics during CO2 disposal into saline aquifers. Environ. Geol. 42, 282–295.

PRUESS, K., & SPYCHER, N. (2007). ECO2N–A fluid property module for the TOUGH2 code for studies of CO2storage in saline aquifers. Energy Conversion and Management, 48(6), 1761-1767.

PRUESS, K., T. XU, J. APPS, AND J. GARCIA (2003), Numerical modeling of aquifer disposal of CO2 (SPE 83695) SPE Journal, 49-60.

REDLICH O. AND KWONG J. N. S. (1949) On the thermodynamics of solutions. V. An equation of state. Fugacities of gaseous solutions. Chem. Rev. 44, 233–244.

RIAZ, A. AND TCHELEPI, H. A. (2008) Dynamics of Vertical Displacement in Porous Media Associated With CO2 Sequestration. SPE Journal, V. 13, pp. 305-313.

RIAZ, A., HESSE, M., TCHELEPI, H. A. & ORR, F. M. (2006) Onset of convection in a gravitationally unstable diffusive boundary layer in porous media. *Journal of Fluid Mechanics*, 548**,** 87-111.

RINGROSE, P., M. ATBI, D. MASON, M. ESPINASSOUS, O. MYHRER, M. IDING, A. MATHIESON, AND I. WRIGHT (2009) Plume development around well KB-502 at the In Salah CO2 storage site, First Break, 27, 85–89.

RINGROSE, P. S., ROBERTS, D. M., GIBSON-POOLE, C. M., BOND, C., WIGHTMAN, R., TAYLOR, M., RAIKES, S., IDING, M. & ØSTMO, S. (2011). Characterisation of the Krechba CO2 storage site: Critical elements controlling injection performance. Energy Procedia, 4, 4672-4679.

RITTENHOUSE, G., (1972) Stratigraphic-Trap Classification: Geologic Exploration Methods, Book Title: Stratigraphic Oil and Gas Fields--Classification, Exploration Methods, and Case Histories, Pub. Id: A010, 14-28.

RUTQVIST, J. (2012). The geomechanics of CO2 storage in deep sedimentary formations. Geotechnical and Geological Engineering, 30(3), 525-551.

RUTQVIST, J., VASCO, D. W., AND MYER, L. (2010) Coupled reservoir-geomechanical analysis of CO2 injection and ground deformations at In Salah, Algeria. International Journal of Greenhouse Gas Control, 4(2), 225-230.

RUTQVIST, J. AND RINALDI, A. (2013) Modeling Ground Deformations and Potential for Induced Micro-Seismicity at the In Salah CO2 Storage Operation, Algeria. Poromechanics V: pp. 1299-1308.

SALES, J. K.,1997, Seal strength vs. Trap closure – A fundamental control on the distribution of oil and gas in R. C. Surdam, ed., Seal, traps, and the petroleum system: AAPG Memoir 67,P.57-83.

SALIMI, H., & WOLF, K. H. (2012). Integration of heat-energy recovery and carbon sequestration. International Journal of Greenhouse Gas Control, 6, 56-68.

SAWAMURA, F. & NAKAYAMA, K. (2005) Estimating the amount of oil and gas accumulation from top seal and trap geometry.

SCHLUMBERGER, (2011)a. Petrel Geological Modelling Software.

SCHLUMBERGER, (2011)b. ECLIPSE Reservoir Simulation Software, Technical Description.

SHARIATIPOUR, S.M., PICKUP, G.E., STOW, D.A.V., AND MACKAY, E.J. (2012) The Effects of Aquifer/Caprock Interface on $CO_2$ Storage Capacity and Security. *3rd EAGE $CO_2$ Geological Storage Workshop.*

SHARIATIPOUR, S.M., PICKUP, G.E., E.J., MACKAY AND Heinemann, N. (2012) Flow Simulation of $CO_2$ Storage in saline Aquifer Using black Oil Simulator" *SPE 151042, Carbon Management Technology Conference*.

SHARIATIPOUR, S. M., MACKAY, E. J., & PICKUP, G. E. (2013, September). Could this be the Future of Secure CO2 Storage?. In Sustainable Earth Sciences 2013.

SHARIATIPOUR, S. M., PICKUP, G. E., & MACKAY, E. J. (2012, June). A Novel Method for CO2 Injection that Enhances Storage Capacity and Security. In 74th EAGE Conference & Exhibition.

SPAN, R.,WAGNER,W. (1996):A newe quation of state for carbon dioxide covering the fluid region from the triple-point temperature to 1100K at pressures up to 800MPa. J. Phys. Chem. Ref. Data 25(6), 1509–1596.

SINGH, V. P., CAVANAGH, A., HANSEN, H., NAZARIAN, B., IDING, M. & RINGROSE, P. S. (2010) Reservoir Modeling of CO2 Plume Behavior Calibrated Against Monitoring Data From Sleipner, Norway. *SPE Annual Technical Conference and Exhibition.* Florence, Italy: Society of Petroleum Engineers.

SLEIPNER PROJECT WEBSITE, 2013 Sleipner project website. www.statoil.com/en/technologyinnovation/newenergy/co2management/pages/Sleipnervest.aspx (accessed 07.08.13).

SMITH, M., CAMPBELL, D, MACKAY, E. AND POLSON, D., (2012) CO2 Aquifer Storage Site Evaluation and Monitoring. SCCS. ISBN: 978-0-9571031-0-8.

SORKHABI, R., TSUJI, Y., 2005, Faults, Fluid Flow, and Petroleum traps.

SPYCHER N.F. AND PRUESS K. (2005) CO2–H2O mixtures in the geological sequestration of CO2. II. Partitioning in chloride brines at 12–100 °C and up to 600 bars, Geochim. Cosmochim. Acta 69 (13), pp. 3309–3320.

SPYCHER N.F., PRUESS K., AND ENNIS-KING J. (2003) CO2–H2O mixtures in the geological sequestration of CO2. I. Assessment and calculation of mutual solubilities from 12 to 100 °C and up to 600 bars, Geochim. Acta 67 (16), pp. 3015–3031.

SPYCHER, N. AND PRUESS, K. (2010) A Phase-Partitioning Model for CO2-Brine Mixtures at Elevated Temperatures and Pressures: Application to CO2-Enhanced Geothermal Systems Transp. Porous Med. Springer. 82: pp.173–196.

STOKER, S.J., GRAY, J.C., HAILE, P., ANDREWS, I.J., CAMERON. T. D. J., (2006) The importance of stratigraphic plays in the undiscovered resources of the UK Continental Shelf, Geological Society, London, Special Publications, v.254 , p153-167.

SUN, R,. DUAN, Z. (2007) An accurate model to predict the thermodynamic stability of methane hydrate and methane solubility in marine environments. Chemical Geology. 244. pp. 248–262.

SWEATMAN, R., CROOKSHANK, S., AND EDMAN, S. (2011) Outlook and Technologies for Offshore CO2 EOR/CCS Project. Offshore Technology Conference, May, Houston, Texas, USA.

TAKU IDE, S., JESSEN, K., & ORR, F. M. (2007). Storage of CO2 in saline aquifers: Effects of gravity, viscous, and capillary forces on amount and timing of trapping. International Journal of Greenhouse Gas Control, 1(4), 481-491.

TENG, YAMASAKI A. M., CHUM K., AND LEE H., (1997) Solubility of liquid CO2 in water at temperatures from 278 K to 293 K and pressures from 6.44 MPa to 29.49 MPa and densities of the corresponding aqueous solutions, J. Chem. Thermodyn. 29, pp. 1301–1310.

VAN WEERT, F., VAN DER GUN, J. & RECKMAN, J. (2009) Global Overview of saline groundwater occurrence and genesis. International Groundwater Resources Assessment Centre.

VESOVIC, V. WAKEHAM, W. A., OLCHOWY, G.A., SENGERS, J.V., WATSON, J.T.R., MILLAT, J. (1990) The Transport Properties of Carbon Dioxide, J. Phys. Chem. Ref. Data, Vol. 19, No.3.

UNDERHILL, J. R. (1998) Development, evolution and petroleum geology of the Wessex Basin. Geol. Soc. (Spec. Publ.) 133.

UNDERHILL, J.R. & STONELEY, R. (1998) Introduction to the development, evolution and petroleum geology of the Wessex Basin. In (Underhill, J.R.; ed.) Development, Evolution and Petroleum Geology of the Wessex Basin. Geological Society, London, Special Publications, 133, 1-18.

WHITE C.J., WILLIAMS A.G., AND CHADWICK R.A., (2013) Thin Layer Detectability in a Growing CO2 Plume: testing the Limits of Time-lapse Seismic Resolution, Energy Procedia, Volume 37, Pages 4356–4365.

WILLIAMS, J. D. O., BENTHAM, M., JIN, M., PICKUP, G., MACKAY, E., GAMMER, D. & GREEN, A. (2013). The Effect of Geological Structure and Heterogeneity on CO2 Storage in Simple 4-way Dip Structures; a Modeling Study from the UK Southern North Sea. *Energy Procedia,* 37**,** 3980-3988.

WINTERFELD P.H.,WU Y.S.,(2011) Parallel Simulation of CO2 Sequestration with Rock Deformation in Saline Aquifers, SPE 141514.

Working Group III of the Intergovernmental Panel on Climate Change (IPCC), (2005) Carbon Dioxide Capture and Storage. United Kingdom and New York, NY, USA.UNT Digital Library. http://digital.library.unt.edu/ark:/67531/metadc12051/

XU, T., APPS, J. A., & PRUESS, K. (2004). Numerical simulation of $CO_2$ disposal by mineral trapping in deep aquifers. Applied geochemistry, 19(6), 917-936.

ZIRRAHI, M., HASSANZADEH, H., & ABEDI, J. (2013). The laboratory testing and scale-up of a downhole device for CO2 dissolution acceleration. International Journal of Greenhouse Gas Control, 16, 41-49.

ZWEIGEL, Z., ARTS, R., LOTHE, A, N., AND LINDEBERG E, B, G. (2004) Rwservoir Geology of the Utsira Formation at the First Industrial-Scale Underground CO2 Storage Site (Sleipner area, North Sea). Geological society, London. Geological Storage of Carbon Dioxide, 233, PP. 165-180.

# Appendix

## Appendix A:

*Geological outcrop and subcrop patterns in southern England and the English Channel (Underhill et al. 1998). The Wessex Basin as defined in this thesis is indicated.*

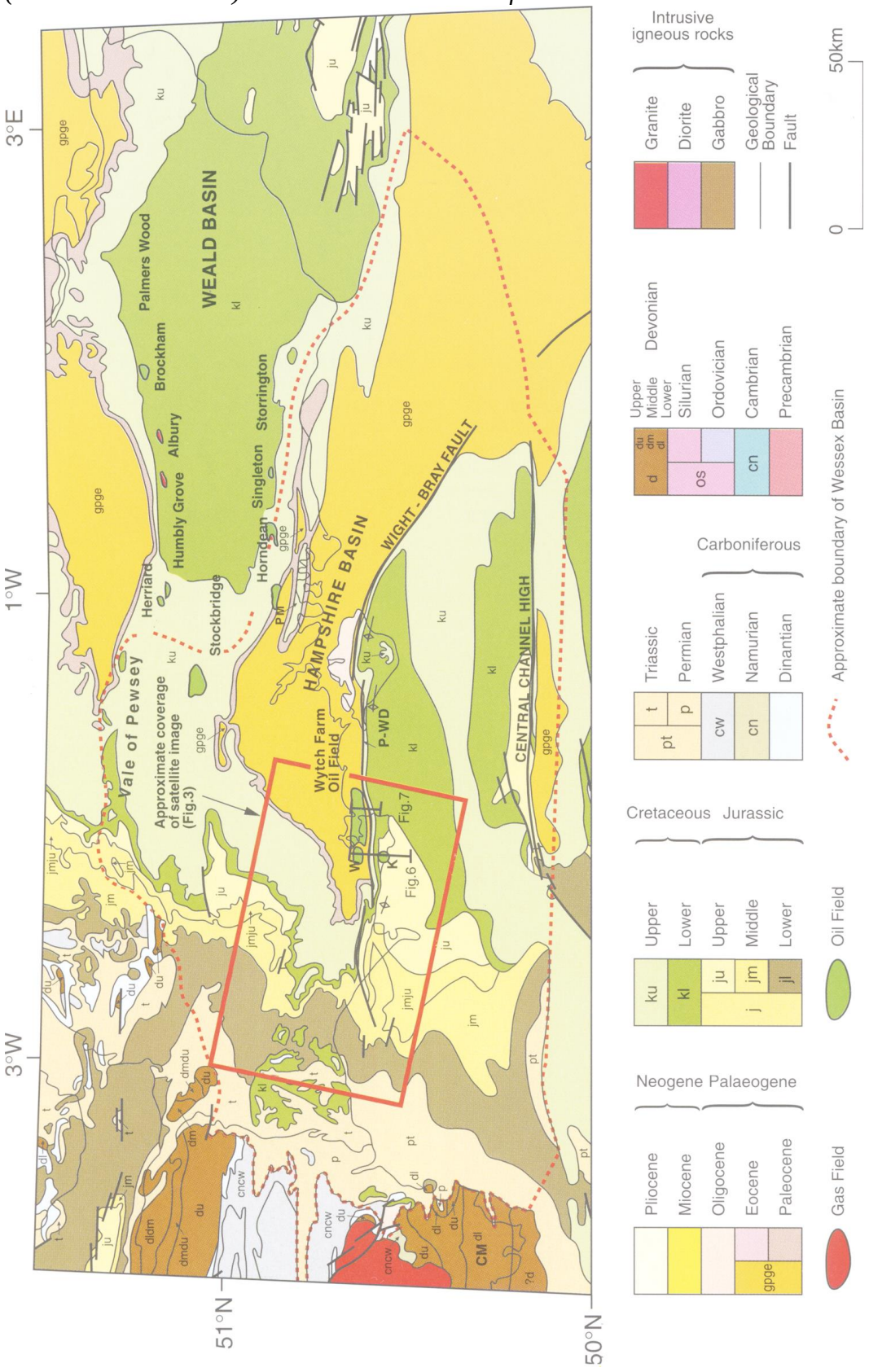

## Appendix B

**Appendix B.1**: Models used in Chapter 3 Section 3, which created by Re-Studio. Last column shows the name of the models and the information about anisotropic ratio, tilt angle and amplitude of ridges of each model are outlined next to it, respectively.

| Branch Number | Branch Title Models | | | | | | | |
|---|---|---|---|---|---|---|---|---|
| 1 | Para | | | | | | | |
| 1.1 | Para | Amplitude | | | | | | |
| 1.1.1 | Para | Amplitude | 0 | | | | | |
| 1.1.1.1 | Para | Amplitude | 0 | Tilt | | | | |
| 1.1.1.1.1 | Para | Amplitude | 0 | Tilt | 0 | | | |
| 1.1.1.1.1.1 | Para | Amplitude | 0 | Tilt | 0 | Kv/Kh | | |
| 1.1.1.1.1.1.1 | Para | Amplitude | 0 | Tilt | 0 | Kv/Kh | 0.01 | |
| 1.1.1.1.1.1.1.1 | Para | Amplitude | 0 | Tilt | 0 | Kv/Kh | 0.01 | Para-A0-D0-K001 |
| 1.1.1.1.1.1.2 | Para | Amplitude | 0 | Tilt | 0 | Kv/Kh | 0.1 | |
| 1.1.1.1.1.1.2.1 | Para | Amplitude | 0 | Tilt | 0 | Kv/Kh | 0.1 | Para-A0-D0-K01 |
| 1.1.1.1.1.1.3 | Para | Amplitude | 0 | Tilt | 0 | Kv/Kh | 1 | |
| 1.1.1.1.1.1.3.1 | Para | Amplitude | 0 | Tilt | 0 | Kv/Kh | 1 | Para-A0-D0-K1 |
| 1.1.1.1.2 | Para | Amplitude | 0 | Tilt | 1 | | | |
| 1.1.1.1.2.1 | Para | Amplitude | 0 | Tilt | 1 | Kv/Kh | | |
| 1.1.1.1.2.1.1 | Para | Amplitude | 0 | Tilt | 1 | Kv/Kh | 0.01 | |
| 1.1.1.1.2.1.1.1 | Para | Amplitude | 0 | Tilt | 1 | Kv/Kh | 0.01 | Para-A0-D1-K001 |
| 1.1.1.1.2.1.2 | Para | Amplitude | 0 | Tilt | 1 | Kv/Kh | 0.1 | |
| 1.1.1.1.2.1.2.1 | Para | Amplitude | 0 | Tilt | 1 | Kv/Kh | 0.1 | Para-A0-D1-K01 |
| 1.1.1.1.2.1.3 | Para | Amplitude | 0 | Tilt | 1 | Kv/Kh | 1 | |
| 1.1.1.1.2.1.3.1 | Para | Amplitude | 0 | Tilt | 1 | Kv/Kh | 1 | Para-A0-D1-K1 |
| 1.1.1.1.3 | Para | Amplitude | 0 | Tilt | 2 | | | |
| 1.1.1.1.3.1 | Para | Amplitude | 0 | Tilt | 2 | Kv/Kh | | |
| 1.1.1.1.3.1.1 | Para | Amplitude | 0 | Tilt | 2 | Kv/Kh | 0.01 | |
| 1.1.1.1.3.1.1.1 | Para | Amplitude | 0 | Tilt | 2 | Kv/Kh | 0.01 | Para-A0-D2-K001 |
| 1.1.1.1.3.1.2 | Para | Amplitude | 0 | Tilt | 2 | Kv/Kh | 0.1 | |
| 1.1.1.1.3.1.2.1 | Para | Amplitude | 0 | Tilt | 2 | Kv/Kh | 0.1 | Para-A0-D2-K01 |
| 1.1.1.1.3.1.3 | Para | Amplitude | 0 | Tilt | 2 | Kv/Kh | 1 | |
| 1.1.1.1.3.1.3.1 | Para | Amplitude | 0 | Tilt | 2 | Kv/Kh | 1 | Para-A0-D2-K1 |
| 1.1.1.1.4 | Para | Amplitude | 0 | Tilt | 5 | | | |
| 1.1.1.1.4.1 | Para | Amplitude | 0 | Tilt | 5 | Kv/Kh | | |
| 1.1.1.1.4.1.1 | Para | Amplitude | 0 | Tilt | 5 | Kv/Kh | 0.01 | |
| 1.1.1.1.4.1.1.1 | Para | Amplitude | 0 | Tilt | 5 | Kv/Kh | 0.01 | Para-A0-D5-K001 |
| 1.1.1.1.4.1.2 | Para | Amplitude | 0 | Tilt | 5 | Kv/Kh | 0.1 | |
| 1.1.1.1.4.1.2.1 | Para | Amplitude | 0 | Tilt | 5 | Kv/Kh | 0.1 | Para-A0-D5-K01 |
| 1.1.1.1.4.1.3 | Para | Amplitude | 0 | Tilt | 5 | Kv/Kh | 1 | |
| 1.1.1.1.4.1.3.1 | Para | Amplitude | 0 | Tilt | 5 | Kv/Kh | 1 | Para-A0-D5-K1 |
| 1.1.2 | Para | Amplitude | 3 | | | | | |
| 1.1.2.1 | Para | Amplitude | 3 | Tilt | | | | |

| | | | | | | | | |
|---|---|---|---|---|---|---|---|---|
| 1.1.2.1.1 | Para | Amplitude | 3 | Tilt | 0 | | | |
| 1.1.2.1.1.1 | Para | Amplitude | 3 | Tilt | 0 | Kv/Kh | | |
| 1.1.2.1.1.1.1 | Para | Amplitude | 3 | Tilt | 0 | Kv/Kh | 0.01 | |
| 1.1.2.1.1.1.1.1 | Para | Amplitude | 3 | Tilt | 0 | Kv/Kh | 0.01 | Para-A3-D0-K001 |
| 1.1.2.1.1.1.2 | Para | Amplitude | 3 | Tilt | 0 | Kv/Kh | 0.1 | |
| 1.1.2.1.1.1.2.1 | Para | Amplitude | 3 | Tilt | 0 | Kv/Kh | 0.1 | Para-A3-D0-K01 |
| 1.1.2.1.1.1.3 | Para | Amplitude | 3 | Tilt | 0 | Kv/Kh | 1 | |
| 1.1.2.1.1.1.3.1 | Para | Amplitude | 3 | Tilt | 0 | Kv/Kh | 1 | Para-A3-D0-K1 |
| 1.1.2.1.2 | Para | Amplitude | 3 | Tilt | 1 | | | |
| 1.1.2.1.2.1 | Para | Amplitude | 3 | Tilt | 1 | Kv/Kh | | |
| 1.1.2.1.2.1.1 | Para | Amplitude | 3 | Tilt | 1 | Kv/Kh | 0.01 | |
| 1.1.2.1.2.1.1.1 | Para | Amplitude | 3 | Tilt | 1 | Kv/Kh | 0.01 | Para-A3-D1-K001 |
| 1.1.2.1.2.1.2 | Para | Amplitude | 3 | Tilt | 1 | Kv/Kh | 0.1 | |
| 1.1.2.1.2.1.2.1 | Para | Amplitude | 3 | Tilt | 1 | Kv/Kh | 0.1 | Para-A3-D1-K01 |
| 1.1.2.1.2.1.3 | Para | Amplitude | 3 | Tilt | 1 | Kv/Kh | 1 | |
| 1.1.2.1.2.1.3.1 | Para | Amplitude | 3 | Tilt | 1 | Kv/Kh | 1 | Para-A3-D1-K1 |
| 1.1.2.1.3 | Para | Amplitude | 3 | Tilt | 2 | | | |
| 1.1.2.1.3.1 | Para | Amplitude | 3 | Tilt | 2 | Kv/Kh | | |
| 1.1.2.1.3.1.1 | Para | Amplitude | 3 | Tilt | 2 | Kv/Kh | 0.01 | |
| 1.1.2.1.3.1.1.1 | Para | Amplitude | 3 | Tilt | 2 | Kv/Kh | 0.01 | Para-A3-D2-K001 |
| 1.1.2.1.3.1.2 | Para | Amplitude | 3 | Tilt | 2 | Kv/Kh | 0.1 | |
| 1.1.2.1.3.1.2.1 | Para | Amplitude | 3 | Tilt | 2 | Kv/Kh | 0.1 | Para-A3-D2-K01 |
| 1.1.2.1.3.1.3 | Para | Amplitude | 3 | Tilt | 2 | Kv/Kh | 1 | |
| 1.1.2.1.3.1.3.1 | Para | Amplitude | 3 | Tilt | 2 | Kv/Kh | 1 | Para-A3-D2-K1 |
| 1.1.2.1.4 | Para | Amplitude | 3 | Tilt | 5 | | | |
| 1.1.2.1.4.1 | Para | Amplitude | 3 | Tilt | 5 | Kv/Kh | | |
| 1.1.2.1.4.1.1 | Para | Amplitude | 3 | Tilt | 5 | Kv/Kh | 0.01 | |
| 1.1.2.1.4.1.1.1 | Para | Amplitude | 3 | Tilt | 5 | Kv/Kh | 0.01 | Para-A3-D5-K001 |
| 1.1.2.1.4.1.2 | Para | Amplitude | 3 | Tilt | 5 | Kv/Kh | 0.1 | |
| 1.1.2.1.4.1.2.1 | Para | Amplitude | 3 | Tilt | 5 | Kv/Kh | 0.1 | Para-A3-D5-K01 |
| 1.1.2.1.4.1.3 | Para | Amplitude | 3 | Tilt | 5 | Kv/Kh | 1 | |
| 1.1.2.1.4.1.3.1 | Para | Amplitude | 3 | Tilt | 5 | Kv/Kh | 1 | Para-A3-D5-K1 |
| 1.1.3 | Para | Amplitude | 6 | | | | | |
| 1.1.3.1 | Para | Amplitude | 6 | Tilt | | | | |
| 1.1.3.1.1 | Para | Amplitude | 6 | Tilt | 0 | | | |
| 1.1.3.1.1.1 | Para | Amplitude | 6 | Tilt | 0 | Kv/Kh | | |
| 1.1.3.1.1.1.1 | Para | Amplitude | 6 | Tilt | 0 | Kv/Kh | 0.01 | |
| 1.1.3.1.1.1.1.1 | Para | Amplitude | 6 | Tilt | 0 | Kv/Kh | 0.01 | Para-A6-D0-K001 |
| 1.1.3.1.1.1.2 | Para | Amplitude | 6 | Tilt | 0 | Kv/Kh | 0.1 | |
| 1.1.3.1.1.1.2.1 | Para | Amplitude | 6 | Tilt | 0 | Kv/Kh | 0.1 | Para-A6-D0-K01 |
| 1.1.3.1.1.1.3 | Para | Amplitude | 6 | Tilt | 0 | Kv/Kh | 1 | |
| 1.1.3.1.1.1.3.1 | Para | Amplitude | 6 | Tilt | 0 | Kv/Kh | 1 | Para-A6-D0-K1 |
| 1.1.3.1.2 | Para | Amplitude | 6 | Tilt | 1 | | | |
| 1.1.3.1.2.1 | Para | Amplitude | 6 | Tilt | 1 | Kv/Kh | | |
| 1.1.3.1.2.1.1 | Para | Amplitude | 6 | Tilt | 1 | Kv/Kh | 0.01 | |
| 1.1.3.1.2.1.1.1 | Para | Amplitude | 6 | Tilt | 1 | Kv/Kh | 0.01 | Para-A6-D1-K001 |
| 1.1.3.1.2.1.2 | Para | Amplitude | 6 | Tilt | 1 | Kv/Kh | 0.1 | |
| 1.1.3.1.2.1.2.1 | Para | Amplitude | 6 | Tilt | 1 | Kv/Kh | 0.1 | Para-A6-D1-K01 |

| | | | | | | | | |
|---|---|---|---|---|---|---|---|---|
| 1.1.3.1.2.1.3 | Para | Amplitude | 6 | Tilt | 1 | Kv/Kh | 1 | |
| 1.1.3.1.2.1.3.1 | Para | Amplitude | 6 | Tilt | 1 | Kv/Kh | 1 | Para-A6-D1-K1 |
| 1.1.3.1.3 | Para | Amplitude | 6 | Tilt | 2 | | | |
| 1.1.3.1.3.1 | Para | Amplitude | 6 | Tilt | 2 | Kv/Kh | | |
| 1.1.3.1.3.1.1 | Para | Amplitude | 6 | Tilt | 2 | Kv/Kh | 0.01 | |
| 1.1.3.1.3.1.1.1 | Para | Amplitude | 6 | Tilt | 2 | Kv/Kh | 0.01 | Para-A6-D2-K001 |
| 1.1.3.1.3.1.2 | Para | Amplitude | 6 | Tilt | 2 | Kv/Kh | 0.1 | |
| 1.1.3.1.3.1.2.1 | Para | Amplitude | 6 | Tilt | 2 | Kv/Kh | 0.1 | Para-A6-D2-K01 |
| 1.1.3.1.3.1.3 | Para | Amplitude | 6 | Tilt | 2 | Kv/Kh | 1 | |
| 1.1.3.1.3.1.3.1 | Para | Amplitude | 6 | Tilt | 2 | Kv/Kh | 1 | Para-A6-D2-K1 |
| 1.1.3.1.4 | Para | Amplitude | 6 | Tilt | 5 | | | |
| 1.1.3.1.4.1 | Para | Amplitude | 6 | Tilt | 5 | Kv/Kh | | |
| 1.1.3.1.4.1.1 | Para | Amplitude | 6 | Tilt | 5 | Kv/Kh | 0.01 | |
| 1.1.3.1.4.1.1.1 | Para | Amplitude | 6 | Tilt | 5 | Kv/Kh | 0.01 | Para-A6-D5-K001 |
| 1.1.3.1.4.1.2 | Para | Amplitude | 6 | Tilt | 5 | Kv/Kh | 0.1 | |
| 1.1.3.1.4.1.2.1 | Para | Amplitude | 6 | Tilt | 5 | Kv/Kh | 0.1 | Para-A6-D5-K01 |
| 1.1.3.1.4.1.3 | Para | Amplitude | 6 | Tilt | 5 | Kv/Kh | 1 | |
| 1.1.3.1.4.1.3.1 | Para | Amplitude | 6 | Tilt | 5 | Kv/Kh | 1 | Para-A6-D5-K1 |
| 1.1.4 | Para | Amplitude | 9 | | | | | |
| 1.1.4.1 | Para | Amplitude | 9 | Tilt | | | | |
| 1.1.4.1.1 | Para | Amplitude | 9 | Tilt | 0 | | | |
| 1.1.4.1.1.1 | Para | Amplitude | 9 | Tilt | 0 | Kv/Kh | | |
| 1.1.4.1.1.1.1 | Para | Amplitude | 9 | Tilt | 0 | Kv/Kh | 0.01 | |
| 1.1.4.1.1.1.1.1 | Para | Amplitude | 9 | Tilt | 0 | Kv/Kh | 0.01 | Para-A9-D0-K001 |
| 1.1.4.1.1.1.2 | Para | Amplitude | 9 | Tilt | 0 | Kv/Kh | 0.1 | |
| 1.1.4.1.1.1.2.1 | Para | Amplitude | 9 | Tilt | 0 | Kv/Kh | 0.1 | Para-A9-D0-K01 |
| 1.1.4.1.1.1.3 | Para | Amplitude | 9 | Tilt | 0 | Kv/Kh | 1 | |
| 1.1.4.1.1.1.3.1 | Para | Amplitude | 9 | Tilt | 0 | Kv/Kh | 1 | Para-A9-D0-K1 |
| 1.1.4.1.2 | Para | Amplitude | 9 | Tilt | 1 | | | |
| 1.1.4.1.2.1 | Para | Amplitude | 9 | Tilt | 1 | Kv/Kh | | |
| 1.1.4.1.2.1.1 | Para | Amplitude | 9 | Tilt | 1 | Kv/Kh | 0.01 | |
| 1.1.4.1.2.1.1.1 | Para | Amplitude | 9 | Tilt | 1 | Kv/Kh | 0.01 | Para-A9-D1-K001 |
| 1.1.4.1.2.1.2 | Para | Amplitude | 9 | Tilt | 1 | Kv/Kh | 0.1 | |
| 1.1.4.1.2.1.2.1 | Para | Amplitude | 9 | Tilt | 1 | Kv/Kh | 0.1 | Para-A9-D1-K01 |
| 1.1.4.1.2.1.3 | Para | Amplitude | 9 | Tilt | 1 | Kv/Kh | 1 | |
| 1.1.4.1.2.1.3.1 | Para | Amplitude | 9 | Tilt | 1 | Kv/Kh | 1 | Para-A9-D1-K1 |
| 1.1.4.1.3 | Para | Amplitude | 9 | Tilt | 2 | | | |
| 1.1.4.1.3.1 | Para | Amplitude | 9 | Tilt | 2 | Kv/Kh | | |
| 1.1.4.1.3.1.1 | Para | Amplitude | 9 | Tilt | 2 | Kv/Kh | 0.01 | |
| 1.1.4.1.3.1.1.1 | Para | Amplitude | 9 | Tilt | 2 | Kv/Kh | 0.01 | Para-A9-D2-K001 |
| 1.1.4.1.3.1.2 | Para | Amplitude | 9 | Tilt | 2 | Kv/Kh | 0.1 | |
| 1.1.4.1.3.1.2.1 | Para | Amplitude | 9 | Tilt | 2 | Kv/Kh | 0.1 | Para-A9-D2-K01 |
| 1.1.4.1.3.1.3 | Para | Amplitude | 9 | Tilt | 2 | Kv/Kh | 1 | |
| 1.1.4.1.3.1.3.1 | Para | Amplitude | 9 | Tilt | 2 | Kv/Kh | 1 | Para-A9-D2-K1 |
| 1.1.4.1.4 | Para | Amplitude | 9 | Tilt | 5 | | | |
| 1.1.4.1.4.1 | Para | Amplitude | 9 | Tilt | 5 | Kv/Kh | | |
| 1.1.4.1.4.1.1 | Para | Amplitude | 9 | Tilt | 5 | Kv/Kh | 0.01 | |
| 1.1.4.1.4.1.1.1 | Para | Amplitude | 9 | Tilt | 5 | Kv/Kh | 0.01 | Para-A9-D5-K001 |

| | | | | | | | | |
|---|---|---|---|---|---|---|---|---|
| 1.1.4.1.4.1.2 | Para | Amplitude | 9 | Tilt | 5 | Kv/Kh | 0.1 | |
| 1.1.4.1.4.1.2.1 | Para | Amplitude | 9 | Tilt | 5 | Kv/Kh | 0.1 | Para-A9-D5-K01 |
| 1.1.4.1.4.1.3 | Para | Amplitude | 9 | Tilt | 5 | Kv/Kh | 1 | |
| 1.1.4.1.4.1.3.1 | Para | Amplitude | 9 | Tilt | 5 | Kv/Kh | 1 | Para-A9-D5-K1 |
| 2 | Trans | | | | | | | |
| 2.1 | Trans | Amplitude | | | | | | |
| 2.1.1 | Trans | Amplitude | 0 | | | | | |
| 2.1.1.1 | Trans | Amplitude | 0 | Tilt | | | | |
| 2.1.1.1.1 | Trans | Amplitude | 0 | Tilt | 0 | | | |
| 2.1.1.1.1.1 | Trans | Amplitude | 0 | Tilt | 0 | Kv/Kh | | |
| 2.1.1.1.1.1.1 | Trans | Amplitude | 0 | Tilt | 0 | Kv/Kh | 0.01 | |
| 2.1.1.1.1.1.1.1 | Trans | Amplitude | 0 | Tilt | 0 | Kv/Kh | 0.01 | Trans-A0-D0-K001 |
| 2.1.1.1.1.1.2 | Trans | Amplitude | 0 | Tilt | 0 | Kv/Kh | 0.1 | |
| 2.1.1.1.1.1.2.1 | Trans | Amplitude | 0 | Tilt | 0 | Kv/Kh | 0.1 | Trans-A0-D0-K01 |
| 2.1.1.1.1.1.3 | Trans | Amplitude | 0 | Tilt | 0 | Kv/Kh | 1 | |
| 2.1.1.1.1.1.3.1 | Trans | Amplitude | 0 | Tilt | 0 | Kv/Kh | 1 | Trans -A0-D0-K1 |
| 2.1.1.1.2 | Trans | Amplitude | 0 | Tilt | 1 | | | |
| 2.1.1.1.2.1 | Trans | Amplitude | 0 | Tilt | 1 | Kv/Kh | | |
| 2.1.1.1.2.1.1 | Trans | Amplitude | 0 | Tilt | 1 | Kv/Kh | 0.01 | |
| 2.1.1.1.2.1.1.1 | Trans | Amplitude | 0 | Tilt | 1 | Kv/Kh | 0.01 | Trans-A0-D1-K001 |
| 2.1.1.1.2.1.2 | Trans | Amplitude | 0 | Tilt | 1 | Kv/Kh | 0.1 | |
| 2.1.1.1.2.1.2.1 | Trans | Amplitude | 0 | Tilt | 1 | Kv/Kh | 0.1 | Trans-A0-D1-K01 |
| 2.1.1.1.2.1.3 | Trans | Amplitude | 0 | Tilt | 1 | Kv/Kh | 1 | |
| 2.1.1.1.2.1.3.1 | Trans | Amplitude | 0 | Tilt | 1 | Kv/Kh | 1 | Trans-A0-D1-K1 |
| 2.1.1.1.3 | Trans | Amplitude | 0 | Tilt | 2 | | | |
| 2.1.1.1.3.1 | Trans | Amplitude | 0 | Tilt | 2 | Kv/Kh | | |
| 2.1.1.1.3.1.1 | Trans | Amplitude | 0 | Tilt | 2 | Kv/Kh | 0.01 | |
| 2.1.1.1.3.1.1.1 | Trans | Amplitude | 0 | Tilt | 2 | Kv/Kh | 0.01 | Trans-A0-D2-K001 |
| 2.1.1.1.3.1.2 | Trans | Amplitude | 0 | Tilt | 2 | Kv/Kh | 0.1 | |
| 2.1.1.1.3.1.2.1 | Trans | Amplitude | 0 | Tilt | 2 | Kv/Kh | 0.1 | Trans-A0-D2-K01 |
| 2.1.1.1.3.1.3 | Trans | Amplitude | 0 | Tilt | 2 | Kv/Kh | 1 | |
| 2.1.1.1.3.1.3.1 | Trans | Amplitude | 0 | Tilt | 2 | Kv/Kh | 1 | Trans-A0-D2-K1 |
| 2.1.1.1.4 | Trans | Amplitude | 0 | Tilt | 5 | | | |
| 2.1.1.1.4.1 | Trans | Amplitude | 0 | Tilt | 5 | Kv/Kh | | |
| 2.1.1.1.4.1.1 | Trans | Amplitude | 0 | Tilt | 5 | Kv/Kh | 0.01 | |
| 2.1.1.1.4.1.1.1 | Trans | Amplitude | 0 | Tilt | 5 | Kv/Kh | 0.01 | Trans-A0-D5-K001 |
| 2.1.1.1.4.1.2 | Trans | Amplitude | 0 | Tilt | 5 | Kv/Kh | 0.1 | |
| 2.1.1.1.4.1.2.1 | Trans | Amplitude | 0 | Tilt | 5 | Kv/Kh | 0.1 | Trans-A0-D5-K01 |
| 2.1.1.1.4.1.3 | Trans | Amplitude | 0 | Tilt | 5 | Kv/Kh | 1 | |
| 2.1.1.1.4.1.3.1 | Trans | Amplitude | 0 | Tilt | 5 | Kv/Kh | 1 | Trans-A0-D5-K1 |
| 2.1.2 | Trans | Amplitude | 3 | | | | | |
| 2.1.2.1 | Trans | Amplitude | 3 | Tilt | | | | |
| 2.1.2.1.1 | Trans | Amplitude | 3 | Tilt | 0 | | | |
| 2.1.2.1.1.1 | Trans | Amplitude | 3 | Tilt | 0 | Kv/Kh | | |
| 2.1.2.1.1.1.1 | Trans | Amplitude | 3 | Tilt | 0 | Kv/Kh | 0.01 | |
| 2.1.2.1.1.1.1.1 | Trans | Amplitude | 3 | Tilt | 0 | Kv/Kh | 0.01 | Trans-A3-D0-K001 |

| | | | | | | | | |
|---|---|---|---|---|---|---|---|---|
| 2.1.2.1.1.1.2 | Trans | Amplitude | 3 | Tilt | 0 | Kv/Kh | 0.1 | |
| 2.1.2.1.1.1.2.1 | Trans | Amplitude | 3 | Tilt | 0 | Kv/Kh | 0.1 | Trans-A3-D0-K01 |
| 2.1.2.1.1.1.3 | Trans | Amplitude | 3 | Tilt | 0 | Kv/Kh | 1 | |
| 2.1.2.1.1.1.3.1 | Trans | Amplitude | 3 | Tilt | 0 | Kv/Kh | 1 | Trans-A3-D0-K1 |
| 2.1.2.1.2 | Trans | Amplitude | 3 | Tilt | 1 | | | |
| 2.1.2.1.2.1 | Trans | Amplitude | 3 | Tilt | 1 | Kv/Kh | | |
| 2.1.2.1.2.1.1 | Trans | Amplitude | 3 | Tilt | 1 | Kv/Kh | 0.01 | |
| 2.1.2.1.2.1.1.1 | Trans | Amplitude | 3 | Tilt | 1 | Kv/Kh | 0.01 | Trans-A3-D1-K001 |
| 2.1.2.1.2.1.2 | Trans | Amplitude | 3 | Tilt | 1 | Kv/Kh | 0.1 | |
| 2.1.2.1.2.1.2.1 | Trans | Amplitude | 3 | Tilt | 1 | Kv/Kh | 0.1 | Trans-A3-D1-K01 |
| 2.1.2.1.2.1.3 | Trans | Amplitude | 3 | Tilt | 1 | Kv/Kh | 1 | |
| 2.1.2.1.2.1.3.1 | Trans | Amplitude | 3 | Tilt | 1 | Kv/Kh | 1 | Trans-A3-D1-K1 |
| 2.1.2.1.3 | Trans | Amplitude | 3 | Tilt | 2 | | | |
| 2.1.2.1.3.1 | Trans | Amplitude | 3 | Tilt | 2 | Kv/Kh | | |
| 2.1.2.1.3.1.1 | Trans | Amplitude | 3 | Tilt | 2 | Kv/Kh | 0.01 | |
| 2.1.2.1.3.1.1.1 | Trans | Amplitude | 3 | Tilt | 2 | Kv/Kh | 0.01 | Trans-A3-D2-K001 |
| 2.1.2.1.3.1.2 | Trans | Amplitude | 3 | Tilt | 2 | Kv/Kh | 0.1 | |
| 2.1.2.1.3.1.2.1 | Trans | Amplitude | 3 | Tilt | 2 | Kv/Kh | 0.1 | Trans-A3-D2-K01 |
| 2.1.2.1.3.1.3 | Trans | Amplitude | 3 | Tilt | 2 | Kv/Kh | 1 | |
| 2.1.2.1.3.1.3.1 | Trans | Amplitude | 3 | Tilt | 2 | Kv/Kh | 1 | Trans-A3-D2-K1 |
| 2.1.2.1.4 | Trans | Amplitude | 3 | Tilt | 5 | | | |
| 2.1.2.1.4.1 | Trans | Amplitude | 3 | Tilt | 5 | Kv/Kh | | |
| 2.1.2.1.4.1.1 | Trans | Amplitude | 3 | Tilt | 5 | Kv/Kh | 0.01 | |
| 2.1.2.1.4.1.1.1 | Trans | Amplitude | 3 | Tilt | 5 | Kv/Kh | 0.01 | Trans-A3-D5-K001 |
| 2.1.2.1.4.1.2 | Trans | Amplitude | 3 | Tilt | 5 | Kv/Kh | 0.1 | |
| 2.1.2.1.4.1.2.1 | Trans | Amplitude | 3 | Tilt | 5 | Kv/Kh | 0.1 | Trans-A3-D5-K01 |
| 2.1.2.1.4.1.3 | Trans | Amplitude | 3 | Tilt | 5 | Kv/Kh | 1 | |
| 2.1.2.1.4.1.3.1 | Trans | Amplitude | 3 | Tilt | 5 | Kv/Kh | 1 | Trans-A3-D5-K1 |
| 2.1.3 | Trans | Amplitude | 6 | | | | | |
| 2.1.3.1 | Trans | Amplitude | 6 | Tilt | | | | |
| 2.1.3.1.1 | Trans | Amplitude | 6 | Tilt | 0 | | | |
| 2.1.3.1.1.1 | Trans | Amplitude | 6 | Tilt | 0 | Kv/Kh | | |
| 2.1.3.1.1.1.1 | Trans | Amplitude | 6 | Tilt | 0 | Kv/Kh | 0.01 | |
| 2.1.3.1.1.1.1.1 | Trans | Amplitude | 6 | Tilt | 0 | Kv/Kh | 0.01 | Trans-A6-D0-K001 |
| 2.1.3.1.1.1.2 | Trans | Amplitude | 6 | Tilt | 0 | Kv/Kh | 0.1 | |
| 2.1.3.1.1.1.2.1 | Trans | Amplitude | 6 | Tilt | 0 | Kv/Kh | 0.1 | Trans-A6-D0-K01 |
| 2.1.3.1.1.1.3 | Trans | Amplitude | 6 | Tilt | 0 | Kv/Kh | 1 | |
| 2.1.3.1.1.1.3.1 | Trans | Amplitude | 6 | Tilt | 0 | Kv/Kh | 1 | Trans-A6-D0-K1 |
| 2.1.3.1.2 | Trans | Amplitude | 6 | Tilt | 1 | | | |
| 2.1.3.1.2.1 | Trans | Amplitude | 6 | Tilt | 1 | Kv/Kh | | |
| 2.1.3.1.2.1.1 | Trans | Amplitude | 6 | Tilt | 1 | Kv/Kh | 0.01 | |
| 2.1.3.1.2.1.1.1 | Trans | Amplitude | 6 | Tilt | 1 | Kv/Kh | 0.01 | Trans-A6-D1-K001 |
| 2.1.3.1.2.1.2 | Trans | Amplitude | 6 | Tilt | 1 | Kv/Kh | 0.1 | |
| 2.1.3.1.2.1.2.1 | Trans | Amplitude | 6 | Tilt | 1 | Kv/Kh | 0.1 | Trans-A6-D1-K01 |
| 2.1.3.1.2.1.3 | Trans | Amplitude | 6 | Tilt | 1 | Kv/Kh | 1 | |
| 2.1.3.1.2.1.3.1 | Trans | Amplitude | 6 | Tilt | 1 | Kv/Kh | 1 | Trans-A6-D1-K1 |

| | | | | | | | | |
|---|---|---|---|---|---|---|---|---|
| 2.1.3.1.3 | Trans | Amplitude | 6 | Tilt | 2 | | | |
| 2.1.3.1.3.1 | Trans | Amplitude | 6 | Tilt | 2 | Kv/Kh | | |
| 2.1.3.1.3.1.1 | Trans | Amplitude | 6 | Tilt | 2 | Kv/Kh | 0.01 | |
| 2.1.3.1.3.1.1.1 | Trans | Amplitude | 6 | Tilt | 2 | Kv/Kh | 0.01 | Trans-A6-D2-K001 |
| 2.1.3.1.3.1.2 | Trans | Amplitude | 6 | Tilt | 2 | Kv/Kh | 0.1 | |
| 2.1.3.1.3.1.2.1 | Trans | Amplitude | 6 | Tilt | 2 | Kv/Kh | 0.1 | Trans-A6-D2-K01 |
| 2.1.3.1.3.1.3 | Trans | Amplitude | 6 | Tilt | 2 | Kv/Kh | 1 | |
| 2.1.3.1.3.1.3.1 | Trans | Amplitude | 6 | Tilt | 2 | Kv/Kh | 1 | Trans-A6-D2-K1 |
| 2.1.3.1.4 | Trans | Amplitude | 6 | Tilt | 5 | | | |
| 2.1.3.1.4.1 | Trans | Amplitude | 6 | Tilt | 5 | Kv/Kh | | |
| 2.1.3.1.4.1.1 | Trans | Amplitude | 6 | Tilt | 5 | Kv/Kh | 0.01 | |
| 2.1.3.1.4.1.1.1 | Trans | Amplitude | 6 | Tilt | 5 | Kv/Kh | 0.01 | Trans-A6-D5-K001 |
| 2.1.3.1.4.1.2 | Trans | Amplitude | 6 | Tilt | 5 | Kv/Kh | 0.1 | |
| 2.1.3.1.4.1.2.1 | Trans | Amplitude | 6 | Tilt | 5 | Kv/Kh | 0.1 | Trans-A6-D5-K01 |
| 2.1.3.1.4.1.3 | Trans | Amplitude | 6 | Tilt | 5 | Kv/Kh | 1 | |
| 2.1.3.1.4.1.3.1 | Trans | Amplitude | 6 | Tilt | 5 | Kv/Kh | 1 | Trans-A6-D5-K1 |
| 2.1.4 | Trans | Amplitude | 9 | | | | | |
| 2.1.4.1 | Trans | Amplitude | 9 | Tilt | | | | |
| 2.1.4.1.1 | Trans | Amplitude | 9 | Tilt | 0 | | | |
| 2.1.4.1.1.1 | Trans | Amplitude | 9 | Tilt | 0 | Kv/Kh | | |
| 2.1.4.1.1.1.1 | Trans | Amplitude | 9 | Tilt | 0 | Kv/Kh | 0.01 | |
| 2.1.4.1.1.1.1.1 | Trans | Amplitude | 9 | Tilt | 0 | Kv/Kh | 0.01 | Trans-A9-D0-K001 |
| 2.1.4.1.1.1.2 | Trans | Amplitude | 9 | Tilt | 0 | Kv/Kh | 0.1 | |
| 2.1.4.1.1.1.2.1 | Trans | Amplitude | 9 | Tilt | 0 | Kv/Kh | 0.1 | Trans-A9-D0-K01 |
| 2.1.4.1.1.1.3 | Trans | Amplitude | 9 | Tilt | 0 | Kv/Kh | 1 | |
| 2.1.4.1.1.1.3.1 | Trans | Amplitude | 9 | Tilt | 0 | Kv/Kh | 1 | Trans-A9-D0-K1 |
| 2.1.4.1.2 | Trans | Amplitude | 9 | Tilt | 1 | | | |
| 2.1.4.1.2.1 | Trans | Amplitude | 9 | Tilt | 1 | Kv/Kh | | |
| 2.1.4.1.2.1.1 | Trans | Amplitude | 9 | Tilt | 1 | Kv/Kh | 0.01 | |
| 2.1.4.1.2.1.1.1 | Trans | Amplitude | 9 | Tilt | 1 | Kv/Kh | 0.01 | Trans-A9-D1-K001 |
| 2.1.4.1.2.1.2 | Trans | Amplitude | 9 | Tilt | 1 | Kv/Kh | 0.1 | |
| 2.1.4.1.2.1.2.1 | Trans | Amplitude | 9 | Tilt | 1 | Kv/Kh | 0.1 | Trans-A9-D1-K01 |
| 2.1.4.1.2.1.3 | Trans | Amplitude | 9 | Tilt | 1 | Kv/Kh | 1 | |
| 2.1.4.1.2.1.3.1 | Trans | Amplitude | 9 | Tilt | 1 | Kv/Kh | 1 | Trans-A9-D1-K1 |
| 2.1.4.1.3 | Trans | Amplitude | 9 | Tilt | 2 | | | |
| 2.1.4.1.3.1 | Trans | Amplitude | 9 | Tilt | 2 | Kv/Kh | | |
| 2.1.4.1.3.1.1 | Trans | Amplitude | 9 | Tilt | 2 | Kv/Kh | 0.01 | |
| 2.1.4.1.3.1.1.1 | Trans | Amplitude | 9 | Tilt | 2 | Kv/Kh | 0.01 | Trans-A9-D2-K001 |
| 2.1.4.1.3.1.2 | Trans | Amplitude | 9 | Tilt | 2 | Kv/Kh | 0.1 | |
| 2.1.4.1.3.1.2.1 | Trans | Amplitude | 9 | Tilt | 2 | Kv/Kh | 0.1 | Trans-A9-D2-K01 |
| 2.1.4.1.3.1.3 | Trans | Amplitude | 9 | Tilt | 2 | Kv/Kh | 1 | |
| 2.1.4.1.3.1.3.1 | Trans | Amplitude | 9 | Tilt | 2 | Kv/Kh | 1 | Trans-A9-D2-K1 |
| 2.1.4.1.4 | Trans | Amplitude | 9 | Tilt | 5 | | | |
| 2.1.4.1.4.1 | Trans | Amplitude | 9 | Tilt | 5 | Kv/Kh | | |
| 2.1.4.1.4.1.1 | Trans | Amplitude | 9 | Tilt | 5 | Kv/Kh | 0.01 | |
| 2.1.4.1.4.1.1.1 | Trans | Amplitude | 9 | Tilt | 5 | Kv/Kh | 0.01 | Trans-A9-D5-K001 |

| | | | | | | | | |
|---|---|---|---|---|---|---|---|---|
| 2.1.4.1.4.1.2 | Trans | Amplitude | 9 | Tilt | 5 | Kv/Kh | 0.1 | |
| 2.1.4.1.4.1.2.1 | Trans | Amplitude | 9 | Tilt | 5 | Kv/Kh | 0.1 | Trans-A9-D5-K01 |
| 2.1.4.1.4.1.3 | Trans | Amplitude | 9 | Tilt | 5 | Kv/Kh | 1 | |
| 2.1.4.1.4.1.3.1 | Trans | Amplitude | 9 | Tilt | 5 | Kv/Kh | 1 | Trans-A9-D5-K1 |
| 3 | Perp | | | | | | | |
| 3.1 | Perp | Amplitude | | | | | | |
| 3.1.1 | Perp | Amplitude | 0 | | | | | |
| 3.1.1.1 | Perp | Amplitude | 0 | Tilt | | | | |
| 3.1.1.1.1 | Perp | Amplitude | 0 | Tilt | 0 | | | |
| 3.1.1.1.1.1 | Perp | Amplitude | 0 | Tilt | 0 | Kv/Kh | | |
| 3.1.1.1.1.1.1 | Perp | Amplitude | 0 | Tilt | 0 | Kv/Kh | 0.01 | |
| 3.1.1.1.1.1.1.1 | Perp | Amplitude | 0 | Tilt | 0 | Kv/Kh | 0.01 | Perp-A0-D0-K001 |
| 3.1.1.1.1.1.2 | Perp | Amplitude | 0 | Tilt | 0 | Kv/Kh | 0.1 | |
| 3.1.1.1.1.1.2.1 | Perp | Amplitude | 0 | Tilt | 0 | Kv/Kh | 0.1 | Perp-A0-D0-K01 |
| 3.1.1.1.1.1.3 | Perp | Amplitude | 0 | Tilt | 0 | Kv/Kh | 1 | |
| 3.1.1.1.1.1.3.1 | Perp | Amplitude | 0 | Tilt | 0 | Kv/Kh | 1 | Perp-A0-D0-K1 |
| 3.1.1.1.2 | Perp | Amplitude | 0 | Tilt | 1 | | | |
| 3.1.1.1.2.1 | Perp | Amplitude | 0 | Tilt | 1 | Kv/Kh | | |
| 3.1.1.1.2.1.1 | Perp | Amplitude | 0 | Tilt | 1 | Kv/Kh | 0.01 | |
| 3.1.1.1.2.1.1.1 | Perp | Amplitude | 0 | Tilt | 1 | Kv/Kh | 0.01 | Perp-A0-D1-K001 |
| 3.1.1.1.2.1.2 | Perp | Amplitude | 0 | Tilt | 1 | Kv/Kh | 0.1 | |
| 3.1.1.1.2.1.2.1 | Perp | Amplitude | 0 | Tilt | 1 | Kv/Kh | 0.1 | Perp-A0-D1-K01 |
| 3.1.1.1.2.1.3 | Perp | Amplitude | 0 | Tilt | 1 | Kv/Kh | 1 | |
| 3.1.1.1.2.1.3.1 | Perp | Amplitude | 0 | Tilt | 1 | Kv/Kh | 1 | Perp-A0-D1-K1 |
| 3.1.1.1.3 | Perp | Amplitude | 0 | Tilt | 2 | | | |
| 3.1.1.1.3.1 | Perp | Amplitude | 0 | Tilt | 2 | Kv/Kh | | |
| 3.1.1.1.3.1.1 | Perp | Amplitude | 0 | Tilt | 2 | Kv/Kh | 0.01 | |
| 3.1.1.1.3.1.1.1 | Perp | Amplitude | 0 | Tilt | 2 | Kv/Kh | 0.01 | Perp-A0-D2-K001 |
| 3.1.1.1.3.1.2 | Perp | Amplitude | 0 | Tilt | 2 | Kv/Kh | 0.1 | |
| 3.1.1.1.3.1.2.1 | Perp | Amplitude | 0 | Tilt | 2 | Kv/Kh | 0.1 | Perp-A0-D2-K01 |
| 3.1.1.1.3.1.3 | Perp | Amplitude | 0 | Tilt | 2 | Kv/Kh | 1 | |
| 3.1.1.1.3.1.3.1 | Perp | Amplitude | 0 | Tilt | 2 | Kv/Kh | 1 | Perp-A0-D2-K1 |
| 3.1.1.1.4 | Perp | Amplitude | 0 | Tilt | 5 | | | |
| 3.1.1.1.4.1 | Perp | Amplitude | 0 | Tilt | 5 | Kv/Kh | | |
| 3.1.1.1.4.1.1 | Perp | Amplitude | 0 | Tilt | 5 | Kv/Kh | 0.01 | |
| 3.1.1.1.4.1.1.1 | Perp | Amplitude | 0 | Tilt | 5 | Kv/Kh | 0.01 | Perp-A0-D5-K001 |
| 3.1.1.1.4.1.2 | Perp | Amplitude | 0 | Tilt | 5 | Kv/Kh | 0.1 | |
| 3.1.1.1.4.1.2.1 | Perp | Amplitude | 0 | Tilt | 5 | Kv/Kh | 0.1 | Perp-A0-D5-K01 |
| 3.1.1.1.4.1.3 | Perp | Amplitude | 0 | Tilt | 5 | Kv/Kh | 1 | |
| 3.1.1.1.4.1.3.1 | Perp | Amplitude | 0 | Tilt | 5 | Kv/Kh | 1 | Perp-A0-D5-K1 |
| 3.1.2 | Perp | Amplitude | 3 | | | | | |
| 3.1.2.1 | Perp | Amplitude | 3 | Tilt | | | | |
| 3.1.2.1.1 | Perp | Amplitude | 3 | Tilt | 0 | | | |
| 3.1.2.1.1.1 | Perp | Amplitude | 3 | Tilt | 0 | Kv/Kh | | |
| 3.1.2.1.1.1.1 | Perp | Amplitude | 3 | Tilt | 0 | Kv/Kh | 0.01 | |
| 3.1.2.1.1.1.1.1 | Perp | Amplitude | 3 | Tilt | 0 | Kv/Kh | 0.01 | Perp-A3-D0-K001 |
| 3.1.2.1.1.1.2 | Perp | Amplitude | 3 | Tilt | 0 | Kv/Kh | 0.1 | |
| 3.1.2.1.1.1.2.1 | Perp | Amplitude | 3 | Tilt | 0 | Kv/Kh | 0.1 | Perp-A3-D0-K01 |

| | | | | | | | | |
|---|---|---|---|---|---|---|---|---|
| 3.1.2.1.1.1.3 | Perp | Amplitude | 3 | Tilt | 0 | Kv/Kh | 1 | |
| 3.1.2.1.1.1.3.1 | Perp | Amplitude | 3 | Tilt | 0 | Kv/Kh | 1 | Perp-A3-D0-K1 |
| 3.1.2.1.2 | Perp | Amplitude | 3 | Tilt | 1 | | | |
| 3.1.2.1.2.1 | Perp | Amplitude | 3 | Tilt | 1 | Kv/Kh | | |
| 3.1.2.1.2.1.1 | Perp | Amplitude | 3 | Tilt | 1 | Kv/Kh | 0.01 | |
| 3.1.2.1.2.1.1.1 | Perp | Amplitude | 3 | Tilt | 1 | Kv/Kh | 0.01 | Perp-A3-D1-K001 |
| 3.1.2.1.2.1.2 | Perp | Amplitude | 3 | Tilt | 1 | Kv/Kh | 0.1 | |
| 3.1.2.1.2.1.2.1 | Perp | Amplitude | 3 | Tilt | 1 | Kv/Kh | 0.1 | Perp-A3-D1-K01 |
| 3.1.2.1.2.1.3 | Perp | Amplitude | 3 | Tilt | 1 | Kv/Kh | 1 | |
| 3.1.2.1.2.1.3.1 | Perp | Amplitude | 3 | Tilt | 1 | Kv/Kh | 1 | Perp-A3-D1-K1 |
| 3.1.2.1.3 | Perp | Amplitude | 3 | Tilt | 2 | | | |
| 3.1.2.1.3.1 | Perp | Amplitude | 3 | Tilt | 2 | Kv/Kh | | |
| 3.1.2.1.3.1.1 | Perp | Amplitude | 3 | Tilt | 2 | Kv/Kh | 0.01 | |
| 3.1.2.1.3.1.1.1 | Perp | Amplitude | 3 | Tilt | 2 | Kv/Kh | 0.01 | Perp-A3-D2-K001 |
| 3.1.2.1.3.1.2 | Perp | Amplitude | 3 | Tilt | 2 | Kv/Kh | 0.1 | |
| 3.1.2.1.3.1.2.1 | Perp | Amplitude | 3 | Tilt | 2 | Kv/Kh | 0.1 | Perp-A3-D2-K01 |
| 3.1.2.1.3.1.3 | Perp | Amplitude | 3 | Tilt | 2 | Kv/Kh | 1 | |
| 3.1.2.1.3.1.3.1 | Perp | Amplitude | 3 | Tilt | 2 | Kv/Kh | 1 | Perp-A3-D2-K1 |
| 3.1.2.1.4 | Perp | Amplitude | 3 | Tilt | 5 | | | |
| 3.1.2.1.4.1 | Perp | Amplitude | 3 | Tilt | 5 | Kv/Kh | | |
| 3.1.2.1.4.1.1 | Perp | Amplitude | 3 | Tilt | 5 | Kv/Kh | 0.01 | |
| 3.1.2.1.4.1.1.1 | Perp | Amplitude | 3 | Tilt | 5 | Kv/Kh | 0.01 | Perp-A3-D5-K001 |
| 3.1.2.1.4.1.2 | Perp | Amplitude | 3 | Tilt | 5 | Kv/Kh | 0.1 | |
| 3.1.2.1.4.1.2.1 | Perp | Amplitude | 3 | Tilt | 5 | Kv/Kh | 0.1 | Perp-A3-D5-K01 |
| 3.1.2.1.4.1.3 | Perp | Amplitude | 3 | Tilt | 5 | Kv/Kh | 1 | |
| 3.1.2.1.4.1.3.1 | Perp | Amplitude | 3 | Tilt | 5 | Kv/Kh | 1 | Perp-A3-D5-K1 |
| 3.1.3 | Perp | Amplitude | 6 | | | | | |
| 3.1.3.1 | Perp | Amplitude | 6 | Tilt | | | | |
| 3.1.3.1.1 | Perp | Amplitude | 6 | Tilt | 0 | | | |
| 3.1.3.1.1.1 | Perp | Amplitude | 6 | Tilt | 0 | Kv/Kh | | |
| 3.1.3.1.1.1.1 | Perp | Amplitude | 6 | Tilt | 0 | Kv/Kh | 0.01 | |
| 3.1.3.1.1.1.1.1 | Perp | Amplitude | 6 | Tilt | 0 | Kv/Kh | 0.01 | Perp-A6-D0-K001 |
| 3.1.3.1.1.1.2 | Perp | Amplitude | 6 | Tilt | 0 | Kv/Kh | 0.1 | |
| 3.1.3.1.1.1.2.1 | Perp | Amplitude | 6 | Tilt | 0 | Kv/Kh | 0.1 | Perp-A6-D0-K01 |
| 3.1.3.1.1.1.3 | Perp | Amplitude | 6 | Tilt | 0 | Kv/Kh | 1 | |
| 3.1.3.1.1.1.3.1 | Perp | Amplitude | 6 | Tilt | 0 | Kv/Kh | 1 | Perp-A6-D0-K1 |
| 3.1.3.1.2 | Perp | Amplitude | 6 | Tilt | 1 | | | |
| 3.1.3.1.2.1 | Perp | Amplitude | 6 | Tilt | 1 | Kv/Kh | | |
| 3.1.3.1.2.1.1 | Perp | Amplitude | 6 | Tilt | 1 | Kv/Kh | 0.01 | |
| 3.1.3.1.2.1.1.1 | Perp | Amplitude | 6 | Tilt | 1 | Kv/Kh | 0.01 | Perp-A6-D1-K001 |
| 3.1.3.1.2.1.2 | Perp | Amplitude | 6 | Tilt | 1 | Kv/Kh | 0.1 | |
| 3.1.3.1.2.1.2.1 | Perp | Amplitude | 6 | Tilt | 1 | Kv/Kh | 0.1 | Perp-A6-D1-K01 |
| 3.1.3.1.2.1.3 | Perp | Amplitude | 6 | Tilt | 1 | Kv/Kh | 1 | |
| 3.1.3.1.2.1.3.1 | Perp | Amplitude | 6 | Tilt | 1 | Kv/Kh | 1 | Perp-A6-D1-K1 |
| 3.1.3.1.3 | Perp | Amplitude | 6 | Tilt | 2 | | | |
| 3.1.3.1.3.1 | Perp | Amplitude | 6 | Tilt | 2 | Kv/Kh | | |
| 3.1.3.1.3.1.1 | Perp | Amplitude | 6 | Tilt | 2 | Kv/Kh | 0.01 | |
| 3.1.3.1.3.1.1.1 | Perp | Amplitude | 6 | Tilt | 2 | Kv/Kh | 0.01 | Perp-A6-D2-K001 |

| | | | | | | | | |
|---|---|---|---|---|---|---|---|---|
| 3.1.3.1.3.1.2 | Perp | Amplitude | 6 | Tilt | 2 | Kv/Kh | 0.1 | |
| 3.1.3.1.3.1.2.1 | Perp | Amplitude | 6 | Tilt | 2 | Kv/Kh | 0.1 | Perp-A6-D2-K01 |
| 3.1.3.1.3.1.3 | Perp | Amplitude | 6 | Tilt | 2 | Kv/Kh | 1 | |
| 3.1.3.1.3.1.3.1 | Perp | Amplitude | 6 | Tilt | 2 | Kv/Kh | 1 | Perp-A6-D2-K1 |
| 3.1.3.1.4 | Perp | Amplitude | 6 | Tilt | 5 | | | |
| 3.1.3.1.4.1 | Perp | Amplitude | 6 | Tilt | 5 | Kv/Kh | | |
| 3.1.3.1.4.1.1 | Perp | Amplitude | 6 | Tilt | 5 | Kv/Kh | 0.01 | |
| 3.1.3.1.4.1.1.1 | Perp | Amplitude | 6 | Tilt | 5 | Kv/Kh | 0.01 | Perp-A6-D5-K001 |
| 3.1.3.1.4.1.2 | Perp | Amplitude | 6 | Tilt | 5 | Kv/Kh | 0.1 | |
| 3.1.3.1.4.1.2.1 | Perp | Amplitude | 6 | Tilt | 5 | Kv/Kh | 0.1 | Perp-A6-D5-K01 |
| 3.1.3.1.4.1.3 | Perp | Amplitude | 6 | Tilt | 5 | Kv/Kh | 1 | |
| 3.1.3.1.4.1.3.1 | Perp | Amplitude | 6 | Tilt | 5 | Kv/Kh | 1 | Perp-A6-D5-K1 |
| 3.1.4 | Perp | Amplitude | 9 | | | | | |
| 3.1.4.1 | Perp | Amplitude | 9 | Tilt | | | | |
| 3.1.4.1.1 | Perp | Amplitude | 9 | Tilt | 0 | | | |
| 3.1.4.1.1.1 | Perp | Amplitude | 9 | Tilt | 0 | Kv/Kh | | |
| 3.1.4.1.1.1.1 | Perp | Amplitude | 9 | Tilt | 0 | Kv/Kh | 0.01 | |
| 3.1.4.1.1.1.1.1 | Perp | Amplitude | 9 | Tilt | 0 | Kv/Kh | 0.01 | Perp-A9-D0-K001 |
| 3.1.4.1.1.1.2 | Perp | Amplitude | 9 | Tilt | 0 | Kv/Kh | 0.1 | |
| 3.1.4.1.1.1.2.1 | Perp | Amplitude | 9 | Tilt | 0 | Kv/Kh | 0.1 | Perp-A9-D0-K01 |
| 3.1.4.1.1.1.3 | Perp | Amplitude | 9 | Tilt | 0 | Kv/Kh | 1 | |
| 3.1.4.1.1.1.3.1 | Perp | Amplitude | 9 | Tilt | 0 | Kv/Kh | 1 | Perp-A9-D0-K1 |
| 3.1.4.1.2 | Perp | Amplitude | 9 | Tilt | 1 | | | |
| 3.1.4.1.2.1 | Perp | Amplitude | 9 | Tilt | 1 | Kv/Kh | | |
| 3.1.4.1.2.1.1 | Perp | Amplitude | 9 | Tilt | 1 | Kv/Kh | 0.01 | |
| 3.1.4.1.2.1.1.1 | Perp | Amplitude | 9 | Tilt | 1 | Kv/Kh | 0.01 | Perp-A9-D1-K001 |
| 3.1.4.1.2.1.2 | Perp | Amplitude | 9 | Tilt | 1 | Kv/Kh | 0.1 | |
| 3.1.4.1.2.1.2.1 | Perp | Amplitude | 9 | Tilt | 1 | Kv/Kh | 0.1 | Perp-A9-D1-K01 |
| 3.1.4.1.2.1.3 | Perp | Amplitude | 9 | Tilt | 1 | Kv/Kh | 1 | |
| 3.1.4.1.2.1.3.1 | Perp | Amplitude | 9 | Tilt | 1 | Kv/Kh | 1 | Perp-A9-D1-K1 |
| 3.1.4.1.3 | Perp | Amplitude | 9 | Tilt | 2 | | | |
| 3.1.4.1.3.1 | Perp | Amplitude | 9 | Tilt | 2 | Kv/Kh | | |
| 3.1.4.1.3.1.1 | Perp | Amplitude | 9 | Tilt | 2 | Kv/Kh | 0.01 | |
| 3.1.4.1.3.1.1.1 | Perp | Amplitude | 9 | Tilt | 2 | Kv/Kh | 0.01 | Perp-A9-D2-K001 |
| 3.1.4.1.3.1.2 | Perp | Amplitude | 9 | Tilt | 2 | Kv/Kh | 0.1 | |
| 3.1.4.1.3.1.2.1 | Perp | Amplitude | 9 | Tilt | 2 | Kv/Kh | 0.1 | Perp-A9-D2-K01 |
| 3.1.4.1.3.1.3 | Perp | Amplitude | 9 | Tilt | 2 | Kv/Kh | 1 | |
| 3.1.4.1.3.1.3.1 | Perp | Amplitude | 9 | Tilt | 2 | Kv/Kh | 1 | Perp-A9-D2-K1 |
| 3.1.4.1.4 | Perp | Amplitude | 9 | Tilt | 5 | | | |
| 3.1.4.1.4.1 | Perp | Amplitude | 9 | Tilt | 5 | Kv/Kh | | |
| 3.1.4.1.4.1.1 | Perp | Amplitude | 9 | Tilt | 5 | Kv/Kh | 0.01 | |
| 3.1.4.1.4.1.1.1 | Perp | Amplitude | 9 | Tilt | 5 | Kv/Kh | 0.01 | Perp-A9-D5-K001 |
| 3.1.4.1.4.1.2 | Perp | Amplitude | 9 | Tilt | 5 | Kv/Kh | 0.1 | |
| 3.1.4.1.4.1.2.1 | Perp | Amplitude | 9 | Tilt | 5 | Kv/Kh | 0.1 | Perp-A9-D5-K01 |
| 3.1.4.1.4.1.3 | Perp | Amplitude | 9 | Tilt | 5 | Kv/Kh | 1 | |
| 3.1.4.1.4.1.3.1 | Perp | Amplitude | 9 | Tilt | 5 | Kv/Kh | 1 | Perp-A9-D5-K1 |

***Appendix B.2**:* Input Date for ECLIPSE, Effect of Aquifer/Caprock Interface.

In this section one example of the script of data file used for the simulation in chapter 3 section 3 (Perp-A9-D5-K1) is presented.

```
--
-- ------------------------------------------------------------------------
-- Office Simulation File (DATA)
-- ------------------------------------------------------------------------
--
--
-- Seyed Shariatipour
--
-- ************************************************************************
-- *                          WARNING                          *
-- *            THIS FILE HAS BEEN AUTOMATICALLY GENERATED.            *
-- *         ANY ATTEMPT TO EDIT MANUALLY MAY RESULT IN INVALID DATA.
*
--
-- ************************************************************************
--
--
--Begin Amarile Project Manager Criteria. Please do not edit.
--Parent=PERP-A9-D4-K1
--End Amarile Project Manager Criteria
RUNSPEC

TITLE
PERP-A9-D5-K1

START
 1 'Apr' 2013 /

-- Metric Units
METRIC

--Unified output files
UNIFOUT


-- Gas and Water present
GAS
WATER

-- Adaptive Implicit – method of solution
AIM

-- 3 components – named below (CO2 water salt)
COMPS
 3 /

-- CO2STORE module
CO2STORE
```

```
-- To do with solution of equations
NSTACK
 100 /


--Dimensions of grid (nx, ny, nz)
DIMENS
80 1 109 /

-- Dimensions of various tables – see manual
TABDIMS
 2 2 52 52 3 /

-- Number of wells, connections/well etc
WELLDIMS
 1 60 1 1/

-- Enable molecular diffusion
DIFFUSE
PARALLEL
4/

-- Use water-gas model for accurate modelling of gas/aqueous phase equilibrium
GASWAT

--NOSIM

-- ************************************************************

GRID

-- Outputs initial data for the model, like perms, so they can be viewed
INIT

DXV
 80*100 /

DYV
 1*8000 /

DZV
 109*1 /

EQUALS

-- TOPS          991   1   80   1   80   1   1/
 PORO     0.0    1     80  1    1   1    9/
 PORO     0.2    1     80  1    1   10   109/
 PERMX    0.0    1     80  1    1   1    9/
 PERMX    500    1     80  1    1   10   109/

/
-- Large aquifer
MULTIPLY

        PORO 10E+6    80   80   1   1   1   109/
```

```
/


COPY
 PERMX PERMY /
 PERMX PERMZ /
/


BOX
 1        80        1        1        1        1/
TOPS
1498.423653     1496.989806     1497.274806     1495.840959     1489.907112     1478.410959
          1462.414806     1444.699806     1428.703653     1417.2075
1411.273653     1409.839806     1410.124806     1408.690959     1402.757112     1391.260959
          1375.264806     1357.549806     1341.553653     1330.0575
1324.123653     1322.689806     1322.974806     1321.540959     1315.607112     1304.110959
          1288.114806     1270.399806     1254.403653     1242.9075
1236.973653     1235.539806     1235.824806     1234.390959     1228.457112     1216.960959
          1200.964806     1183.249806     1167.253653     1155.7575
1149.823653     1148.389806     1148.674806     1147.240959     1141.307112     1129.810959
          1113.814806     1096.099806     1080.103653     1068.6075
1062.673653     1061.239806     1061.524806     1060.090959     1054.157112     1042.660959
          1026.664806     1008.949806     992.9536529     981.4575
975.5236529     974.0898059     974.3748059     972.9409588     967.0071118     955.5109588
          939.5148059     921.7998059     905.8036529     894.3075
888.3736529     886.9398059     887.2248059     885.7909588     879.8571118     868.3609588
          852.3648059     834.6498059     818.6536529     807.1575
/

ENDBOX

CARFIN
 LGR1  1        45        1        1        1        109      45       80       109/
CARFIN
 LGR2  46       79        1        1        1        34       34       80       34/


--*****************************************************

EDIT

PROPS

-- Diffusion Coefficients
DIFFCGAS
--for CO2  Water
   0.0001   0.0001 /

DIFFCWAT
--For CO2 Water NaCl
    0.0001   0.0005  0.0005 /

-- For Report
RPTPROPS
'PVTW' 'PVTG' 'PVDG'  'PVTWSALT' 'SOLU'
/
```

```
CNAMES
  'CO2' 'H2O' 'NACL' /

-- Rock Compressibility
ROCK

  150 5e-05 /
  150 5e-04 /
-- reservoir termperature, in degrees C
RTEMP
 45 /

-- initial molar fractions
ZI
-- mole fractions (CO2 H2O NaCl)
 0.0 0.967 0.033 /


--Gas rel perm – table has gas sat, rel perm and Pc
GSF
-- Sand Drainage **Table 1
--   Sg        Krg        Pcg

0         0         0.1000
0.02      0         0.1016
0.08      0         0.1070
0.12      0.0001    0.1110
0.16      0.0003    0.1156
0.2       0.0007    0.1208
0.24      0.0015    0.1267
0.28      0.0028    0.1337
0.32      0.0047    0.1419
0.36      0.0074    0.1518
0.4       0.0112    0.1642
0.44      0.0161    0.1801
0.48      0.0225    0.2019
0.52      0.0305    0.2342
0.56      0.0404    0.2893
0.6       0.0525    0.4203
0.636     0.0654    1.4142
/
---- Sg   Krgi      Pc for SSG Fm
0.38      0         0.1576
0.42      0.001     0.1716
0.46      0.0046    0.1901
0.5       0.0116    0.2163
0.52      0.0165    0.2342
0.56      0.0292    0.2893
0.6       0.0461    0.4203
0.636     0.065     1.4142
/
WSF
--Sand ** Table 1
--   Sw        Krw
--
0.364     0
```

```
0.4       0.0004
0.44      0.0033
0.48      0.0104
0.52      0.0232
0.56      0.043
0.6       0.071
0.64      0.1084
0.68      0.1563
0.72      0.2157
0.76      0.2877
0.8       0.3732
0.84      0.4731
0.88      0.5885
0.92      0.7201
0.98      0.95
1         1
/
-- Sw    Krwi for SSG Fm
0.364     0
0.4       0.0034
0.44      0.0157
0.48      0.0374
0.5       0.0518
0.54      0.0879
0.58      0.1338
0.62      0.1892
/
-- ***************************************************************
REGIONS

FIPNUM
800*1  7920*2

/

-- ***************************************************************
SOLUTION

EQUIL
--
-- Equilibration Data Specification
--   DATUM DATUM   OWC   OWC   GOC   GOC   RSVD  RVVD  SOLN
--   DEPTH PRESS   DEPTH  PCOW DEPTH  PCOG TABLE TABLE  METH
--
     1500  150   200    1*   500    1*    1*    1*    1*    1*
/

-- To do with reporting the initial values
RPTRST
'RESTART' 'PRES' 'BWAT' 'BGAS' 'DENW' 'DENG' 'PGAS' 'PSAT' 'PWAT' 'SGAS'
'SWAT' 'VWAT' 'VGAS' 'XMF' 'YMF' 'AQPH' 'FIP' 'OILPOT' /

-- ***************************************************************

SUMMARY
ELAPSED
EXCEL
```

```
--FAQR

--FAQT
FCGMR
 1 /
FGCDI
RGCDI
1 2 3 /
FGCDM
RGCDM
1 2 3 /
FGIP
RGIP
1 2 3 /
FGIPG
RGIPG
1 2 3 /
FGIPL
RGIPL
1 2 3 /

FGIR
FGIT
FGMT
FGOR
FGPP
FGPR
FGSAT
RGSAT
1 2 3 /
FPR
FPRP
RPR
1 2 3 /
FVIR
FVIT
FWCD
RWCD
1 2 3 /
FWGR
FXMF
 1 /
FXMF
 2 /
FYGR
 1 /
FYGR
 2 /
FYMF
 1 /
FZMF
 1 /
FZMF
 2 /
NEWTON
RPTONLY
RUNSUM
```

```
--SEPARATE
TCPU
TIMESTEP
WBHP
 /
WGIR
 /
WGIT
 /
WTHP
 /

-- ************************************************************************

SCHEDULE

-- For outputting to restart files
RPTRST
'RESTART' 'PRES' 'DENW' 'DENG' 'PGAS' 'PWAT' 'SGAS'
'SWAT' 'VWAT' 'VGAS' 'XMF' 'YMF' 'OILPOT' /


-- Names of wells, location, datum depth, etc
--      Well  Well   Location   BHP    Pref.   Drainage  Inflow  automatic cross pressure density
well
--      name  group  I    J    datum   phase   radius    eqn     shut-in   flow  table  calcltn     model
--     -----  ----   -    -   -----   -----   ------    ------  -------   ----  ------  -------     -----
WELSPECS
      INJ1   G     1   1    1500    GAS     1*      STD     SHUT     YES   1*     SEG     3*   STD
/
 /

-- Completions for wells – completed from layer 190 - 200
-- WELL     I    J    K1   K2  CONNECTION  SAT trans  DIAM   Kh Skin D-factr directn
peacemn radius
-- ----     --   --   --   --  ----------  --- -----  -----  -- ---- ------- ------- --------------
COMPDATl
  INJ1    LGR1  1    40   59  109     OPEN        2*      0.2      3*           Z       1* /

/



-- Specify composition of injected gas
WELLSTRE
-- name    CO2  H2O NaCl
--         mol  mol mol
--         ---  --- ----
 'CO2GAS'   1    0    0 /
/


-- well   Fluid    Fluid
-- Name   inject   name
-- ----   ------   -----
WINJGAS
  INJ1    STREAM 'CO2GAS'         2* /
```

```
/

-- Injection rate
--  Well  Type  Well   Control surface  resv   BHP    THP
--  name        status  mode   rate     rate  target target
--  ----  ----  ------  ----   ----     ----   ----  -----
WCONINJE
     INJ1   GAS   OPEN    RATE   2737206     1*     600     1* /
 /


---- To do with solution of equations
TUNING
0.01 60 0.01 7* / -- limiting time step to 60 days
14* /
20 1 100 7* /

-- Times of printouts.
TSTEP
 1 364 5*365 /


-- Shut after 20 years and continue to simulate for 100 years

WCONINJE
--  Well  Type  Well   Control surface  resv   BHP    THP
--  name        status  mode   rate     rate  target target
--  ----  ----  ------  ----   ----     ----   ----  -----
     INJ1   GAS   SHUT    RATE   2737206     1*     600     1* /
 /


-- To do with solution of equations
TUNING
30 365 0.01 7* / -- time step limit now 1 year
14* /
20 1 100 7* /

TSTEP
 10*3650 /

END
```

***Appendix C:***

***Conversion for Salinity Units***

Concentrations of salt are entered into the ECLIPSE package as mole fractions. Here the calculation for converting molality to mole fraction is presented. Mole fraction of component $i$ in the aqueous phase:

$$x_i = molality_i \times \frac{M_{Solvent}}{1000} \times x_{Solvent}$$

(C.7.1)

Where:

Mole fraction of solvent in the aqueous phase:

$$x_{Solvent} = \frac{n_{Solvent}}{n_{total}} = \frac{n_{Solvent}}{n_{solvent} + \sum_{i \neq solvent} n_i}$$

(C.7.2)

Molality of component i:

$$molality_i = \frac{n_i}{m_{solvent}} [mol/kg]$$

(C.7.3)

where,

$M_{solvent}$ is the molecular weight of solvent (g/mol) and *n* represents the number of mole.

Therefore:

$$molality_{solvent} = \frac{1000}{M_{solvent}} [mol/kg]$$

(C.7.4)

In this calculation the solvent is $H_2O$, $M_{H_2O} = 18.014 g/mol$ and $molality_{H_2O} = 55.508 mol/kg$.

Concentration in mg/L can be converted to mole fraction through:

$$x_i = \frac{\left(\frac{c_i}{M_i}\right)}{\sum_j \left(\frac{c_j}{M_j}\right)} = \frac{[i]}{\sum_j [j]}$$

(C.7.5)

Where:

$[i]$ denotes the molarity of component $i$ in mol/L.

$c_i$ denotes the concentration in mg/L.

$M_i$ the molecular weight in mg/mol.